How an Arginine Switch Promotes the Self-preservation of an Hydrogen Peroxide-degrading Enzyme KatG: the Strategic Use of an Active-Site Tryptophan

by

Hui Xu

A dissertation submitted to the Graduate Faculty of
Auburn University
in partial fulfillment of the
requirements for the Degree of
Doctor of Philosophy

Auburn, Alabama
August 08, 2020

Keywords: catalase-peroxidase (KatG), peroxidase electron donors (PxEDs), the arginine switch, proximal tryptophan, protein-based radicals

Approved by

Douglas C. Goodwin, Chair, Professor of Chemistry and Biochemistry
Holly R. Ellis, Professor of Chemistry and Biochemistry
Steven O. Mansoorabadi, Associate Professor of Chemistry and Biochemistry
Christopher J. Easley, Professor of Chemistry and Biochemistry

Abstract

Catalase-peroxidase (KatG) is a heme-dependent enzyme and an effective H_2O_2 disposal catalyst, sustaining life for many archaea, bacteria, and lower eukaryotes. Many pathogens employ KatG catalase activity ($2\ H_2O_2 \rightarrow 2\ H_2O + O_2$) to manage oxidative stress. Notably, the intracellular human pathogen *Mycobacterium tuberculosis* survives within the harsh acidic and highly oxidizing phagolysosomes of host neutrophils and macrophages with KatG as one of its two catalase-active enzymes and research suggests *M. tuberculosis* with *katG* gene knocked out is more susceptible to oxidative stress induced by host cells.

With a unique active site incorporated into a peroxidase fold, KatG has robust catalase activity that no other member of its superfamily possesses. KatG carries out its catalase activity by a novel radical-based mechanism involving a protein-derived cofactor, the Met-Tyr-Trp (MYW) adduct. In connection with this mechanism, KatG also undergoes inactivation resulting from off-catalase radical transfer events. A central participant in this process is the active site's proximal tryptophan, (Trp 321 according to *M. tuberculosis* KatG (*Mt*KatG) numbering). Interestingly, KatG also has an arginine "*switch*" (Arg 418 in *Mt*KatG), the conformational position of which is pH dependent. Above pH 6.5, its side chain points predominantly toward the phenolic oxygen of the MYW tyrosine (i.e., "*in"* conformation), and below pH 6.5 it points away from the MYW cofactor and toward the protein surface (i.e., "*out*" conformation). It has been observed that susceptibility of KatG catalase to inactivation increases below pH 6.5. Prior to the research described in this dissertation, any connection between inactivation and arginine switch conformation was unknown and uninvestigated. Similarly, the strict conservation of the proximal Trp across all KatGs even though it appears to contribute to KatG inactivation has raised questions about its role that have remained unexplored.

To investigate the connection between the arginine switch, off-pathway radical transfer, and KatG inactivation, as well as to shed light on the role of Trp 321 oxidation in enzyme inactivation, we evaluated four KatG variants: 1) The fully functional wild-type KatG, 2) enzyme missing a functional arginine switch (R418N KatG), 3) enzyme lacking an oxidizable proximal Trp (W321F KatG), and enzyme lacking both features (W321F/R418N KatG). Each variant was investigated for its reactions with H_2O_2 to determine not only standard steady-state kinetic parameters, but also to evaluate the kinetics of enzyme inactivation. Likewise, enzyme intermediates involved in active catalatic turnover as well as those observed during inactivation were monitored by optical stopped-flow and rapid freeze-quench (RFQ) EPR. Across all of these studies, the impact of pH and the presence or absence of peroxidatic electron donor (PxED), were also evaluated.

Compared to the wild-type enzyme, our R418N KatG variant showed a 38-fold decrease in catalase catalytic efficiency (i.e., k_{cat}/K_M), but a 60-fold *increase* in peroxidase efficiency (i.e., k_{cat}/K_M with respect to H_2O_2). The catalase activity of R418N KatG was susceptible to inactivation, a phenomenon that varied little with pH. In contrast, the wild-type enzyme was vulnerable to inactivation, but only at acidic pH. These data suggested that withdrawal of the arginine switch, either by pH-dependent conformational change (e.g., wild-type KatG at pH 5) or by mutagenesis (e.g., R418N substitution), created an enzyme more susceptible to inactivation. Inclusion of PxEDs prevented inactivation of KatG in all cases where its susceptibility to inactivation was observed. Interestingly, much greater PxED oxidation per H_2O_2 consumed was observed for R418N KatG than for wild-type during the catalatic depletion of H_2O_2. In light of the fact that most PxEDs are too large to transit the narrow substrate access channel leading to the enzyme active site, their peroxidatic oxidation relies on through-protein radical transfer

oxidation. As such, peroxidase activity would seem to constitute a record of off-catalase electron transfer events that occur during KatG catalase turnover. The dramatically elevated peroxidase activity of R418N KatG suggests that more PxED intervention is needed by the variant to prevent the accumulation of inactive states. Stated another way, these data indicate a much greater participation of off-pathway electron transfer during H_2O_2 processing by R418N KatG compared to the wild-type enzyme.

Though the kinetics were distinct, enzyme-monitored stopped-flow experiments indicated that upon reaction with H_2O_2, wild-type (e.g., pH 5) and R418N KatG (e.g., pH 5 and 7) both accumulated catalase-inactive intermediates characterized by spectra with compound II-like (i.e., Fe^{IV}=O) features. Consistent with this conclusion, the rates of conversion of these intermediates to the Fe^{III} (i.e., resting) state were not catalytically competent to account for the catalase activity of either protein. For both wild-type and R418N KatG, inclusion of a PxED stimulated catalatic H_2O_2 consumption, prevented accumulation of Fe^{IV}=O-like states, *and* produced the rapid return of the Fe^{III} enzyme after H_2O_2 depletion. These data suggest that PxEDs act to prevent accumulation of catalase-inactive species.

In our RFQ-EPR studies upon reaction of either wild-type or R418N KatG with H_2O_2 at pH 5.0, an intense narrow-doublet EPR spectrum was observed at the earliest reaction quench times. This signal has been assigned as an MYW adduct radical. Likewise, for both variants, at a time estimated to correspond to the depletion of H_2O_2, an exchange-broadened singlet dominated the spectrum. This species has been assigned as a radical centered on the proximal Trp (Trp 321). An identical species has been observed upon reaction of wild-type enzyme with peracetic acid, a peroxide that can oxidize Fe^{III} peroxidases to their compound I (i.e., Fe^{IV}=O[porphyrin]$^{\bullet+}$) state, but does not support full catalase turnover. Spectral features indicative of exchange broadening

diminished over time, suggesting that the radicals migrate away from the active site heme iron toward the protein surface. Inclusion of a PxED did not interfere with the $MYW^{\bullet+}$, but fully prevented the accumulation of other radicals, and produced the fast return of the ferric enzyme. Though the kinetics were different, reaction of R418N KatG at pH 7 showed the same steady-state radical migration from MYW to Trp 321, *and* to remote oxidizable amino acids. Likewise, only the catalase-essential $MYW^{\bullet+}$ species were detected upon inclusion of a PxED. These results suggest that Trp-321 is the primary participant for off-pathway electron transfer when the Arg switch is withdrawn by mutagenesis or by the conformational adjustments induced under low-pH conditions. Further, PxEDs serve to prevent accumulation of catalase-inactive species.

To further investigate the participation of the proximal tryptophan, a double variant was prepared wherein the Trp was replaced by Phe, a residue that is not oxidizable under typical biological conditions (i.e., W321F/R418N KatG). The double variant produced catalase steady-state kinetic parameters (i.e, k_{cat}, k_{cat}/K_M) highly similar to R418N under standard assay conditions. However, the double variant showed almost no resistance to H_2O_2-dependent catalase inactivation, regardless of pH or the presence or absence of a PxED. On the other hand, the peroxidase activities and the extent of PxED oxidation for H_2O_2 consumed by the double variant were nearly identical or even higher, compared to R418N KatG, suggesting facile off-catalase through-protein electron transfer via conduit(s) bypassing Trp 321 occurred in the double variant. The disparity between effective peroxidatic oxidation and failure to restore catalase activity by inclusion of a PxED suggested that the off-pathway electron transfer by route(s) bypassing Trp 321 are not effective for PxED-based prevention of KatG inactivation. Further, off-catalase radicals handled by another route(s) appeared to produce the more rapid demise of the enzyme as compared to variant where the proximal Trp was present.

KatG variants with an arginine switch (e.g., *wt* and W321F) are relatively insensitive to H_2O_2-dependent inactivation at pH 7 but become increasingly so as pH decreases below 6.5. KatG variants without an arginine switch (e.g., R418N and W321F/R418N) showed relatively high sensitivity to H_2O_2-dependent inactivation across the pH range. This suggests that the absence of the arginine switch either induced by low pH or by mutagenesis produces a KatG more susceptible to inactivation. The peroxidase activities of these enzymes and the extent of PxED oxidation for H_2O_2 consumed all point to a higher propensity toward off-catalase electron transfer when the arginine switch is absent. At pH 7, where the off-catalase electron transfer is not an issue, the tolerance to H_2O_2-dependent inactivation followed *wt*KatG ≈ W321F >> R418N > W321F/R418N. In contrast, at pH 5, where there is much greater frequency of off-pathway electron transfer, the order followed *wt*KatG > R418N > W321F > W321F/R418N. Taken together, our data suggest that Trp 321 enables KatG to most effectively cope with the off-catalase electron transfer events when they occur.

In conclusion, the results of the research described in this dissertation indicate the arginine switch is the central player in managing the frequency of off-pathway radical transfer, whereas the proximal tryptophan is an essential residue for handling these events when they occur. These data have potentially far reaching implications. First, they inform the mechanism by which KatG preserves its catalase activity. KatG, on one hand, is the frontline defense against H_2O_2 in many pathogens, important for pathogen colonization. However, on the other hand, KatG is prone to inactivation at pH 5, the condition coincides with host defense mechanism like neutrophil oxidative stress (i.e., pH 5, large [H_2O_2]). Understanding the mechanism by which KatG preserves its central catalase activity will lead to better understanding of the overall host-pathogen interaction. This knowledge may allow intervention into the host-pathogen interaction

for developing a treatment which enhances a host's ability to combat pathogenic infections in general. Second, KatG is an ideal system to investigate how oxidoreductases cope with the potentially destructive chemistry they catalyze.

This work was supported by a grant from the National Science Foundation (MCB 1616059).

Acknowledgments

I give my sincerest gratitude to Dr. Douglas Goodwin, my major advisor. I could not have reached today's achievement without your guidance, encouragement, persistence, and sacrifice. You are a model mentor, who dedicates yourself to helping all your graduate students achieve at a high level in academics and also in their personal life. You guided me through the entire research process and helped me become a well-trained and independent researcher. I am greatly indebted to you for all you have done for me.

I want to give special thanks to all of my committee members, Dr. Holly Ellis, Dr. Steven Mansoorabadi, and Dr. Christopher Easley for your contributions and support during this journey. I also want to extend thanks to outside reader Dr. Angela Calderón. Your strong work ethics and sincere willingness to help me any time I needed assistance have set great examples for me to emulate. I will always be grateful for your help and support.

I also want to give special thanks to Dr. Eduardus Duin for your encouragement and special assistance with use of the X-band EPR spectrometer. I will always remember your passion and kindness. In reference to my RFQ-EPR work, I also wish to extend my deep appreciation to Bryan Cronin, Robel Ghebreab, Carly Engel, and Katherine Clohan from Dr. Duin's lab who provided help for my RFQ experiments. All of you as well as my group members, especially Jessica Krewall have provided me with a lot of help to make this amazing sample-getting, data-collecting of RFQ-EPR journey much easier.

I would like to thank Dr. Aimin Liu and Ian Davis for your timely help and advice in setting up the home-made liquid ethane apparatus we used. Your collegiality means a lot to me. Your encouragement has made me a better researcher that gains happiness when helping others. I am also very excited to have the opportunity to join Dr. Liu's group as a postdoc fellow soon.

I would like to thank Dr. Angela Calderón and Eli for your assistance in setting up and using the mass spectrometer. Your positive attitudes and encouragement stood out and kept me focused during this "trial and error" process. I am grateful for that.

I wish to thank former members of the Goodwin research group, including Rene Fuanta, Olive Njuma, Yu Wang, and Haijun Duan, as well as current members of that group, to include Jessica Krewall, Tarfi Azis, Rejaul Islam, Callie Jackson, and Jahangir Alam. I also want to thank the undergrad (Kirklin McWhorter), who worked closely with me, for his stimulating discussions of our research. As a member of that group, I will always be grateful for your collegiality, constant support and friendship.

I would like to thank Dr. Rik Blumenthal and Dr. Konrad Patkowski, faculty members in my department, for guiding me and supporting me from the time I arrived at Auburn University.

Many thanks to all the friends I have made while in graduate school, especially Xingchen Huang, Rene Fuanta, Richard Hagen, Katie Tombrello, Shuxin Li, Robel Ghebreab, Jessica Krewall and Md Mohibullah.

Special thanks to the ladies of the Department of Chemistry and Biochemistry main office to include Rebbcca Folmar, Carol Nixon (retired), Lynn Walker (retired) and all the other departmental support staff.

I also wish to extend my deep appreciation to Dr. Stewart Schneller (Papa) and his wife Aina (Nanny) for taking on the role as American family members for me. Many thanks for your unconditional love and support, and for being my cheerleaders throughout my program of study.

Deep gratitude also goes to another American family, James (Dad) and Ruth (Mom) Hairston. You two have had positive impacts that transformed my life. Because of you, not only did I have family members in the USA to spend weekends and holidays with, you helped me

become more assertive, more optimistic and more confident in myself and my abilities. I appreciate all the invaluable love you give me. I would not be the person I am now without you. I am also very grateful that you invited me to live with you before I move to UTSA for the postdoc position.

I would like to give my greatest appreciation to my Mom (Lei Wang) and Dad (Feng Xu). You are the best parents I could have ever asked for. I would not be the person I am now without you and your love. My greatest gratitude goes to my committed boyfriend (Nianjun Fu). You are the best soul mate that I could ever hope for. My special appreciation also goes to my other family members for your love and support to include step mom (Liling Li), step dad (Yiping Song), my half-brother (Zhihong Xu), grandparents (Jingsong Xu, Lipeng Xie, Haowen Wang, Xiufang Zhu). I am also so grateful to my additional Dad (Lipeng Hong) for your unconditional love which brightens my life. I also want to extend my appreciation to my sweet uncle (Decai Luo) for your wonderful support and encourangement.

Looking back, I made the courageous decision to transition from the route that would allow me to be a physician specialized in physical medicine and rehabilitation to the route to be a biochemist. I have faced many difficulties in this transition, especially my efforts to become proficient in the English language. Fortunately, with the tremendous support from all of you and many others, this dream is being realized. I am very grateful to all of you who gave me your friendship and assistance during this wonderful PhD program in chemistry and biochemistry at Auburn University.

Table of Contents

List of Figures

List of Tables

Chapter One: Literature Review

1.1 Molecular oxygen activation

Dioxygen plays a central role in respiration which provides enormous amounts of energy and that energy supports the metabolisms of aerobic organisms on earth. However, molecular oxygen in its triplet ground state is very stable and it is relatively unreactive toward most biological molecules which are in singlet ground state, because this type of reaction is spin-forbidden (Fig. 1.1A).[1,2] To overcome this O_2 activation barrier, organisms in nature have developed at least two methods. One method is to excite triplet O_2 so that it is converted to one of two singlet states ($^1O_2$) by reversing the spin of one electron.[3,4] More commonly, a second method is to use redox-active transition metals to facilitate one electron transfer from singlet biological molecules to O_2. The reason why transition metals circumvent spin restriction is because they accommodate multiple oxidation and spin states. Therefore, they can donate or accept electrons from O_2 by forming a metal-dioxygen complex, which activates dioxygen. In this univalent reduction process, superoxide ($O_2^{\bullet-}$), hydrogen peroxide (H_2O_2), hydroxyl radical ($OH^{\bullet}$), and/or water (H_2O) will be generated (Fig. 1.1B).[3,4] Indeed, transition metals, such as Fe (the most common), Cu, Co, Mo, and Mn, are widely observed in enzyme systems which relate to oxygen transport, manipulation and reaction.

Transition metals make oxidizing power of dioxygen accessible; however, this comes at a cost: the inevitable generation of partially reduced reactive oxygen species (ROS) such as $O_2^{\bullet-}$, H_2O_2, and $OH^{\bullet}$. These molecules are notoriously responsible for oxidative damage to biomolecules of different kinds, posing a threat to living organisms that must occupy an aerobic

Figure 1.1 (A) Molecular orbital diagram for triplet ground state O_2, and its two singlet excited states. (B) The four step electron-reduction of molecular O_2 to water with standard (pH 7) reduction potentials.

environment. Even though the interaction and reaction of metalloenzymes and O_2 is tightly controlled *in vivo*, inadvertent ROS production can not be eliminated.

1.2 Reactive oxygen species (ROS) and reactive nitrogen species (RNS)

Reactive oxygen species (ROS) are a class of oxygen-containing molecules and ions formed as a result of partial reduction of dioxygen. These include the three major species superoxide radical ($O_2^{\bullet-}$), hydrogen peroxide (H_2O_2), and hydroxyl radical ($OH^{\bullet}$), along with lesser amounts of peroxyl ($ROO^{\bullet}$) and alkoxyl ($RO^{\bullet}$) radicals, singlet oxygen ($^1O_2$), and ozone (O_3).[3] Reactive nitrogen species (RNS) are nitrogen-containing molecules, including the parent radical nitric oxide (NO), peroxynitrite ($ONOO^-$), and nitric dioxide (NO_2).[5] Peroxynitrite ($ONOO^-$) is primarily from the reaction of NO and $O_2^{\bullet-}$. Both ROS and RNS are highly reactive, and thus lead to a wide range of biomolecular damages, for example, protein oxidation, protein nitration, lipid peroxidation and nitration, and DNA damage.[6,7] For the purposes of this literature review focus will be on the three major ROS species.

1.2.1 Major sources of ROS

Aerobic organisms must confront the threats of ROS. There are numerous sources for ROS formation. The largest contributor is the electron transport chain (ETC) in mitochondria, where oxygen serves as the terminal electron acceptor. Indeed, nonspecific electron transfer to O_2 either by mitochondrial electron transfer proteins or by nonenzymatic mitochondrial reactions leads to the production of ROS as inevitable but unwanted byproducts.[8] Although ETC machinery has adopted sophisticated mechanisms to ensure continuous ATP production while minimizing ROS generation, mitochondria are still the most prominent *in vivo* source of ROS production due to the high amount of O_2 consumed.[9,10]

Both generation of $O_2^{\bullet-}$ and H_2O_2 have been detected in the ETC. Superoxide radical ($O_2^{\bullet-}$), a product of the one-electron reduction of dioxygen, is the precursor of most ROS. The generation of superoxide radical in this context is mainly non-enzymatic, and happens when a single electron is transferred to O_2 inadvertently from reduced coenzymes or prosthetic groups. Because the univalent reduction potential of O_2 is negative (-0.16 V), O_2 will most likely take electrons from good univalent electron donors, such as flavins, respiratory quinones and metal centers. Since the respiratory chains are rich in these cofactors, it is not surprising that mitochondrial respiration ranks as the biggest contributor. Specifically, generation of $O_2^{\bullet-}$ has been detected in Complex I, II and III. H_2O_2 is mainly produced by dismutation of $O_2^{\bullet-}$ either spontaneously or through a reaction catalyzed by superoxide dismutases (SODs). That said, the sources for generation of $O_2^{\bullet-}$ are likely to produce H_2O_2 as well. The majority of ROS produced in this context is thought to be accidental and can pose grave consequences, although the minority of ROS in mitochondria serves as the signaling molecule from an organelle to the rest of the cell.[9]

Another big contributor of ROS production is autoxidation of flavoprotein. Because flavoproteins are abundant across metabolism, accidental autoxidation of non-respiratory flavoproteins has been suggested to be another substantial source of $O_2^{\bullet-}$ and H_2O_2.

Another prominent source of ROS production is the professional immune cells, such as neutrophils and macrophages. Interestingly, it seems that living organisms have taken note of the "destructive" nature of ROS, and use them for antimicrobial defenses. In contrast to cell respiration, where the ROS are generated primarily as byproducts, in this defense context ROS are deliberately generated by specialized enzyme systems in immune cells to defend a host against invading microorganisms. For example, mammalian neutrophils stimulated for

phagocytosis have specialized enzymatic systems that generate ROS as key intermediates in microbicidal mechanisms. Specifically, the NADPH-oxidase complex catalyzes the formation of $O_2^{\bullet-}$ at the expense of NADPH oxidation.[11] The NADPH oxidases are mainly expressed in professional phagocytes. As such, ROS production is under tight control to prevent collateral damage to surrounding tissues. There is clinical significance to NADPH oxidase production in host cell defense. For instance, if there are defects in the genes that encode the subunits of the NADPH oxidase, this leads to chronic granulomatous disease (CGD), characterized by recurrent infections with microorganisms including some bacteria and fungi.[12,13] Then, superoxide dismutation (SOD-catalyzed + nonenzymatic) yields millimolar quantities of H_2O_2. Myeloperoxidase uses H_2O_2 to oxidize chloride to hypochlorous acid (HOCl), one of the most lethal antimicrobial agents.[14,15] Additionally, $OH^{\bullet}$ is generated via Fenton reactions with a metal ion catalyst ($O_2^{\bullet-} + H_2O_2 \rightarrow O_2 + OH^- + OH^{\bullet}$).[11] Likewise, the reaction of H_2O_2 and HOCl yields singlet oxygen ($^1O_2$), a highly energetic oxygen species that breaks double bonds.[11] It is noteworthy to mention that, despite the toxicity of $O_2^{\bullet-}$ and H_2O_2, the multitude of microbicidal agents derived from them (HOCl, $OH^{\bullet}$, $^1O_2$ and peroxynitrite) are far more destructive.

1.2.2 Detrimental effects of ROS

As previously mentioned, ROS have the capacity to lead to a wide range of molecular damages. For example, superoxide radical ($O_2^{\bullet-}$) readily oxidizes Fe/S clusters. Therefore, dehydratase enzymes in bacteria that utilize [4Fe-4S] clusters, like aconitase, dihydroxy-acid dehydratase and isopropylmalate dehydratase are the potential targets of $O_2^{\bullet-}$.[2,16,17] Since some of these enzymes are involved in the citric acid cycle and amino acid biosynthesis, elevated level of $O_2^{\bullet-}$ impairs a range of metabolic pathways. Even worse, Fe which is released upon Fe/S cluster oxidation can be the catalyst for formation of other ROS, especially $OH^{\bullet}$ (the most

reactive species) via Fenton reactions ($O_2^{\bullet-} + H_2O_2 \rightarrow O_2 + OH^- + OH^{\bullet}$). Notably, $OH^{\bullet}$ is an indiscriminant oxidant that reacts at diffusion-limited rates with essentially any biomolecule. In addition, $O_2^{\bullet-}$ inactivates catalases[18] and glutathione peroxidases,[19] and thereby has the ability to interfere with H_2O_2 detoxification. It also reacts with nitric oxide (NO) to form the more reactive peroxynitrite ($ONOO^-$), which modifies an array of amino acids, such as cysteine, tyrosine, methionine, tryptophan, and histidine. Interestingly, NO is generated by NO synthases whose expression and increased activity often coincide with the same circumstance that produces increased $O_2^{\bullet-}$.

H_2O_2 is well known for readily oxidizing both of the sulfur-containing amino acid residues in proteins, namely, cysteine (more reactive) and methionine. In addition, copious amounts of H_2O_2 with limited reducing substrates can inactivate typical peroxidases, which are among the front-line defenses against H_2O_2. However, the most detrimental effects of H_2O_2 are not itself *per se*, but its derivatives, such as $OH^{\bullet}$, HOCl, $ONOO^-$ and so forth, all of which are generated in the immune responses of a host against infection.

Hydroxyl radical ($OH^{\bullet}$) attacks almost all of the macromolecules of cells indiscriminately at a diffusion-limited rate: RNA, DNA, protein, lipids and so forth, because of its extraordinary reactivity ($E^{o'} = +2.33$ V). There is no enzymatic mechanism to detoxify $OH^{\bullet}$. Because $OH^{\bullet}$ has a very short half-life and reacts within a very small radius of its site of generation; it is indiscriminately reactive to most biological molecules, and it seems that there is no point to set aside enzyme systems to cope with $OH^{\bullet}$. In this context, small antioxidant molecules, such as ascorbate, tocopherol, uric acid, GSH, etc., are the means to mitigate $OH^{\bullet}$ damage. That said, detoxification of H_2O_2, prior to its transformation to the more destructive $OH^{\bullet}$, is of paramount importance.

1.2.3 Mechanisms of ROS detoxification

Aerobic organisms have evolved non-enzymatic and enzymatic strategies to scavenge ROS, which enable them to thrive from exploiting the oxidizing power of oxygen without succumbing to oxidative damages. Non-enzymatic strategies include generation of low-molecular-weight compounds, such as ascorbate, tocopherol, uric acid, and reduced GSH, a tripeptide (L-g-glutamyl-L-cysteinyl-L- glycine) that is comprised of a thiol (sulfhydryl) group.

In biology, multiple superoxide dismutases (SODs) have evolved to disproportionate the superoxide radical which is the precursor for production of other more aggressive ROS, such as H_2O_2, $OH^{\bullet}$, and $ONOO^-$. These SODs include the cytoplasmic iron- and manganese-dependent enzymes (Fe SOD and Mn SOD, respectively) and copper-zinc-dependent enzyme (Cu-Zn SOD). Cu-Zn SOD is found in the cytoplasm of eukaryotes and in the periplasm of some bacteria. All the SODs catalyze $O_2^{\bullet-}$ disproportionation to form H_2O_2 and O_2. The rate constant for the uncatalyzed $O_2^{\bullet-}$ dismutation is optimal at pH 4.5 according to a second-order rate constant of $2 \times 10^7\ M^{-1}\ s^{-1}$ and decreases to $5 \times 10^5\ M^{-1}\ s^{-1}$ at pH 7.0. However, in the presence of SOD, the rate constant approaches the diffusion limit ($1.6 \times 10^9\ M^{-1}\ s^{-1}$) at pH 7.[20]

Because H_2O_2 is destructive in its own right and more so because it is a precursor for far more destructive oxidants, it is not surprising that biology developed a wide variety of enzymes to scavenge H_2O_2. These enzymes can be divided into two main categories, catalases and peroxidases. Catalases disproportionate H_2O_2 into O_2 and H_2O, whereas peroxidases, reduce H_2O_2 to H_2O at the expense of a wide range of inorganic and organic electron donors. For the sake of completeness and flow, the details will be given in section 1.7.

1.3 Common oxidative modifications of amino acids in proteins by ROS

ROS lead to all kinds of oxidative modifications of proteins, including cleavage of

peptide bonds, formation of oligomers, and oxidation of amino acid residue side chains.[21] For the purpose of this dissertation, only the oxidation of side chains of amino acid residues in proteins by ROS will be discussed. All amino acids are susceptible to oxidation.[22] However, the most oxidation-prone amino acids include Cys, Met, Tyr, Trp and His (Fig. 1.2). Sulfur-containing amino acids Cys and Met are readily oxidized by a wide variety of reactive species, including H_2O_2, HOCl, peroxynitrite, hydroxyl radicals and other oxidants.[23,24,25] Oxidation of Tyr, Trp and His by HOCl, peroxynitrite, and hydroxyl radicals has been reported. However, direct oxidation of Tyr, Trp and His by H_2O_2 is less likely to occur. Rather, their oxidation can be achieved by the hydroxyl radical generated by H_2O_2 reacting with Fe (II), or by enzyme systems that use metal-mediated H_2O_2 oxidation, such as cytochrome c peroxidase and lignin peroxidase.

Oxidation products of Cys by ROS are manifold and include thiyl radical, sulfenic acid (SOH), disulfide, sulfinic acid (SO_2H), and sulfonic acid (SO_3H) among others (Fig. 1.2A).[26] Oxidation products of Met include methionine sulfoxide and methionine sulfone derivatives (Fig. 1.2B).[25] Tyr oxidation products include tyrosyl radical, dityrosine, and dihydroxyphenylalanine (Fig. 1.2C).[21,25,27] Trp oxidation products include hydroxytryptophan, N-formylkynurenine (Trp metabolite), kynurenine (Trp metabolite), and hydroxykynurenine (Fig. 1.2D).[21,25] His is oxidized to 2-oxo-histidine, aspartic acid, and asparagine(Fig. 1.2E).[28]

Repair of the damage to amino acids *in vivo* appears limited to the reduction of certain oxidized derivatives of the two sulfur-containing amino acids, such as Cys and Met. Most organisms have elegant enzymatic systems to reverse the oxidation products of Cys oxidation products, such as sulfenic acid and disulfide bond, back to their original thiol states. For example, thioredoxin and thioredoxin reductase systems have been demonstrated to reduce disulfide bond at the expense of NADPH.[29] Likewise, many cells carry methionine sulfoxide reductases, which

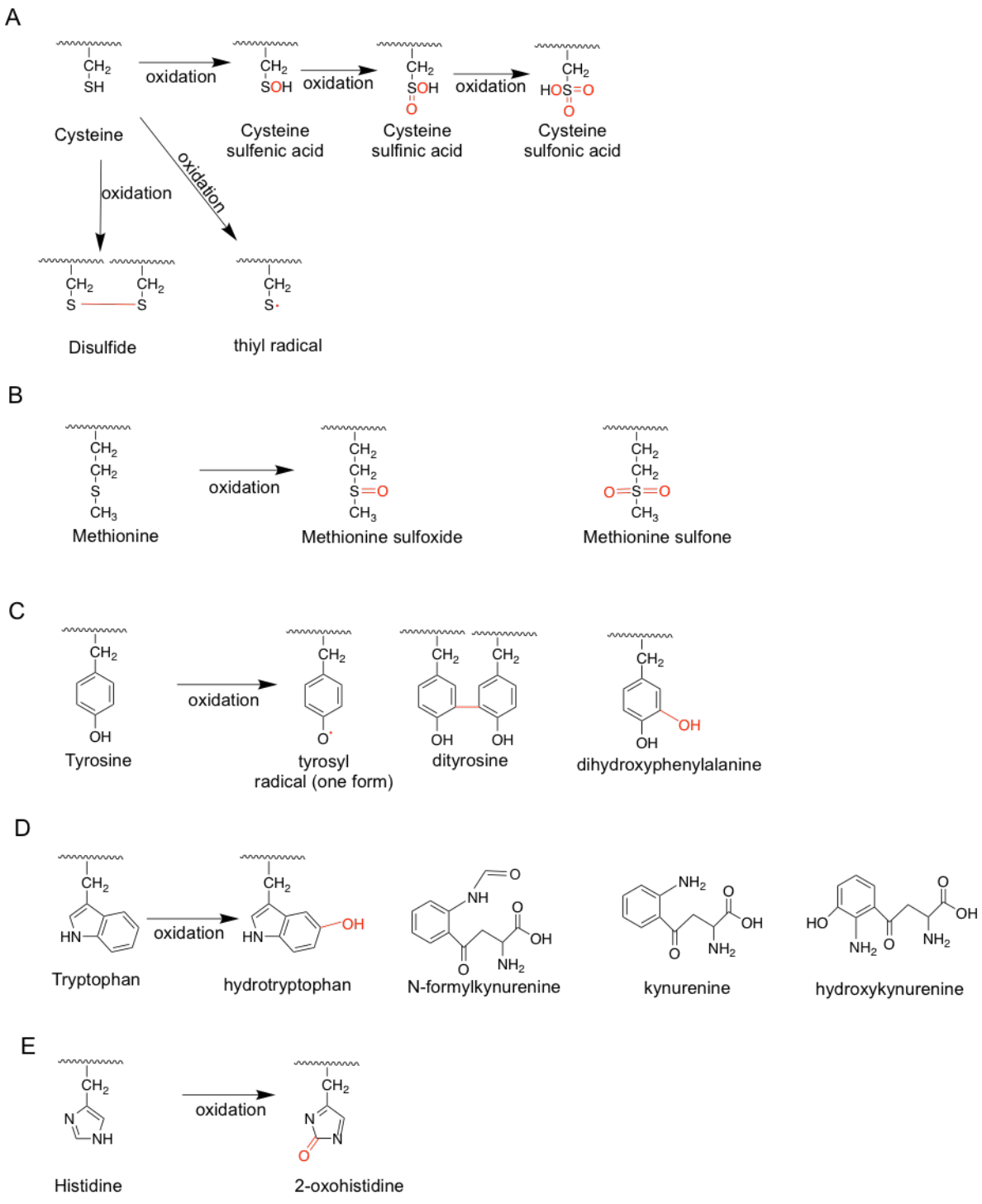

Figure 1.2. Common amino acid oxidation products. 〰 represents the main chain.

catalyze a thioredoxin-dependent reduction of methionine sulfoxide to methionine at the expense of NADPH.[30] It has been established that the methionine sulfoxide reductase can reduce either the free or the protein-bound methionine sulfoxide back to methionine *in vitro*.[31] However, repair of covalent oxidation products of Tyr, Trp and His *in vivo* has not been documented.[32]

Interestingly, it seems that biological systems of aerobes not only note the vulnerability of biomolecules to ROS attack, but also explore oxidation-prone features of these amino acids to conquer the oxidative stress from the oxidants. The following review covers how aerobic organisms capitalize on amino acids' oxidation to address problems of ROS and/or highly oxidizing intermediates generated during catalysis from three aspects. First, organisms purposely designate ROS sensor proteins for the detection of elevated levels of reactive species. This is generally achieved by oxidative modifications of a certain part of the enzyme. Then this signal is amplified via a cascade of reactions to recruit antioxidant defenses. Secondly, there is increased production of sacrificial redox-active amino acids in protein, especially on the protein surface. These oxidizable amino acids have the potential to neutralize environmentally proximate oxidants, and thereby spare other essential parts of the protein, such as the active site, from oxidative damage. Lastly, organisms seem to also note "the oxidative stress" can be endogenously generated within the enzyme active site during catalysis. This is especially true for oxidoreductases which usually use an activated cofactor/highly oxidizing intermediate(s) to perform the demanding chemistry. In these cases, evolution seems to have strategically populated the enzymes with a cluster of redox-active amino acid residues, which connects the active site (where reactions occur) and the remote solvent-exposed surface. This arrangement constructs the route(s) for off-loading the oxidizing equivalent(s) which failed from the primary reactions, to the solvent-exposed surface. And, the oxidizing equivalent(s) can be rescued by the

reducing agents when present. This mechanism, commonly known as hole hopping, has recently been proposed to be the protective method for enzymes under oxidative stress during catalysis, especially the O_2-utilizing oxidoreductase enzymes.[33]

1.4 ROS sensor proteins

1.4.1 H_2O_2 signaling mechanisms

For a long time, all ROS were viewed as exclusively deleterious. But in recent years, the discovery that certain ROS molecules serve as a key signaling molecule that modulates diverse biological processes from cell proliferation to differentiation to migration to apoptosis is now appreciated.[34,35] This, of course, depends on the ROS in question and its relative concentration. As a general rule of thumb, the features fulfilling the requirements to be signaling molecules (2nd messengers) should at least include specificity and sensitivity to its target (fast reaction).[36] That said, $OH^{\bullet}$ at any concentration is not suitable to be a signaling molecule, due to its non-specificity of reaction in the diffusion limit. In fact, H_2O_2 is the only ROS known to be clearly involved in signaling.

H_2O_2 signaling is achieved via multiple methods. The most common mechanism is the oxidation of the thiolate group of cysteine by H_2O_2 making it a signaling protein, which then modulates protein function, akin to phosphorylation. The representatives include some transcription factors from both prokaryotes and eukaryotes (i.e., OxyR, Yap 1) and other enzymes, such as protein tyrosine phosphatase (PTP) and glutathione peroxidase 3 (Gpx3). Importantly, not all thiol groups are reactive toward H_2O_2 in a manner kinetically competent for signaling purposes. In other words, only thiols in the signaling protein that readily react with H_2O_2 may fulfill the signal role. Although it is still not completely understood, the pK_a of the thiolates is an important factor, because thiolates are much more reactive than their protonated

forms. That said, low pK_a of Cys is the prime candidate. The typical pK_a of a cysteine residue thiol is approximately 8.5. However, the presence of polar or positively charged amino acids, such as arginine, can stabilize the thiolate form through electrostatic interactions and decrease the pK_a to roughly 3.5. Indeed, the pK_a value for Cys known to be reactive in OxyR is around 3.5. And the pK_a value for PTP1B is around 5.4.[37] Another important factor is the protein environment which facilitates the stability of the oxidized products of thiols. Another widely used mechanism is oxidation of the thioether group of methionine. Because Met oxidation product (i.e., methionine sulfoxide) is a reversible covalent modification, cyclic oxidation and reduction of Met residues function as regulatory processes. Lastly, a less common but novel mode of H_2O_2 signaling that has emerged within the last 15 years is metal-catalyzed protein oxidation. The only two known examples are PerR from *B.subtilis*[38] and cytochrome c peroxidase from *Saccharomyces cerevisiae*.[39]

H_2O_2 is a key signaling molecule involved not only in cellular metabolism but also in apoptosis. As such, cells must quickly sense and tightly control this "double-edged" sword to strike a homeostasis. It appears that organisms take advantage of the oxidation-prone protein feature to sense the elevated ROS levels and recruit a wide array of antioxidant defenses in response. It is also worth pointing out that signaling embraces very broad topics, but only those involved in sensing H_2O_2 stress will be the concern here.

1.4.1.1 Thiol-based H_2O_2 signaling proteins

Cysteine is oxidized to various forms by a series of ROS, including thiyl radical, sulfenic acid (SOH), disulfide, sulfinic acid (SO_2H), and sulfonic acid (SO_3H) among others (Fig. 1.2A). Among these, formation of Cys sulfenic acid or disulfides is relevant as thiol redox switches in signaling, because those oxidation products can be reverted to the reduced thiol by biological

processes that are well established.[40] Although irreversible modifications are not unprecedented in signaling, SO_2H and SO_3H modifications, mostly considered irreversible, are not involved in signaling. Generally, regulation of gene expression by thiol-based transcription factors (TF) involves oxidative transformation of cysteine to a disulfide or sulfenic acid which results in: (1) modulation of (increase or decrease) TF affinity for the NDA promoter sequence, or (2) change of the subcellular location, or (3) change in the activity.

The well documented example is *E.coli* OxyR transcription factor, whose function is activated by ROS modification. Specifically, it changes from the free thiol state (inactive state) to the disulfide linkage state (active state) upon reaction with H_2O_2. In its oxidized state, it binds to the DNA and rapidly induces the expression of *katG* (catalase peroxidase)*, gorA* (glutathione reductase), and other activities likely to defend against ROS. Once H_2O_2 concentration decreases, OxyR is reduced.[26] Likewise, the transcription factor Yap 1 from *Saccharomyces cerevisiae* activates expression of antioxidant genes upon its own oxidation by peroxides. It also employs the redox chemistry of cysteine, although another protein (Gpx3) is required for the formation of the disulfide bond in Yap1.[41] OhrR repressor uses a similar method even though it only has one cysteine.[42]

1.4.1.2 Metal-based H_2O_2 signaling proteins

1.4.1.2.1 PerR

Bacillus subtilis PerR is a metal-dependent peroxide sensor that regulates inducible peroxide-defense genes, including *katA* (catalase) and *ahpCF* (alkyl hydroperoxide reductase).[43] This factor typically binds two different metals, a structural Zn^{2+} and a regulatory Fe^{2+} ion.

Initially, it was proposed that PerR used a reactive Cys-based peroxide sensing mechanism, because oxidation of Cys was observed *in vitro* upon reaction of PerR and H_2O_2.[44]

However, the problem with this study was that the concentration of H_2O_2 employed was far higher than would be expected physiologically. In addition, other possible forms of enzyme oxidation were not investigated and therefore, cannot be ruled out.

In a subsequent investigation, Helmann and coworkers showed that PerR senses very low levels of peroxides by iron-mediated histidine oxidation.[38] In particular, oxygenation of His 37 or His 91 generates the 2-oxo derivative through the iron-catalyzed formation of hydroxyl radical. Oxidation of the histidine results in release of the protein-bound Fe^{2+} ion and dissociation of PerR-DNA complex, producing expression of the PerR regulon which includes catalase and alkyl-hydroperoxide reductase to detoxify H_2O_2. This finding is the first characterized transcription factor to use a H_2O_2-based signaling mechanism that is independent of sulfur-containing amino acids. Thus far, no mechanism for repair of the 2-oxo-histidine modification has been identified *in vivo.* It is possible that PerR is a sacrificial protein that may be degraded following its oxidation.

1.4.1.2.2 Cytochrome c peroxidase (Ccp)

Cytochrome *c* peroxidase (C*c*P) has been well established as an efficient H_2O_2 scavenger owing to its peroxidase activity.[45] As with all peroxidases, C*c*P catalyzes H_2O_2 reduction to H_2O, but it is unique in its ability to use ferrocytochrome c as the reducing substrate:

2 ferrocytochrome *c* + H_2O_2 + $H^+ \rightarrow$ 2 H_2O + ferricytochrome *c*

English and Jiang showed that C*c*P1, a heme peroxidase which targeted the mitochondrial intermembrane space, protects yeast *Saccharomyces cerevisiae* from H_2O_2 challenge.[46] This was not surprising since C*c*P1 functions as a highly efficient H_2O_2 detoxifier in the presence of donor ferrocytochrome c *in vitro*.[46] Ironically English *et al.* later found that H_2O_2 accumulation in (*ccp1*Δ-*ccp1*^{W191F}) cells, which produce only the catalytically inactive C*c*P1-W191F variant, is

lower than wild-type cell.[47] These results suggest the benefits that C*c*P1 offer should not be attributed to H_2O_2 scavenging ability *per se*, since *ccp1*Δ-*ccp1*^{W191F} cells do not even have peroxidase activity. It was demonstrated elsewhere that C*c*P1 in *Saccharomyces cerevisiae* has separate H_2O_2 scavenging and H_2O_2 signaling roles and both C*c*P1 and C*c*P1-W191F variant convey an oxidative stress signal to the nuclear transcription factor Skn7, which regulates the expression of many antioxidant enzymes to defend against oxidative damage.[48] English *et al*. observed that intracellular H_2O_2 level follows the order that *ccp1*Δ cells > wild-type cells > (*ccp1*Δ-*ccp1*^{W191F}) cells.[47] The fact that *ccp1*-null cells accumulate a higher level of H_2O_2 than that of (*ccp1*Δ-*ccp1*^{W191F}) cells is indicative of a sensing role of C*c*P1. English *et al*. concluded that C*c*P1 serves primarily as a mitochondrial H_2O_2 sensing and signaling protein to maintain reactive oxygen species homeostasis, rather than serve as an H_2O_2 scavenger.[47] In addition, they found that C*c*P1-mediated H_2O_2 signaling increases catalase (Cta1) activity. Indeed, intracellular H_2O_2 levels (*ccp1*Δ > wildtype > *ccp1*^{W191F}) correlated inversely with the activity of the mitochondrial (and peroxisomal) heme catalase, Cta1 (*ccp1*Δ < wildtype < *ccp1*^{W191F}). They further hypothesized that H_2O_2-activated C*c*P1 transferred its heme cofactor to apo Catalase A (apoCta1) for the maturation of apoCta1, based on their data.

In subsequent studies, English *et al*. identified Cta1 as a likely recipient of C*c*P1 heme.[39] They observed that: (1) respiration triggers apoCcp1 exit from mitochondria; (2) Cta1 activity increases in parallel with extramitochondrial apoCcp1 buildup; and (3) low Cta1 activity in *ccp1Δ* cells occurs with the accumulation of holoCcp1 in *cta1Δ* mitochondria.[39] They also hypothesized that heme was labilized by hyperoxidation of the protein by H_2O_2. To test this idea, they did *in vitro* experiments where they reacted C*c*P1 with excess H_2O_2 in the presence of apomyoglobin, which served as the surrogate heme acceptor. They not only observed heme

transfer to apomyoglobin, but also identified the tentative molecular cause of heme labilization-that is, heme-mediated oxidation of proximal Fe ligand, His175, to predominantly oxo-histidine. Taken together, English *et al*. concluded that C*c*P1 functions as a H_2O_2 sensor protein via a novel mechanism involving H_2O_2-activated heme transfer to apoCat1, and that it is the catalase activity of Cta1, not C*c*P1 activity, that contributes to mitochondrial H_2O_2 detoxification.

For C*c*P1 to be the H_2O_2 sensor protein, it must be modified by H_2O_2. This prompted Kathiresan and English to use LC-MS/MS to investigate in detail the oxidation of C*c*P1 by up to 10 molar excess of H_2O_2 in the absence of ferrocytochrome c.[49] Indeed, they observed extensive oxidation of C*c*P1, with the incorporation of around 20 oxygen atoms predominantly at the sites of methionine and tryptophan residues. They also observed extensive intramolecular crosslinking via dityrosine. The clusters of oxidizible amino acids exhibited a remarkable ability to facilitate hole hopping from the active site to the protein surface. As these redox-active amino acid residues were exhausted by oxidation, the proximal heme ligand His was oxidized to oxo-histidine, and thereby liberated intact heme. The heme is subsequently transferred to apoCta1. This constitutes the first example heme-mediated His oxidation being used for H_2O_2 sensing.

1.5 High composition of Cys/Met in protein-antioxidant roles

The feature of cyclic oxidation and reduction of methionine and cysteine is not only used for sensing purposes. It appears that natural cell biochemistry goes a step further and make general use of these amino acids as an antioxidant strategy by increasing their population in the protein composition, especially on the enzyme surface. As such, this pool of redox-active residues can spare the catalytically crucial components from oxidative damage by acting as sacrificial reductants themselves. As previously mentioned, some oxidation products of Cys and Met (i.e., sulfenic acid, disulfide bond, methionine sulfoxide) are reversible by enzyme systems

in vivo, at the ultimate expense of NADPH. Accordingly, this cyclic oxidation and reduction ensures their catalytic efficiency as antioxidants, rather than as stoichiometric reactants. Yet, other oxidation products of Cys, such as sulfinic acid (SO_2H) and sulfonic acid (SO_3H), as well as methionine sulfone, are usually irreversible. In these cases, they may be sacrifice-able.

The tentative antioxidant role of solvent exposed methionine residues in a variety of enzyme systems have been reviewed extensively.[23,50,51] Adding to those, Benoitand and Maier recently reported that methionine-rich *Helicobacter* catalase plays a prominent defensive role in oxidative stress, independent of its catalase activity.[52] Rather, this protective role is achieved by quenching hazardous oxidants through reversible oxidation and reduction of surface-exposed Met residues. A similar role of cysteine residues on the protein surface has just been emerging.[53] Likewise, it was reported that during oxidative stress, a key cysteinyl residue in methionine synthase (MetE) prevents ROS damage to the active site by being glutathionylated.[54] This modification then blocks the substrate access channel and spares further damage to preserve enzyme function. This modification is reversed once the stress is diffused.[54] Another way that methionine and cysteine serve as the antioxidant is that they can funnel damage away from other amino acids.[53]

1.6 Hole hopping as an oxidant-defense mechanism

The previously mentioned, redox-active transition metals such as, Fe (the most common), Cu, Co, Mo, and Mn, have been widely used in catalysis that involves O_2, and they constitute O_2 activation strategies to support metabolism of all kinds. Transition metals alone and/or with other cofactors (i.e., porphyrin, flavin) facilitate the formation of highly reactive intermediates which are crucial catalytic intermediates. These high-energy chemical intermediates include, histidine-bonded heme iron-oxo in peroxidases, tyrosine-bonded heme iron-oxo in catalases, cysteine-

bonded heme iron-oxo in P450, histidine-bonded heme iron-oxo in cytochrome c oxidase, and manganese-oxo in the oxygen evolving complex of photosystem II. However, these unstable highly oxidizing species formed during enzyme catalysis have the potential to be destructive, provided the primary chemistry is unsuccessful (i.e., physiological substrates are absent). With highly reactive intermediates confined near the vulnerable active site, they will very likely damage the catalytic components, thus ultimately leading to inactivation of the enzyme. In sharp contrast to environmentally proximate ROS discussed previously, this "oxidative stress" is confined in the core of the enzyme and endogenously generated during catalysis when the activated intermediates fail to achieve the primary chemistry. Consequently, enzymes are left to cope with radical bombs of their own making in this situation. Fortunately, these enzymes appear to have evolved a means to manage this "oxidative stress" as well.

In this regard, Gray and Winkler recently proposed that chains of tyrosine and/or tryptophan residues may serve to protect the active site and the whole enzyme from oxidative damage by rapidly offloading uncommitted oxidizing equivalents (holes) to the protein surface via a multistep hole hopping mechanism.[33,55,56] In most cases, the distance between the active site and the protein periphery is too far for single electron hopping, thus multiple redox-active Tyr and Trp residues are positioned in a manner that bridge the buried active site and protein solvent-exposed surface to facilitate the charge shuttling process. Once oxidizing holes are outside the protein, they can be scavenged by the cellular reductants, if present. To support their hypothesis, Gray and Winkler searched for such Tyr/Trp chains in the protein structural database, and found that about one-third of all proteins contain Tyr/Trp chains which are composed of three or more residues.[33] But more to the point, these researchers presented correlations between the occurrence of these chains and the biological functions of the enzymes.[33] Specifically, these

findings are consistent with the hypothesis that Tyr/Trp has a redox-protective role, since these chains appear with greatest frequency in dioxygen-using oxidoreductases.

Reports of various heme-dependent oxidoreductases being inactivated upon reaction with H_2O_2 without reducing substrates, are consistent with the Gray and Winkler hypothesis. These enzymes include cytochrome P450,[57] cytochrome c peroxidase,[49] chloroperoxidases,[58] horseradish peroxidases, prostaglandin H synthases, and MauG.[59] Admittedly, detailed inactivation mechanisms are likely to be different among these diverse enzymes. However, the highly oxidizing intermediates formed during catalysis, yet uncommmitted to the primary chemistry, are invariably the culprits in these cases. The vulnerability of these redox-active enzymes makes the potential protective mechanism very likely. Gray and Winkler also stressed an important feature of these Tyr/Trp chains, suggesting they serve as internal antioxidants. That is, the deactivation of high energy intermediates by Tyr/Trp chains should not outperform catalysis when a substrate is present, thereby interupting the primary chemistry.

Hole hopping using aromatic amino acids, mainly Tyr and Trp, as hole carriers, has been exploited for the function of many enzymes including MauG,[60,61] cytochrome c peroxidases,[49] DNA photolyases,[62,63] and ribonucleotide reductases,[64,65] since this mechanism ensures fast electron transfer rate over a long distance to support biological activity. However, its tentative protective role has not been noted before. This fascinating hypothesis has ignited the enthusiasm of various research studies of a variety of enzyme systems.

As mentioned before, Kithiresan and English reported various hole-hopping pathways in cytochrome c peroxidase upon reaction with H_2O_2 in the absence of ferrocytochrome c.[49] Their data suggest the hole hopping mechanism in CcP offloads the harmful oxidants to the protein exterior and thus spares the heme from damage in Ccp1. As such, the intact heme cofactor in

Ccp1 is subsequently transferred to apoCta1 for apoCta1 maturation and to combat oxidative stress.

MnSODs are important enzymes due to the correlation between their superoxide dismutation role and their above-average content of redox-active amino acids. These characteristics stimulated an investigation by Italian scholars using computational methods.[66] Particularly, these Italian researchers calculated the oxidation potential difference among a four-residue chain composed of Try-Trp-Trp-Trp in the MnSOD2 enzyme, to test the feasibility of multistep hole hopping along a chain of Tyr and Trp residues in human MnSOD2. They showed the oxidation potential values along the chains of these four residues evidently decreased from the active site to the protein exterior. Therefore, hole hopping along the chain is thermodynamically favored in MnSOD2.

The hole-hopping mechanism as a protective method for oxidoreductases has a grear bearing on the research discussed in this dissertation. Indeed, the data reported in this dissertation suggest that KatG capitalizes on the hole-hopping mechanism to protect itself from oxidative damage during its highly demanding catalase activity. With a conformationally-dynamic Arginine switch (^{Sw}Arg) to deliberately control two activities (its central catalase activity *vs.* off-pathway electron transfer/peroxidase activity for self-protection), KatG is capable of detoxifying H_2O_2 sustainably. In this manner, the protective peroxidase activity will not outcompete/disrupt catalase activity, but rather, serve as a protective mechanism that only operates when needed.

1.7 Catalases and peroxidases

In nature, organisms have evolved two methods to detoxify H_2O_2, either by the catalase mechanism or peroxidase mechanism. Catalases are enzymes that catalyze the decomposition of H_2O_2 to water and oxygen ($2\ H_2O_2 \rightarrow 2\ H_2O + O_2$). In contrast, peroxidases are enzymes that

catalyze the reduction of peroxides at the expense of various organic chemicals which serve as electron donors ($H_2O_2 + 2\ RH \rightarrow 2\ H_2O + 2\ R^{\bullet}$).

1.7.1 Catalases

Catalases are ubiquitous enzymes that are widely distributed among Eubacteria, Archaeabacteria, Protista, Fungi, Plantae, and Animalia.[67] They prevent cell damage by scavenging hydrogen peroxide and converting it to water and oxygen with high efficiency. Catalases are subdivided into two main groups, namely the typical heme-containing catalases and the non-heme Mn-containing catalases. Although both groups dismutate H_2O_2, the mechanisms are completely different. Only typical heme-containing catalases will be discussed in the scope of this dissertation.

1.7.1.1 Heme-dependent catalases

Heme-dependent catalases are distributed among Bacteria, Archaea, and Eukarya. These typical catalases are homotetramers, where each subunit bears a heme prosthetic group. In most catalases, heme *b* is used, with some exceptions where heme *d* is observed.

The catalase cycle is performed as a two-step catalytic mechanism where H_2O_2 is used both as an oxidant and a reductant (Fig. 1.3A). The first step involves the heterolytic reduction of H_2O_2 to H_2O, yielding two-electron oxidation of the ferric enzyme to a ferryl-oxo-porphyrin π-cation radical intermediate, referred to as compound I (i.e., Fe^{IV}=O[porphyrin]$^{\bullet+}$). In the second step, the compound I is reduced by another molecule of H_2O_2 to generate H_2O and O_2.

Catalases have a highly conserved active site (Fig. 1.3B). The invariant phenolate tyrosine ligand is coordinated to the heme iron on the proximal side. (By convention, the side of the heme where the protein-based ligand coordinates the iron is referred to as its proximal side, with the other side referred to as the distal side.) This anionic character of the ligand gives rise to

a very negative Fe^{III}/Fe^{II} reduction potential of the heme, which is proposed to help oxidation of Fe(III) to Fe(IV) and help removal of an electron from the heme upon compound I formation.[68] On the distal side of the heme are the strictly conserved triad "histidine-asparagine-serine". The distal histidine imidazole plane is parallel to the heme. The distal histidine is proposed to serve as the general base to abstract a proton from H_2O_2 during compound I formation.[69,70] The distal asparagine stabilizes the negative charge which develops on the distal side when the O-O bond is heterolytically cleaved. The serine residue participates in a hydrogen bonding interaction with the N^{δ} of the imidazole of the histidine and increases its nucleophilicity, thus stabilizing the heme pocket for H_2O_2 oxidation.[69,70] For compound I reduction, the distal histidine is proposed to act as an acid-base catalyst to oxidize H_2O_2 which facilitates release of O_2 and H_2O.[71]

Two features common to all monofunctional catalases will be discussed. First, catalase activity of typical catalases is optimal over a wide pH range (i.e., pH 5 to pH 10). This property is in sharp contrast to catalase-peroxidases (KatGs), which also have catalase activity. However, their optimal H_2O_2 dismutation occurs in a very narrow pH range (i.e., neutral pH to slightly acidic depending on KatG source). Second, typical catalases tend to have a very restricted, narrow substrate access channel. This channel allows passage of H_2O_2 and other very small molecules (i.e., peracetic acid, *etc.*). And, their heme edge is not accessible to larger molecules like the typical aromatic electron donors which support peroxidase activity. This feature is purported to facilitate catalase turnover by preventing heme reduction by molecules other than H_2O_2. Therefore, catalases are usually very poor at peroxidase activity.

Heme-dependent catalases can be divided into three main clades based on difference in sequence, structure, and identity of the prosthetic group.[72] Clade 1 contains eubacterial, algal,

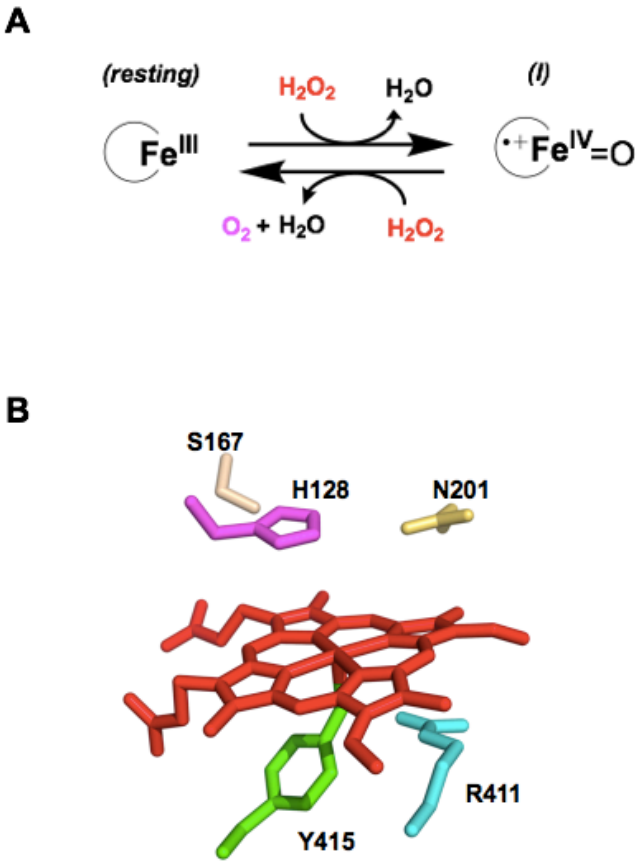

Figure 1.3. (A) Catalase mechanism of typical catalases; (B) The active site of *E.coli* catalase. PDB accession numbers for *E.coli* catalase is 1IPH.

and plant catalases of small-subunit size (55-69 kDa) and heme *b* as the prosthetic group. Clade 2 contains eubacterial and fungal catalases of large-subunit size (75-84 kDa). Clade 2 mainly uses heme *d* as the prosthetic group and they have an additional "flavodoxin-like" domain. Clade 3 is the most abundant heme-dependent catalase, and is widely found in archaebacteria, fungi, plants and animals.[73] These enzymes are small-subunit (43-75 kDa) catalases containing heme *b*. They are unique in that they use NADPH as a second redox-active cofactor. NADPH binds 20 Å from the heme in a highly conserved environment. The proposed role of NADPH is to prevent formation of inactive intermediates during catalase activity, although the exact mechanism is not clear. The general idea is that in some cases, after compound I (i.e., Fe^{IV}=O[porphyrin]$^{\bullet+}$) is formed during catalase turnover, it may undergo an intramolecular one-electron reduction that leads to a catalatically inactive species (i.e., Fe^{IV}-OH[porphyrin]AA$^{\bullet+}$), referred to as compound II, where the protein amino acid (AA) donates an electron to the porphyrin ring. And, the tightly bound NADPH is proposed to rescue this inactive compound II, thus preserving enzyme activity.[72,73] Representative Clade 3 examples are bovine liver catalase and human erythrocyte catalase.

1.7.2 Peroxidases

While H_2O_2 dismutation is the activity of typical catalases, peroxidases are the enzymes that utilize different peroxides as electron acceptors to catalyze a wide range of oxidative transformations. Peroxidases are ubiquitous and widely found in all classes of organisms. They are divided into two large groups depending on whether they contain heme as a cofactor or not. The non-heme peroxidases are classified into five independent families.[74] These include the thiol peroxidases (i.e., glutathione peroxidases and peroxiredoxines), alkylhydroperoxidases (AhpC), NADPH peroxidases, manganese catalases, and non-heme haloperoxidases.

The non-heme peroxidases are especially important for detoxification of endogenously generated H_2O_2. However, due to their very low k_{cat} and a very low apparent K_M using H_2O_2 as one substrate, they are easily overwhelmed as the H_2O_2 level becomes elevated. Therefore, these common enzymes will not provide adequate protection to the microorganisms that carry them when they encounter a host immune response which by design generates copious amounts of H_2O_2 to kill the invaders. The non-heme peroxidases are out of the scope of this literature review.

Most heme-dependent peroxidases are classified into two large superfamilies: (1) peroxidase-cyclooxygenases and (2) non-animal peroxidases. Peroxidase-cyclooxygenases are found primarily in vertebrate organisms. And the non-animal peroxidases include representatives from fungal, plant and bacterial species.

1.7.2.1 Peroxidase-cyclooxygenases

Peroxidase-cyclooxygenases play an important role in the immune system of mammals. These enzymes include myeloperoxidase (MPO), eosinophil peroxidase (EPO), lactoperoxidase (LPO) and thyroid peroxidase (TPO). The first three of these four mammalian enzymes are central to the formation of hypohalous acids (hypohalide ions) and hypothiocyanate, all of which form a formidable defense against invading microorganisms, whereas thyroid peroxidase is central to the production of thyroxine, a metabolic regulatory hormone. Among the first three mammalian enzymes involved in immune defenses, myeloperoxidase deserves special attention. Not only can MPO oxidize I^- to OI^- (most peroxidases are capable), and oxidize Br^- to OBr^- (some peroxidases are capable), it can also oxidize Cl^- to OCl^- with H_2O_2 reduction to H_2O. Indeed, HOCl, as mentioned earlier, is a highly effective antimicrobial agent in host immune defense. It fact, it is far more effective than its precursor H_2O_2.

1.7.2.2 Non-animal peroxidases

This group of enzymes is found predominantly in plants, fungi and bacteria.[75,76] All non-animal peroxidases share some structural similarities. First, they all have a so-called peroxidase fold which is composed of 10 alpha helices (A-J) linked by loops and turns, and with little or no beta sheets. Second, there is a remarkable conservation of active site structure and catalytic residues among all of them. Specifically, not only do all of these non-animal peroxidases contain heme *b* prosthetic group, they also have five residues strictly conserved in the active site. These residues include the proximal His which is modulated through a strong H-bond to an Asp, the distal His modulated by an H-bond to an Asn, and the distal Arg. All of these residues are important for peroxidase function. Third, in sharp contrast to typical catalases, these peroxidases tend to have a more open active site, where typical aromatic electron donors are accessible to the heme cofactor.

The superfamily of non-animal peroxidase has been divided into three classes based on amino acid sequence alignment and similarity of biological function. Class I contains intracellular peroxidases like ascorbate peroxidase (APX), yeast cytochrome c peroxidase (CcP) and catalase-peroxidase (KatG). As the name suggests, APX uses ascorbate as a reducing substrate to facilitate H_2O_2 reduction to water. APX plays a prominent role in protecting chloroplasts of higher plants as they combat H_2O_2 generation, the inevitable byproduct of photosynthesis and respiration. In contrast, CcP uses the protein ferrocytochrome c to reduce toxic peroxide to water.

Class II peroxidases of this superfamily are mainly secretory fungal peroxidases. Examples include lignin peroxidases (LiP), manganese-dependent peroxidases (MnP) and

versatile peroxidases from lignin-degrading fungi. This class also includes many novel heme peroxidase sequences from fungi, that are not used to degrade wood.

Class III peroxidases of the superfamily include the secretory plant peroxidases, such as horseradish peroxidase (HRP), as well as soybean, peanut, and barley peroxidases. Of note, Class III peroxidases are not primarily used for H_2O_2 degradation, but instead are involved in a wide range of physiological processes in the plant life cycle.

These three non-animal peroxidase classes are highly similar with respect to both the conserved amino acid and detailed peroxidase mechanisms. Since the main work in this dissertation deals with KatG, the catalase-peroxidase that belongs to Class I of the non-animal peroxidases, the active site structure and peroxidase mechanism for only the Class I peroxidases will be reviewed.

Generally, the peroxidase mechanism involves three steps (Fig. 1.4A). The first step involves the heterolytic reduction of H_2O_2 to H_2O, yielding a ferryl-oxo-porphyrin π-cation radical intermediate, referred to as compound I (i.e., Fe^{IV}=O[porphyrin]$^{\bullet+}$), two oxidizing equivalents above the ferric enzyme. In some cases, it is the amino acid that holds the radical, instead of the porphyrin ring. A well-established case is CcP, in which Trp-191 is the radical site (i.e., Fe^{IV}=O, W191$^{\bullet+}$).[77] To complete the peroxidase cycle, compound I returns to the ferric enzyme, usually by two sequential one-electron reductions at the expense of the two equivalents of an exogenous electron donor. The compound I is first reduced to a ferryl intermediate, compound II (i.e., Fe^{IV}=O), yielding one equivalent of the donor radical. Afterwards, compound II is reduced to the ferric state, yielding a second equivalent of the donor radical and water.

Class I peroxidases all use heme *b* as the prosthetic group and share the Arg/Trp/His triad on the distal side as well as the His/Asp/Trp triad on the proximal side (Fig. 1.4B). The proximal

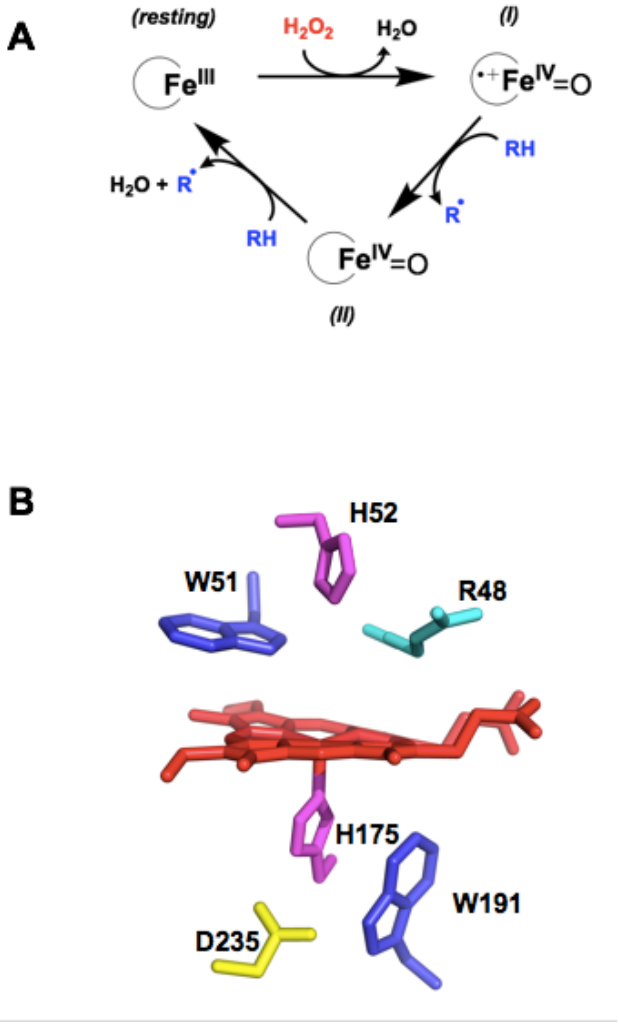

Figure 1.4. (A) Peroxidase mechanism of typical peroxidases; (B) The active site of cytochrome c peroxidase (CcP) PDB accession numbers for CcP is 1CCP.

His (H175 in CcP) serves as the ligand to the heme iron. The proximal Asp (D235 in CcP) forms the hydrogen bonding interaction with the N^{δ} of the imidazole of the His, and thus imparts a substantial anionic character to the imidazole ligand. This produces a much lower reduction potential (-186 to -226 mW). As such, peroxidases are isolated in the ferric oxidation state and thereby stabilize the higher oxidation state (i.e., Fe^{IV}=O) during catalysis. This Asp is also hydrogen bonded to the nitrogen atom of the indole group of the proximal Trp (W191 in CcP). The role of distal His (H52 in CcP) serves as a general base to facilitate the heterolytic cleavage of H_2O_2 to form H_2O and compound I.[78,79,80] The conserved Arg (R48 in CcP) stabilizes compound I by electrostatic interactions between the positive charge of its side chain and the developing negative charge on the distal oxygen of the bound H_2O_2 during heterolytic O-O bond cleavage.[78]

1.8 Catalase-peroxidases (KatGs)

1.8.1 Oddity of KatG

Up to this point, only the degradation of H_2O_2 by either the catalase ($2\ H_2O_2 \rightarrow 2\ H_2O + O_2$) or the peroxidase ($H_2O_2 + 2\ RH \rightarrow 2\ H_2O + 2\ R^{\bullet}$) mechanism has been covered. Interestingly, these two mechanisms are mostly segregated. That is, monofunctional catalases are usually poor peroxidases and vice versa. However, catalase-peroxidases (KatG) stand out as the only class of enzymes that can effectively degrade H_2O_2 through both mechanisms using a single active site.

Catalase-peroxidases (KatGs) are widely found in many archaea, bacteria, and lower eukaryotes.[81] Based on sequence, overall structure and active site homology, KatGs are within Class I of the non-animal peroxidases superfamily, along with cytochrome c peroxidases (CcP), ascorbate peroxidase (APX) and hybrid-type A peroxidases.[76,82] Indeed, the active site of CcP, APX and KatG are virtually superimposable (Fig. 1.5). But KatG is the only enzyme in the entire

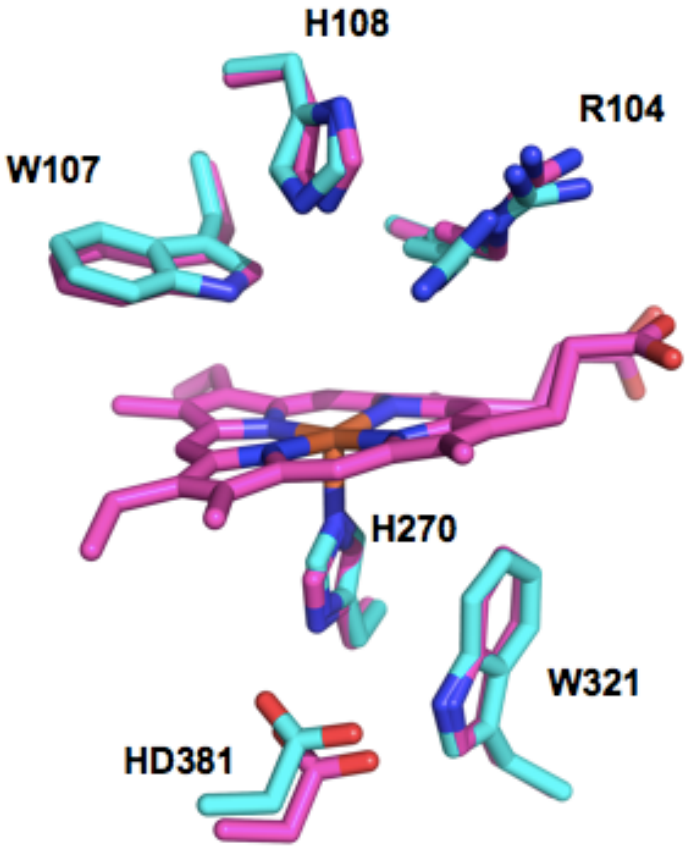

Figure 1.5. Overlay of the active sites of *Mt*KatG and CcP. PDB accession numbers for *Mt*KatG and CcP are 2CCA and 1CCP respectively.

superfamily that has appreciable catalase activity. In fact, other peroxidases within the same superfamily have almost no catalase activity (i.e., k_{cat} of KatG is around 5000 s^{-1} *vs.* typical monofunctional peroxidases around 10 s^{-1}). On the other hand, KatG does H_2O_2 dismutation (catalase activity) with an apparent second-order rate constant ($\sim 1\times10^6$ M^{-1} s^{-1}) similar to that of canonical (i.e., monofunctional) catalases, with which KatG shares no structural and sequence homology.[83,84]

Exactly how KatG in a peroxidase scaffold can effectively dismutate H_2O_2 while no other peroxidases in the same superfamily can, is a question that has not yet been fully resolved. This intriguing question, among others, has attracted copious amounts of focus on elucidating the structure and function relationships of KatG.

1.8.2 A peroxidase fold

Based on the recently reconstructed phylogeny of catalase-peroxidases, the evolution of a peroxidase-catalase superfamily began with predecessors of KatG, which were composed of two domains per subunit, namely a catalytically-active N-terminal heme-containing domain and a catalytically-inactive C-terminal domain, lacking the heme.[85,86] Both the N-terminal and C-terminal domains share high structure and sequence resemblance, including the typical 10 α helix, yet only the N-terminal domain bears the heme and is catalytically active. Similarity of the domains is believed to be the outcome of gene duplication and a fusion event followed by subsequent loss of heme binding and catalytic activity in the C-terminal domain.[87] It is further believed that during evolution of the peroxidase-catalase superfamily, the (KatG-typical) C-terminal domain was lost, and thereby so was the H_2O_2-dispropotionation ability (catalase activity). That said, all other members of the peroxidase-catalase superfamily, namely typical

(monofunctional) peroxidases, only contain a single domain with high homology to the N-terminal domain of KatGs.

Crystal structures reveal an arrangement of the active site of KatGs that is highly similar to that of Class I peroxidases, such as CcP and APX (Fig. 1.5).[88,89,90] Specifically, they all use heme b as the prosthetic group and all of them share the Arg 104/Trp 107/ His 108 triad on the distal side as well as the His 270/Asp 381/Trp 321 triad on the proximal side (*Mt*KatG numbering throughout) at almost identical places.[91] Furthermore, in all of them, the proximal His is coordinated to the heme cofactor as the fifth ligand, and also hydrogen bonded to the carboxylate side chain of the Asp residue, which is also hydrogen bonded to the nitrogen atom of the indole group of the proximal Trp. This hydrogen bonding network on the proximal side has been shown to stabilize the heme architecture.[92] Moreover, the role of distal His-Arg residues is very similar among KatG and other heme peroxidases within the Class I superfamily, which is proposed to work in concert to stabilize the charge separation necessary for heterolytic O-O bond cleavage upon reaction of KatG with H_2O_2 to form the compound I intermediate.[93,94] Specifically, the distal histidine serves as a general base to facilitate the deprotonation of H_2O_2.[78,79,80] And, the distal arginine stabilizes compound I by electrostatic interactions between the positive charge of its side chain and the developing negative charge on the distal oxygen of the bound H_2O_2 during heterolytic O-O bond cleavage.[78] The enigmatic distal Trp 107 is essential for the catalatic activity of KatG, yet CcP and APX with an exactly analogous Trp are catalase inactive.[78,79] The difference between KatG and the others did not get untangled until the first crystal structure of KatG from *Haloarcula marismortui* was published and revealed that this Trp was covalently linked to an invariant Tyr 229 as part of an unprecedented Met-Tyr-Trp covalent adduct.[88] The catalase activity of KatG is now attributed to this novel adduct.

1.8.3 Catalatic-specific structures

Since KatG is the only enzyme that can perform as a catalase within the entire peroxidase-catalase superfamily, many distinct features of KatG have emerged that are absent in the other Class I peroxidases.

1.8.3.1 Additional C-terminal domain

As stated earlier, the most conspicuous feature of KatG is that each subunit contains two domains. This is in sharp contrast to all other heme peroxidases in the Class I superfamily which have only a single domain. Although the KatG C-terminal domain lacks a heme cofactor and some of the catalytically-essential amino acids, and thus does not perform catalysis directly, it appears to support the architecture of the active site.[95] Indeed, the truncated version of KatG, which abolishes the C-terminal domain, eliminates both catalase and peroxidase activities. Incubation with a separately expressed C-terminal domain partly restores the catalytic activities and appears to restabilize the accurate fold of the N-terminal domain.[95] It is reasonable to assume that all other single-domain heme peroxidases within the Class I superfamily are not able to degrade H_2O_2 in the absence of electron donors.

1.8.3.2 Highly constricted substrate access channel

The active site heme of KatG is buried deep with a long, highly restricted and narrow substrate channel from its exterior surface. This arrangement sharply contrasts with that of most heme peroxidases, which have a much more open active site. The additional restriction is due to the presence of extra interhelical loops (LL1, LL2) in proximity to the entrance channel which leads to the heme cofactor in KatG. Specifically, KatG has a funnel-shaped channel that progressively narrows to the most constricted point where conserved Asp 137 and Ser 315 are located (*Mt*KatG number). It is generally agreed that most aromatic electron donors are denied

access to the heme site in KatG due to this narrow channel. As such, their oxidation is accomplished by hole hopping from the deep core where heme resides towards the surface via clusters of redox-active amino acids. And consistent with this idea, KatG is loaded with an unusually high percentage of oxidizable amino acids. Interestingly, although the active site arrangements are vastly different between KatG and monofunctional catalases, they all have a very narrow substrate access channel. This unique feature is believed to be critical in facilitating catalase activity, by allowing only a small molecule like H_2O_2 into the channel, rather than peroxidatic electron donors.

1.8.3.3 Met-Tyr-Trp covalent adduct

All crystal structures of KatGs to date have revealed a novel covalent bond between the distal Trp (Cη2) and an adjacent Tyr (Cε1) which is also covalently linked via Cε2 to the sulfur of a Met residue.[88,89,90,96,97] Mass spectrometric studies have revealed the presence of the adduct in KatGs in solution.[98,99] All these data indicate that the novel covalent adduct is likely a common feature harbored by all KatGs.

The integrity of this Met-Tyr-Trp (MYW) adduct is integral for catalase activity. Site-directed mutagenesis studies suggest that replacement of any of these three amino acids eliminates catalase activity but retains peroxidase activity.[78,79,100,101,102,103,104] It has been further demonstrated that the MYW serves as a redox cofactor which bears a radical (i.e., $MYW^{\bullet+}$) in the catalase turnover.

The formation of MYW adduct requires the heme and peroxides. The proposed mechanism for MYW cofactor formation is sequential.[100,101] The W and Y are each oxidized to their corresponding radical states followed by formation of the W(Cη2)-Y(Cε1) bond. Another

oxidation converts the YW adduct to a quinoid state, creating an electrophilic center for formation of the Y(Cε2)-Met(Sδ) sulfonium structure to complete the cofactor.

The MYW adduct is unique to KatGs, although covalently modified aromatic amino acids are not uncommon in metalloenzymes. Some examples include but are not limited to cytochrome c oxidase (His240-Tyr244)[105,106], galactose oxidase (Tyr272-Cys228)[107], and catalase 1 (Cys356-Tyr379)[108], all of which are believed to occur via metal mediated autocatalytic processes.[109,110,111] The mechanism by which MYW is involved in the catalase function of KatG is covered in 1.8.4.1.

1.8.3.4 Arginine switch (^{Sw}Arg)

A strictly conserved "arginine switch" (^{Sw}Arg) has sparked a lot of interest since it interacts with the catalase-essential MYW cofactor in a pH-dependent manner, albeit remote from the heme (20 Å). The side chain of the ^{Sw}Arg can adopt two conformations depending on pH. In one position, the guanidinium moiety of the switch forms a salt bridge with the tyrosal phenoxide anion of the MYW cofactor ("*in*" position), found at high pH where the ^{MYW}Y is deprotonated and the guanidinium group is protonated. In the other position, the arginine side chain is oriented away from the MYW cofactor and toward the surface of KatG ("*out*" position), found at low pH where the ^{MYW}Y is protonated.[112] At a pH that is equal to pK_a of the phenolate oxygen of ^{MYW}Tyr, "*out"* and "*in"* conformation is shown to be 50/50, and importantly, this is the condition that yields the optimum catalase activity of KatG with respect to k_{cat} and k_{cat}/K_M. This feature seems to be common to prokaryotic and fungal KatGs, albeit the pK_a of the phenolate oxygen of ^{MYW}Tyr may vary from case to case. For example, a comprehensive study of changes in the *Bp*KatG crystals as a function of pH (from 4.5 to 8.5) shows >90% "*out"* position at pH 4.5, and >95% "*in"* position at pH 8.5, and the intermediate pH (i.e., pH 6.5) where

"*out"*= "*in"* is where maximum catalase activity occurs.[112] For all the differences, *Mag*KatG2 shows a lower pH optimum (ie., pH 4.5) for catalase function, and has lower pH where the two conformations are equally populated.[113] It is worth pointing out that the remarkably low pK_a of the phenolate oxygen of ^{MYW}Tyr compared to the unmodified Tyr is attributed to: (1) the electronic effects of the MYW sulfonium cation and (2) the conformation of the positive side chain of ^{Sw}Arg.

Moreover, the dominant position of the switch is also dictated by the oxidation state of the heme. In particular, even at pH 7.5, where "*in"* conformation is favored, the switch is 100% in the "*out"* conformation when the heme is in its ferryl state.[114]

Substitution of the ^{Sw}Arg with Ala, Asn, Leu, but not Lys, greatly diminishes the catalase activity of KatG, suggesting it plays a prominent role in high catalase turnover.[112,114,115]

1.8.3.5 Distal Aspartate

Distal Asp (^{Ds}Asp) is strictly conserved and is positioned in the narrowest point of the KatG substrate access channel. The ^{Ds}Asp is necessary for high catalase activity but not peroxidase activity, indicative of its role after compound I formation.[115,116,117] The mechanism by which ^{Ds}Asp facilitates catalase activity is not yet defined. Because D137S KatG is able to form the $MYW^{\bullet+}$ at essentially the same rate and to the same extent as observed for the *wt*KatG, but is far defective in forming dioxyheme (Fe^{III}-$O_2^{\bullet-}$), it has been proposed that ^{Ds}Asp is necessary to facilitate the formation of the Fe^{III}-$O_2^{\bullet-}$ intermediates in the catalatic turnover, although how this is achieved is unclear.[115]

1.8.4 Catalatic mechanism of KatG

It is clear that KatG performs the catalatic turnover via a novel mechanism, distinct from that of the monofunctional catalases with which it shares no structural resemblance.[115,118,

[119,120,121,122,123,124,125] It is generally agreed that the initial step of the KatG catalase mechanism is oxidation of the ferric enzyme to an oxo-ferryl porphyrin π cation radical intermediate, known as compound I (i.e., Fe^{IV}=O [porphyrin]$^{\bullet+}$), which is widely shared by members of the peroxidase-catalase superfamily (Fig. 1.6A). Due to the very fast catalase turnover of KatG, this canonical compound I has only been captured by either *wt*KatG reacting with alternative peroxide which does not support catalase turnover (i.e., PAA), or from catalase-inactive variants reacting with H_2O_2.[102,126,127] This highly unstable species undergoes an intramolecular electron transfer where the porphyrin radical migrates to the MYW adduct forming the compound I* species (i.e., Fe^{IV}=O[MYW]$^{\bullet+}$/Fe^{IV}-OH[MYW]$^{\bullet+}$).[118,119,120] Afterwards, compound I* (i.e., Fe^{IV}-OH[MYW]$^{\bullet+}$) is proposed to react with a second equivalent of H_2O_2 in a nonscrambling mechanism to form an (Fe^{III}-$O_2^{\bullet-}$[MYW]$^{\bullet+}$) intermediate, termed as compound III*. [118,119,120,121] This ferric-superoxide complex is analogous to peroxidase compound III, which is catalytically inert. Monofunctional peroxidases which have no catalase activity are stuck in the compound III state in the absence of PxED. However, in KatG with the MYW adduct radical only about 3.4 Å from the heme, another intramolecular electron transfer is proposed to occur from the Fe^{III}-$O_2^{\bullet-}$ intermediate to the MYW$^{\bullet+}$, thereby releasing O_2 and returning the ferric enzyme to the resting state along with the closed shell MYW adduct.

1.8.4.1 Evidence of MYW adduct radical in the catalatic mechanism

Based on the fact that the MYW adduct, in its integrity, is required for catalase activity, it was first proposed that the [MYW]$^{\bullet+}$ intermediate may be catalatically competent.[121] Rapid freeze-quenched reactions of *Mt*KatG with steady-state concentrations of H_2O_2 have shown a narrow doublet signal detected by X-band EPR for the first time.[118] The fact that this radical is the sole radical species present in the reaction, and that its presence corresponds well to the time

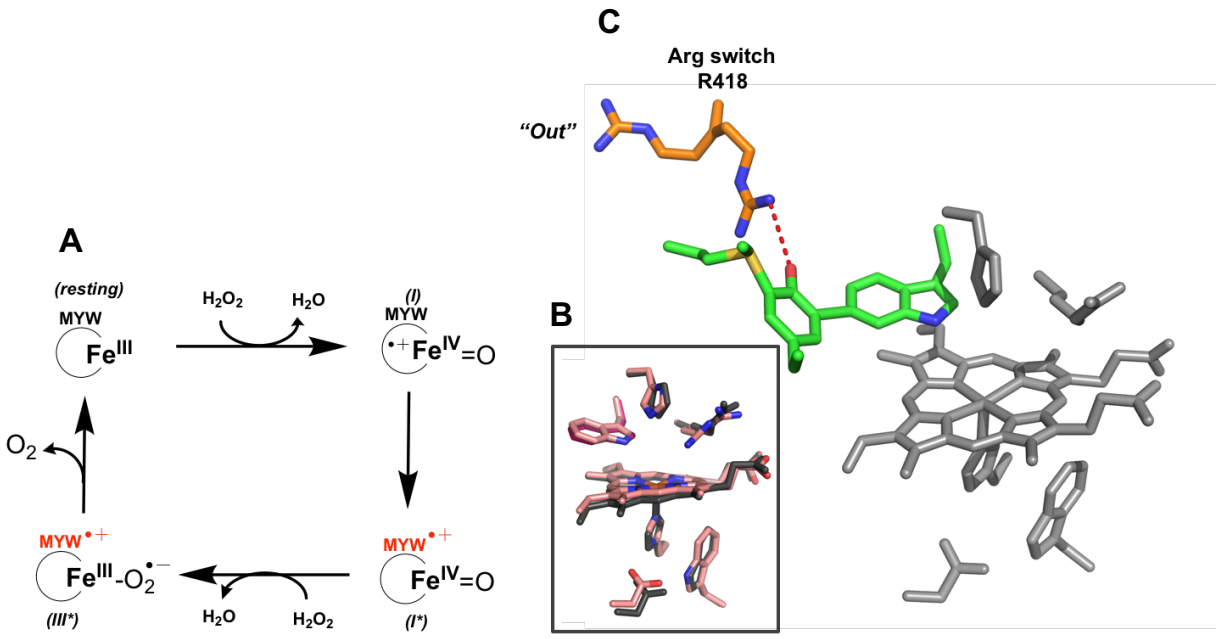

Figure 1.6. (A) Proposed catalase mechanism of KatG. (B) Overlay of the active sites of *Mt*KatG and CcP. (C) Other important residues in the active site of *Mt*KatG are highlighted in color. PDB accession numbers for *Mt*KatG and CcP are 2CCA and 1CCP respectively.

regime of H_2O_2 consumption, indicate that this radical is likely catalatically competent. With the complete loss of catalase activity, variants in which the formation of the MYW adduct is disrupted (i.e., M255I, Y229F, W107F) can not form this radical species.[118] Simulation of HF EPR data reveal that g-value anisotropy of this species slightly deviates from that of an unmodified tyrosyl radical, suggesting the possibility of an electronically modified tyrosyl radical. Moreover, the hyperfine parameters obtained by simulations of X- and D-band EPR spectra also suggest the absence of ring hydrogens in this tentative tyrosyl radical site. This is consistent with the modified structure of MYW covalent adduct (where 3' and 5' ring hydrogens are absence due to bonds to the ^{MYW}M, ^{MYW}W), provided ^{MYW}Y holds the radical.[118] A comprehensive study that used isotopic labeling, EPR and site-directed mutagenesis has assigned the narrow doublet radical species to be the $[MYW]^{\bullet+}$ intermediate, based on the following results.[119] First, a change from the doublet to the singlet with reduced line width was observed when reactions of *wt*KatG labeled with β-methylene-deuterated tyrosine with H_2O_2 were compared to that of unlabeled *wt*KatG. This indicates that the radical is tyrosine-based. Second, in contrast, 3', 5'-dideuterotyrosine-labeling of KatG did not change the parameter of the narrow doublet in comparison to that of unlabeled *wt*KatG, thereby suggesting the tyrosyl site lacked the 3' and 5' hydrogen. Third, replacement of each MtKatG Tyr with Phe produced variants with catalase activity close to that of *wt*KatG, and the ability to yield the narrow doublet, except in the case of ^{MYW}Y229F KatG.

1.8.4.2 Role of the arginine switch (^{Sw}Arg) in the catalatic mechanism

It has already been mentioned that ^{Sw}Arg is a positive effector for high catalase activity by KatG. Indeed, its presence boosts catalase activity more than an order of magnitude with respect to k_{cat} at catalase pH optimum. However, the mechanism by which the Arg switch

facilitates catalase turnover is still not clear. In general, its "*out*" conformation is associated with MYW oxidation, whereas the "*in*" conformation is associated with MYW radical reduction. Observations have revealed that the Arginine switch variants lead to dramatically decreased catalase activity but not peroxidase activity, indicating that the Arginine switch is only involved after compound I formation.[115] Moreover, it has been reported that in the absence of the Arg switch (i.e., R418L), a compound III-like intermediate dominates in the UV-vis spectrum and the adduct radical is formed at essentially the same rate and to the same extent as observed for the *wt*KatG.[115] All these effects suggest that ^{Sw}Arg assists the step(s) after compound III* (Fe^{III}-$O_2^{\bullet-}$ [MYW]$^{\bullet+}$) intermediate formation. Specifically, ^{Sw}Arg is proposed to facilitate the optimum electron transfer between the superoxide/dioxygen intermediate and the adduct radical, to restore the ferric heme, triplet O_2 and the closed-shell MYW adduct.[113,115] Indeed, a recent computational study suggests that R418 ensures electron transfer from Fe^{III}-$O_2^{\bullet-}$ heme to the MYW radical by facilitating the rotation of the Y and W aromatic rings with respect to one another.[123]

1.8.5 Peroxidatic mechanism of KatG

Consistent with its peroxidase-typical scaffold, KatG also possesses peroxidase activity (i.e., the ability to oxidize exogenous peroxidatic electron donors [PxEDs] at the expense of H_2O_2 reduction). Since its physiological peroxidatic electron donor is unknown, artificial electron donors are routinely used for testing KatG peroxidase activity in the laboratory. The mechanism of peroxidase activity for KatG is not defined. Howver, it is generally agreed and proposed that this mechanism starts from oxidation of the ferric enzyme to compound I (i.e., Fe^{IV}=O [porphyrin]$^{\bullet+}$) by H_2O_2, the same intermediate involved in the catalatic mechanism of KatG as well as the peroxidase mechanism of most peroxidases. Thereafter, PxED oxidation (peroxidase

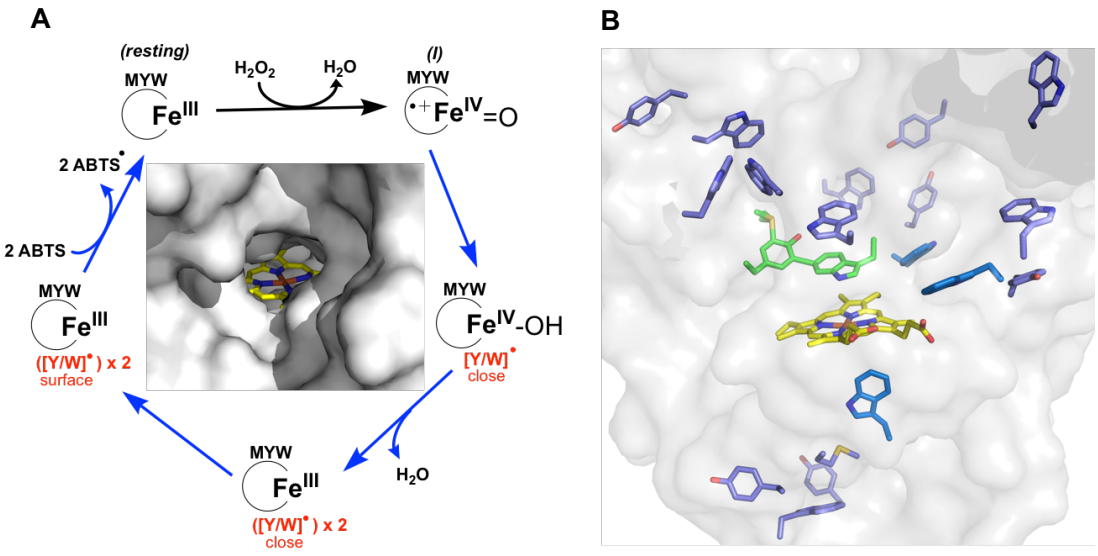

Figure. 1.7. Proposed peroxidase mechanism of KatG and surface presentation to the active site (A). Oxidizable amino acids in KatG matrix (B).

activity) is accomplished by a hole-hopping mechanism where radicals hop via a series of redox-active amino acid residues leading to the remote protein surface (Fig. 1.7A). This mechanism is plausible since most well-known PxEDs are too large to get access to the deeply buried heme directly.

1.8.5.1 KatG protein matrix loaded with redox-active amino acids

Consistent with the proposed hole-hopping mechanism of KatG peroxidase activity, is its remarkably high number of oxidation-prone amino acids (i.e., 18 Trp, 4.2%; 16 Tyr, 3.7%; 14 Met, 3.2%; 2 Cys, 0.5%; and 50 total, 11.6%) within the active site-containing N-terminal domain (Fig.1.7B). Substantial empirical data from KatG reacting with organic peroxide (i.e., PAA) suggest that intramolecular electron transfer and protein oxidation are common. Even though KatG from different sources can preferentially support distinct intramolecular electron transfer pathways, it is agreed that the sequence of radical hopping starts from the active site to the more remote protein surface, where Trp and/or Tyr can be the electron source for Fe^{IV}=O [porphyrin]$^{\bullet+}$.[125]

Ivancich *et al.* have intensively elucidated the protein-based radical intermediates produced in reactions of KatGs from various sources with PAA, using a combination of isotopic labeling, mutagenesis and multifrequency EPR.[126] They reported that whereas the distal site Trp which is 14.5 Å away from the heme iron is the sole Trp radical site in the case of *Sy*KatG, the proximal tryptophan (^{Px}Trp) is assigned to be the radial site in *Mt*KatG and *Bp*KatG. This ^{Px}Trp radical intermediate gives rise to the exchange-coupled feature in X-band EPR. Of note, CcP also forms the analogous ^{Px}Trp radical intermediate in its catalytic turnover with H_2O_2 and cytochrome c.

The roles of the intramolecular electron transfer processes are not defined. It is proposed that many electron donors in the peroxidase mechanism could be oxidized by transferring the oxidizing equivalent from the heme active site via these Trp/Tyr amino acids. However, no electron donor *in vivo* has been identified yet. It is also proposed that these amino acids may also serve an antioxidant role in KatG.[128]

1.8.5.2 Proximal Trp

Among all 18 Trp in *Mt*KatG, the conserved proximal Trp in KatG (W321 in MtKatG) is a peculiarity and deserves attention. Notably, the proposed catalase mechanism(s) of KatG does not directly involve this proximal Trp residue. Consistent with this, W321F produced by us and by Anabella and coworkers showed highly comparable catalase activity to *wt*KatG,[129,130] even though the earlier report by Magliozzo and co-workers stated that W321F retained catalase activity which was only 38% that of *wt*KatG.[131] As mentioned earlier, proximal Trp oxidation was detected when reacting *Mt*KatG or *Bp*KatG with PAA (the reagent that does not support the catalase mechanism). Likewise, as was previously reported by us, *Mt*KatG is prone to inactivation during catalase turnover at low pH due to off-pathway electron transfer events with W321 being the central participant in this event.[129] Indeed, we showed the coexistence of $MYW^{\bullet+}$ and $W321^{\bullet+}$ during KatG catalatic turnover. This is consistent with the previous computational study which showed that the distribution of spin in the two-electron oxidized state (i.e., Fe^{IV}=O[porphyrin]$^{\bullet+}$, Fe^{IV}=O[MYW]$^{\bullet+,}$ or Fe^{IV}=O[Trp]$^{\bullet+}$) is greatly influenced by the position of the Arginine switch.[132] However, if oxidation of W321 leads to KatG inactivation, why is it still conserved?

1.8.6 Interrelationship between KatG catalase and peroxidase mechanism

The interplay between catalase and peroxidase activities of KatG is not well understood. It seems more logical that these two activities should be mutually antagonistic to each other. Specifically, peroxidatic electron donors should inhibit the catalase activity of KatG. In accordance with this idea, conditions which favor KatG catalase activity (neutral pH, high [H_2O_2]) do not favor its peroxidase activity (low pH, low [H_2O_2]), and vice versa.[83,125] Moreover, catalase-negative variants almost invariably exhibit enhanced peroxidase activity.[78,79,120] More so, it has been reported that a common peroxidatic electron donor, *o*-dianisidine inhibited the catalase activity of KatG at pH 7.5.[133]

Contrary to all the above observations, the Goodwin group first reported that PxEDs stimulate the catalase activity of KatG.[134] They found this stimulatory effect to be most pronounced at acidic pH (i.e., pH 5.0), where catalase activity is normally diminished and peroxidase activity increases.[134] These results are fascinating, since it points toward a mechanism in which far more efficient scavenging of H_2O_2 can be achieved, especially at low pH, which mirrors the physiological conditions that pathogens are facing (i.e., phagolysosomes of neutrophils and macrophages). The Goodwin group has also reported that *Mt*KatG is prone to inactivation during catalase turnover at low pH due to off-pathway electron transfer, primarily via W321 oxidation.[129] PxED is able to restore catalase activity by rescuing the catalase-inactive species from the solvent-exposed surface. Two questions need to be resolved. First, what is the structural element(s) that minimize off-catalase protein oxidation to ensure that KatG continues to be an effective catalase? Second, what is the role of off-catalase protein oxidation, considering no physiological peroxidatic substrate has yet been determined? That is to say, if protein oxidation is the culprit of KatG inactivation, why does evolutionary biology appear to purposely

load KatG with such a high percentage of redox-active residues. In this work, attempts are made to seek these answers.

1.8.7 Biomedical ramifications

Many pathogens, such as *Magnaporthe grisea, Legionella pneumophia,* and *Yersinia pestis*, employ KatG catalase activity ($2\ H_2O_2 \rightarrow 2\ H_2O + O_2$) to manage copious amounts of H_2O_2 induced by a host immune response (e.g. oxidative stress). Specifically, the organism *Mycobacterium tuberculosis* is able to survive within the harsh acidic and highly oxidizing phagolysosomes of neutrophils and macrophages with KatG as one of only two catalase-active enzymes present. This particular study intends to elucidate the catalytic mechanism of KatG, specifically the mechanism by which KatG promotes its self-preservation through modulating off-pathway electron transfer. This knowledge may allow for methods to intervene in the host-pathogen interaction by developing a treatment which enhances a host's ability to combat pathogenic infections. In addition, it will shed light on how an oxidoreductase copes with the oxidative stress generated by its own potentially destructive catalysis.

Chapter Two: Strategy and Methodology

2.1 Overview of this project

We previously reported that *wt*KatG is prone to inactivation at low pH due to off-pathway electron transfer and the proximal Trp (W321) appears to be the primary oxidation site that initiates this inactivation process.[129] Because (1) the pH condition where this inactivation is observed seems to correlate with the condition where the arginine switch (^{Sw}Arg) (Arg-418 in *Mt*KatG) is predominantly pointing away from the active site and towards the protein surface (i.e., "*out"* conformation); and (2) previous calculations have showed that compound I (i.e. two-electron oxidized KatG) has substantial spin density on W321, when the ^{Sw}Arg is oriented away from the MYW cofactor (i.e., "*out"* conformation) and tyrosine in the MYW is protonated,[135] we surmised that the presence and/or the conformation of ^{Sw}Arg may play a prominent role in favoring catalase activity *vs.* inactivation by minimizing off-catalase radical transfer. To investigate the connection between the arginine switch, off-pathway radical transfer, and KatG inactivation, as well as to shed light on the role of Trp 321 oxidation in enzyme inactivation, we evaluated four KatG variants: 1) The fully functional wild-type KatG, 2) enzyme missing a functional arginine switch (R418N KatG), 3) enzyme lacking an oxidizable proximal Trp (W321F KatG), and enzyme lacking both features (W321F/R418N KatG). Each variant was investigated for its reactions with H_2O_2 to determine not only standard steady-state kinetic parameters, but also to evaluate the kinetics of enzyme inactivation. Likewise, enzyme intermediates involved in active catalatic turnover as well as those observed during inactivation were monitored by optical stopped-flow and rapid freeze-quench (RFQ) EPR. Across all of these studies, the impact of pH and the presence or absence of peroxidatic electron donor (PxED),

were also evaluated. Specifically, pH values of 5 and pH 7 were chosen as representatives. pH 5 is where inactivation occurs and where optimum PxED-stimulated KatG catalase activity, in terms of k_{cat}, is observed.[129,134] pH 7 is where optimum unassisted catalase activity with respect to k_{cat} and k_{cat}/K_M are seen.

2.2 Overview of major techniques

All KatGs are heme-dependent enzymes that use radical-based catalytic mechanisms. These allow investigating the enzymatic mechanism by a vast range of spectroscopic techniques. The tools routinely used for monitoring heme oxidation and coordination states include UV-visible absorption, circular dichroism, magnetic circular dichroism, resonance raman, electron paramagnetic resonance (EPR), and Mossbauer spectroscopies. Of course, EPR is the most reliable technique for the paramagnetic species. Consequently, EPR is widely used for detection and characterization of the organic radicals, including protein-based species. In this work, extensive use of UV-visible absorption and EPR spectroscopies were applied in conjunction with rapid mixing kinetic techniques (i.e., stopped-flow and rapid freeze quench [RFQ]) to evaluate the heme intermediates and protein-based radicals during KatG's reactions with H_2O_2.

2.2.1 Evaluation of heme states by UV-vis absorption spectroscopy

Generally speaking, heme and heme-dependent proteins have two types of transitions (π-π^* and charge transfer) that are readily detected by UV-visible absorption spectroscopy. The π-π^* transitions are originated from excitation of electrons within the conjugated π system of the porphyrin. These transitions give rise to at least three prominent absorption bands in a typical heme absorption spectrum. In order of increasing energy and intensity, these are α (Q_{00}), β (Q_{0v}), and γ (Soret). The Soret band (γ) is the most intense band, which occurs at the lowest wavelength of these three transitions. The β band is observed at shorter wavelength (520- 540 nm) than the α

band (550- 580 nm). Charge-transfer (CT) bands occur when an electron from the porphyrin π system is transferred from highest energy-filled orbital to lowest energy unfilled orbitals of the iron. Two charge transfer bands are hallmarks of high-spin ferric heme. They are not observed in low-spin ferric complexes, and they are too weak in the ferrous heme states to be reliably observed. Specifically, in low spin complexes, the charge transfer is blocked because an electron is dropped from the porphyrin π∗ orbital into a d-orbital of the iron to completely fill it. The characteristic absorption bands of KatG in its resting state occur at 408 nm (Soret), 502 nm (CT2), and 640 nm (CT1). In the high-spin complex of KatG, the α, β bands are detectable but obscured by the charge transfer bands.

The identity of ligands and oxidation states of iron have a dramatic impact on the properties of both π-π∗ and CT transitions, thus giving distinct absorption features. Therefore, UV-visible spectroscopy can discern different iron states, such as ferrous (Fe^{II}), ferric (Fe^{III}), ferryl (Fe^{IV}=O), and ferric-superoxide (Fe^{III}-$O_2^{\bullet -}$) and/or coordination states.

In free hemin (i.e., Fe^{III}), the Soret band occurs at 380 nm. When incorporated in a protein, the absorption will usually red shift to a wavelength above 400 nm. As isolated, the dominant form of heme in KatG is high-spin ferric, including populations of hexacoordinate and pentacoordinate states. In the hexacoordinate high-spin state of KatG, a water molecule is likely the sixth ligand. When a strong-field ligand (i.e., CN^-, N_3^-) is introduced into the KatG heme ligand sphere, a substantial red shift in the Soret band to 418 nm is observed along with prominent α, β transitions at 570 nm and 535 nm, and the CT bands are no longer detected.[95] Occasionally, the distal His can act as a strong-field sixth ligand, producing a low-spin ferric state in some KatG variants, such as $KatG^{Nterm}$.[95,136]

When KatG reacts with peroxides, different species can be observed. Compound I (i.e., Fe^{IV}=O[porphyrin]$^{\bullet+}$) exhibits little or no shift of the Soret band with about 40% hypochromicity compared to the native enzyme, together with a broad increase in absorbance above 520 nm.[91,121] This signature is typical for compound I of both KatGs and that of most peroxidases. Compound II (i.e., Fe^{IV}=O) of KatGs has its Soret band red shift to 416 nm and the prominent α, β transitions at 560 nm and 530 nm, respectively.[121,137] Among different peroxidases, λ_{max} of Soret, α, and β bands are highly similar. For example, compound II of horseradish peroxidase (HRP) exhibits red shift Soret band at 420 nm, and the double peak in the visible spectrum at 527 and 554 nm.[91] A ferric superoxide (i.e. Fe^{III}-$O_2^{\bullet-}$) has its Soret band red shift to 418 nm and the α, β transitions at 580 nm and 540 nm, respectively.[121] These ferric superoxide absorption features have been captured when KatG reacts with steady-state concentrations of H_2O_2 at the earliest turnovers.[118,121,138] Before this discovery, the characteristic absorption features were invariably assigned as the inactive species in most peroxidases reacting with H_2O_2 in the absence of electron donors.[91]

One caveat is that UV-visible absorption is a general tool used to gauge heme oxidation state and coordination environment, however, it can be ambiguous. Thus, definitive assignment of states and relative abundance require other techniques, with one being EPR. Additionally, the overwhelming absorption bands of the heme in the electronic absorption spectra make it impossible to discern the formation of protein-based radicals. Thus, EPR was used to detect and characterize the free radical intermediates, and also to track the disappearance and re-appearance of ferric state in KatG catalase reactions.

2.2.2 EPR basics and application in KatG

EPR is the resonance spectroscopy of molecular systems with unpaired electrons (paramagnetic species). Many biomolecules that involve transition metal and/or protein-based radical species in their enzymatic turnover are highly suitable for EPR investigation. In this work, EPR was used to evaluate the disappearance and appearance of the ferric form of KatG (paramagnetic species) and its protein-based radicals (paramagnetic species) that evolved in the reactions of KatG with H_2O_2. During KatG reactions, other iron states (i.e., Fe^{IV}=O, Fe^{III}-$O_2^{\bullet-}$) can be formed, however, these species are silent to the standard perpendicular mode EPR used in this work. The parallel mode EPR which can detect these species is out of the scope of this dissertation.

EPR requires four major components: a source of radiation, a sample, an external magnetic field and a detector. In contrast to most other magnetic spectroscopies (i.e., NMR, magnetic circular dichroism, Mossbauer) in which the radiation frequency is changed with the static magnetic field, the approach used in EPR is to vary the magnetic field while the frequency is kept constant. The sample (i.e., a molecule with a single unpaired electron) can exist in two different states with identical energies in the absence of a magnetic field, but these two energy states are different in the presence of a magnetic field. The strength of the field is used to tune the energy differences of the two molecular states. The resonance condition for a two-level system in EPR (a net absorption) occurs when the energy of the radiation produced by the source is equal to the energy difference between the two molecular states produced by the external magnet (Equation 1).

$$h\nu = g\beta B \qquad \text{(Eq. 1)}$$

The interaction between the compound and the magnetic field is called the *electronic Zeeman interaction*. In this equation, h is Planck's constant (6.62607×10^{-34} J × s), β is Bohr magneton (9.27401×10^{-24} J× T^{-1}), v is frequency of radiation, B is the external magnetic field, and g is a proportionality constant, whose value can be obtained from the experiments. The value of g gives information on the electronic structure of a paramagnetic species. Generally speaking, the most important information gained from EPR is the g value. First derivative spectra are recorded so that instead of an absorption peak, a curve with positive and negative components is obtained.

2.2.2.1 Evaluation of heme states by EPR

As stated above, ferric heme is detectable by standard perpendicular mode of EPR, the one used for this work. EPR spectra of resting KatGs show signals mainly from the high-spin (HS) ferric heme [139,140,141,142,143] with minimal of low-spin (LS) ferric form if any.[139,144,145] KatGs have shown a number of HS states. They are easily distinguished by their g-tensor anisotropy, located in the $g \sim 6$ and $g \sim 2$ region of the spectrum in EPR. A wide rhombic signal ($g_x \sim 6.6$, $g_y \sim 5.1$, $g_z \sim 1.95$), a narrow rhombic signal ($g_x \sim 6.0$, $g_y \sim 5.6$, $g_z \sim 1.99$), as well as an intermediate rhombic ($g_x \sim 6.3$, $g_y \sim 5.3$, $g_z \sim 1.97$) have been documented. An axial signal ($g_{//} \sim 5.9$, $g_{\perp} \sim 2$) has also been observed.[127,139,142, 143] The distribution of these different HS states presumably arise from different bonding strengths of the sixth coordinated H_2O molecule, from strongly bounded (axial form) to unbounded (rhombic form with maximal distortion).[125,142] It is agreed that the relative population of these HS states heavily depend on pH, buffer components, enzyme age and mutations around the active site and the substrates.[139,142] Thus, in this work, not only were the structural changes of heme active-site between the variants and *wt*KatG monitored, but the disappearance and appearance of the resting enzyme in kinetics were also monitored.

2.2.2.2 Evaluation of protein-based radicals and porphyrin radicals by EPR

Upon reaction of catalases, peroxidases, and KatGs with peroxides, an intermediate named compound I is formed. This compound is two oxidizing equivalents above the ferric enzyme. This intermediate invariably contains an oxoferryl moiety (Fe^{IV}=O) and another oxidizing equivalent can either be on porphyrin (i.e., [porphyrin]$^{\bullet+}$) or on redox-active amino acid (Tyr, Trp in most cases). EPR is well suited to elucidate the electronic nature of these redox intermediates.

The EPR spectra that originate from the canonical compound I (i.e., Fe^{IV}=O [porphyrin]$^{\bullet+}$) have been well characterized in some catalases, peroxidases and KatGs.[146,147] This intermediate exhibits a very broad (about 2000 G) EPR spectrum with effective g value $g_{\perp}$ = 2.35 and $g_{//}$ = 2.0, due to exchange-coupling to the iron.

X-band EPR (9 GHz) EPR is the most commonly used technique to probe the electronic nature of protein-based radicals by assigning the *g* values.[148,149] However, this conventional X-band is not able to resolve *g*-tensor anisotropy. Because tyrosyl and tryptophanyl radials exhibit similar *g* values, it is not possible to differentiate different protein-based radicals by using X-band EPR alone. Multifrequency EPR is required to resolve the *g* anisotropy of protein- based radicals. And based on their line shapes and resolution of g-anisotropies at the x,y, and z-directions, radical intermediates are more likely to be assigned.

In most cases, a combination of isotopic labeling, mutagenesis and multifrequency EPR and/or ENDOR is necessary for definitive assignment of the radical sites. For example, the proximal Trp has been identified as the radical site in CcP reacting with H_2O_2.[77,149] And the tyrosyl radical generated upon reaction of KatG with H_2O_2 at the ms time regime, has been assigned to the MYW$^{\bullet+}$.[118,119] Likewise, Ivancich and coworkers have assigned the protein-based

radical intermediates produced in reactions of KatGs from various sources with PAA using a powerful combination of isotopic labeling, mutagenesis and multifrequency EPR.[126,128,130,140,150,151]

These substantial empirical data from multifrequency EPR investigation of KatGs mentioned above can be used to compared our X-band EPR data with those results and support our assignments. Notably, X-band EPR can discern $MYW^{\bullet+}$ *vs.* $porphyrin^{\bullet+}$ *vs.* $W321^{\bullet+}$ *vs.* $W/Y^{\bullet}$ due to their distinct line shapes and saturation behaviors.

2.3 Experimental procedures

2.3.1 Reagents

Chlorpromazine (CPZ), N,N,N',N'-tetramethyl-*p*-phenylenediamine dihydrochloride (TMPD), 2,2'-azino-bis (3-ethylbenzthiazoline-6-sulfonic acid) (ABTS), L-ascorbic acid, hemin, ampicillin, hydrogen peroxide (30%), imidazole, calcium chloride hydrate and sodium dithionite were purchased from Sigma. Tetracycline hydrochloride, mono and dibasic sodium phosphate, sodium chloride, sodium acetate trihydrate, potassium chloride, magnesium chloride and magnesium sulfate were purchased from Fisher (Pittsburg, PA). P*fu* polymerase, Herculase polymerase, T4 DNA ligase, and all *E. coli* (XL-1 Blue) were gotten from Agilent (La Jolla, CA). Phusion High Fidelity PCR Master Mix with GC Buffer and all restriction enzymes were purchased from New England Biolabs (Beverly, MA). All oligonucleotide primers for site-directed mutagenesis as well as sequencing were purchased from Invitrogen (Carlsbad, CA). Benzonase nuclease, Bugbuster, nickel-nitrilotriacetic acid resin were bought from Novagen (Madison, WI). Isopropyl-β-D-thiogalactopyranoside was purchased from Gold Biotechnology (St. Louis, MO). Buffer exchange chromatography columns (10DG) and Macro-Prep High Q resin were acquired from BioRad (Hercules, CA). Centrifugal filters (50 kD cutoff) were

obtained from Millipore (Billerica, MA). All buffers and media were prepared using water purified through a Barnstead EASY pure II UV ultrapure water system (18.2 MΩ/cm resistivity).

2.3.2 Mutagenesis

The W321F KatG variant was previously generated and the sequence of its expression construct was confirmed by DNA sequence analysis.[129] Site-directed mutagenesis to generate the R418N and W321F/R418N variants were carried out by applying the "Round-the-horn" approach.[152] The template for mutagenesis was pMRLB11, a pET23b-derived plasmid bearing the *M. tuberculosis* katG gene and was obtained from the TB vaccine Testing and Research Materials Contract at Colorado State University. The forward primer designed for the R418N substitution was 5'-CAC**AAC***GAT*ATGGGTCCCGTTGCGA-3'. This primer included a site for codon replacement (bold) as well as mutations designed to introduce diagnostic restriction digest sites by PshAI for screening. The reverse primer was (5'-GATCAGCTTGTACCAGGCCTTGGCGAA-3'). Both primers were modified to include 5'-phophoryl groups, allowing for the blunt-end ligation of PCR products. To generate the W321F/R418N double variant, the same primers were used but the template was the plasmid for expression of W321F KatG. All PCR reactions were carried out using Phusion High-Fidelity polymerase in GC buffer-containing Master-Mix and 3% DMSO. All PCR products were initially treated with DpnI to degrade the starting template and then ligated using T4 DNA ligase. Ligation products were used to transform *E. coli* (XL-1 Blue) by a standard hear shock protocol. Transformants were selected using ampicillin-containing media, and candidate plasmids were screened by PshAI digestion as successful mutation would eliminate one PshAI restriction site. Successful candidates were sent for full DNA sequence analysis (Laragen Sequencing, CA) to

verify the intended mutation was present and that no unintended mutations had occurred during PCR amplification. Full sequence for R418N and W321F/R418N KatG variants was confirmed.

2.3.3 Protein expression and purification

E. coli C41 (DE3) bearing the heme protein expression plasmid, pHPEX3,[153] were transformed with the appropriate expression constructs. Transformants were selected on the basis of tetracycline and ampicillin resistance. Expression of wild-type *Mt*KatG and all variants were carried out as described previously.[134] Similar to wild-type *Mt*KatG, R418N and W321F/R418N KatG variants were expressed in a soluble form. Thus, purification was carried out as reported previously,[134] with the exception that lysis was carried out by sonication. A Branson 250 Sonifier (Danbury, CT) fit with a standard tip was set to constant output and 3.5 duty. Sonication was carried out in eight cycles (42 s on, 42 s off). Benzonase nuclease (250 units) was added to the lysate following sonication. The supernatant was loaded onto a Ni-NTA column by recirculating the solution through the column bed overnight (1 mL/min) as reported previously.[129] The column was washed with 50 mM Tris, pH 8, followed by a second wash with buffer A (50 mM phosphate, pH 7.0; 200 mM NaCl). Subsequent washes were carried out using buffer A supplemented with 2, 20, and 50 mM imidazole. The protein was then eluted off the column with buffer A supplemented with 100 mM imidazole. The final eluent was concentrated by ultrafiltration using a 30 kDa molecular cutoff filter. Following concentration, excess imidazole was removed using a 10 DG size exclusion column. Then protein was then separated by anion exchange using a Macro-Prep High Q resin as reported previously.[129]

2.3.4 UV-visible absorption spectra

Following purification, UV-visible spectra for *wt*KatG and KatG variants were evaluated in 100 mM phosphate, pH 7.0, as described previously.[134] Holoenzyme concentration was

determined by the pyridine hemichrome assay of Falk.[154] The absorption features, Soret band, charge transfer (CT) transitions, and optical purity ratio A_{408}/A_{280} (i.e., R_z values) for *wt*KatG and variants are provided in Table 3.1.1.

2.3.5 Peroxidase activity assays

Peroxidase activity was evaluated by monitoring 2,2'-azino-bis 3-ethylbenzthiazoline-6-sulfonic acid (ABTS) (the PxED) oxidation to $ABTS^{\bullet+}$ (ε_{417} =34.7 $mM^{-1}cm^{-1}$) spectrophotometrically.[134,155] To evaluate the effect of H_2O_2 concentration on peroxidase activity, ABTS concentration was typically held constant at 0.1 mM. To determine the effect of ABTS concentration on peroxidase activity, H_2O_2 concentration was held constant at 1.0 mM. All assays contained 20 nM KatG, and were carried out in 50 mM acetate, pH 5.0 at room temperature. When evaluated, TMPD oxidation to $TMPD^{\bullet+}$ at 610 nM (ε = 11.6 $mM^{-1}cm^{-1}$)[156] or CPZ oxidation to $CPZ^{\bullet+}$ at 525 nm (ε = 121,000 $M^{-1}cm^{-1}$) spectrophotometrically.[157]

2.3.6 Catalase activity assays

Two methods were used to evaluate catalase activity. The first monitored decreases in H_2O_2 concentration at 240 nm ($\varepsilon_{240=}$ 39.4 $M^{-1}cm^{-1}$) over time.[158] Typical assays contained 20 nM KatG and were carried out at room temperature in 100 mM phosphate, pH 7.0. Alternatively, O_2 production was monitored using a Clark-type O_2-sensitive electrode.[134] Calibration was achieved using N_2 and sodium dithionite to establish a zero O_2 level within the reaction chamber prior to experimental measurements. All reactions were carried out at room temperature (23 ºC). Data collection was started with buffer, KatG, and PxED (when present) in the reaction chamber for 20 seconds to establish a baseline, at which point H_2O_2 was injected to initiate O_2 production. The initial rate was measured after 10 seconds of reaction initiation, to avoid the artifact of the O_2-sensitive electrode. In most cases, these two methods worked interchangeably. Only in two

scenarios, O_2 sensitive electrode was preferred. First, when PxED was included in the catalatic assays, catalase activity was measured for O_2 production, because PxED oxidation products likely obscure the electronic absorption spectra. Second, in some variants (i.e., R418 mutation-bearing variants) where catalase activity was highly compromised, O_2 production measurement is preferentially used, because absorption coefficient of H_2O_2 at 240 nm is low, making it difficult to evaluate the activity.

Analysis of steady-state kinetic data were carried out as described previously to obtain kinetic parameters k_{cat} and k_{cat}/K_M (k_{on}).[134] In all situations where these terms are applied, k_{cat} is the maximum rate divided by the concentration of holo-enzyme as estimated by heme concentration. The apparent K_M is not intended to mean anything more than the concentration of substrate necessary to produce ½ of the maximum rate. And k_{cat}/K_M represents the catalytic efficiency.

If a standard rectangular hyperbolic increase in rate as a function of increasing substrate concentration was detected, the data were fit using a standard Michaelis-Menten, Equation 2 to obtain the apparent kinetic parameters k_{cat} and k_{cat}/K_M (indicated as k_{on} in Equation 2)

$$v_o/[E]_T = \frac{k_{cat}[H_2O_2]}{k_{cat}/k_{on} + [H_2O_2]} \quad \text{(Eq. 2)}$$

As before, *wt*KatG catalase activity showed a two-component response to H_2O_2 at pH 5, necessitating the use of Equation 3,

$$v_o/[E]_T = \frac{k_{cat}[H_2O_2]}{k_{cat}/k_{on} + [H_2O_2]} + k_{app}[H_2O_2] \quad \text{(Eq. 3)}$$

which permits determination of the apparent second-order rate constant (k_{app}) for a "high K_M" response to H_2O_2. In addition, data were fit to directly estimate k_{cat}/K_M (indicated as k_{on} in equation 3) and k_{cat}.

2.3.7 Inactivation assays

Two methods were used for inactivation assays. In first method, extent of O_2 production by reacting KatG (5 nM) with a single concentration of H_2O_2 was monitored. At the end of catalase activity (as judged by O_2 production cessation), either fresh enzyme or H_2O_2 was added. If 2nd addition of enzyme rather than H_2O_2 yielded more O_2 production, the reaction ceased due to enzyme inactivation. Alternatively, if 2nd addition of H_2O_2 instead of enzyme produced another O_2 evolution, the reaction ceased due to substrate depletion. These experiments have a couple of applications in this work. On one hand, in cases where inactivation is observed, catalase cycle numbers that enzyme sustains prior to irreversible inactivation are calculated, from O_2 concentration divided by enzyme concentration. Further, O_2 extent traces are fitted to a single exponential equation, to obtain k_{obs} of inactivation. On the other hand, in cases where enzyme is active enough to deplete substrate, % remaining catalase activity is obtained by the initial rate of O_2 production following the 2nd addition of H_2O_2 relative to the initial rate observed following the 1st addition of H_2O_2. Notably, extent of O_2 production provides insight of enzyme sustainability (i.e., catalase cycle number) whereas the initial rate fails to do so. When PxED (i.e., ABTS, TMPD, CPZ) was included, the concentration is 0.1 mM.

In second method, preincubation of KatGs with varying H_2O_2 concentration in the corresponding buffer (pH 5.0 or 7.0) was performed for 1 hour, then a fraction was withdrawn and the catalase activity was measured afterwards. % remaining catalase activity is calculated by catalase activity of the withdrawn sample relative to the catalase activity of the control. The control underwent the same procedure except no H_2O_2 but H_2O was added. Catalase activity measurements were performed in 100 mM phosphate pH 7, with 10 mM H_2O_2 by O_2-sensitive electrode. When PxED (i.e., ABTS) was included, the concentration is 0.1 mM. This type of

experiments also allowed for evaluating % remaining peroxidase activity and UV-visible spectra. Peroxidase activity was performed in 50 mM acetate pH 5, with 1 mM H_2O_2, 0.1 mM ABTS. % remaining peroxidase activity is calculated by peroxidase activity of the withdrawn sample relative to the peroxidase activity of the control. Before UV-visible spectra were investigated, a fraction was withdrawn and centrifuged with rpm 4000 for 40 s to precipitate the aggregated enzyme by oxidative damage to avoid light scattering effects.

2.3.8 Stopped-flow

Optical stopped-flow method was used to observe the dominant heme intermediates of *wt*KatG and variants under multiple turnover conditions. We used a PC-upgraded SX18.MV rapid reaction analyzer from Applied Photophysics (leatherhead, UK) for all measurements. All reactions were carried out in the single-mixing mode using diode array detection. The intense absorption spectra of electron donor radical oxidation products (e.g., $ABTS^{\bullet+}$) often obscured a clear view of spectral characteristics due to heme. To circumvent this challenge, we included ascorbate to rapidly reduce these accumulating radical products.[134,159,160] Single-mixing experiments were set up such that 6 μM KatG was placed in syringe A in 5 mM phosphate buffer, pH 7.0. Syringe B contained varying concentrations of H_2O_2 in 100 mM acetate buffer, pH 5.0 or in 200 mM phosphate buffer, pH 7.0. When ascorbate and ABTS included, the concentration was 1 mM and 0.2 mM respectively.

2.3.9 Quantification of PxED oxidation products generated during catalase catalysis

Two methods to quantify PxED oxidation products were used, either benchtop spectrometric assays or stopped-flow. The advantages of using stopped-flow to quantify the generation of $ABTS^{\bullet+}$ are as follows. It allows fast reaction and easy validation of ABTS oxidation as a result of enzymatic catalysis, since much higher concentration of KatG is included

compared to benchtop spectrometric assays. Furthermore, it allows us to evaluate $ABTS^{\bullet+}$ yields upon reaction of R418N with as little as 1 equivalent (1 eq.) of H_2O_2. We observed the same phenomenon using both methods with ABTS as PxED.

In benchtop spectrometric assays, we set up reactions containing 0.1 mM ABTS, 20 nM enzyme, initiated the reaction by adding H_2O_2 and allowed the reaction to go completion (30 min). Reaction completion was confirmed by addition of enzyme yield no $ABTS^{\bullet+}$. Samples were withdrawn and $ABTS^{\bullet+}$ was quantified at 417 nM (ε_{417} =34.7 $mM^{-1}cm^{-1}$). In these experiments, we either vary H_2O_2 concentration at the desired pH, or vary pH with a fixed H_2O_2 concentration. When H_2O_2 concentration was varied, reactions contained 0.1 mM ABTS, 20 nM enzyme in 50 mM acetate, pH 5 or 100 mM phosphate, pH 7. Alternatively, when pH was varied, reactions contained 0.1 mM ABTS, 20 nM enzyme, 0.8 mM H_2O_2. The reaction solution from pH 6- 7.5 were buffered with 100 mM phosphate, and the reaction solution from pH 5- 5.5 were buffered with 50 mM acetate. CPZSO was also quantified by benchtop spectrometric assays. Similarly, the reaction contained 20 nM KatG or variants, 0.08 nM H_2O_2, 0.1 mM CPZ in the corresponding buffer. CPZSO is measured at 340 nM (ε_{340} = 5900 $M^{-1}cm^{-1}$)[157]

Alternatively, we use stopped-flow to evaluate the quantity of PxED oxidation products during reaction. When evaluated, $ABTS^{\bullet+}$ was quantified at 645 nm (ε_{645} nm = 0.012 μM^{-1} cm^{-1}). TMPD radical was quantified at 610 nm (ε_{610} = 11.6 $mM^{-1}cm^{-1}$). CPZ radical was quantified at 525 nm (ε_{525} = 121000 $M^{-1}cm^{-1}$). Similarly, we vary H_2O_2 concentration at the desired pH values, or vary pH with a fixed H_2O_2 concentration. When H_2O_2 concentration (3 μM- 4 mM) was varied, reactions contained 0.1 mM ABTS, 3 μM enzyme in 50 mM acetate, pH 5 or 100 mM phosphate, pH 7. When pH was varied, reactions contained 0.1 mM ABTS, 3 μM enzyme, 0.05 mM H_2O_2.

The reaction solution from pH 6- 7.5 were buffered with 100 mM phosphate, and the reaction solution from pH 5- 5.5 were buffered with 50 mM acetate.

2.3.10 Freeze-quench preparation of EPR samples

R418N, and W321F/R418N *Mt*KatG were each concentrated to 300 μM using an Amicon Ultra-4 centrifuge filter (MW cutoff of 30 kD). One syringe contained 300 μM enzyme in 5 mM phosphate, pH 7.0. and the other syringe contained 667 molar equivalents of H_2O_2 in 100 mM acetate buffer, pH 5.0 or 200 mM phosphate buffer, pH 7.0. This applied to R418N at pH 5 and pH 7, as well as W321F/R418N at pH 7. Exception was the reactions of W321F/R418N at pH 5, although one syringe still contained 300 μM enzyme, the other syringe only contained 66.7 molar equivalents of H_2O_2 in pH 5. Reactions testing the impact of PxED included ABTS (2 mM) and ascorbate (10 mM) along with H_2O_2.

We access a range of reaction times by rapid-freeze quench (RFQ) (10- 50 ms), and manual-freeze quench (12 s- 5 min).

Samples of reaction time in ms range were mixed by rapid-freeze quench apparatus, and after a defined time the reaction mixture was quenched by spraying directly into liquid ethane, and then packed in quartz EPR tubes. Samples of reaction time longer than 12 s, the reactions were initiated by hand mixing, gently mixed by inversion and transferred to quartz EPR tubes, and quenched manually in liquid N_2 and ethanol mixture. All samples were stored in liquid N_2 until analyzed by EPR spectroscopy.

2.3.11 EPR measurements

All X-band (9 GHz) EPR spectra were collected using a Bruker spectrometer operating in perpendicular mode at 100 kHz modulation frequency in a 4119HS resonator. The spectrometer was equipped with an ESR910 liquid helium cryostat and an ITC503S temperature controller,

and spectra were recorded at 4.5 K and/ or 77 K as previously reported.[129] For spectra recorded at 4.5 K instrument parameters, unless otherwise indicated, were as follows: microwave frequency, 9.393 GHz; modulation amplitude, 1 G; modulation frequency, 100 kHz; microwave power, 1 mW; time constant, 163.84 ms; sweep time 335.54 s; number of scans, 1; conversion 327.68 ms; resolution, 1024 point; receiver gain, 1.0×10^4; and phase 0 degree.

For spectra recorded at 77 K, all parameters were the same except the modulation amplitude was 1 G, the receiver gain was 1.0×10^5, and the microwave power was 15.84 uW (41 dB).

Power saturation for select species was examined by fitting normalized signal intensities using

$$I \propto 1/(1 + P/P_{1/2})^{b/2} \quad \text{(Eq. 4)}$$

2.3.12 Circular Dichroism

Far-UV CD spectra (180-300 nm) were recorded for both variants along with *wt*KatG by using 2.5 μM of each enzyme in 5 mM phosphate buffer, pH 7.0. A Jasco J-180 spectropolarimeter was used to record all CD spectra by using 0.05 cm pathlength quartz cell, 0.05 nm data pitch, continuous scanning mode, scanning speed of 50 nm/min, and 8 accumulations. Baseline correction and data analysis were done using J-720 software from Jasco.

Chapter Three: Results

3.1 Activities and Spectral Properties of R418N and W321F/R418N KatG Variants

As previously mentioned, KatG carries out its catalase activity by a novel radical-based mechanism involving a protein-derived cofactor, the Met-Tyr-Trp (MYW) covalent adduct. We have previously reported that *wt*KatG is prone to inactivation, particularly at acidic pH. This appears to be due to off-pathway electron transfer, and the proximal tryptophan (W321) is a hotspot for off-catalase protein oxidation.[129] KatG has a strictly conserved arginine which adopts one of two conformations depending on pH. Accordingly, it is referred to as the arginine switch (^{Sw}Arg). The acidic conditions which favor KatG inactivation coincide with the conditions where the ^{Sw}Arg (Arg 418 in *Mt*KatG) is predominantly in a conformation that points away from the active site and towards the protein surface. This is referred to as as the "*out*" conformation. When the cationic guanidinium side chain of the ^{Sw}Arg interacts with the phenolate oxygen of the MYW cofactor tyrosine, it is occupying its "*in*" conformation. To investigate the potential connection between the ^{Sw}Arg and KatG inactivation, we produced R418A and R418N KatG variants to effectively remove the ^{Sw}Arg. Our results suggest that both the R418A and R418N variants have a much higher propensity for off-pathway electron transfer than wild-type, and protein oxidation events for both variants appear to start at the proximal tryptophan (^{Px}Trp) (Trp 321 by *Mt*KatG numbering). To determine the extent to which the ^{Px}Trp and ^{Sw}Arg coordinate together in managing off-catalase electron transfer events, we produced the double variant in which the ^{Sw}Arg was absent and the oxidizable ^{Px}Trp was replaced with non-oxidizable Phe. Our attempts to express soluble W321F/R418A were not successful, but we were able to obtain W321F/R418N KatG. Because R418N and R418A KatG were nearly identical in every respect,

the research described in this dissertation has focused on the R418N and W321F/R418N variants, drawing comparisons to wild-type and W321F KatG.

3.1.1 Optical and circular dichroism spectra for R418N and W321F/R418N

We successfully expressed and purified soluble R418N and W321F/R418N KatG variants. The UV-vis absorption spectra for both variants were consistent with those of *wt*KatG. They exhibited the typical bands of a heme *b*-containing peroxidase. Specifically, the Soret band showed an λ_{max} at 408 nm together with two charge-transfer bands bands at around 500 and 633 consistent with a His-coordinated heme dominated by a hexacoordinate high-spin heme with a relatively small contribution from a pentacoordinate high-spin state (Table 3.1.1, Fig. 3.1.1A).[102,161] Here the sixth ligand is an active-site H_2O. The optical purity ratio (i.e., A_{408}/A_{280}) was consistent with full heme occupancy given the amino acid composition of the KatG monomer (Table 3.1.1). The optical purity ratios of R418N and W321F/R418N KatG were slightly lower than that of *wt*KatG. This difference may because of the lower absorption coefficient number of the heme or the lower heme incorporation for the variants, compared to the *wt*KatG.

Circular dichroism (CD) spectra for KatG are consistent with an enzyme dominated by α helices (Fig. 3.1.1B). The spectra for R418N and W321F/R418N variants were indistinguishable from those observed for *wt*KatG, indicating that the substitutions did not result in disruption of the KatG structure at a secondary structural level.

3.1.2 Steady-state kinetic evaluation of R418N and W321F/R418N KatG

Under typical assay conditions (i.e., pH 7.0), R418N and W321F/R418N KatG showed significantly diminished catalase activities relative to the wild-type enzyme. For example, R418N KatG showed a 27-fold decrease in maximum catalatic output (i.e., k_{cat}), as well as a

Table 3.1.1 Spectral features of *MtKatG* and R418 variants[a]

	Absorption Feature			
Protein	Soret (γ) (nm)	CT[b]2 (nm)	CT 1 (nm)	RZ[c]
*Mt*KatG	408	500	633	0.63
R418N	408	500	633	0.56
W321F/R418N	408	500	633	0.53

[a]All spectra were recorded at 23 ℃ using 100 mM phosphate, pH 7.0.

[b]CT = charge transfer band. CT 1 is usually near 640 nm, and CT 2 is usually near 500 nm.

[c]RZ = optical purity ratio. Ratio of absorbance at the Soret λ_{max} versus absorbance at 280 nm.

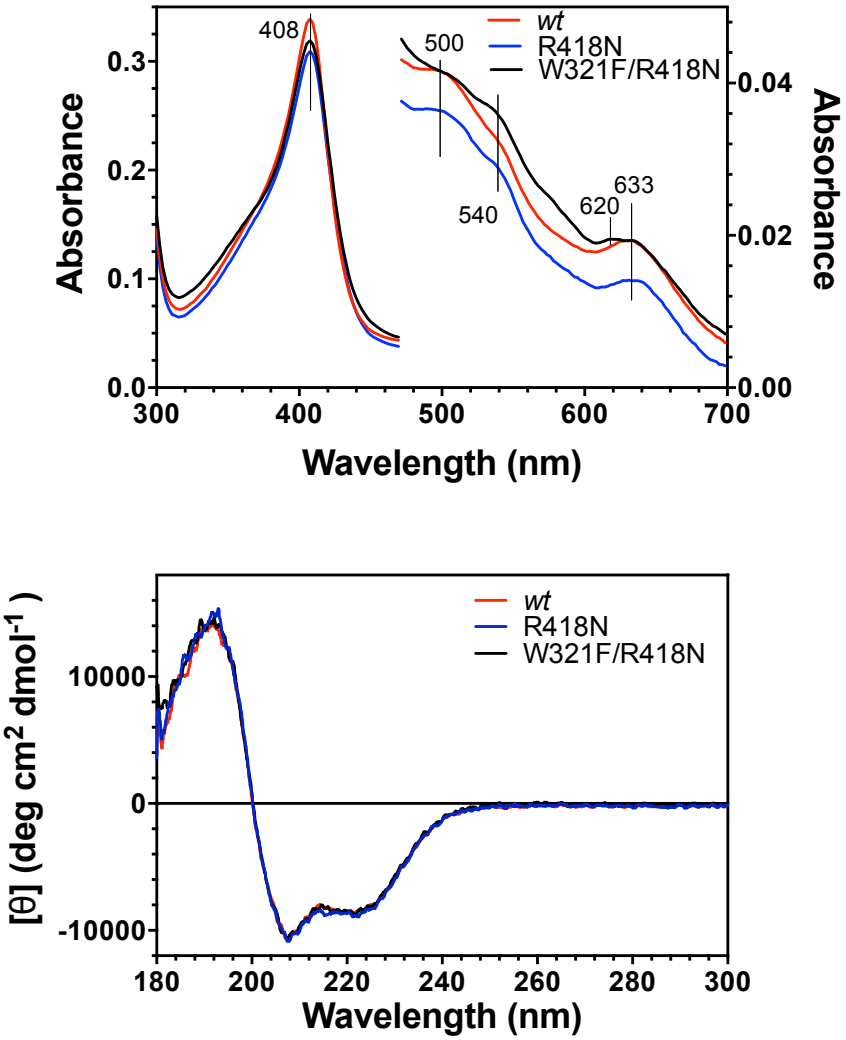

Figure 3.1.1. Optical (A) and CD (B) spectra for *wt*KatG and its variants. All optical spectra (A) were recorded at 4 °C using 100 mM phosphate, pH 7.0. Enzyme concentration was 3 μM. Far-UV CD spectra (B) were all recorded at 23 °C with 2.5 μM enzyme in 5 mM phosphate, pH 7.0.

37-fold decrease in catalase efficiency (i.e., k_{cat}/K_M with respect to H_2O_2) (Table 3.1.2). The data for R418N KatG are highly similar to reports for the analogous variants of KatGs from *M. tuberculosis* and other organisms.[112,113,114,115,127] This is the first report of a double variant targeting both the ^{Sw}Arg and the ^{Px}Trp; however, at first glance its spectral and catalytic properties are quite similar to the single variant. At pH 5 where the side chain of the ^{Sw}Arg is predominantly in its "*out*" conformation, the catalase activity of *wt*KatG is decreased by over an order of magnitude in k_{cat}. Indeed, *wt*KatG, R418N, and W321F/R418N KatG all showed highly similar catalase activity at this pH, despite that *wt*KatG did not exhibit standard Michaelis-Menten behaviors as R418N. The k_{cat} for R418N KatG catalase activity was essentially pH independent from 7 to 5 (Table 3.1.2). These are consistent with data for an R461A variant of extracellular KatG from *Magnaporthe grisea*.[113] In contrast, the efficiency (k_{cat}/K_M) of the catalase activity of our R418N variant clearly increased at acidic pH, registering ~ 10-fold higher at pH 5.0 than at pH 7.0.

By contrast, R418N and W321F/R418N KatG both showed 27- to 160-fold increases in peroxidase activity relative to the wild-type enzyme in terms of catalytic efficiency (i.e., k_{cat}/K_M) with respect to the H_2O_2 substrate (Tables 3.1.2 and 3.1.3). The value of k_{cat}/K_M varied to some extent with the identity of the peroxidatic electron donor substrate (i.e., PxED) (Table 3.1.3). For example, R418N KatG exhibited a 30-fold and 150-fold increase in the k_{cat}/K_M with respect to H_2O_2 with CPZ *vs* TMPD as PxEDs, respectively.

This drastic enhancement in k_{cat}/K_M of peroxidase activity with the Arg switch variant was reported by others.[114] Consistent with previous reports, R418N substitution showed very little impact on the k_{cat} of the peroxidase activity,[112,115,127] the same was determined for the W321F/R418N KatG variant.

Table 3.1.2. Catalase and peroxidase kinetic parameters for *Mt*KatG and variants.

Activity (substrate) Parameter	KatG Protein		
	*Mt*KatG	R418N	W321F/R418N
Catalase (pH 7.0)[a]			
k_{cat} (s^{-1})	3800 ± 430 [h]	137 ± 5	359 ± 25
k_{cat}/K_M ($M^{-1}s^{-1}$)	$(1.0 \pm 0.3) \times 10^6$ [h]	$(2.6 \pm 0.2) \times 10^4$	$(4.1 \pm 0.5) \times 10^4$
Peroxidase[b] (H_2O_2)[c]			
k_{cat} (s^{-1})	17.6 ± 0.1	9.3 ± 0.1	8.7 ± 0.2
k_{cat}/K_M ($M^{-1}s^{-1}$)	$(5.2 \pm 0.2) \times 10^4$	$(3.1 \pm 0.3) \times 10^6$	$(1.4 \pm 0.3) \times 10^6$
Peroxidase (ABTS)[d]			
k_{cat} (s^{-1})	25.0 ± 0.1	40.4 ± 1.6	40.1 ± 0.6
k_{cat}/K_M ($M^{-1}s^{-1}$)	$(1.8 \pm 0.1) \times 10^5$	$(3.6 \pm 0.5) \times 10^5$	$(4.3 \pm 0.2) \times 10^5$
Catalase (pH 5.0)[e]			
k_{cat} (s^{-1})[f]	170 ± 10	77.0 ± 1.8	140 ± 4
k_{cat}/K_M ($M^{-1}s^{-1}$)[f]	$(2.8 \pm 0.4) \times 10^5$	$(3.0 \pm 0.3) \times 10^5$	$(1.00 \pm 0.06) \times 10^4$
k_{app} ($M^{-1}s^{-1}$)[g]	$(9.2 \pm 0.3) \times 10^3$	-	-

[a]Activity was determined by O_2 production at 23 °C in 100 mM phosphate buffer, pH 7.0.
[b]All peroxidase activity assays were performed at 23 °C in 50 mM acetate buffer, pH 5.0.
[c]Peroxidase parameters with respect to H_2O_2 were determined using 0.1 mM ABTS.
[d]Peroxidase parameters with respect to ABTS were determined using 1.0 mM H_2O_2.
[e]Activity was determined by O_2 production at 23 °C in 50 mM acetate buffer, pH 5.0.
[f]Kinetic parameters for low K_M component.
[g]Apparent second-order rate constant for high-K_M component.
[h]From reference number 129 and the value adjusted for stoichiometry.

Table 3.1.3. Peroxidase kinetic parameters for *Mt*KatG and variants.[a]

Parameter[b]	KatG Protein		
	*Mt*KatG	R418N	W321F/R418N
Peroxidase (ABTS)			
k_{cat} (s^{-1})	17.6 ± 0.1	9.3 ± 0.1	8.7 ± 0.2
k_{cat}/K_M ($M^{-1}s^{-1}$)	$(5.2 \pm 0.2) \times 10^4$	$(3.1 \pm 0.3) \times 10^6$	$(1.4 \pm 0.3) \times 10^6$
Peroxidase (CPZ)			
k_{cat} (s^{-1})	56.0 ± 4.7	62.8 ± 3.1	70.2 ± 0.6
k_{cat}/K_M ($M^{-1}s^{-1}$)	$(2.8 \pm 0.3) \times 10^4$	$(8 \pm 2) \times 10^5$	$(5.0 \pm 0.3) \times 10^6$
Peroxidase (TMPD)			
k_{cat} (s^{-1})	51.7 ± 1.5	32.9 ± 0.8	64.0 ± 0.7
k_{cat}/K_M ($M^{-1}s^{-1}$)	$(4.2 \pm 0.3) \times 10^4$	$(6.3 \pm 0.7) \times 10^6$	$(6.6 \pm 0.3) \times 10^6$

[a]All assays were carred out using 50 mM acetate, pH 5.0, at 23 °C.
[b]Parameters are with respect to H_2O_2 using 0.1 mM of the PxED indicated in parentheses.

3.2 The ^{Sw}Arg in catalysis and inactivation: Properties and intermediates of R418N KatG

3.2.1 Inactivation of KatG during catalatic O_2 production

Inactivation of KatG catalase activity is observed at pH 5.0.[129] This corresponds to conditions where the ^{Sw}Arg is predominantly in its "*out*" conformation and is not in an ion pairing interaction with the phenolate oxygen of the MYW cofactor. To investigate the impact of pH on inactivation, and to determine the extent to which inactivation is linked to the ^{Sw}Arg, we compared the vulnerability of *wt* and R418N KatG to H_2O_2-dependent inactivation at pH 5.0 and 7.0.

When *wt*KatG was reacted with 0.5 mM H_2O_2 (molar ratio of H_2O_2 : KatG = 100,000) at pH 7, catalatic O_2 production ceased once 0.25 mM had been generated. Consistent with the 2:1 catalase stoichiometry of H_2O_2 consumed to O_2 generated, a second addition of the enzyme did not yield more O_2, instead only addition of more H_2O_2 resumed O_2 production (Fig. 3.2.1A). Thus, the reaction ceased due to substrate depletion not enzyme inactivation. In contrast, O_2 production by R418N KatG ceased at ~ 60 μM generated, only 24% of that anticipated from catalase stoichiometry. Only the addition of fresh R418N KatG ***not*** H_2O_2 produced a new burst of O_2 evolution (Fig. 3.2.1A). Therefore, R418N was inactivated during catalase turnover without fully consuming the substrate.

Reactions of *wt*KatG and R418N with H_2O_2 at pH 5 resulted in inactivation of both proteins (Fig. 3.2.1B). First, between 50% (*wt*) and 75% (R418N) of the H_2O_2 reacted was unaccounted for in O_2 production. Second, in both cases only the addition of more enzyme not H_2O_2 yielded more O_2 evolution (Fig. 3.2.1B). Notably, *wt*KatG reproducibly yielded more O_2 (~100 μM) prior to inactivation than R418N (~ 60 μM) at pH 5. We calculated that *wt*KatG performed roughly 21,000 ± 3000 catalatic cycles prior to irreversible inactivation, whereas

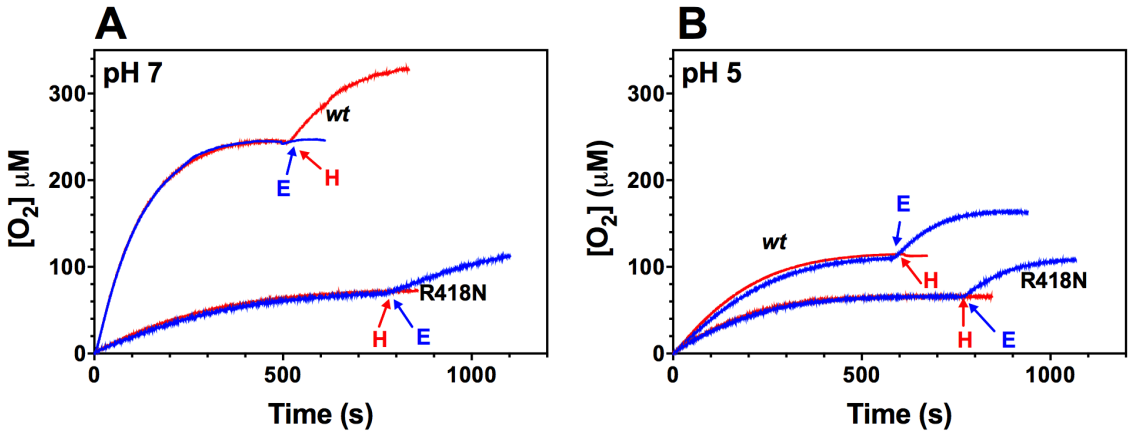

Figure 3.2.1. Catalatic O_2 production by *wt* and R418N KatG at pH 7 and 5. Reactions at pH 7.0 (A) contained 100 mM phosphate, and reactions at pH 5.0 (B) contained 50 mM acetate. The time of a second addition of H_2O_2 (H) or enzyme (E) are indicated by the arrows. All reactions contained 5 nM KatG and were initiated by the addition of 0.5 mM H_2O_2. All reactions were carried out at 23 °C. Each trace is a representative from 5 replicates. Each 5 replicates is repeated three times.

R418N only achieved 12000 ± 1500 cycles.

In addition, we have tested alternative buffer-components system (i.e., the reactions were buffered with 50 mM acetate and 100 mM phosphate) to rule out the possibility that this phenomenon is merely the artifact of the buffer. We have got nearly identical results in both buffer systems to verify the susceptibility to inactivation was the true reflection of the enzyme properties (data not shown).

Preincubation of *wt*KatG and R418N with increasing concentrations of H_2O_2 produced decreases in catalase activity for *wt* and R418N KatG at pH 5.0 and 7.0 (Fig. 3.2.2). For both enzymes, full catalase activity was maintained up to at least a 1,000 fold excess of H_2O_2. *wt*KatG at pH 7 showed the greatest resistance to catalase inactivation with 100% activity still detected after reaction with 5000 molar equivalents of H_2O_2. Further, the wild-type enzyme still retained >50% of its activity following preincubation with 200,000 molar equivalents of H_2O_2. This was in contrast to *wt*KatG at pH 5 and R418N KatG at either pH 5 or 7. In all three cases, the complete loss of catalase activity was observed upon preincubation with ≤100,000 molar equivalents of H_2O_2. Accordingly, resistance to H_2O_2-dependent inactivation by these measurements followed the order *wt*KatG at pH 7 >> *wt*KatG at pH 5 > R418N at pH 5 ≈ R418N at pH 7. This was in close agreement with the extent of catalatic O_2 production shown in Fig. 3.2.1.

Taken together, these data suggest that whether the ^{Sw}Arg is absent by orientation (i.e., *wt*KatG at low pH) or by mutagenesis (i.e., R418N regardless of pH), KatG becomes more susceptible to inactivation. Notably, elimination of the ^{Sw}Arg by mutagenesis created an enzyme (i.e., R418N KatG) more compromised in sustaining activity than by the manipulation of its orientation by pH. Though the dominant conformation of the ^{Sw}Arg at pH 5.0 is "*out*" (given an

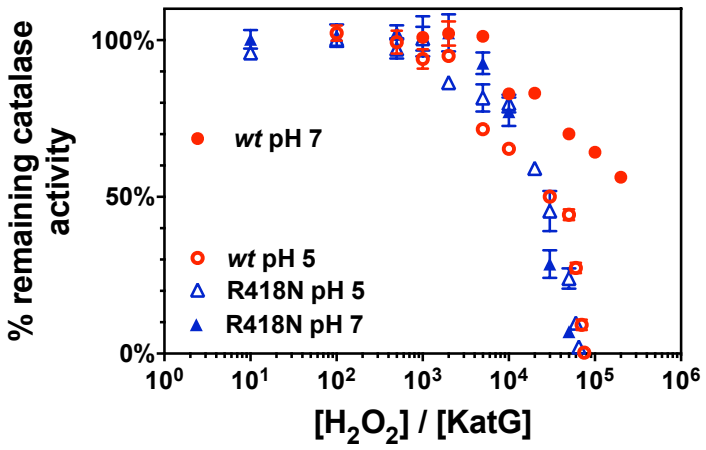

Figure 3.2.2. Effect of preincubation with H_2O_2 on the catalase activity of *wt* and R418N KatG at pH 7 and 5. Either *wt* or R418N KatG (200 nM) was preincubated with the indicated concentration of H_2O_2. Preincubations were carried out in either 100 mM phosphate, pH 7.0, or 50 mM acetate, pH 5.0. Following a 1 hour preincubation, an aliquot was withdrawn and catalase activity was measured with 10 mM H_2O_2 in 100 mM phosphate, pH 7.0 by O_2-senstive electrode. All reactions were carried out at 23 °C.

apparent pK_a of 6.5), the ability to occupy the "*in*" conformation for a limited time/to a limited extent appears to mitigate some of the enzyme's sensitivity to inactivation.

3.2.2 The effect of peroxidatic electron donor (PxED) on KatG catalase inactivation

We previously reported that several PxEDs did not inhibit but unexpectedly stimulated the catalase activity of KatG at pH 5.0.[134] We propose that PxEDs are stimulatory due to their ability to sacrificially reduce KatG's catalatically inactive species. Inclusion of ABTS (0.1 mM) as a PxED prevented inactivation and enabled the complete depletion of H_2O_2 under all conditions where susceptibility to catalase inactivation had been previously observed (i.e., *wt*KatG at pH 5, R418N KatG at pH 5 and pH 7) (Fig. 3.2.3). Accordingly, in all three cases it was the addition of more H_2O_2 not fresh enzyme that resulted in more catalase activity. Because *wt*KatG already maintained activity to the full consumption of H_2O_2 at pH 7, ABTS produced little improvement. Interestingly, even though the full depletion of H_2O_2 was observed, it appeared that it was not all directed toward catalatic O_2 production, especially with R418N KatG at pH 5 and 7 and with wtKatG at pH 5. These data suggest that H_2O_2 consumption was directed toward the oxidation of something else. Stoichiometric decomposition of 0.5 mM H_2O_2 by catalase activity should produce 0.25 mM O_2. Instead, values close to 0.2 mM O_2 were reproducibly generated under all conditions except with *wt*KatG at pH 7.

We observed ABTS-based preservation of KatG catalase activity in two ways. The first was observed as the stimulation of the *rate* of catalatic O_2 production which occurred in all cases except *wt*KatG at pH 7.0 (compare Figs. 3.2.1 and Fig. 3.2.3). The second was observed as an increase in the *extent* of O_2 production. For example, inclusion of ABTS in R418N KatG catalase assays at pH 7 roughly doubled the initial rate of O_2 production. At pH 5, the effect was more

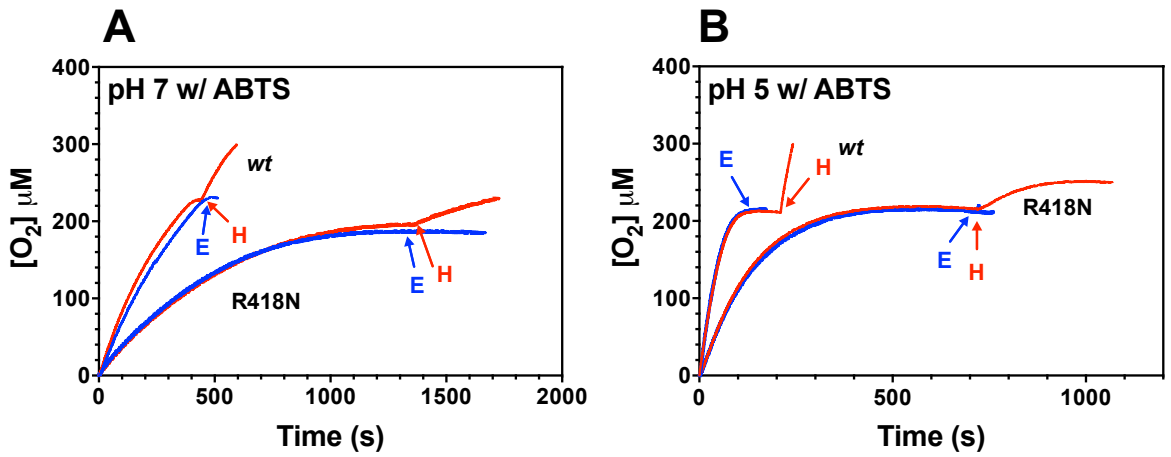

Figure 3.2.3. Catalatic O_2 production by wild-type and R418N KatG in the presence of PxED at pH 7 (A) and 5 (B). Reactions at pH 7.0 (A) contained 100 mM phosphate, and reactions at pH 5.0 (B) contained 50 mM acetate. The time of the second addition of H_2O_2 (H) or enzyme (E) are indicated by the arrows. All reactions contained 5 nM KatG, 0.1 mM ABTS and were initiated by the addition of 0.5 mM H_2O_2.

dramatic, producing a rate enhancement of about an order of magnitude. In terms of the *extent* of O_2 production, inclusion of ABTS resulted in the complete depletion of H_2O_2 and the generation of 3.3 times more O_2 at acidic and neutral pH. In addition, R418N still retained some activity under both conditions even after fully consuming 10^5 molar equivalents H_2O_2. In a similar manner, inclusion of ABTS enabled *wt* and R418N KatG to resist peroxide-dependent inactivation to at least an order of magnitude higher concentrations of H_2O_2 (Compare Figs. 3.2.4, and 3.2.2). For instance, *wt*KatG at pH 5 with ABTS present maintained full catalase activity even following reaction with 100,000 fold H_2O_2, a concentration of H_2O_2 which fully inactivated *wt*KatG otherwise. ABTS provided decent protection for R418N at pH 7, although not as pronounced as that observed at pH 5.

In the absence of any PxED, R418N KatG lost all catalase activity upon preincubation with as little as 0.2 mM H_2O_2; this was observed at all pH investigated from 5 to 7.5 (Fig. 3.2.5A). In contrast, *wt*KatG was able to retain activity and deplete all the H_2O_2 added in preincubation across all pH conditions evaluated. However, *wt*KatG showed greater resistance to H_2O_2-dependent inactivation as the pH increased from 5 (25% catalase activity retained) to 7.5 (75% catalase activity retained).

With ABTS present, *wt*KatG lost little if any catalase activity across all pH conditions tested (Fig. 3.2.5B). Similarly, in the presence of ABTS, R418N KatG retained catalase activity at all the pH values tested; however, the level of catalase activity remaining diminished with increasing pH. Indeed, ABTS was as effective for the R418N variant as for *wt*KatG under the most acidic conditions tested (i.e., pH 5 and 5.5). These data suggest sacrificial oxidation of ABTS preserves catalase activity for R418N across pH 5 to pH 7.5 as well as for *wt*KatG from pH 5 to 7 tested.

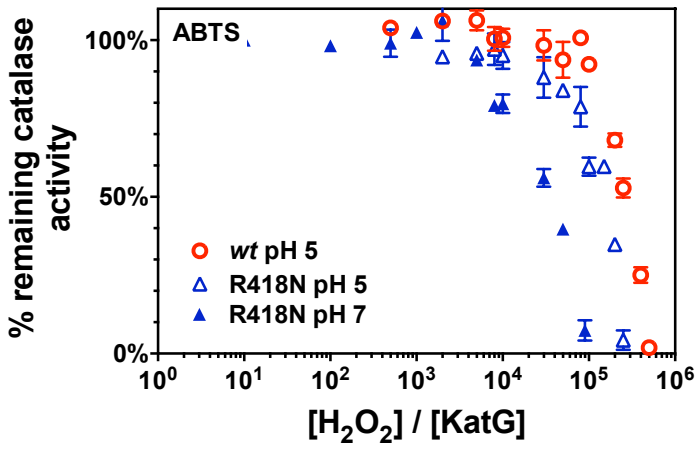

Figure 3.2.4 Effect of H_2O_2 on the catalase activity of *wt* and R418N KatG in the presence of ABTS at pH 5 and 7. Either *wt* or R418N KatG (200 nM) was preincubated with the indicated concentration of H_2O_2. Preincubations were carried out in either 100 mM phosphate, pH 7.0 or 50 mM acetate, pH 5.0 in the presence of 0.1 mM ABTS. Following a 1 hour preincubation, an aliquot was withdrawn and catalase activity was measured with 10 mM H_2O_2 in 100 mM phosphate, pH 7.0 by O_2-senstive electrode. All reactions were carried out at 23 °C.

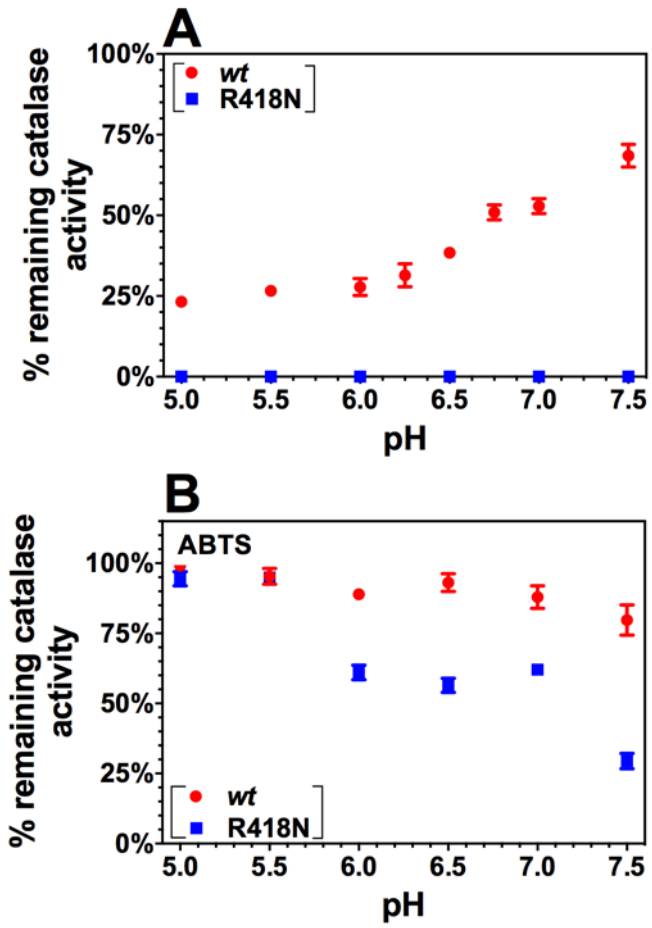

Figure 3.2.5. Effect of pH on *wt* and R418N KatG catalase inactivation. All reactions (Panel A) contained 5 nM KatG and were initiated by the addition of 0.2 mM H_2O_2. All reactions (Panel B) contained 5 nM KatG, 0.1 mM ABTS and were initiated by the addition of 0.2 mM H_2O_2. All reactions were carried out at 23 °C by O_2 sensitive electrode. When reaction completed (O_2 production ceased), more H_2O_2 was added. The % remaining catalase activity was obtained by the initial rate O2 production following the 2nd addition relative to the initial rate observed following the 1st addition of H_2O_2. Reactions at pH 5.0 and pH 5.5 were buffered with 50 mM acetate, and reactions at pH 6.0, 6.25, 6.5, 7, 7.5 were buffered with 100 mM phosphate.

3.2.3 The extent of ABTS oxidation during KatG catalase catalysis

Thus far, the data indicate that the stimulatory effect of PxEDs on KatGs catalase activity is through the prevention of enzyme inactivation during catalatic consumption of H_2O_2. In comparison to other superfamily members, KatG is well known to have a very restricted access channel for H_2O_2 to approach the active-site heme. Because most PxEDs, such as ABTS, are too large to access the active site through this channel, their oxidation requires the delivery of oxidizing equivalents to the protein surface by way of through-protein radical transfer. Interestingly, the net result of this phenomenon is that the extent of PxED oxidation (i.e., $ABTS^{\bullet+}$ accumulation) during catalatic H_2O_2 consumption by KatG serves to record off-catalase electron transfer events. Thus, calculating the ratio of $ABTS^{\bullet+}$ generated per H_2O_2 consumed gauges not only the effect of amino acid substitutions (e.g., *wt vs*. R418N KatG), pH, and other factors on the propensity toward off-pathway electron transfer, but it also indicates the extent to which PxED intervention is necessary to sustain KatG catalase activity. The extent of $ABTS^{\bullet+}$ production increased with an increase in initial H_2O_2 concentration in a hyperbolic relationship for *wt* and R418N KatG reacting with varying concentrations of H_2O_2 at pH 5 by optical stopped-flow (Fig.3.2.6A). However, R418N produced substantially greater quantities of $ABTS^{\bullet+}$ at all H_2O_2 concentrations tested, compared to *wt*KatG. Moreover, the ratio of $ABTS^{\bullet+}$ generated to H_2O_2 consumed for R418N was inversely dependent on H_2O_2 concentration to a much greater degree than with *wt*KatG at pH 5 (Fig.3.2.6B). For example, at pH 5, with 4 mM H_2O_2 R418N variant produced 0.014 equivalents of $ABTS^{\bullet+}$, around three-fold greater than that produced by *wt*KatG. Conversely, with 0.25 mM H_2O_2, R418N variant produced 0.135 equivalents of $ABTS^{\bullet+}$, around 17-fold greater than that produced by *wt*KatG. This ratio continued to increase with lower H_2O_2 concentrations such that 0.94 equivalents of $ABTS^{\bullet+}$ (0.82 μM) was generated when R418N

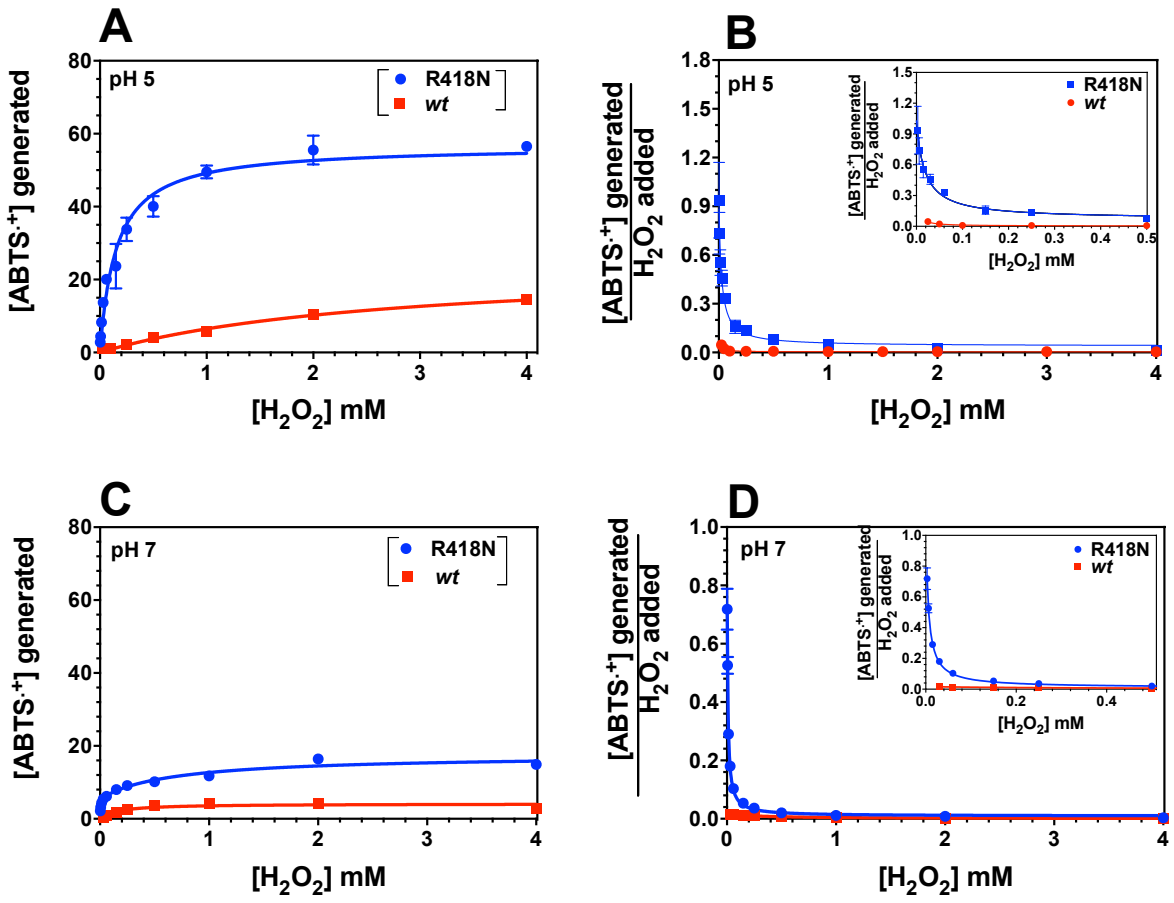

Figure 3.2.6. Effect of H_2O_2 concentration and pH on ABTS oxidation by *wt* and R418N KatG. All reactions contained 3 μM KatG, and 0.1 mM ABTS. Concentration of $ABTS^{\bullet+}$ was calculated using ε (645 nm) = 0.012 $\mu M^{-1}\,cm^{-1}$. All reactions were carried out at 4 °C. Panels B and D depict the $ABTS^{\bullet+}$ generated to H_2O_2 consumed by *wt*KatG (red) and R418N (blue). Reactions at pH 5.0 (Panels A and B) contained 50 mM acetate, and reactions at pH 7.0 (Panels C and D) contained 100 mM phosphate.

KatG was reacted with 1 equvalent of H_2O_2 (3 μM) at pH 5. Similar to pH 5, much greater quantities of $ABTS^{\bullet+}$ were produced by R418N than *wt*KatG at pH 7. Further, the ratio of $ABTS^{\bullet+}$ generated to H_2O_2 consumed showed much greater inverse dependence on concentration of H_2O_2 by R418N than *wt*KatG. We observed the highly similar trend using alternative benchtop spectrometric assays (data not shown). These data suggest off-pathway electron transfer becomes a much more frequent event when the Arg switch is abolished by mutagenesis. Notably, the extent of $ABTS^{\bullet+}$ by both enzymes at pH 7 is lower than those at pH 5, suggestive of higher propensity for off-pathway electron transfer for both enzymes at pH 5 compared to pH 7. The extent of $ABTS^{\bullet+}$ by R418N at pH 7 exhibited dual hyperbolic response to H_2O_2, in contrast to other three cases which showed single hyperbolic response.

Consistent with the higher participation of off-pathway electron transfer in the Arg variant, reaction of R418N KatG with H_2O_2 in the presence of ABTS reproducibly generated greater quantities of ABTS oxidation to $ABTS^{\bullet+}$, and this was actually visually apparent in O_2 production assays (Fig. 3.2.3A and B). Qualitatively, $ABTS^{\bullet+}$ color intensity followed the order R418N at pH 5 > R418N at pH 7 > *wt*KatG at pH 5 >> *wt*KatG at pH 7.

Taken together, these data suggest off-pathway electron transfer becomes a much more frequent event when the Arg switch is abolished by mutagenesis. While inclusion of a PxED prevents KatG inactivation for both *wt* and R418N, clearly more PxED intervention is needed for R418N variant.

We also quantified the generation of the ABTS oxidation product ($ABTS^{\bullet+}$) during the consumption of H_2O_2 as a function of pH by stopped-flow (Fig. 3.2.7A) or by benchtop spectrometric assays (Fig. 3.2.7B). They showed the same trend, although the molar ratio of H_2O_2 to KatG used in two experiment were far apart from each other (16.7-fold by stopped-flow

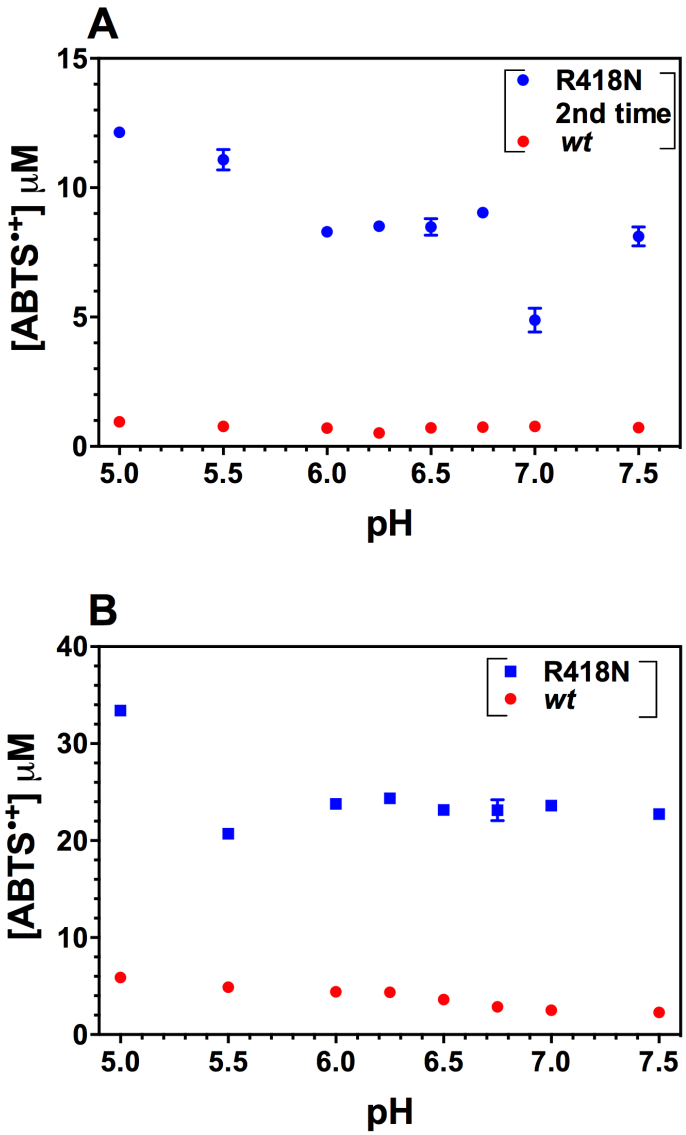

Figure 3.2.7. Effect of pH and H_2O_2 concentration on ABTS oxidation by *wt* and R418N KatG. All reactions (Panel A) contained 3 µM KatG, 0.05 mM H_2O_2 and 0.1 mM ABTS. All reactions (Panel B) contained 20 nM KatG, 0.8 mM H_2O_2 and 0.1 mM ABTS. Concentration of $ABTS^{\bullet+}$ was calculated using ε (645 nm) = 0.012 μM^{-1} cm^{-1}. Reactions (Panel A) were carried out by stopped-flow at 4 °C, and Reactions (Panel B) were carried out manually at 23 °C and concentration of $ABTS^{\bullet+}$ was measured by UV-visible spectroscopy post 30 minutes of reaction. Reactions at pH 5.0 and pH 5.5 were buffered with 50 mM acetate, and reactions at pH 6.0, 6.25, 6.5, 7, 7.5 were buffered with 100 mM phosphate.

vs. 40,000-fold by benchtop assays). That is: R418N variant produced substantially greater quantities of $ABTS^{\bullet+}$ during consumption of H_2O_2 at all the pH tested, compared to *wt*KatG. Based on the premise that the extent of ABTS oxidation reports the frequency of off-pathway electron transfer, our data again suggest that off-catalase electron transfer becomes a much frequent event across the pH tested when the Arg switch is eliminated.

Our data from ***3.2.1*** to ***3.2.3*** suggest the Arg switch minimizes the frequency of off-catalase through-protein electron transfer of KatG for self-preservation. In other words, withdrawal of the Arg switch makes KatG higher susceptibility to inactivation due to largely increased frequency of off-pathway electron transfer. PxEDs oxidation at the protein surface resolves inactive catalatic species thus preserving catalase function of KatG, however, substantially more PxEDs oxidation is required for correction of off-catalase electron transfer for R418N than *wt*KatG. Because catalase mechanism requires precise electron transfer involving a novel MYW adduct cofactor, our next question is what the participant is for off-pathway electron transfer in the absence of the Arg switch. We previously reported the Trp 321 is the hot spot for off-catalase oxidation of *wt*KatG at low pH (i.e., pH 5) by paired stopped-flow and RFQ-EPR techniques. In order to examine the off-pathway route(s) for the variant, we performed similar experiments.

3.2.4 R418N KatG intermediates observed upon reaction with H_2O_2 at pH 5

To evaluate the dominant heme intermediate(s) present during catalatic H_2O_2 degradation, we used stopped-flow to react wild-type and R418N KatG with varying H_2O_2 concentration in the absence and presence of PxED at pH 5. As previously reported, we used the ascorbate-based method to suppress spectral interference due to the accumulation of $ABTS^{\bullet+}$.[134] As such, the term "PxED" in these experiments refers to a mixture of ABTS and ascorbate.

We observed R418N took longer to consume a comparable concentration of H_2O_2 in the absence of PxED than *wt*KatG, consistent with the proposed role of the Arg switch in facilitating O_2 release in catalase turnover.[123] However, despite that R418N had slower steady-state turnover, we consistently observed that the return of the ferric state of the enzyme lagged behind the cessation of H_2O_2 consumption, in both the *wt* and R418N variant. For example, reaction of 3 μM R418N with 2.0 mM H_2O_2 at pH 5.0, H_2O_2 consumption ceased at about 18-23 s (some variations were seen between R418N in different expression/ purifications) (monitored at 408 nm), but it took about 100 s for the ferric enzyme to completely reemerge (Fig. 3.2.8A). By contrast, it only took *wt*KatG 6 s to deplete the same amounts of H_2O_2, but more than 50 s were required for the ferric enzyme to return (data not shown). We have previously reported that catalase-inactive intermediates accumulate during catalatic turnover of *wt*KatG at pH 5.[129] The slow return of the ferric state is an indicator of that phenomenon. These data suggest R418N is likely to accumulate similar inactive states during catalatic turnover.

As we have observed for *wt*KatG, we also observed highly identical spectra of R418N reacting with 667 molar excess of H_2O_2 at the earliest time regime (i.e., 2.5 ms); it included a Soret at 416 nm and α, β bands maxima at 578 and 542 nm (Fig. 3.2.8B). A conspicuous feature of this spectrum compared to the enzyme's resting state is the lack of absorbance at both 500 (CT 1) and 637 nm (CT 2), both of which are the hallmarks of the ferric state. The species was consistent with the oxyferrous/ferric superoxide intermediate (i.e. Fe^{III}-$O_2^{\bullet-}$), which has been observed with a range of KatGs upon reaction with H_2O_2 and has been associated with catalase activity.[118,121] This spectra was followed by a rapid and broad increase in absorption at wavelength above 520 nm within 546 ms, with α, β bands maxima at 583 nm and 550 nm (Fig. 3.2.8B), similar to reaction of *wt*KatG we previously reported.[129] This same spectra progression

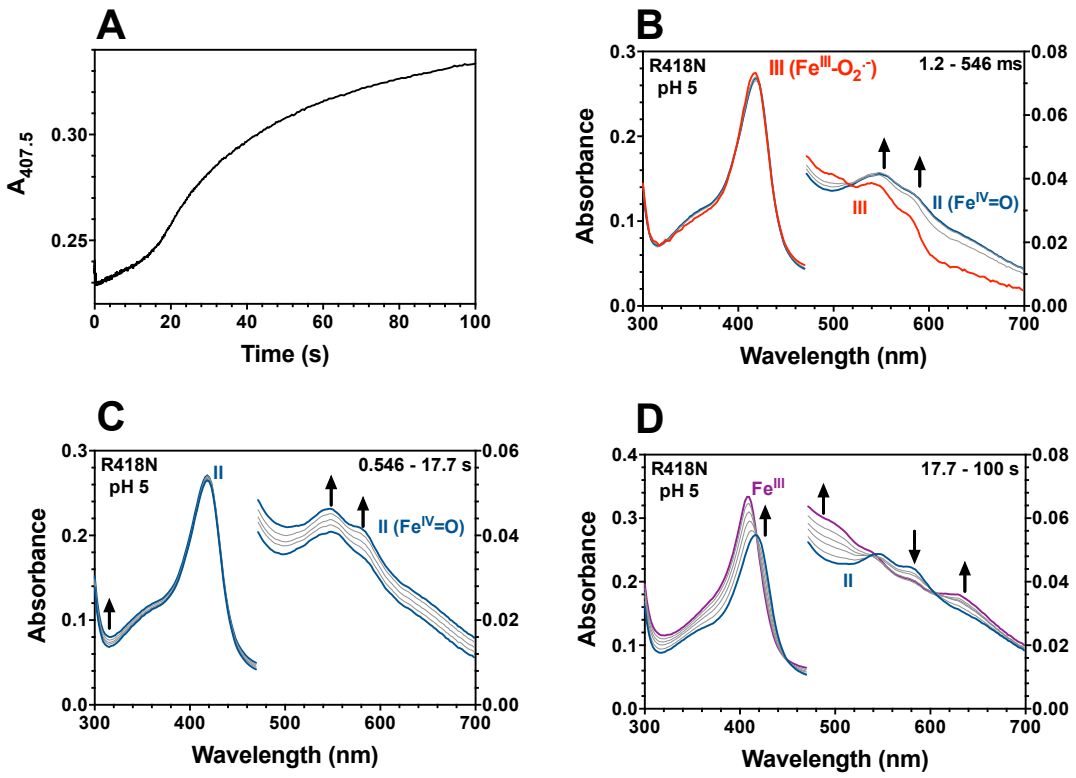

Figure 3.2.8. Spectra collected during reaction of R418N KatG with 2.0 mM H_2O_2. The change in absorbance at 407.5 nm over the entire course of the reaction (A) is also shown. Spectra corresponded to 1.2-546 ms (B) (1.2 ms trace shown in red, 546 ms trace shown in ocean), 0.546-17.7 s (C), and 17.7-100 s (D) following mixing of 3 μM enzyme and 2.0 mM H_2O_2. This reaction was carried out using 50 mM acetate pH 5 at 4 °C.

has also been observed across several KatGs reacting with H_2O_2.[118,121] A species with identical spectral features to the latter has been reported in several KatGs by reaction with peracetic acid (PAA), the reagent that does that support catalase activity.[121,128,162] This has been assigned through a combination of EPR and X-ray crystallographic studies as a ferryl-oxo (most likely protonated) species with a protein-centered radical where the proximal Trp has been identified as a prominent site of oxidation.[114,130,151] We think this represents the accumulation of catalase-inactive species. From 0.5 to 17.7 s, there was little if any change in spectra (Fig. 3.2.8C). Very slow return of the ferric state was observed thereafter. From 0.5 s to 100 s, we consistently observed a progressive increase in the absorbance at 320 nm (Fig. 3.2.8C,D), suggestive of a light scattering effect. This is likely due to the crosslinking of the enzyme resulting from surface radicals generated by off-pathway electron transfer events. This was not observed or not as pronounced, if seen at all, for *wt*KatG under identical conditions, consistent with the conclusion that off-pathway electron transfer is a more frequent event in the R418N variant than *wt*KatG.

Attempts to monitor H_2O_2 degradation at 240 nm with the photomultiplier were not successful. In light of the higher propensity for off-pathway electron transfer during catalase activity of R418N, we reasoned potential oxidative crosslinking of the enzyme could interfere with the absorption at all wavelengths, but especially so at 240 nm. Indeed, we saw a progressive increase in absorbance at 240 nm following the initial decrease in A_{240}, which was attributed to the disappearance of H_2O_2. These absorptions suggest the species accumulated during catalase catalysis strongly absorbed at this UV wavelength range, and thereby masked the decrease in absorption of H_2O_2. But based on what we and others have established, the time point when the ferric enzyme starts to return post to the steady-state turnover phase corresponds to the substrate

depletion time.[113,121,129] Therefore, the substrate depletion time for R418N reacting with 2 mM H_2O_2 was estimated to be around 18 s.

Inclusion of PxED not only stimulated H_2O_2 consumption, but also ensured a much faster regeneration of the resting state of R418N across H_2O_2 concentrations (data not shown). For example, it took less than 5 s to deplete 2 mM H_2O_2 in the presence of PxED, compared to that in the absence (i.e., 18 s). In similarity to the reactions in the absence of PxED, we also observed the spectra reminiscent of a Fe^{III}-$O_2^{\bullet-}$ heme state at the earliest time point upon reaction of R418N KatG with H_2O_2 with PxED included. But what was distinct from the reactions in the absence of PxED was the fast return of this Fe^{III}-$O_2^{\bullet-}$ heme intermediate to the ferric resting state after substrate depletion, without accumulation of some other species. We observed the same phenomenon for *wt*KatG. These data suggest PxED rescues inactive catalatic intermediates to restore the ferric enzyme for R418N and *wt*KatG at pH 5. However, the time to consume a comparable amount of H_2O_2 by *wt*KatG was much faster than by R418N, irrespective of whether PxED present or not, consistent with the direct participation of ^{Sw}Arg in catalase turnover.[113,123] Somewhat not surprising, for the same conditions (i.e., 3 μM KatG, 2 mM H_2O_2 at pH 5) we included 0.5 mM ascorbate for reactions of R418N *vs.* 0.1 mM ascorbate for *wt*KatG. Because R418N required more ABTS intervention to restore its inactive species, and the ABTS concentration needed to remain constant, more ascorbate was needed in the case of R418N, to prevent the generation of $ABTS^{\bullet+}$ that obscures the spectra.

Our data suggest R418N also accumulates inactive species during catalase turnover, similar to *wt*KatG at pH 5. These inactive species can be resolved by inclusion of PxED.

We then performed rapid freeze-quench (RFQ)-EPR experiments to trap and characterize protein-based radical(s), and to track the disappearance and appearance of the high spin ferric

enzyme during the reaction. We retained a 667 molar ratio of H_2O_2 : enzyme in RFQ experiments for R418N to ensure the rigid comparison.

3.2.5 EPR signal of high spin ferric resting R418N KatG variant

The 9-GHz EPR spectrum of the ferric form of R418N KatG recorded at 4.5 K at pH 7 and 5 showed the main resonances at g ~ 6 and g ~ 2 (Fig. 3.2.9). Such spectra are characteristic of heme iron in the ferric high spin state (S = 5/2). Consistent with the resting KatGs reported by others, we also observed a multiplicity of high spin states. The contributions from at least two different ferric high-spin species, were observed: 1) an axial signal with $g_{//} \sim 6.0$ and $g_{\perp} \sim 1.99$, 2) a rhombically distorted signal with $g_x \sim 6.4$, $g_y \sim 5.3$ and $g_z \sim 1.98$ (Fig. 3.2.9). Our results were highly similar to the *Mt*KatG reported by Singh, *et al.* in which one axial and one rhombic ferric high spin signal were observed.[130]

Changes in pH induced slight differences in the relative population of axial and rhombic signals of our resting *Mt*KatG. That is, the "axial" fraction of the high spin ferric signal observed at pH 7 was greater than at pH 5. This trend was not shown in data by Singh, *et al.* However, this is in resemblance to the trend of pH dependence of wild-type *Synechocystis* KatG, although the latter exhibited more remarkable change as a function of pH.[126] In addition, our spectra were very similar to the previously published low temperature EPR spectrum of *Syn*KatG and *Mt*KatG.[140]

3.2.6 R418N KatG intermediates observed upon reaction with H_2O_2 at pH 5

The EPR spectrum of R418N freeze-quenched 10-ms after mixing with H_2O_2 showed an near complete loss of signals corresponding to high spin ferric heme, concomitant with formation of an intense narrow doublet radical signal (Fig. 3.2.10B,C). Taking into account the relative susceptibility to power saturation of the signal at 4.5 K, this radical is in agreement with the so-called narrow doublet assigned by others as the cation radical of the MYW adduct.[118,119]

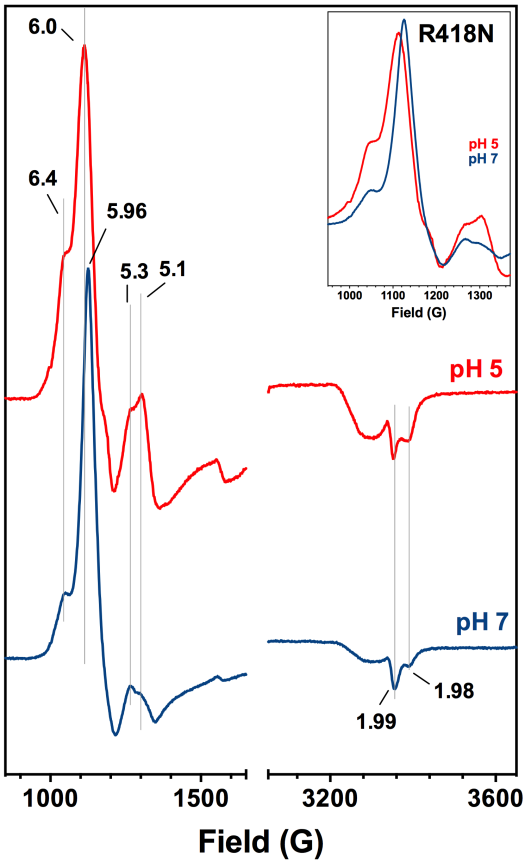

Figure 3.2.9. 9 GHz EPR spectra of resting R418N KatG at pH 5 and 7. The samples contained 150 μM R418N KatG in either 50 mM acetate, pH 5, or in 100 mM phosphate, pH 7. All spectra were recorded at 4.5 K. Instrument parameters were as follows: microwave frequency, 9.393 GHz; modulation amplitude, 1 G; modulation frequency, 100 kHz; microwave power, 1 mW; time constant, 163.84 ms; sweep time 335.54 s; number of scans, 1; conversion 327.68 ms; resolution, 1024 point; receiver gain, 1.0×10^4; and phase 0 degree.

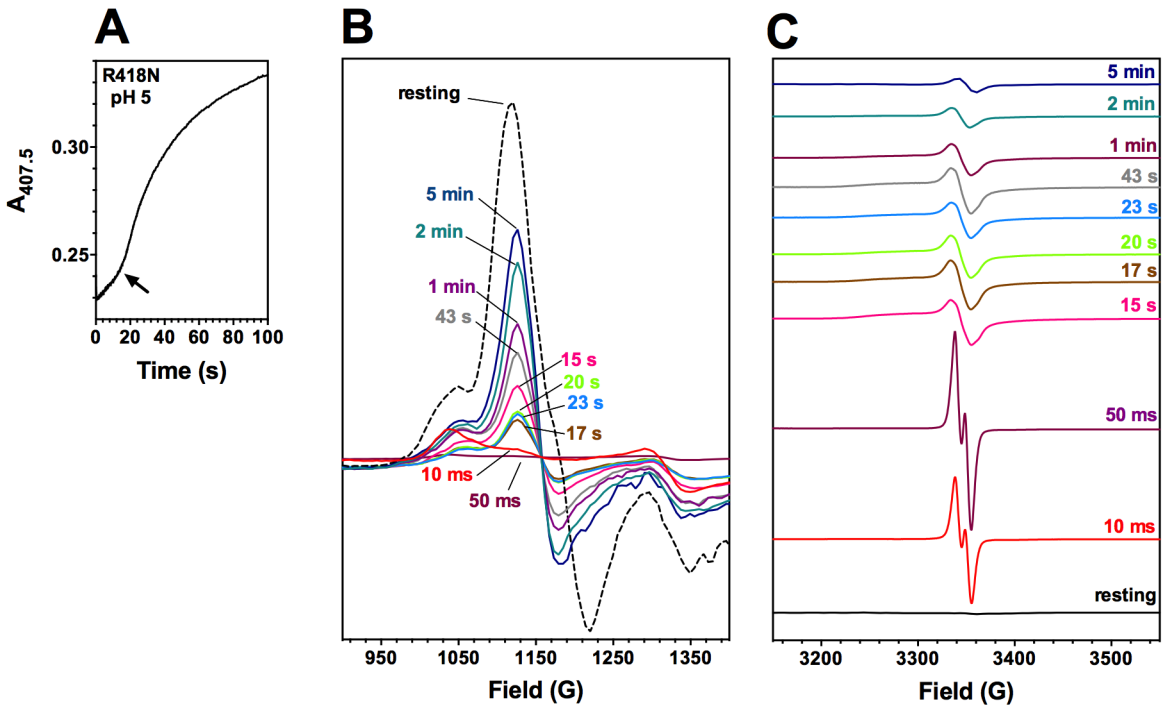

Figure 3.2.10. EPR spectra of freeze-quenched samples from reaction of R418N KatG with H_2O_2 at pH 5. The stopped-flow trace monitoring return of ferric enzyme at 407.5 nm during R418N reaction with 667eq. H_2O_2 are shown in A. High spin ferric species typical of KatG resting state (g ~ 6) are shown in B, and the g// component of the resting state as well as protein-based radicals (g ~ 2) of R418N are shown in C. The molar proportions of enzyme to H_2O_2 used for stopped-flow experiments (1:667) were maintained for these experiments. Consequently, ferric enzyme (150 μM after mixing) was reacted with H_2O_2 (100 mM after mixing) for the time indicated prior to freeze-quenching. Reactions were carried out at 4 °C in 50 mM acetate, pH 5. The resting R418N KatG was prepared the same way except no H_2O_2 included and it was quenched manually. All spectra were recorded at 4.5 K, if not indicated otherwise. Spectrometer settings were as described under "Experimental procedures." Specifically, Instrument parameters were as follows: microwave frequency, 9.393 GHz; modulation amplitude, 2 G for g ~ 6 and 1 G for g ~ 2; modulation frequency, 100 kHz; microwave power, 1 milliwatt; time constant, 163.84 ms; sweep time 335.54 s; number of scans, 1; conversion, 327.68 ms; resolution, 1024 point; receiver gain, 1.0×10^4; and phase, 0 degrees.

This same radical has been associated with the catalase activity of KatG.[118,119] We also captured this narrow doublet signal with higher intensity in sample quenched after a 50-ms reaction time with H_2O_2 (Fig. 3.2.10B). In this sample, the high spin ferric signal was completely absent. Thus, the combination of our optical stopped-flow and RFQ-EPR data suggest that the dominant steady-state intermediate of KatG catalase activity at the earliest turnover, bears a $MYW^{\bullet+}$, and a spectrum reminiscent of a Fe^{III}-$O_2^{\bullet-}$ heme state, which are aligned with previous results by us and others.[118,129]

In samples quenched 15-s after reaction with H_2O_2, the ferric state was slightly shown (Fig. 3.2.10B). The narrow doublet was completely replaced by a broad (~ 300 G) singlet signal at g ~ 2 at 15-s reaction time (Fig. 3.2.10C). The overall width and lineshape of this signal (Fig. 3.2.10C; 3.2.11A), power saturation characteristics as well as the temperature dependence of its features were highly similar to the exchange-coupled radical intermediate observed with CcP upon its reaction with H_2O_2.[149] A nearly identical exchange-coupled radical species has been observed with KatG from *M. tuberculosis* and *Burkholderria pseudomallei* upon their reactions with PAA. In each case, the signal has been assigned to the proximal Trp (Trp 321 and Trp 330, respectively).[130,151] With the caveat that similarity in lineshape and relaxation behavior of the signal detected in 9 GHz EPR is not sufficient for a definitive assignment of the protein-based radicals, its high resistance to power saturation was consistent with $W321^{\bullet+}$ (*Mt*KatG numbering) (Fig. 3.2.12D).

The EPR spectrum of R418N freeze-quenched 17-s, 20-s, 23-s after mixing with H_2O_2 showed a similar intensity of the high spin ferric signal (Fig. 3.2.10B), concomitant with formation of the broad singlet signal at g ~ 2 (Fig. 3.2.10C, 3.2.11A). The high spin ferric signal in these samples were less intense compared to that of the sample quenched at 15-s, however,

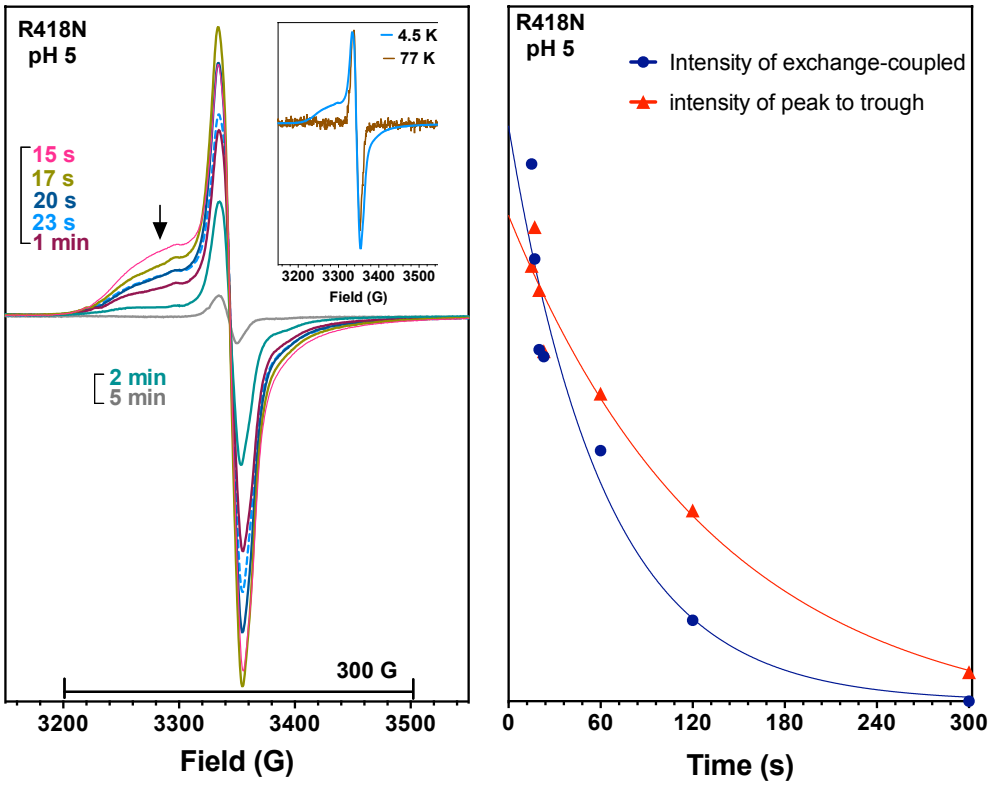

Figure 3.2.11. Overlay of protein-based radicals detected during R418N KatG reaction with H_2O_2 at pH 5. Spectrometer settings were as described under "Experimental procedures." Specifically, Instrument parameters were as follows: microwave frequency, 9.393 GHz; modulation amplitude, 1 G; modulation frequency, 100 kHz; microwave power, 1 milliwatt; time constant, 163.84 ms; sweep time 335.54 s; number of scans, 1; conversion, 327.68 ms; resolution, 1024 point; receiver gain, 1.0×10^4; and phase, 0 degrees.

.

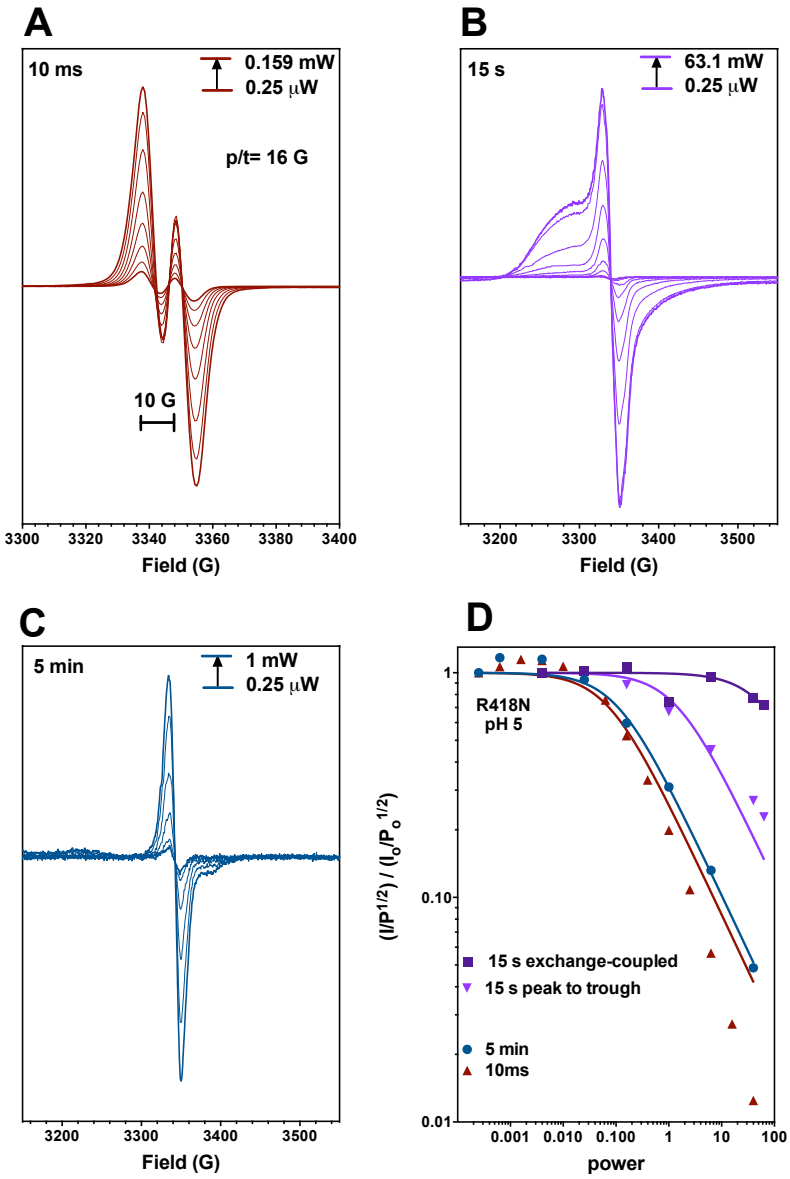

Figure 3.2.12. Evaluation of protein-based radicals detected during R418N KatG reaction with H_2O_2 at pH 5. The doublet radical observed 10 ms after mixing with H_2O_2 (A) was recorded across a range of microwave power setting from 0.25 μW to 0.159 mW. The effect of microwave power 0.25μW to 63.1 mW on the spectra recorded for the sample quenched 15 s after R418N reaction with H_2O_2 was shown (B). The effect of microwave power 0.25μW to 1 mW on the spectra recorded for the sample quenched 5 min after R418N reaction with H_2O_2 was shown (C). The normalized signal intensities for samples collected 10 ms, 15 s and 5 min after R418N KatG reaction with H_2O_2 as a function of microwave power are shown in (D). For exchanged coupled radical at 15 s, the intensity at 3300 G as well as that of the peak to trough were used. For 10 ms and 5 min samples, the peak to trough intensity (I at 3338.5 G- I at 3344.4 G) was used. Unless otherwise indicated, all spectra were recorded at 4.5 K with all other spectrometer settings as described in "Experimental procedures" Samples were prepared and evaluated as described for Fig. 3.2.10.

they showed nearly identical proportions of the rhombical and axial signals. In samples quenched 43-s after reaction with H_2O_2, a more intense signal of the ferric state was observed, consistent with the slow return of the ferric enzyme by stopped-flow after substrate depletion (i.e., 18 s). The exchange-coupled radical intermediate was still prominent.

In samples quenched 1-min, 2-min and 5-min after reaction with H_2O_2, we observed greater contribution of the ferric state over time, albeit still less intense than that of the resting state enzyme even in sample quenched after 5-min (Fig. 3.2.10B). The exchange-coupled radical intermediate was still evident in sample quenched at 1-min (Fig. 3.2.11A). But the broadening feature was much less pronounced in sample quenched at 2-min compared to that at 1-min (Fig. 3.2.11A). In sample quenched at 5-min, only a narrow singlet radical was shown (Fig. 3.2.11A). The intensity of the exchange-coupled feature decayed exponentially over time (fig. 3.2.11B). This protein-based radical progression indicates the predominant exchange-coupled W321 radical migrates further away from the active site at later time points (i.e., 2-min, 5-min). These off-catalase radical species takes longer time to resolve, consistent with the slow return of the resting enzyme.

The power saturation profiles for the narrow doublet (i.e., 10 ms and 50 ms), the exchange-coupled radical (i.e., 15 s, 17 s, 20 s, 23 s, 43 s, 1 min and 2 min) and the narrow singlet (i.e., 5 min) are very different. We used the spectra samples reacted after a 10-ms, 15-s and 5-min as representatives (Fig. 3.2.12). It is worth highlighting that the normalized intensity of the narrow doublet species and the exchange-coupled radical species detected across all the samples cannot be well-fitted to the equation, suggesting that more than one radical species are present. No good $P_{1/2}$ was obtained due to the poor fitting, however, manifestly the power saturation characteristic of the narrow doublet was largely different from that of the exchange-

coupled radical species. The narrow doublet was easily saturated, consistent with that it is a relatively isolated organic radical tentatively assigned to MYW adduct radical. In contrast, the exchange-coupled radical was much more resistant to power saturation than the narrow doublet, whether measured at 3300 G or by peak to trough (p/t) intensity. Notably, the broadening feature measured at 3300 G was even more resistant to power than that measured by peak to trough intensity, consistent with its assignment to exchange-coupling to the heme. The fact that different regions of the exchange-coupled singlet showed different power saturation characteristics suggests more than one radical species are overlapping. In support of this idea, when spectra were recorded at 77 K, the exchange-coupled feature observed at 4.5 K dropped out, and a narrow singlet was detected, suggesting more remote radical species coexist with the proximal Trp radical.

Interestingly, this narrow doublet (R418N 10 ms) contrasted to that detected in a 10-ms reaction time of *wt*KatG with H_2O_2 at pH 5, in that the normalized signal intensites of the later species were well-fitted to the equation. This difference suggests that radical species other than the catalase-competent MYW adduct radical accumulate during the earliest time regimes of catalase activity by R418N, whereas this phenomenon may not be as prominent in *wt*KatG at pH 5 to be detected. In fact, we observed the rapid spectra change from compound III to a compound II-like intermediate by stopped-flow upon reaction of both R418N variant and *wt*KatG with H_2O_2 at pH 5 within 500 ms (Fig. 3.2.8A). But the frequency of off-pathway electron transfer is much more higher when the Arg switch is abolished completely by mutagenesis.

The narrow singlet radical observed at 5-min was relatively susceptible to power saturation with $P_{1/2} \sim 1.05$ μW (Fig. 3.2.12C,D). Interestingly, it is the only one that can be well-

fitted, indicating that the remote protein-based radicals observed far after reaction was done were likely have similar power saturation characteristics.

We also recorded EPR spectra at 77 K, along with the 4.5 K. The rationales are (1) low temperature (< 10 K) is optimum for detection of exchange-coupled signals or ferric heme signals, whereas at higher temperature (i.e., 77 K) other organic signals can be detected without interference from either exchange-coupled signals and/or ferric heme signals; and (2) the narrow doublet signal easier to be saturated at 4.5 K, can be better resolved at 77 K.

We observed the narrow doublet radical species detected in samples quenched at 10-ms and 50-ms were well resolved when spectra were recorded at 77 K, sharply contrast to those recorded at 4.5 K and 1 mW, where it was saturated (Fig. 3.2.13).

The spectra recorded at 77 K for samples quenched after a 17-s, 20-s, 23-s, 60-s reaction time showed only the narrow singlet. These were attributed to more remote radicals. The combination of 4.5 K and 77 K data suggest the co-existence of Trp 321 radical and more remote protein-based radical species (Fig. 3.2.14).

Taken together, our freeze-quench EPR data are in good agreement with our stopped-flow results where the re-emergence of the ferric state lags behind the depletion of H_2O_2. This is an indication of off-pathway electron transfer. Indeed, the primary catalase-inactive intermediate to accumulate during R418N catalase catalysis contains a protein-based radical distinct from the $MYW^{\bullet+}$ narrow doublet. The exchanged coupling observed from this species is consistent with the proximal tryptophan (Trp 321) as the site of protein radical accumulation with subsequent radical migration away from the active site. R418N showed exactly the same sequence of radical intermediates transition (i.e., $[MYW^{\bullet+}] \rightarrow [W321^{\bullet+}] \rightarrow [W/Y^{\bullet+}]$) as *wt*KatG during catalase catalysis at pH 5, we previously reported (Fig. 3.2.15).[129] These suggest that the proximal

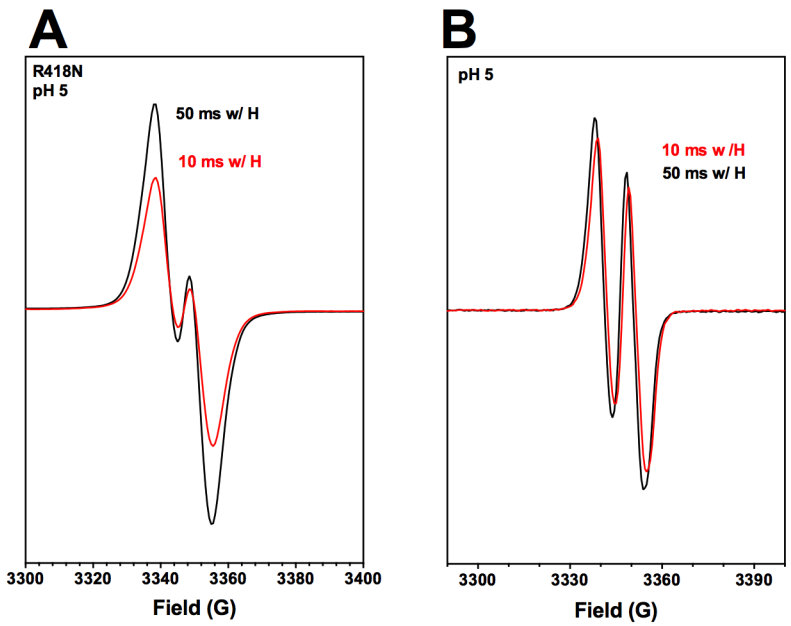

Figure 3.2.13. Comparison of the narrow doublet recorded at 4.5 K and 77 K. Spectra (A) were recorded at 4.5 K. Spectra (B) were recorded at 77 K. All spectrometer settings were as described under "Experimental procedures."

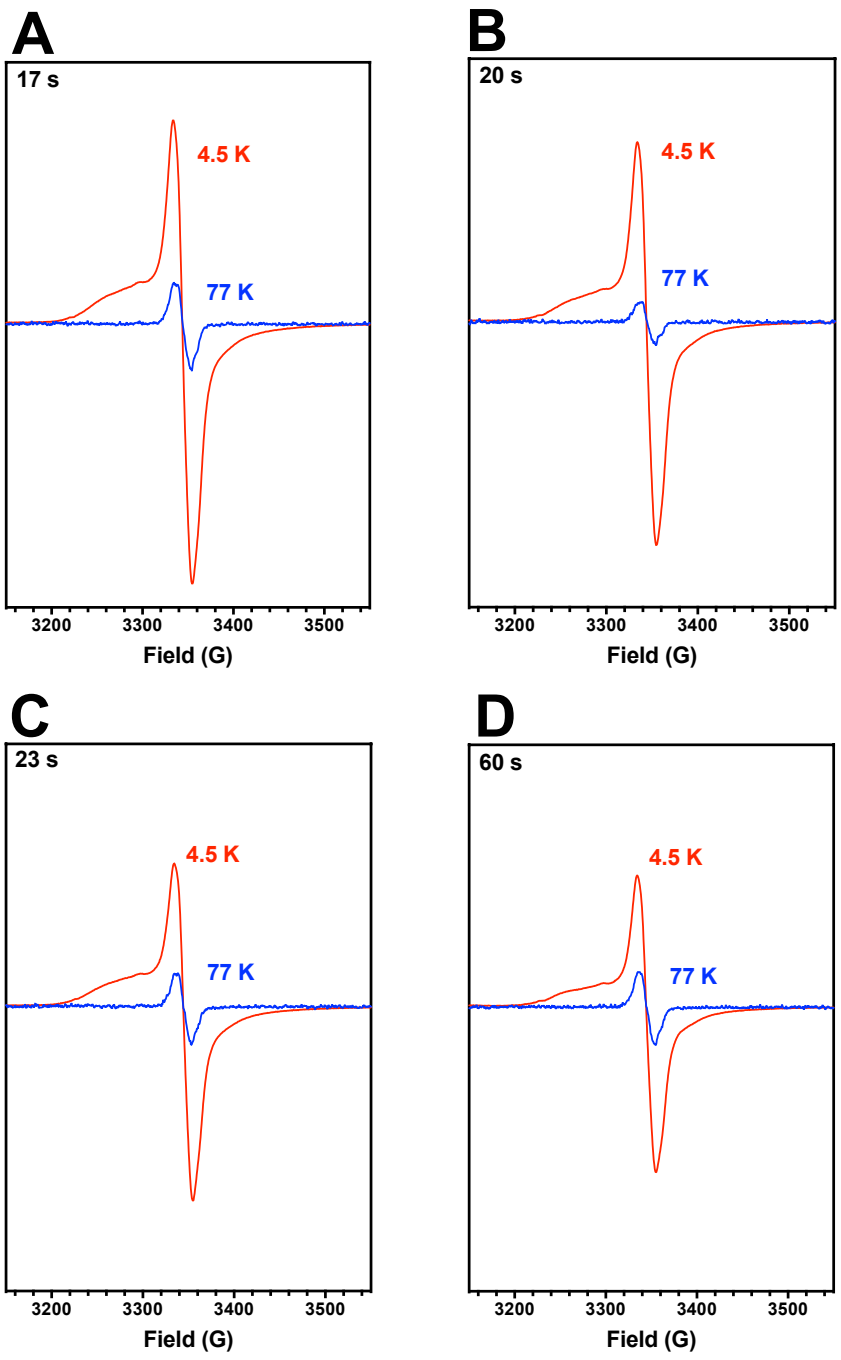

Figure. 3.2.14. Comparison of protein-based radicals recorded at 4.5 K and 77 K during R418N KatG reaction with H_2O_2 at pH 5. Protein-based radicals (g ~ 2) of R418N reacting with 667 molar excess of H_2O_2 over time are shown. Spectrometer settings were as described under "Experimental procedures." 4.5 K data are shown in *red line*. 77 K data are shown in *blue line*. A, B,C, D panels are shown samples quenched at time 17-s, 20-s, 23-s, 60-s respectively.

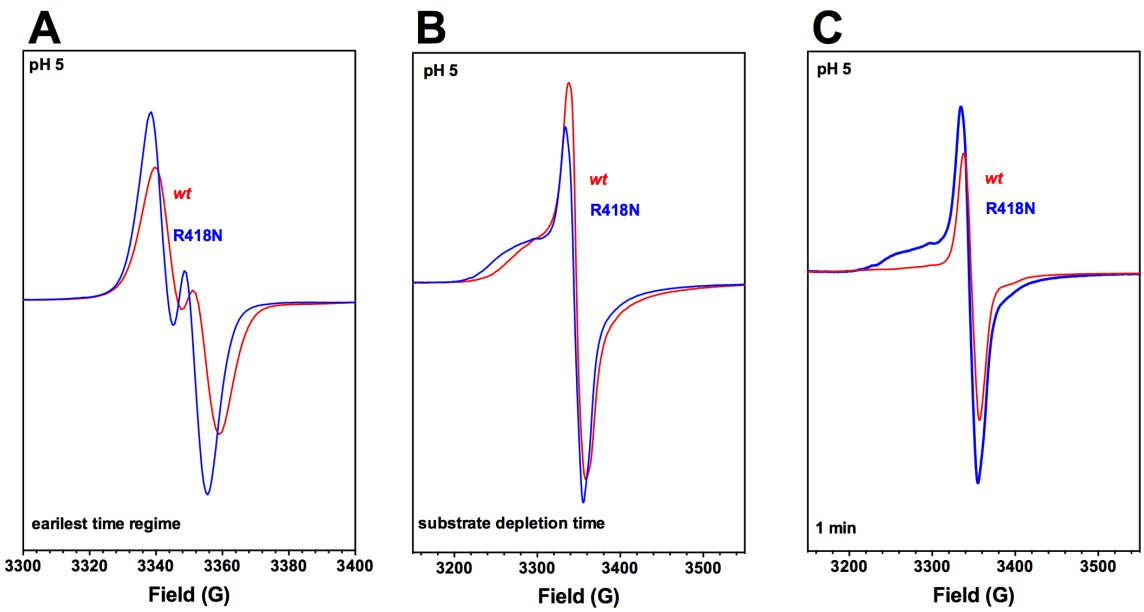

Figure 3.2.15. Comparison of protein-based radicals detected at crucial time points during *wt* and R418N KatG reaction with H_2O_2 at pH 5. The signals at g ~ 2 regime are shown. R418N is compared to *wt*KatG reacting with 667 molar excess of H_2O_2 at pH 5. (A) shows the radical signal in 10 ms samples. (B) shows the radical signal in the samples quenched at substrate depletion time, 23-s for R418N *vs.* 6-s for *wt*KatG. (C) shows the radical signal in the samples quenched 1-min. (D) shows the radical signal in the samples quenched 5-min. Reactions were carried out at 4 °C in 50 mM acetate, pH 5. All spectra were recorded at 4.5 K, Spectrometer settings were as described under "Experimental procedures." Samples were prepared and evaluated as described for Fig. 3.2.10.

tryptophan (Trp 321) is the primary conduit for off-catalase electron transfer, when the Arg switch is withdrawn either by mutagenesis (i.e., R418N at pH 5) or by lower pH (i.e., *wt*KatG at pH 5).

3.2.7 Effect of PxEDs on protein-based radicals of R418N KatG reactions with H_2O_2 at pH 5

To examine the effects of PxED on the intermediates formed upon reaction of R418N with H_2O_2, similar rapid freeze-quench EPR experiments at pH 5 were performed in the presence of PxED (ABTS/ascorbate). With PxED included in the reaction mixture, R418N showed a complete loss of the high spin ferric signal as well as formation of the same narrow doublet 10 ms after mixing with H_2O_2 as was observed without PxED (Fig. 3.2.16; 3.2.17). Thus, PxED did not interfere with the formation of the catalatic-essential MYW cofactor radical intermediate. The sample quenched at near-substrate depletion time (4.5 s) showed a narrow doublet with substantially lower intensity (Fig. 3.2.16C), which represented the decreasing steady-state level of the radical intermediate as the peroxidase concentration dropped. The sample quenched at 20-s and 50-s reaction time both showed the return of ferric enzyme, with 50-s sample showing higher contribution of the resting state. Neither of them had detectable protein-based radicals at 20-s and 50-s reaction time (Fig. 3.2.16C).

Therefore, we observe inclusion of ABTS in the reaction of R418N KatG with H_2O_2 does not interfere with the formation of MYW radical, which is essential for catalase activity (Fig. 3.2.17A,B). But all other protein-based radicals are undetected in samples quenched at later time points when PxED is present. For example, the exchanged coupled radical detected in sample quenched at 20-s without PxED included was completely eradicated when PxED was present (Fig. 3.2.17B). We previously reported the same phenomenon for *wt*KatG. These data suggest

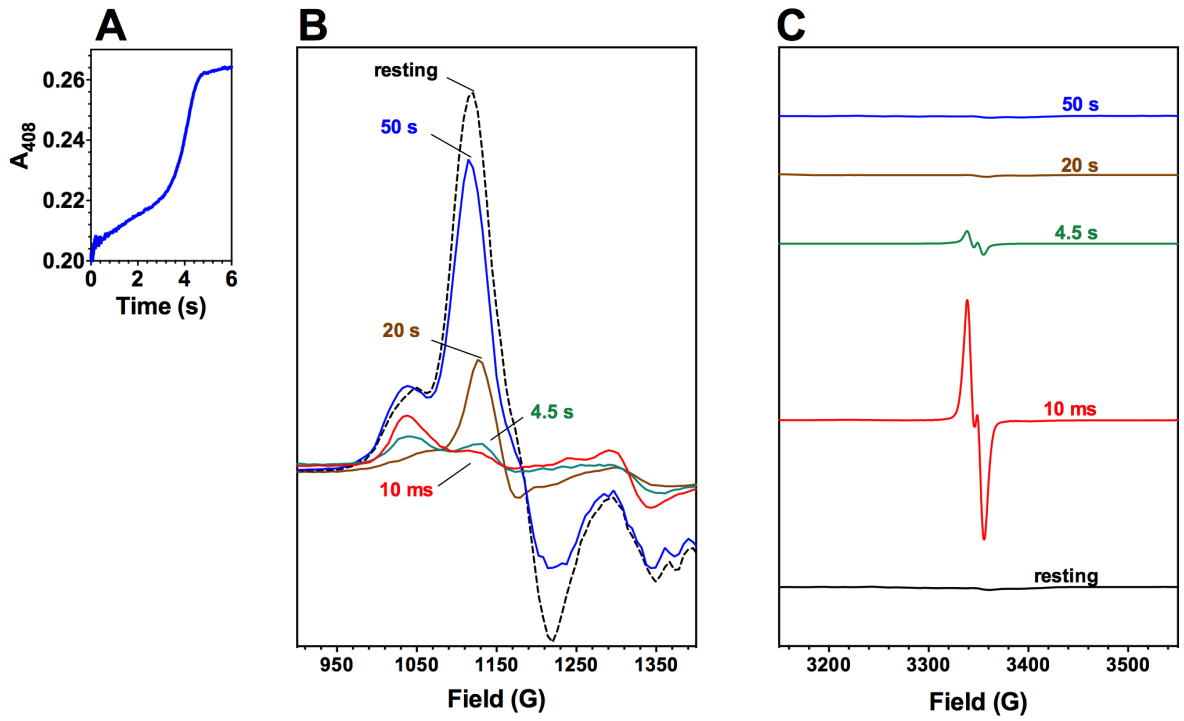

Figure 3.2.16. EPR spectra of freeze-quenched samples from reaction of R418N KatG with H_2O_2 in the presence of ABTS at pH 5. The stopped-flow trace monitoring return of ferric enzyme at 408 nM during R418N reaction with 667eq. H_2O_2 in the presence of 0.1 mM ABTS are shown in A. High spin ferric species typical of KatG resting state (g ~ 6) are shown in B, and the g// component of the resting state as well as protein-based radicals (g ~ 2) of R418N are shown in C. The molar proportions of enzyme to H_2O_2 used for stopped-flow experiments (1:667) were maintained for these experiments and ABTS. The concentration of ABTS and ascorbate were 1.0 and 5.0 mM, respectively. Reactions were carried out at 4 °C in 50 mM acetate, pH 5. All spectra were recorded at 4.5 K. Reaction conditions, sample preparation, and evaluation were as described for Fig. 3.2.10. Spectrometer settings were as described under "Experimental procedures."

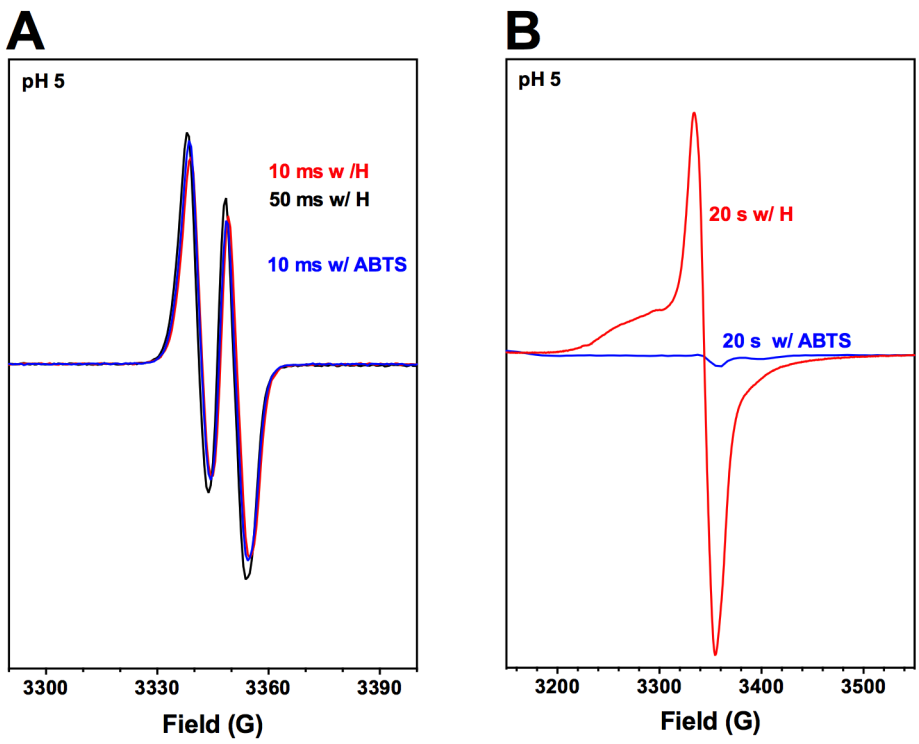

Figure 3.2.17. Effect of PxED on the protein-based radicals at earliest time regime and later time points for R418N reacting with H_2O_2 at pH 5. Spectra in (A) were recorded at 77 K to minimize power saturation of the narrow doublet radical observed at 4.5 K. Spectra in (B) were recorded at 4.5 K. All spectrometer settings were as described under "Experimental procedures."

that PxED rescues the inactive catalatic intermediates, primarily starts from W321 oxidation, thus preserves KatG catalase activity.

3.2.8 R418N KatG intermediates observed upon reaction with H_2O_2 at pH 7

We performed similar stopped-flow experiments by reacting wild-type and R418N KatG with varying H_2O_2 concentration in the absence and presence of PxED at pH 7, to evaluate the dominant heme intermediate(s) present during catalatic H_2O_2 degradation. Similarly, we used the ascorbate-based method to suppress spectral interference due to the accumulation of $ABTS^{\bullet+}$.[134] As such, the term "PxED" in these experiments refers to a mixture of ABTS and ascorbate.

We observed R418N exhibited much slower rate of consuming a certain concentration of H_2O_2 (relatively lower molar excess of H_2O_2 in stopped-flow) at pH 7 than pH 5. This was consistent with that R418N showed around 10-fold increase of k_{on} of the catalase activity at pH 5 compared to pH 7, even though k_{cat} remained unchanged at pH 5 and 7 (Table 3.1.2). Despite of these differences, the reemergence of the ferric enzyme lagged much behind the substrate depletion during reaction of R418N with H_2O_2 at pH 7, similar to R418N at pH 5 and *wt*KatG at pH 5. In contrast, *wt*KatG at pH 7 was 35-fold faster than R418N variant to deplete 2 mM H_2O_2 (i.e., ~ 2 s for *wt vs.* ~ 70 s for R418N). Further, ferric state returned immediately after *wt*KatG depleted H_2O_2.

We observed the spectra at the earliest time regime (i.e., 5 ms) of R418N reacting with 2 mM H_2O_2 included a Soret at 418 nm and α, β bands maxima at 580 and 542 nm (Fig. 3.2.18B). These spectra were consistent with the oxyferrous/ferric superoxide intermediate (i.e. Fe^{III}-$O_2^{\bullet-}$), which is catalatic competent. We observed nearly identical spectra (i.e. Fe^{III}-$O_2^{\bullet-}$) at the earliest time points for R418N and *wt*KatG at both pH 5 and 7. The spectra were almost unchanged from 5 ms to 3.7 s, except very slight decrease in the Soret band at 418 nm. During this time regime

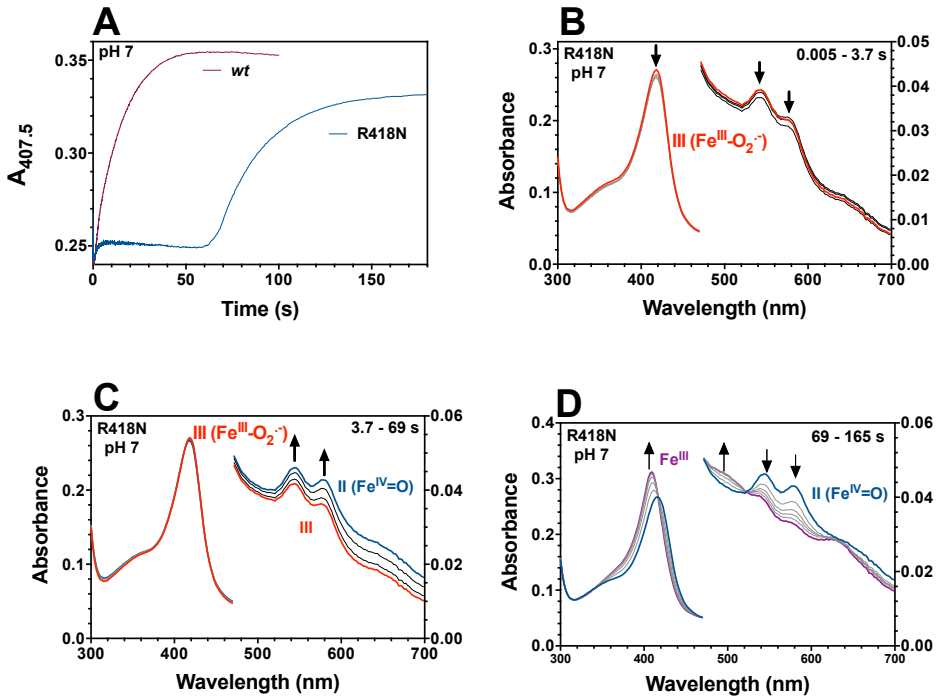

Figure 3.2.18. Spectra collected during reaction of R418N KatG with 2.0 mM H_2O_2 at pH 7. The change in absorbance at 407.5 nm over the entire course of the reaction (A) is shown. Spectra corresponded to 0.005 – 3.7 s (B), 3.7 – 69 s (C), and 69 – 165 s (D) following mixing of 3 μM enzyme and 2.0 mM H_2O_2. This reaction was carried out in 100 mM phosphate pH 7 at 4 °C.

the slight increase of the absorbance at 408 nm was observed (Fig. 3.2.18A). This increase of the absorbance at 408 nm did not seem to be H_2O_2 concentration dependent. From 3.7 s to 69 s (the steady-state phase), we observed the broad increase in absorption above 520 nm, with α, β bands maxima at 584 and 546 nm (Fig. 3.2.18C), with the Soret peak absorbance unchanged. The ferric enzyme slowly returned afterward (Fig. 3.2.18D). We are not sure about what occurs in the first stage (i.e., 5 ms to 3.7 s). This is only observed at pH 7, not at pH 5. But we reason it is not a primary concern. Instead, the highly similar spectra progression from an oxyferrous intermediate to a state featured with a broad increase in absorption above 520 nm was worth highlighting. We saw a highly similar spectra progression upon reaction of R418N with H_2O_2 at pH 5, as well as that of *wt*KatG at pH 5. These data suggest that accumulation of inactive intermediates due to off-catalase electron transfer during catalase catalysis of R418N at pH 7 is a likelihood. And supportive of this idea is the slow return of the ferric enzyme.

Inclusion of PxED also stimulated H_2O_2 consumption and ensured a much faster regeneration of the resting state for R418N reaction with H_2O_2 at pH 7, similar to that at pH 5 (data not shown). We observed nearly the same spectrum included a Soret at 416 nm and α, β bands maxima at 580 and 542 nm at the earliest turnover (i.e., 10 ms), as was observed in the absence of ABTS. But what was distinct from the reactions in the absence of PxED was the fast return of this Fe^{III}-$O_2^{\bullet-}$ heme intermediate to the ferric resting state after substrate depletion without accumulation of other species. In contrast, inclusion of PxED offered little improvement to *wt*KatG at the same condition with respect to both the steady-state turnover and the return of the ferric enzyme afterwards, consistent with that PxED-unassisted *wt*KatG is robust enough at pH 7.

We also examined the protein-based radical(s), tracked the disappearance and appearance of the high spin ferric enzyme during the reaction of R418N with H_2O_2 at pH 7 by RFQ-EPR. Reaction of R418N with 667 eq. of H_2O_2 produced a nearly identical narrow doublet radical at 10 ms, as at pH 5 (Fig. 3.2.19C). This radical was also observed with the reaction quenched at 50 ms. These two samples showed a near complete loss of the ferric heme (Fig. 3.2.19B). Thus, similar to R418N KatG at pH 5, the combination of our optical stopped-flow and RFQ-EPR data suggest that the dominant steady-state intermediate catalase activity at the earliest turnover at neutral pH is still consistent with Fe^{III}-$O_2^{\bullet-}$ $[MYW]^{\bullet+}$.

The narrow doublet was replaced by a protein-based singlet radical species at 15 s, similar to that at pH 5 (Fig. 3.2.19; 3.2.20). This radical was very broad (>300 G), suggesting that there was exchange coupling with the heme iron. Based on its high resistance to saturation and temperature dependence, it was consistent with $W321^{\bullet+}$ (Fig. 3.2.21). Notably, its wing intensity at 3300 G was much lower than that of R418N sample quenched at 15 s at pH 5 (Fig. 3.2.20).

The broadening was still visible in the sample quenched at 20 s (Fig. 3.2.20). Some feature of the broadening was noticeable with the samples quenched at 30 s and 40 s. In the samples quenched thereafter (i.e., 60 s, 70 s, 100 s, 5 min), only the narrow singlet was seen. The g_z component of the high spin ferric signal was shown in samples quenched at 40 s and thereafter, consistent with the presence of high spin ferric enzyme in g ~ 6 region. This feature was not seen with samples quenched at 15 s, 20 s and 30 s, likely was masked by the broadening of the signal. We also observed the protein-based radicals persisted far longer after substrate depletion (70 s).

The power saturation profiles for the narrow doublet (i.e., 10 ms and 50 ms), the exchange-coupled radical (i.e., 15 s, 20 s) and the narrow singlet (i.e., 70 s) are very different.

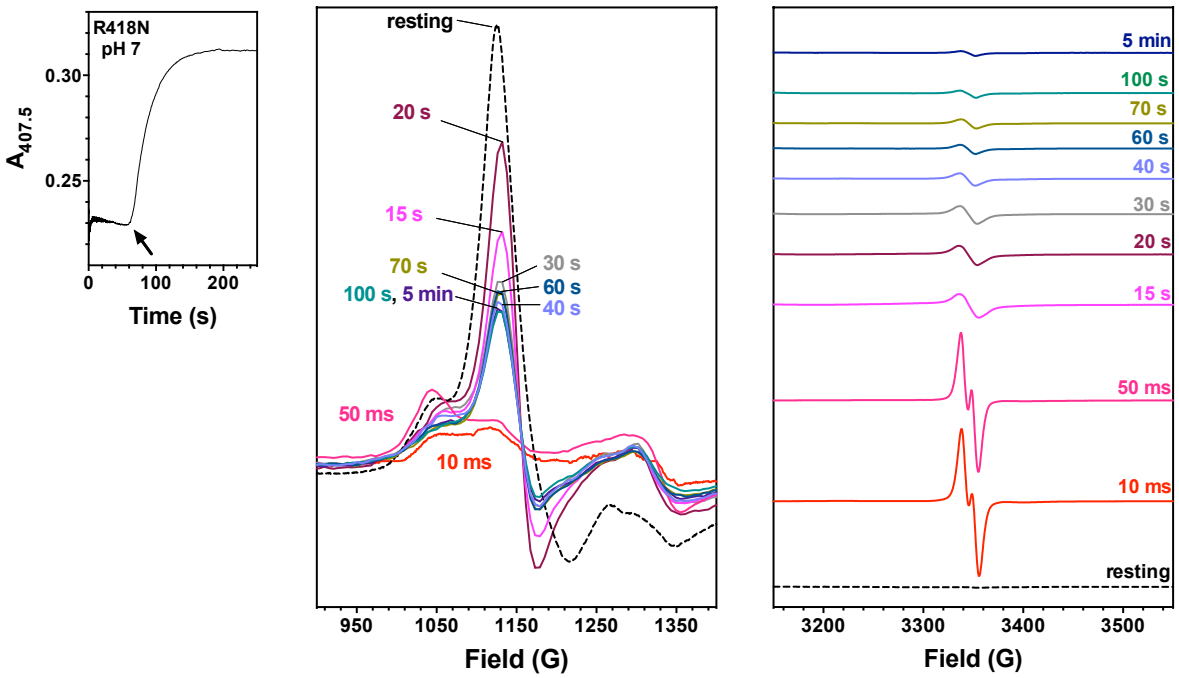

Figure 3.2.19. EPR spectra of freeze-quenched samples from reaction of R418N KatG with H_2O_2 at pH 7. The stopped-flow trace monitoring return of ferric enzyme at 408 nm during R418N reaction with 667eq. H_2O_2 are shown in A. High spin ferric species typical of KatG resting state (g ~ 6) are shown in B, and the g// component of the resting state as well as protein-based radicals (g ~ 2) of R418N are shown in C. The molar proportions of enzyme to H_2O_2 used for stopped-flow experiments (1:667) were maintained for these experiments. Consequently, ferric enzyme (150 μM after mixing) was reacted with H_2O_2 (100 mM after mixing) for the time indicated prior to freeze-quenching. Reactions were carried out at 4 °C in 100 mM phosphate, pH 7. The resting R418N KatG was prepared the same way except no H_2O_2 included and quenched manually. (grammer OK?) All spectra were recorded at 4.5 K, if not indicated otherwise. Spectrometer settings were as described under "Experimental procedures." Specifically, Instrument parameters were as follows: microwave frequency, 9.393 GHz; modulation amplitude, 2 G; modulation frequency, 100 kHz; microwave power, 1 milliwatt; time constant, 163.84 ms; sweep time 335.54 s; number of scans, 1; conversion, 327.68 ms; resolution, 1024 point; receiver gain, 1.0×10^4; and phase, 0 degrees.

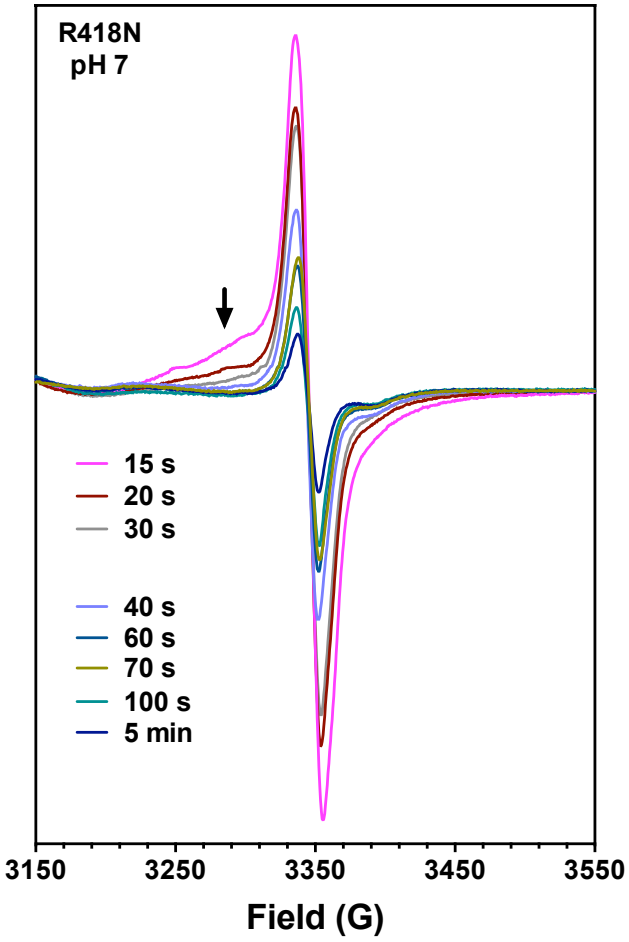

Figure 3.2.20. comparison of the singlet radicals detected in freeze-quenched samples from reaction of R418N KatG with H_2O_2 at pH 7. Reaction conditions, sample preparation, and evaluation were as described for Fig. 3.2.19. Spectrometer settings were as described under "Experimental procedures."

We used the spectra samples reacted after a 10-ms, 15-s and 70-s as representatives (Fig. 3.2.21). The normalized intensities of the narrow doublet species and the exchange-coupled radical species as well as the singlet detected across all the samples cannot be well fitted to the equation, suggestive of the heterogeneity of the radical species present. No good $P_{1/2}$ was obtained due to the poor fitting, however, the power saturation characteristic of the exchange-coupled radical species was largely different from both the narrow doublet and narrow singlet species. The exchange-coupled radical was much more resistant to power saturation than the narrow doublet, whether measured at 3300 G or by peak to trough (p/t) intensity. Notably, the broadening feature measured at 3300 G was even more resistant to power than that measured by peak to trough intensity, consistent with its assignment to exchange-coupling to the heme. The fact that different regions of the exchange-coupled singlet showed different power saturation characteristics suggests more than one radical species are overlapping. In support of this idea, when spectra were recorded at 77 K, the exchange-coupled feature observed at 4.5 K dropped out, and a narrow singlet was detected, suggesting more remote radical species coexist with the proximal Trp radical. In contrast, the narrow doublet and narrow singlet were both easily saturated, consistent with that it is a relatively isolated organic protein-based radical species.

We detected the exchange-coupled radical after a 15-s time upon reaction of R418N KatG variant with H_2O_2 at both pH 7 and 5, suggesting W321 is a hot spot of oxidation in the absence of the Arg switch. Two major differences observed in reactions of R418N with H_2O_2 at pH 5 *vs.* pH 7 are worth highlighting (Fig. 3.2.22). First, the timeline during which the exchange-coupled radical is detected upon reaction of R418N with H_2O_2 at pH 5 (15 s → 2 min), is much longer than that by R418N at pH 7 (15 s → 40 s). Second, the intensity of later radical detected

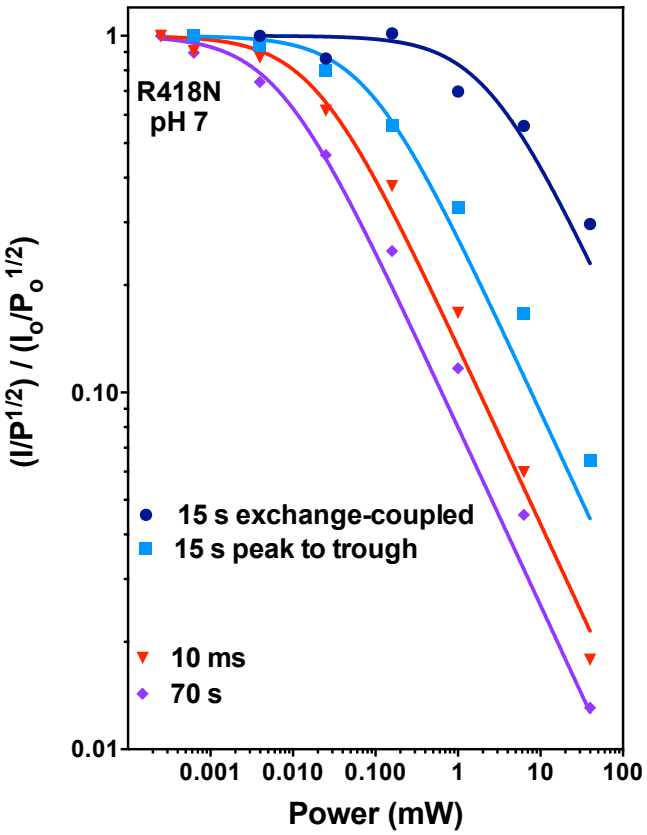

Figure 3.2.21 Evaluation of protein-based radicals detected during R418N KatG reaction with H_2O_2 at pH 7. The normalized signal intensities for samples collected 10 ms, 15 s and 70 s after R418N KatG reaction with H_2O_2 at pH 7 as a function of microwave power are shown. For exchanged coupled radical at 15 s, the intensity at 3300 G as well as that of the peak to trough were used. For 10 ms and 70 s samples, the peak to trough intensity was used. Unless otherwise indicated, all spectra were recorded at 4.5 K with all other spectrometer settings as described in "Experimental procedures" Samples were prepared and evaluated as described for Fig. 3.2.19.

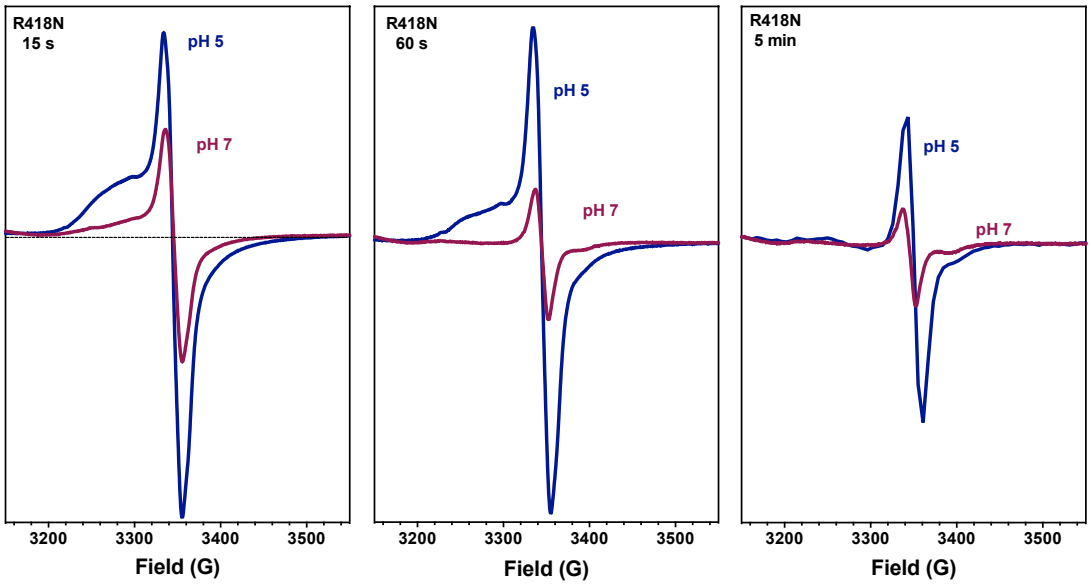

Figure 3.2.22. Comparison of intensity of later radical species detected in reaction of R418N with 667 eq. of H_2O_2 at pH 5 and pH 7. Reaction conditions, sample preparation, and evaluation were as described in Fig 3.2.10 (pH 5 reactions) and Fig. 3.2.19 (pH 7 reactions). Spectrometer settings were as described under "Experimental procedures."

during R418N reacting with H_2O_2 at pH 5 are much higher than that at pH 7 across the reaction timeline. We attribute these differences to a much frequent off-catalase electron transfer at pH 5 than pH 7, as demonstrated by a higher $ABTS^{\bullet+}$ generated with consumption of 2 mM H_2O_2 at pH 5 compare to pH 7 (Refer to Fig. 3.2.6A,C). And it is also likely the participation of Trp 321 oxidation increased as the frequency for off-pathway electron transfer increased at pH 5 for the variant. With all the differences, we highlight Trp 321 is the primary conduit for off-pathway electron transfer for R418N at both pH.

In addition, at variance to what we observed at pH 5, a high fraction of ferric signal was present in all samples quenched at 15-s, 20-s, 30-s, 40-s, and 60-s, prior to the substrate depletion time (i.e., 70 s) as estimated by SF at pH 7 (Fig. 3.2.19A). But we did not find evidence of the ferric enzyme in the corresponding stopped-flow experiment (Fig.3.2.18). Indeed, charge-transfer band at 640 nM, the hallmark of the ferric enzyme, was absent during steady-state turnover of catalase activity of R418N at pH 7 by stopped-flow. Moreover, the Soret peak was red shifted to 414 nm during steady-state turnover. Given the fact that we observed the ferryl species replaced the oxyferrous heme species as turnover proceeded towards substrate depletion, it was possible that the ferric signal was masked by other species due to the dubious nature of UV-visible spectroscopy. And this may be captured by EPR, because of its rigorousness and sensitivity for ferric species. Alternatively, it is likely the condition of the RFQ is not comparable to SF in this case. Specifically, although we maintained the same substrate to enzyme ratio for SF (3 μM enzyme and 2 mM H_2O_2) and RFQ (150 μM enzyme and 100 mM H_2O_2) experiment, they may not behave exactly the same due to factors such as solubility, packing of the EPR samples, and so on.

We compared the radical spectra recorded at both 77 K and 4.5 K in reactions quenched at 15-s, 20-s, 60-s, 70-s, 80-s, and 5-minute. We saw the radical intensity diminished over time, regardless of the temperature (Fig. 3.2.23). Furthermore, the exchanged feature observed in the samples quenched at 15-s and 20-s at 4.5 K was absent when recorded at 77 K, consistent with its temperature-sensitive characteristic. These data also suggest reactions quenched at 15-s and 20-s have multiple protein-based radical species present: the coexistence of W321 radical (featured by exchange-coupled radical) and remote radicals (featured by narrow singlet radical).

With all the differences between R418N reacting with 667 molar excess of H_2O_2 at pH 7 and that at pH 5, we emphasize some similarities. First, the narrow doublet radical assigned to $MYW^{\bullet+}$ does not persist throughout the time course of turnover of H_2O_2, and is replaced by the catalase-inactive species whose signal was distinct from the narrow doublet. Second, the exchange-coupled radical is consistent with the proximal trypotophan (Trp 321) as the primary site of oxidation. Third, subsequent radical hopping towards remote amino acids occur over time and protein-based radical were persistent for a long time after reaction. These data suggest R418N also uses the Trp 321 as the primary route for off-pathway electron transfer during catalase catalysis at pH 7, as it does at pH 5.

3.2.9 Effect of PxEDs on protein-based radicals of R418N KatG reactions at pH 7

To examine the effects of PxED on the intermediates formed upon reaction of R418N with H_2O_2, we performed similar rapid freeze-quench EPR experiments at pH 7 reacting R418N with 667 molar excess of H_2O_2 in the presence of PxED (ABTS/ascorbate) (Fig. 3.2.24B,C). R418N showed the same narrow doublet at 10 ms after mixing with H_2O_2 as was observed without PxED (Fig. 3.2.24C, 3.2.25A) Spectra recorded for samples quenched at the time of

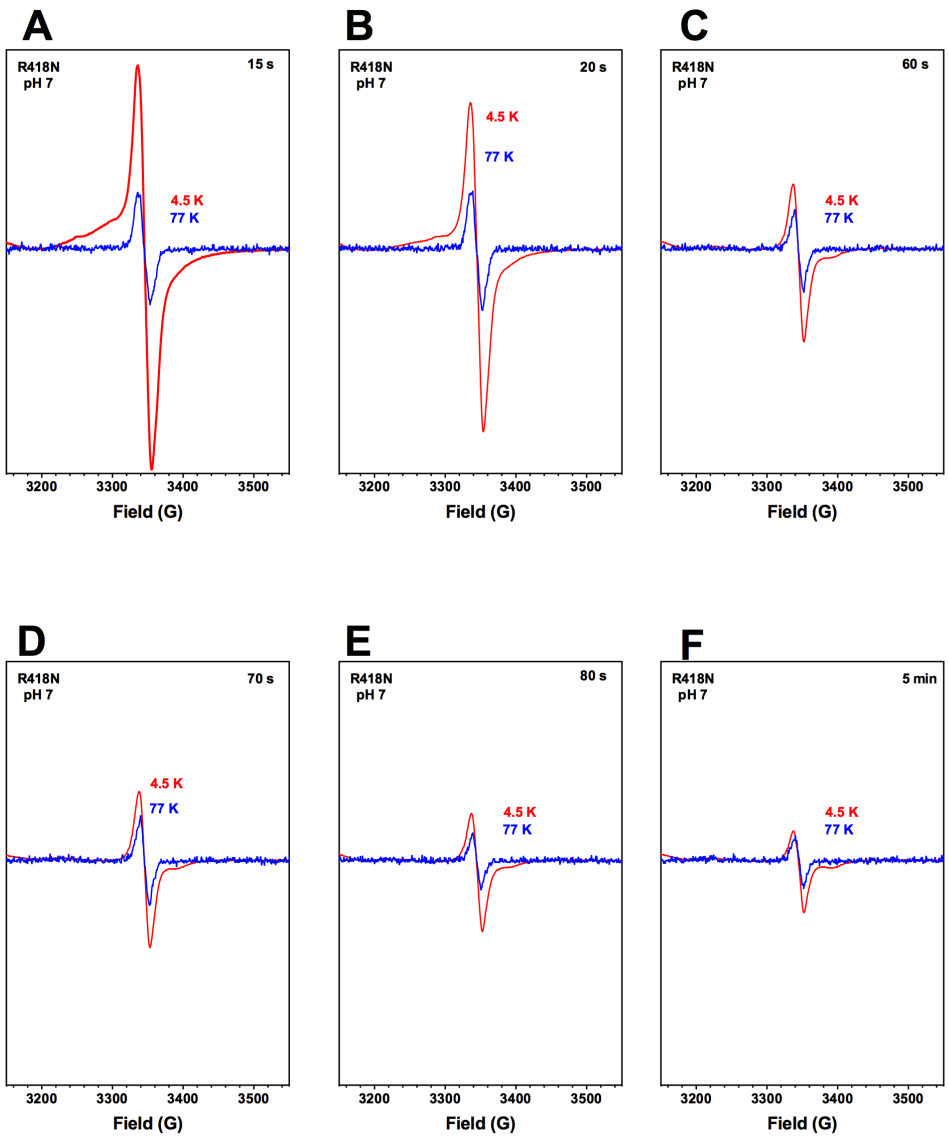

Figure 3.2.23 Comparison of protein-based radicals recorded at 4.5 K and 77 K during R418N KatG reaction with H_2O_2 at pH 7.

protein-based radicals (g ~ 2) of R418N reacting with 667 molar excess of H_2O_2 over time are shown. Spectrometer settings were as described under "Experimental procedures." 4.5 K data are shown in *red line*. 77 K data are shown in *blue line*.

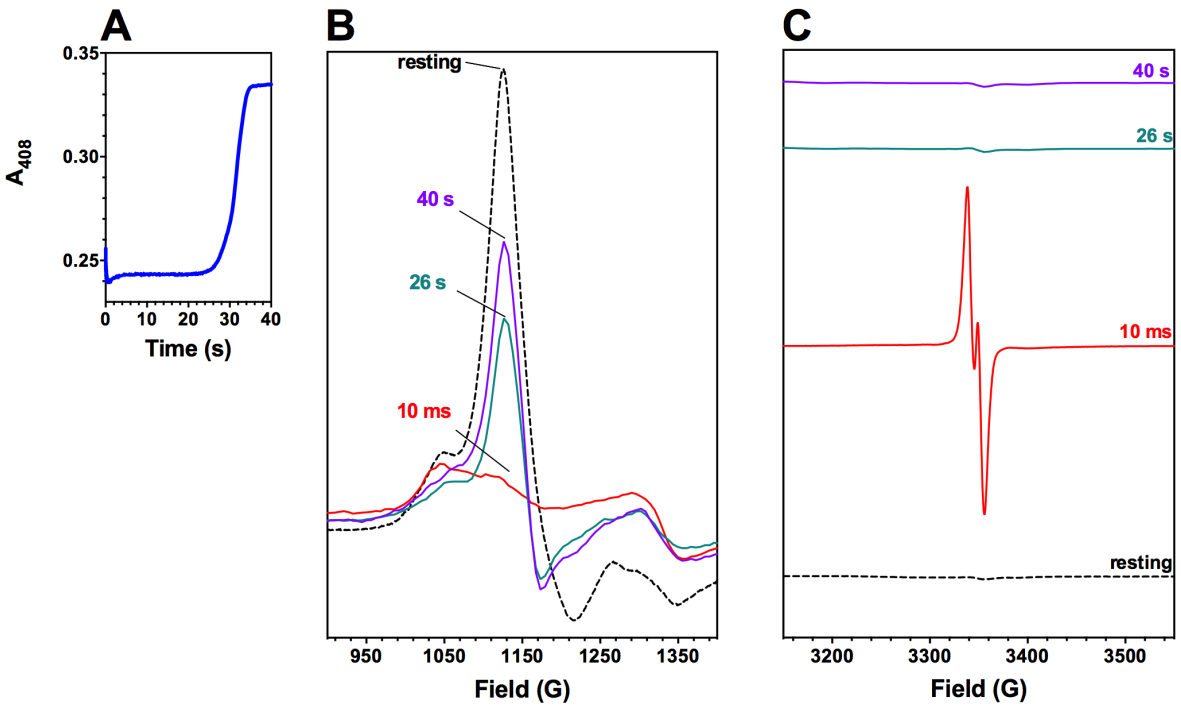

Figure 3.2.24 EPR spectra of freeze-quenched samples from reaction of R418N KatG with H_2O_2 in the presence of ABTS at pH 7. The stopped-flow trace monitoring return of ferric enzyme at 408 nM during R418N reaction with 667eq. H_2O_2 in the presence of 0.1 mM ABTS are shown in A. High spin ferric species typical of KatG resting state (g ~ 6) are shown in B, and the g// component of the resting state as well as protein-based radicals (g ~ 2) of R418N are shown in C. The molar proportions of enzyme to H_2O_2 used for stopped-flow experiments (1:667) were maintained for these experiments and ABTS. The concentration of ABTS and ascorbate were 1.0 and 5.0 mM, respectively. Reactions were carried out at 4 °C in 50 mM acetate, pH 5. All spectra were recorded at 4.5 K. Reaction conditions, sample preparation, and evaluation were as described for Fig. 3.2.19, except in the presence of ABTS (2 mM) and ascorbate (4 mM) Spectrometer settings were as described under "Experimental procedures."

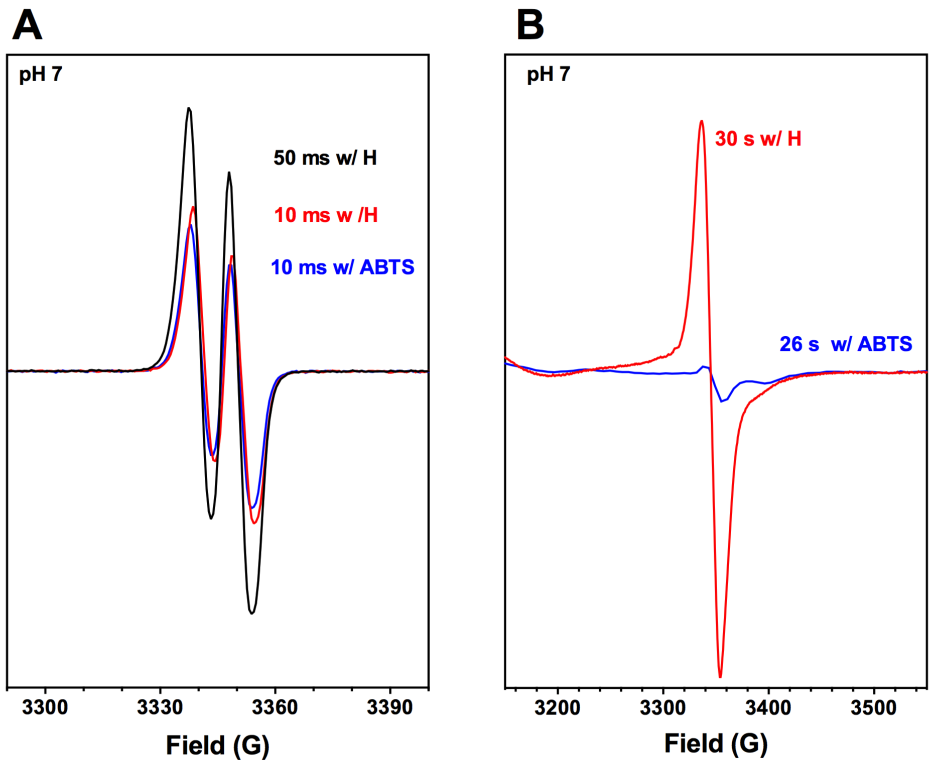

Figure 3.2.25 Effect of PxED on the protein-based radicals at earliest time regime and later time points for R418N reacting with H_2O_2 at pH 7. Spectra in (A) were recorded at 77 K to minimize power saturation of the narrow doublet radical observed at 4.5 K. Spectra in (B) were recorded at 4.5 K. All spectrometer settings were as described under "Experimental procedures."

substrate depletion or thereafter showed minimal, if any, contribution from protein-based radicals, as well as the return of ferric enzyme (Fig. 3.2.24B,C). Clearly, the singlet radical detected in sample quenched after a 30-s mix without PxED was not detected in the sample quenched after a 26-s mix with PxED present (Fig. 3.2.25B), suggesting that PxED rescues inactive species, and thereby preserves the catalase activity.

3.2.10 Conclusions

The presence and conformation of Arg switch preserves KatG catalase activity by limiting off-pathway electron transfer, the primary candidate of which is through Trp 321. Indeed, we established that the absence of the Arg switch by orientation (*wt*KatG at pH 5) or by mutagenesis (R418N) leads to an increased frequency of off-pathway electron transfer events as well as higher susceptibility to H_2O_2-dependent inactivation of KatG. The proximal Trp 321 is the primary conduit leading to inactive catalatic intermediates, the continuation of which eventually results in inactivation of KatG. PxEDs resolve inactive species and restore catalase activity through Trp 321 conduit.

3.3 The ^{px}Trp in catalysis and inactivation: Properties and intermediates of W321F/R418N KatG

Because the proximal Trp 321 is the conduit for off-pathway electron transfer when the Arg switch is withdrawn either by manipulating pH (i.e., *wt*KatG at pH 5) or by mutagenesis (i.e., R418N at pH 5 and 7), two questions need to be resolved. First, is W321 the sole route for off-pathway electron transfer or does other route(s) bypassing W321 also operate? Second, why is Trp 321 strictly conserved across all KatGs by evolutionary biology, if its oxidation kicks of inactivation? To answer these questions, we first characterize the W321F/R418N KatG variant and compare it with the R418N KatG variant and *wt*KatG.

3.3.1 Inactivation of W321F/R418N KatG variant during catalatic O_2 production

We performed the same type of experiment as described in Fig. 3.2.1. by reacting W321F/R418N with 100,000 fold H_2O_2 to figure out the cause of reaction cessation at both pH 5 and pH 7. W321F/R418N was inactivated at both pH values, as indicated by the addition of enzyme not H_2O_2 yielding another burst of O_2 production (data not shown). Both W321F/R418N and R418N got inactivated at pH 5 and 7, however, strikingly the oxygen extent of the double variant prior to inactivation was much lower than that of R418N at both pH, indicative of the higher vulnerability of the double variant (Fig. 3.3.1A,B). The difference was especially pronounced at pH 5, W321F/R418N only sustained 1200 ± 110 catalase cycles prior to irreversible inactivation, around 10% of that by R418N, which achieved 12000 ± 1500 catalase cycles. Clearly, the sustainability of catalase activity followed the order *wt*KatG > R418N > W321F/R418N, at both pH 5 and 7, based on the O_2 extent (Fig. 3.3.1A,B). We then performed the same experiment as described in Fig. 3.2.5A by reacting W321F/R418N with 40,000 fold H_2O_2 across pH 5 and 7.5. We confirmed W321F/R418N was inactivated in all the pH values we tested without depleting the substrate, similar to R418N (data not shown). We calculated the

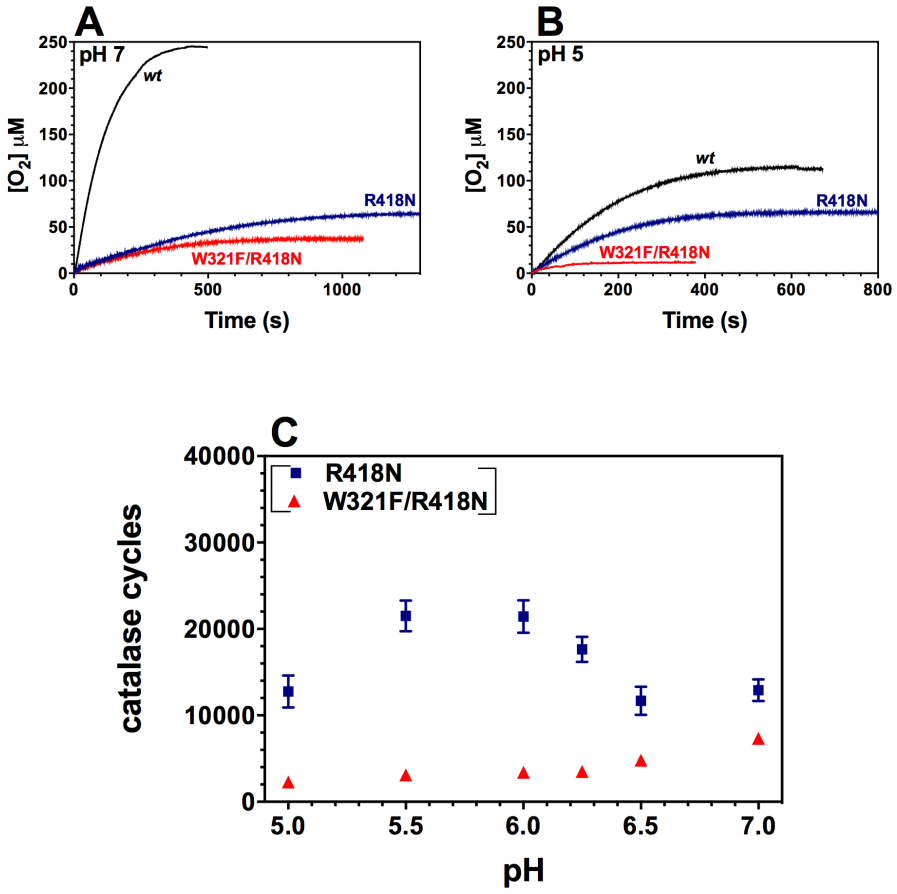

Figure 3.3.1. The effect of pH on catalatic O_2 production by R418N and W321F/R418N KatG. The oxygen extent of *wt,* R418N and W321F/R418N at pH 7.0 (Panel A) and the oxygen extent of *wt*, R418N and W321F/R418N at pH 5.0 (Panel B) are shown. All reactions in (A, B) contained 5 nM KatG, and were initiated by the addition of 0.5 mM H_2O_2. The catalase cycle numbers prior to inactivation are calculated and shown (Panel C). All reactions contained 5 nM KatG, and were initiated by the addition of 0.2 mM H_2O_2. Reactions at pH 6.0, 6.5, 7 were buffered with 100 mM phosphate, and reactions at pH 5.0 and 5.5 were buffered with 50 mM acetate. All reactions were carried out at 23 °C.

catalase cycles that both enzymes sustained accordingly (Fig. 3.3.1C). We observed the double variant was much more vulnerable to inactivation than R418N across the pH tested. Indeed, it became notoriously susceptible to H_2O_2-dependent inactivation as pH went down (i.e., pH 5, pH 5.5). As pH goes up, W321F/R418N was more sustainable as a catalase. However, even that, it was still inferior to R418N as a catalase and only achieved 50 % catalase cycles as that of R418N at pH 7.

This was perplexing, since W321 served as an internal electron donor for off-pathway electron transfer which eventually resulted in the inactivation of KatG. We reasoned eliminating this pathway by mutating oxidizable Trp to non-oxidizable Phe should produce a more robust catalase enzyme in terms of sustainability.

We also pre-incubated W321F/R418N with a range of concentration of H_2O_2, measured catalase activity relative to the control sample after reaction done at pH 7 and 5 (post 1 hour) (Fig. 3.3.2). In sharp contrast to R418N, which showed a clear H_2O_2 threshold beyond which the loss of catalase activity was observed at pH 7, W321F/R418N was much less tolerant to H_2O_2-dependent inactivation and started losing catalase activity from very early turnovers. This is surprising for a catalase that uses H_2O_2 as sole substrate. Consistent with the oxygen extent data, much less molar excess of H_2O_2 inactivates W321F/R418N, compared to that of R418N. The attempts to perform the preincubation of W321/R418N with H_2O_2 at pH 5 and measure residual catalase activity afterwards were not successful. Because of the hyper-vulnerability to cope with H_2O_2 at low pH, it appeared that W321F/R418N did not survive long enough after H_2O_2 challenge to make this type of experiment feasible.

These data again suggest that the sustainability of catalase activity followed the order *wt*KatG > R418N > W321F/R418N at pH 7. And the failure to perform the same experiments

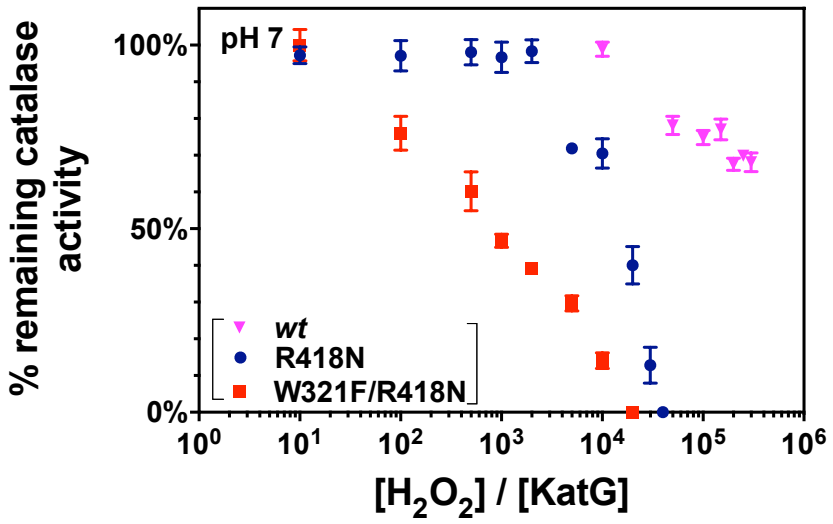

Figure 3.3.2 Effect of H_2O_2 preincubation on the catalase activity of *wt*, R418N and W321F/R418N KatG. Enzyme (200 nM) was preincubated with the indicated concentration of H_2O_2. Preincubations were carried out in either 100 mM phosphate, pH 7.0. Following a 1 hour preincubation, an aliquot was withdrawn and catalase activity was measured with 10 mM H_2O_2 in 100 mM phosphate, pH 7.0 by O_2-senstive electrode. All reactions were carried out at 23 °C.

with the double variant at pH 5 suggests this order holds true at pH 5 as well and the double variant is even more vulnerable at low pH (Refer to Fig. 3.2.2). Therefore, our data are suggestive of the advantageous role of Trp 321 in coping with the off-pathway electron transfer events.

3.3.2 The effect of PxED on W321F/R418N KatG catalase inactivation

Inclusion of ABTS, the double variant was still inactivated during the reaction with 100,000 molar excess of H_2O_2 (Fig. 3.3.3). The inactivation was observed at both pH 5 and 7. At pH 5, W321F/R418N produced 2-fold more O_2 in the presence of ABTS than absence, substantially less than 250 μM O_2 based on the catalase stoichiometry (Fig. 3.3.3A). ABTS did not seem to stimulate the initial rate of catalase activity at pH 5 with this dose of H_2O_2. But the key point was that enzyme was inactivated even with ABTS present. These were in sharp contrast to R418N at pH 5 (Fig. 3.3.3B). Indeed, ABTS not only extended the catalase cycle number to the extent that R418N was still active after depletion of H_2O_2, but also largely stimulated the initial rate of O_2 production (~ 10-fold). At pH 7, ABTS did not seem to either stimulate the initial rate or extend the catalase cycle number upon reaction of W321F/R418N with H_2O_2. These data were again distinct from R418N, where both extension of catalase cycle number and stimulation of the initial rate (pH 7 < pH 5) provided by ABTS were evident (Fig. 3.3.3D). This stood out because this was the first case in which PxED failed to preserve catalase activity of KatG variant in our experience.

Preincubation of W321F/R418N with H_2O_2 in the presence of ABTS at pH 7 showed ABTS provided very limited protection to the remaining catalase activity of the doublet variant (Fig. 3.3.4). In fact, this marginal protection was also reflected by the fact that the

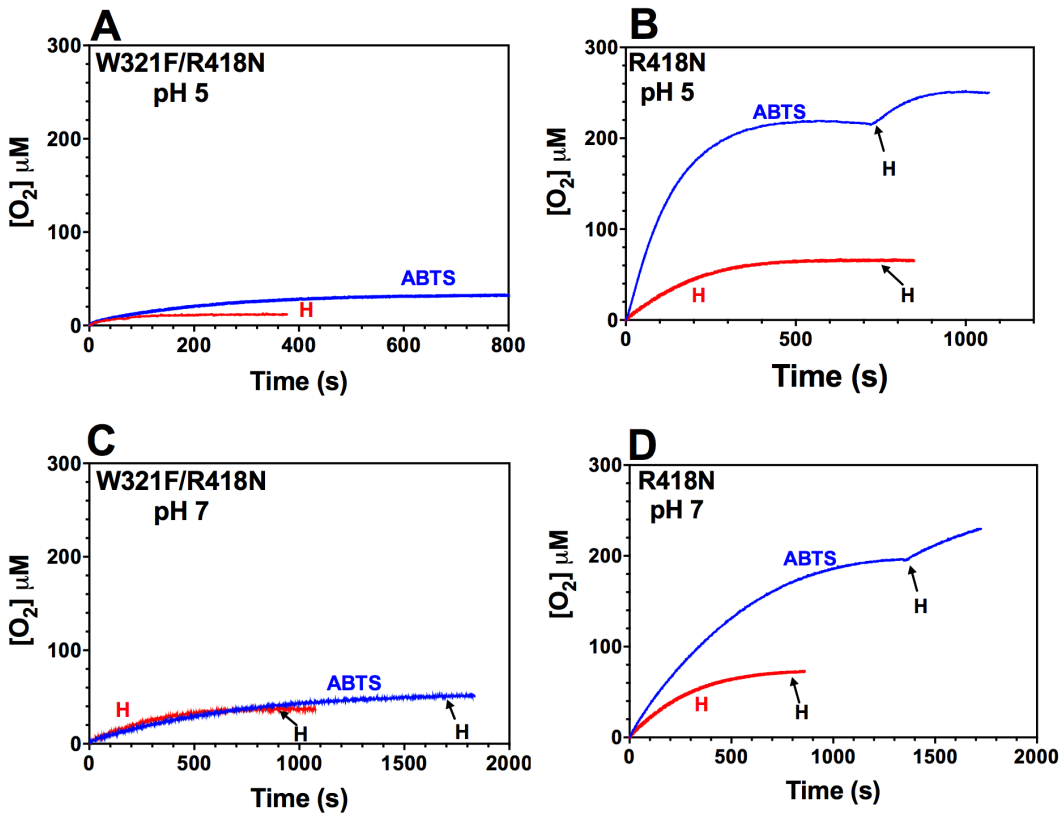

Figure 3.3.3. The effect of ABTS and pH on catalatic O_2 production by R418N and W321F/R418N KatG. The time of the second addition of H_2O_2 (H) are indicated by the arrows. All reactions contained 5 nM KatG, and were initiated by the addition of 0.5 mM H_2O_2. ABTS, when included, was 0.1 mM. All reactions were carried out at 23 °C. Reactions at pH 5.0 (Panel A,B) were buffered with 50 mM acetate and reactions at pH 7.0 (Panel C,D) were buffered with 100 mM phosphate,

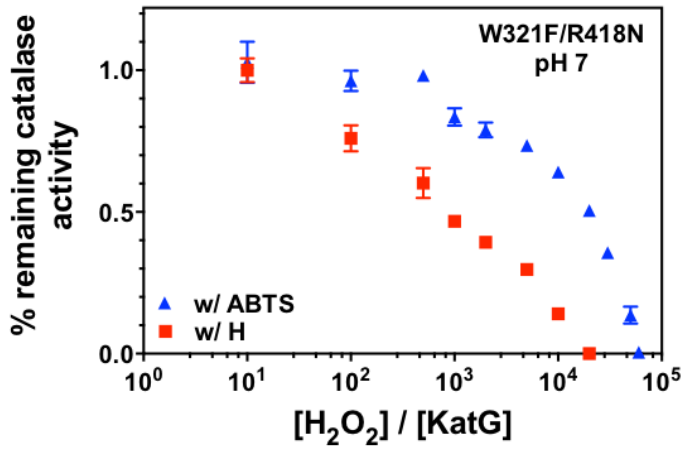

Figure 3.3.4. Effect of H_2O_2 preincubation and ABTS on the catalase activity of W321F/R418N KatG at pH 7. Enzyme (200 nM) was preincubated with the indicated concentration of H_2O_2. Preincubations were carried out in 100 mM phosphate, pH 7.0 in the absence and presence of 0.1 mM ABTS. Following a 1 hour preincubation, an aliquot was withdrawn and catalase activity was measured with 10 mM H_2O_2 in 100 mM phosphate, pH 7.0 by O_2-senstive electrode. All reactions were carried out at 23 °C.

PxED-unassisted R418N was even slightly more sustainable compared to ABTS-assisted W321F/R418N. We reasoned that the seemingly different conclusions suggested by two types of the inactivation assays (compare Fig. 3.2.3C and Fig. 3.2.4) are due to very different molar excess ratio of H_2O_2 to enzyme in two experiment set-up. In fact, we observe that ABTS stimulates the initial rate of the double variant during catalase activity but only at a relatively low molar excess of H_2O_2 (i.e, < 500 molar excess of H_2O_2 to enzyme). One the other hand, reaction of W321F/R418N with a higher molar excess of H_2O_2 invariably leads to substantial light scattering effects, potentially due to large scale protein oxidative damage. And in this situation, ABTS protective effects were bare minimal, if any. We reason that a PxED can help to a certain extent in the basis of enzyme's intrinsic sustainability. Because the double variant was only able to cope with relatively small amounts of H_2O_2, ABTS can only exert some protection in lower H_2O_2 concentration range. However, It is worth highlighting that the stimulation and/or protection by PxED is far less for W321F/R418N compared to that for R418N, even at low H_2O_2 concentration.

In the absence of any PxED, W321F/R418N KatG exhibited full catalase inactivation across all pH values investigated from 5 to 7.5, similar to R418N (Fig. 3.3.5A). In contrast, *wt*KatG retained enough activity to deplete the substrate across all pH, but at lower pH, a 75% loss of catalase activity was observed. With ABTS present, *wt*KatG lost little if any catalase activity across the tested pH range (Fig. 3.3.5B). Similarly, the R418N variant retained catalase at all the pH tested in the presence of ABTS. But this was not the case for W321F/R418N. Indeed, the double variant was inactivated without consuming the substrate at all pH tested even in the presence of ABTS. We also tested other two aromatic PxEDs (i.e., TMPD, CPZ) (Fig. 3.3.5C,D). In both cases, with assistance of PxED, *wt*KatG and R418N were able to maintain full

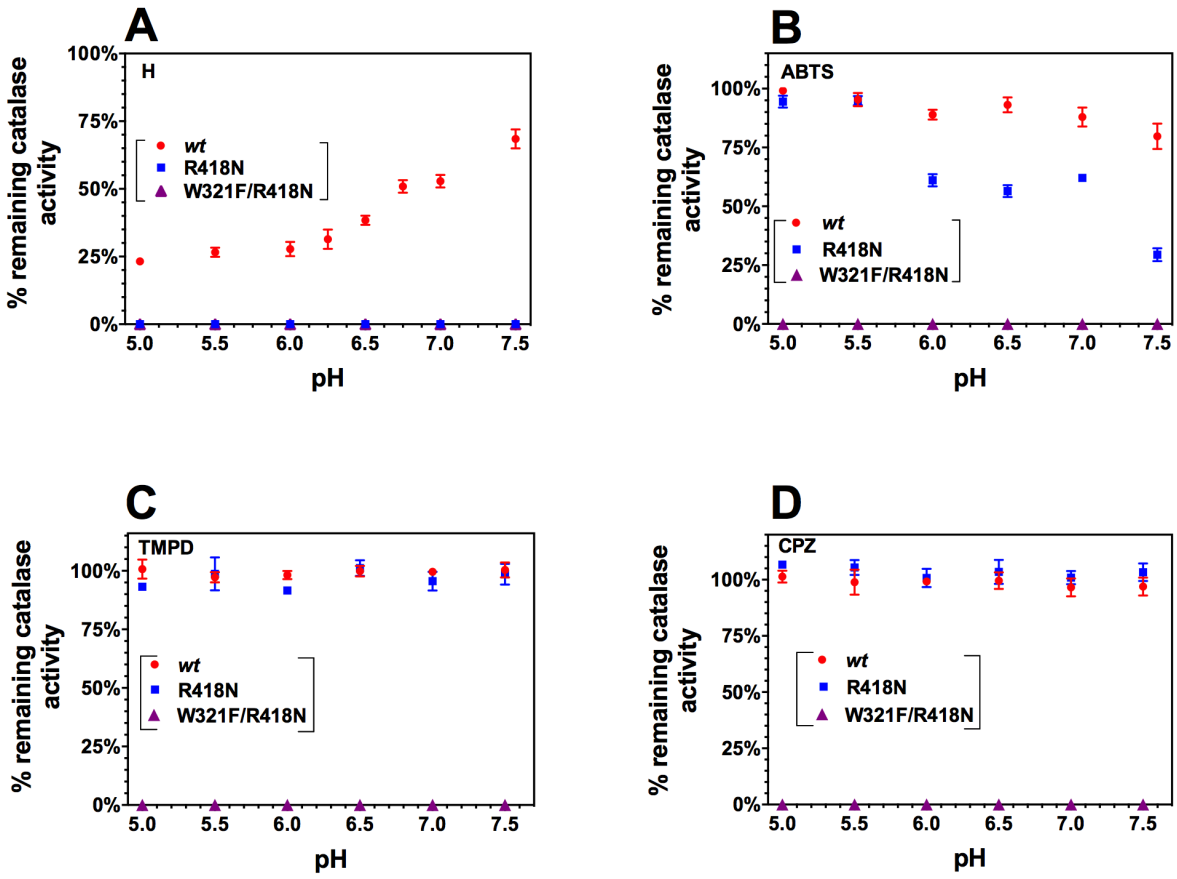

Figure 3.3.5. Effect of pH and PxEDs on catalase activity of KatGs. All reactions (Panel A) contained 5 nM KatG and were initiated by the addition of 0.2 mM H_2O_2. All reactions (Panel B) contained 5 nM KatG, 0.1 mM ABTS and were initiated by the addition of 0.2 mM H_2O_2. All reactions (Panel C) contained 5 nM KatG, 0.1 mM TMPD and were initiated by the addition of 0.2 mM H_2O_2. All reactions (Panel D) contained 5 nM KatG, 0.1 mM CPZ and were initiated by the addition of 0.2 mM H_2O_2. All reactions were carried out at 23 °C by O_2 sensitive electrode. When reaction completed (O_2 production ceased), 2nd addition of 0.2 mM H_2O_2 was added. The % remaining catalase activity was obtained by the initial rate of O_2 production on the 2nd addition over the initial rate of O_2 production on the 1st addition of H_2O_2. Reactions at pH 5.0 and pH 5.5 were buffered with 50 mM acetate, and reactions at pH 6.0, 6.25, 6.5, 7, 7.5 were buffered with 100 mM phosphate.

catalase activity after depletion of 40,000 molar excess of H_2O_2 across the pH 5.0 to 7.5. However, the double variant failed to do so, regardless of the presence of TMPD or CPZ.

We also examined the effect of these PxEDs on the k_{cat} enhancement of catalase activity at low pH (i.e., pH 5) (Fig. 3.3.6), where we observed substantial stimulation of k_{cat} due to the presence of PxEDs. Again, all PxEDs we tested failed to enhance the k_{cat} of the double variant, but were able to stimulate k_{cat} for R418N and *wt*KatG dramatically (more than 8-fold were seen across the board).

3.3.3 The extent of PxED(s) oxidation during catalase catalysis

As stated previously, taking the premise that most PxEDs, such as ABTS, are too big to transit through the long restricted substrate channel of KatG, their oxidation reports off-catalase electron transfer events during catalase catalysis. As such, quantification of PxED oxidized products during catalatic consumption of H_2O_2 informs the frequency of off-pathway electron transfer events. And we also calculate the ratio of $ABTS^{\bullet+}$ generated per H_2O_2 consumed during the consumption of H_2O_2, to determine the partition between peroxidase activity/rescue events and catalase activity. The extent of $ABTS^{\bullet+}$ production increased with an increase in initial H_2O_2 concentration for W321F/R418N reacting with varying concentrations of H_2O_2 at pH 5 (Fig. 3.3.7A). W321F/R418N produced nearly identical quantities of $ABTS^{\bullet+}$ at all H_2O_2 concentrations tested as R418N, far greater than *wt*KatG. We also observed the ratio of $ABTS^{\bullet+}$ generated to H_2O_2 consumed for W321F/R418N was inversely dependent on H_2O_2 concentration to a much greater degree than with *wt*KatG, nearly identical to that of R418N (Fig. 3.3.7B). The double variant produced substantially greater quantities of $ABTS^{\bullet+}$ at all H_2O_2 concentrations tested at pH 7 than R418N (Fig. 3.3.7C,D). These data suggest that (1) off-catalase electron

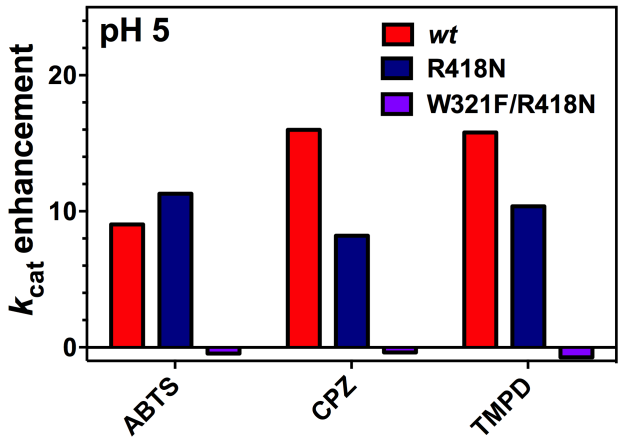

Figure 3.3.6. k_{cat} enhancement of catalase activity of KatGs by PxEDs at pH 5. All activities were measured by O_2 production using a Clark-type of electrode in 50 mM acetate at pH 5, 23 °C. Concentration of each electron donor was 0.1 mM.

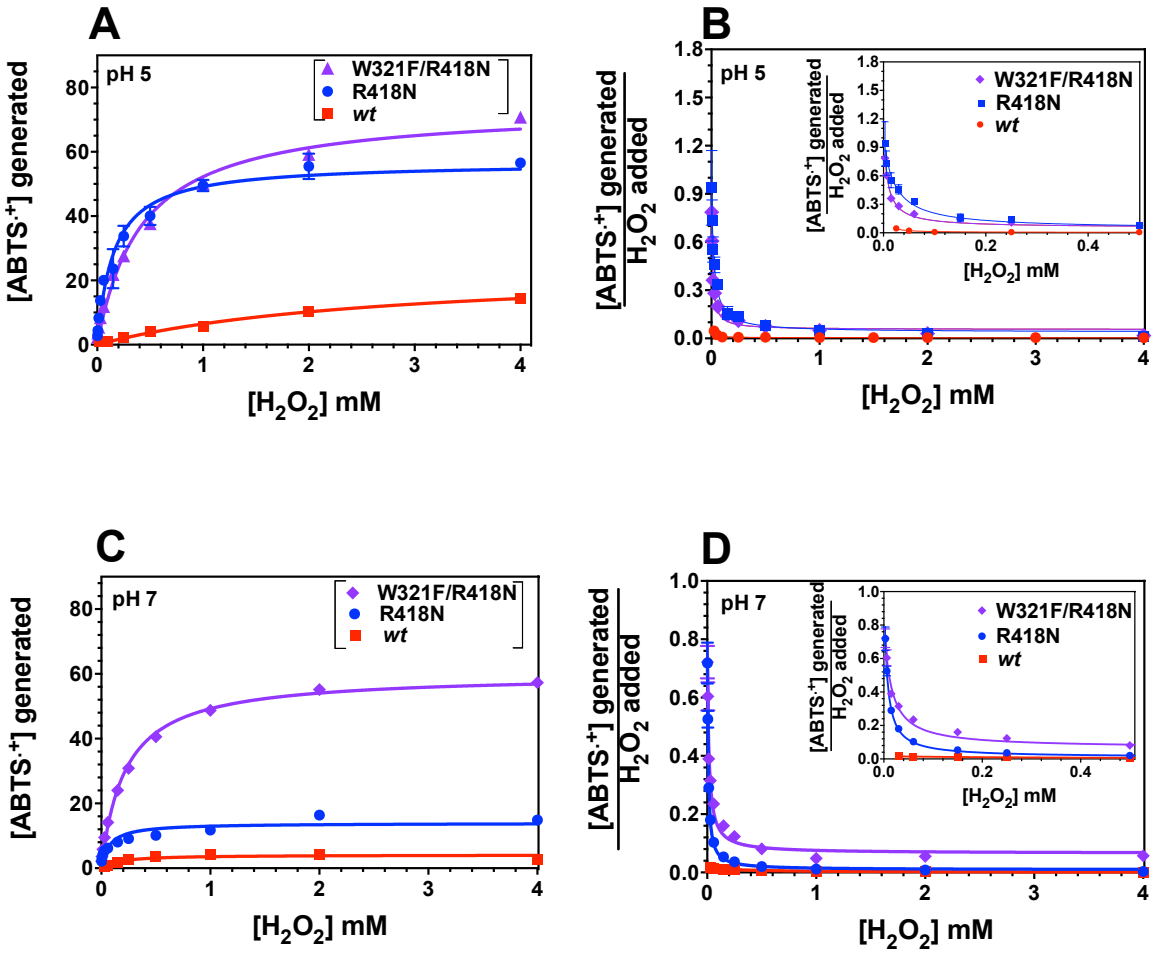

Figure 3.3.7. Effect of H_2O_2 concentration and pH on ABTS oxidation by KatGs. All reactions contained 3 μM KatG, and 0.1 mM ABTS. Concentration of $ABTS^{\bullet+}$ was calculated using ε (645 nm) = 0.012 μM^{-1} cm^{-1}. All reactions were carried out at 4 °C. Reactions at pH 7.0 (Panels A and B) were buffered with 100 mM phosphate and reactions at pH 5.0 (Panels C and D) were buffered with 50 mM acetate.

transfer becomes a much more prominent situation when Arg switch is abolished by mutagenesis; and (2) the conduit(s) bypass Trp 321 also operates.

We quantified the generation of the ABTS oxidation product ($ABTS^{\bullet+}$) during the consumption of H_2O_2 as a function of pH by stopped-flow (Fig. 3.3.8A) by the W321F/R418N KatG variant to compare with the *wt* and R418N KatG, as we previously did. We observed substantially greater quantities of $ABTS^{\bullet+}$ were detected during the reaction of W321F/R418N with H_2O_2 at all the pH tested, than that with R418N. Therefore, W321F/R418N exhibits a much higher frequency for off-catalase electron transfer across the pH tested than R418N. There data suggest Trp 321 is not the sole route for off-pathway electron transfer of KatG, when off-catalase electron transfer is favored by abolishing the Arg switch.

We also quantified the generation of the TMPD oxidation products ($TMPD^{\bullet+}$) by stopped-flow during catalase activity of *wt*KatG, R418N, W321F/R418N (Fig. 3.3.8B). The fastest oxidation of TMPD to $TMPD^{\bullet+}$ (monitored at 610 nM) was accomplished within the time regime prior to recovery of the resting state (monitored at 407 nM), upon reaction of KatGs with H_2O_2. Thus, its oxidation was enzymatically-relevant. Overwhelmingly intense absorption of $TMPD^{\bullet+}$ in the case of both variants swamped the CT band of the ferric enzyme (i.e., 640 nm), making the accurate quantification of $TMPD^{\bullet+}$ products possible. Only generation of $TMPD^{\bullet+}$ during enzymatic turnover was considered. The quantity of TMPD oxidation followed the order exactly the same as using ABTS as PxED : W321F/R418N > R418N > *wt*KatG.

Because CPZ oxidation product (i.e., $CPZ^{\bullet+}$) is not stable due to the secondary oxidation afterwards to form CPZSO, we quantified CPZ oxidation products ($CPZ^{\bullet+}$) as well as CPZSO (Fig. 3.3.8C,D) to be exhaustive. Notably, W321F/R418N yielded CPZ oxidation products to the same extent as that for R418N, which far exceeded that by *wt*KatG, whether $CPZ^{\bullet+}$ or CPZSO

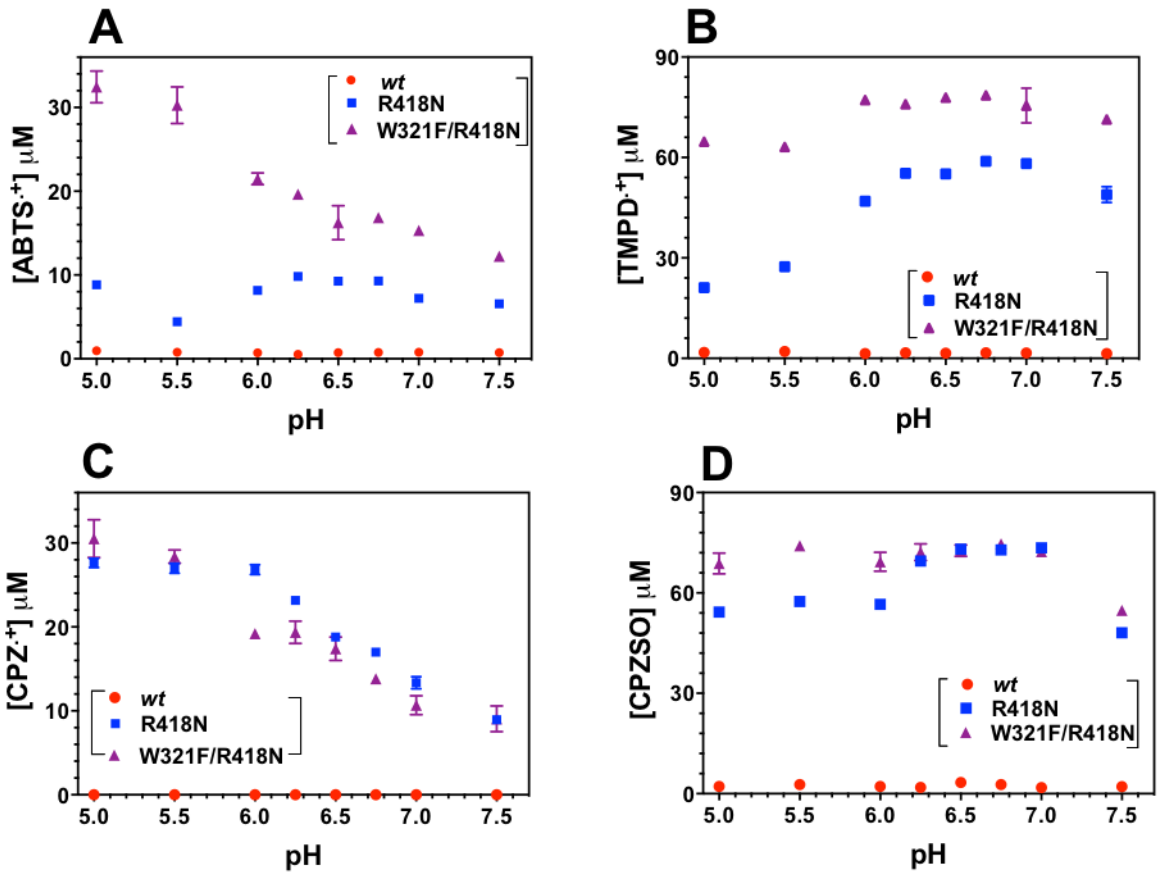

Figure 3.3.8. Effect of pH on PxED oxidation by KatGs. All reactions (Panel A) contained 3 µM KatG, 0.05 mM H_2O_2 and 0.1 mM ABTS. All reactions (Panel B and C) contained 3 µM KatG, 0.05 mM H_2O_2 and 0.1 mM TMPD, CPZ respectively. Reactions (Panel D) contained 20 nM KatG, 0.08 mM H_2O_2, 0.1 mM CPZ in the corresponding buffer. CPZSO is measured at 340 nM by UV-visible spectroscopy. Reactions at pH 5.0 and pH 5.5 were buffered with 50 mM acetate, and reactions at pH 6.0, 6.25, 6.5, 7, 7.5 were buffered with 100 mM phosphate.

was measured. The difference in the yield of CPZ oxidation products was attributed to the different experimental conditions.

Our data suggest that withdrawal of Arg. switch leads to higher frequency of off-catalase through-protein radical hopping. Clearly Trp 321 is not the sole route that delivers the oxidizing equivalents to the protein surface. In other words, other route(s) bypassing Trp 321 operates. But the disconnection between substantial intervention of PxED (i.e., PxED oxidation) and failure to preserve catalase activity for the double variant (Refer to Figs. 3.3.3, 3.3.5, 3.3.6, 3.3.7 and 3.2.8) suggests that the off-pathway electron transfer bypassing the Trp 321 is not resolve-able. This further suggests the advantageous role of Trp 321 and Trp 321 is the residue to handle the off-pathway electron transfer when it occurs.

Our Data from ***3.3.1*** to ***3.3.3*** suggest that devoid of Trp 321 while increasing off-pathway electron transfer (i.e., R418N mutation) generates KatG with almost no tolerance to H_2O_2-dependent inactivation. Further, the absence of the Trp 321 creates the discrepancy between substantial PxED intervention and failure to preserve catalase activity for the double variant. These data indicate that Trp 321 is the residue to handle the off-pathway electron transfer when it occurs.

3.3.4 Heme intermediates observed during W321F/R418N KatG catalase catalysis at pH 5

To evaluate the dominant heme intermediate(s) present during catalatic H_2O_2 degradation, we also reacted W321F/R418N with varying H_2O_2 concentration. Consistent with the hyper-vulnerability of W321F/R418N to H_2O_2-dependent inactivation at pH 5, mixing W321F/R418N with [H_2O_2] routinely employed for *wt*KatG or R418N (i.e., range from 0.25 mM to 4 mM) showed substantial light scattering effect characterized by undescriptive increase of absorption at all wavelength. The higher the concentration of H_2O_2, the more dramatic light scattering was

observed. For examples, upon reaction of W321F/R418N reacting with 2 mM H_2O_2, the earliest spectra we observed included a Soret peak at 418 nm and α, β bands maxima at 580 and 542 nm (Fig. 3.3.9). These spectra were consistent with the oxyferrous/ferric superoxide intermediate (i.e. Fe^{III}-$O_2^{\bullet-}$) associated with catalase activity. But after that, we saw substantial light scattering effect which prevents us to examine the intermediates. We interpret this phenomenon as that the enzyme is under massive oxidative damage upon reaction with H_2O_2.

We validated W321F/R418N was stable at pH 5, and the light scattering effect was only observed after mixing with H_2O_2. When 0.2 mM H_2O_2 or less (molar ratio of H_2O_2 : enzyme = < 66.7 fold) was included, W321F/R418N was able to deplete the substrate and return to the ferric state without remarkable/substantial interference from the light scattering effect. Thus, we used 66.7 molar excess of H_2O_2 as the condition for FRQ-EPR experiment at pH 5 for W321F/R418N.

We observed the spectrum at the earliest time regime (i.e., 5 ms) of W321F/R418N reacting with 0.2 mM H_2O_2 included a Soret at 412 nm and α, β bands maxima at 542 and 580 nm (Fig. 3.3.10B). This spectrum was consistent with the oxyferrous intermediate (i.e. Fe^{III}-$O_2^{\bullet-}$), which is the intermediate in catalase turnover. We observed the nearly identical spectra (i.e. Fe^{III}-$O_2^{\bullet-}$) at the earliest time points for R418N and *wt*KatG at both pH 5 and 7. The spectra showed progressive increased absorption across the whole wavelength during 63 ms to 19.8 s, suggestive of light scattering effect (Fig. 3.3.10C). The light scattering effect made it hard to examine the intermediates accumulated. After that, the ferric enzyme slowly returned (Fig. 3.3.10D). These data indicate the accumulation of some other species in the catalase catalysis of W321F/R418N, likely due to off-pathway electron transfer.

We observed ABTS provided marginal protective effects on W321F/R418N catalatic degradation of H_2O_2 at pH 5. Indeed, the stimulation of rate of the steady-state turnover and the

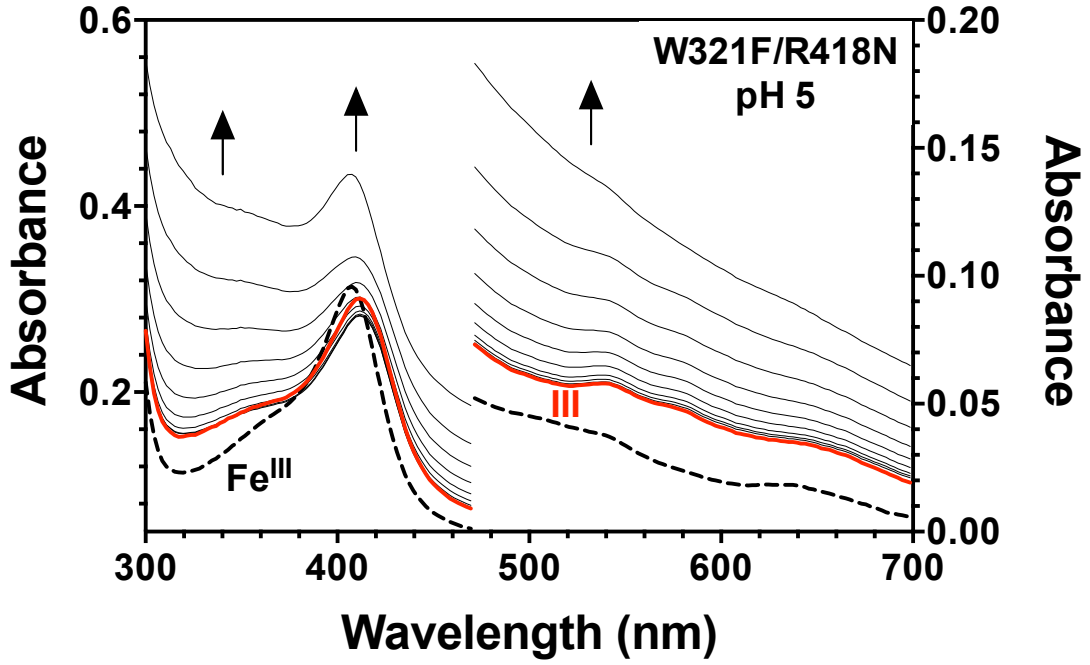

Figure 3.3.9. Light scattering effect during catalatic turnover of W321F/R418N reacting with 667 eq. H_2O_2 (2 mM) at pH 5. The reaction contained 3 μM W321F/R418N KatG and 2 mM H_2O_2 in 50 mM acetate, pH 5.0. Reactions were carried out at 4 °C. Reaction was monitored for 50 s.

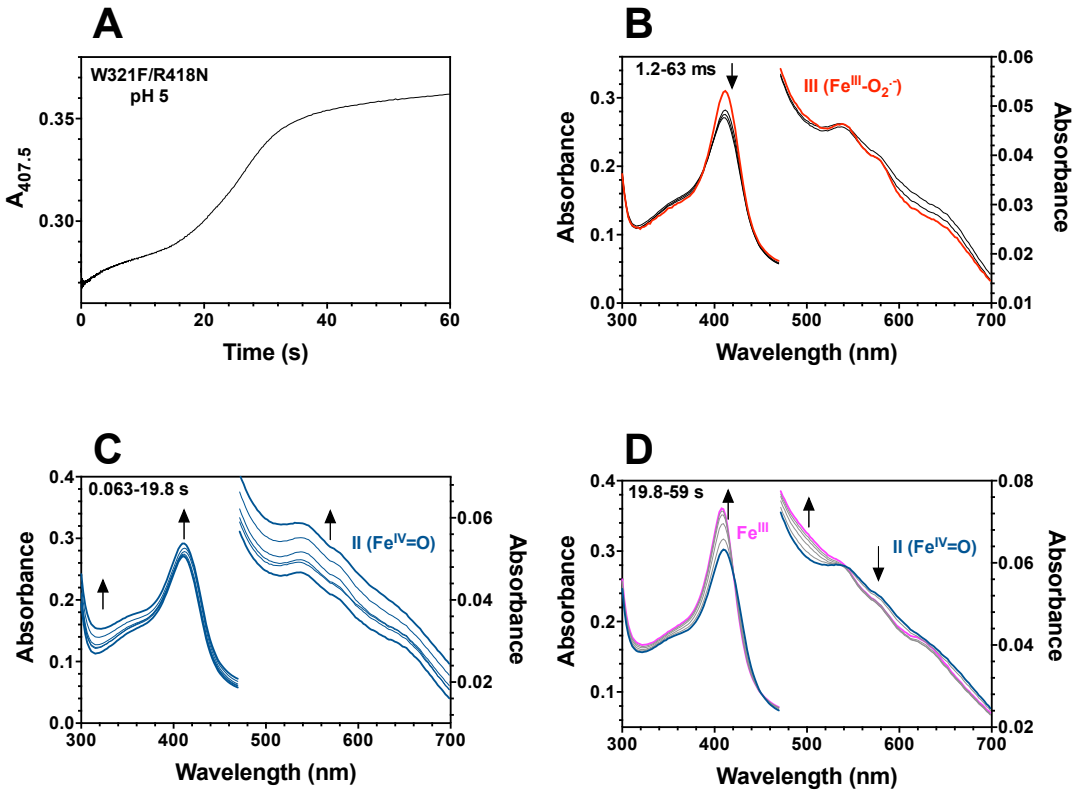

Figure 3.3.10. Spectra collected during reaction of W321F/R418N KatG with 0.2 mM H_2O_2 at pH 5. The change in absorbance at 407.5 nm over the entire course of the reaction (A) is shown. Spectra corresponded to 1.2 – 63 ms (B) 0.063– 19.8 s (C), and 19.8-60 s (D) following mixing of 3 μM enzyme and 0.5 mM H_2O_2. This reaction was carried out in 50 mM acetate pH 5 at 4 °C.

return of the ferric enzyme was far less pronounced than that for R418N across H_2O_2 concentration. In addition, light scattering effect was prominent during catalase reaction of the double variant even in the presence of PxED, especially from 0.25 mM to 4 mM H_2O_2 (data not shown). These data indicate the PxED-assisted double variant was still compromised and the substantial off-pathway electron transfer events were not remediated. In other word, the off-pathway electron transfer bypassing Trp 321 is mostly un-fixable.

3.3.5 EPR signal of high spin ferric resting W321F/R418N KatG

The 9-GHz EPR spectrum of the ferric form of W321F/R418N KatG recorded at 4.5 K was much less intense compared to R418N, although the EPR samples were prepared in the same way (Fig. 3.3.11). This was likely because the W321F mutation slightly perturbed the active site microenvironment. Indeed, we have previously observed that the ferric high spin signal of our W321F was much less intense compared to *wt*KatG. In addition, we suspect that the double mutations in W321F/R418N results in some population of the enzyme expressed in some EPR-silent state(s), such as oxyferrous heme. However, our UV-Vis spectrum of the double variant was typical for high-spin ferric enzyme (Refer to Fig. 3.1.1). We reasoned it was likely oxyferrous heme species existed and was masked by other species due to the ambiguous nature of the UV-Vis. Another possibility we could not rule out is the high spin ferric signal of the double variant detected by EPR is enzyme-age dependent, which we have not explored yet. Similar to R418N, we also observed a multiplicity of high spin states of the double variant at both pH. It at least contained an axial signal and the rhombic distorted signal. The signal did not seem to be pH-dependent. Both the axial and rhombic signals were much less intense for the double variant compared to R418N.

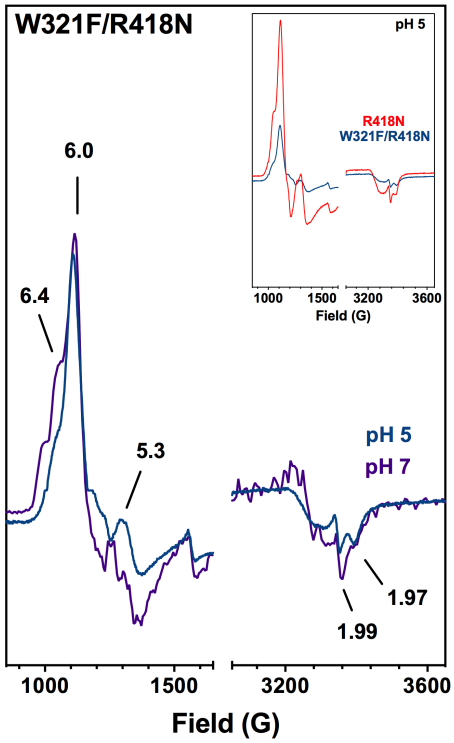

Figure 3.3.11 9 GHz EPR spectra of resting W321F/R418N KatG at pH 5 and 7. The samples contained 150 μM W321F/R418N KatG in either 50 mM acetate, pH 5, or in 100 mM phosphate, pH 7. The comparison of the 9 GHz EPR spectra of R418N and W321F/R418N at pH 5 is shown in the inset. All spectra were recorded at 4.5 K. Instrument parameters were as follows: microwave frequency, 9.393 GHz; modulation amplitude, 1 G; modulation frequency, 100 kHz; microwave power, 1 mW; time constant, 163.84 ms; sweep time 335.54 s; number of scans, 1; conversion 327.68 ms; resolution, 1024 point; receiver gain, 1.0×10^4; and phase 0 degree.

3.3.6 W321F/R418N KatG protein-based radicals upon reaction with H_2O_2 alone at pH 5

The EPR spectra of W321F/R418N freeze-quenched after a 10-ms reaction time with H_2O_2 showed formation of an intense doublet radical signal (Fig. 3.3.12B). In the sample quenched at 50-ms time, the narrow doublet signal was more intense. These suggest W321F/R418N formed Fe^{III}-$O_2^{\bullet-}$ $[MYW]^{\bullet+}$ at the earliest time regime during catalase turnover. Since W321F/R418N was able to form catalase active MYW radical, its vulnerability to H_2O_2-dependent inactivation was likely due to other disadvantages.

The EPR spectra of W321F/R418N quenched at 26 s showed a narrow singlet radical species (Fig. 3.3.12B). The narrow singlet radical species was still evident in samples quenched at 1-min and 5-min. Thus, other conduit(s) bypassing W321 still served as internal electron donor(s) during catalase turnover of W321F/R418N with H_2O_2 at pH 5. The power saturation profile for 10-ms, 26-s, and 1-min all showed that the radical was relatively susceptible to saturation (Fig. 3.3.13). None of them are well-fitted to the equation, suggestive of a multitude of radical species.

Two key points need to be highlighted. First, we did not observe the exchange-coupled radicals, consistent with Trp 321 being eliminated in W321F/R418N KatG. Second, the off-pathway electron transfer bypassing W321 operated during catalase catalysis for the double variant.

3.3.7 W321F/R418N catalase catalysis intermediates observed at pH 7

W321F/R418N took longer to consume a certain concentration of H_2O_2 than R418N at pH 7 (Fig. 3.3.14A). For examples, W321F/R418N took more than 100 s to deplete 2 mM H_2O_2 *vs.* R418N only used 70 s. This was consistent with the fact that although two variants showed nearly identical state-state catalatic parameters, W321F/R418N was much less sustainable than

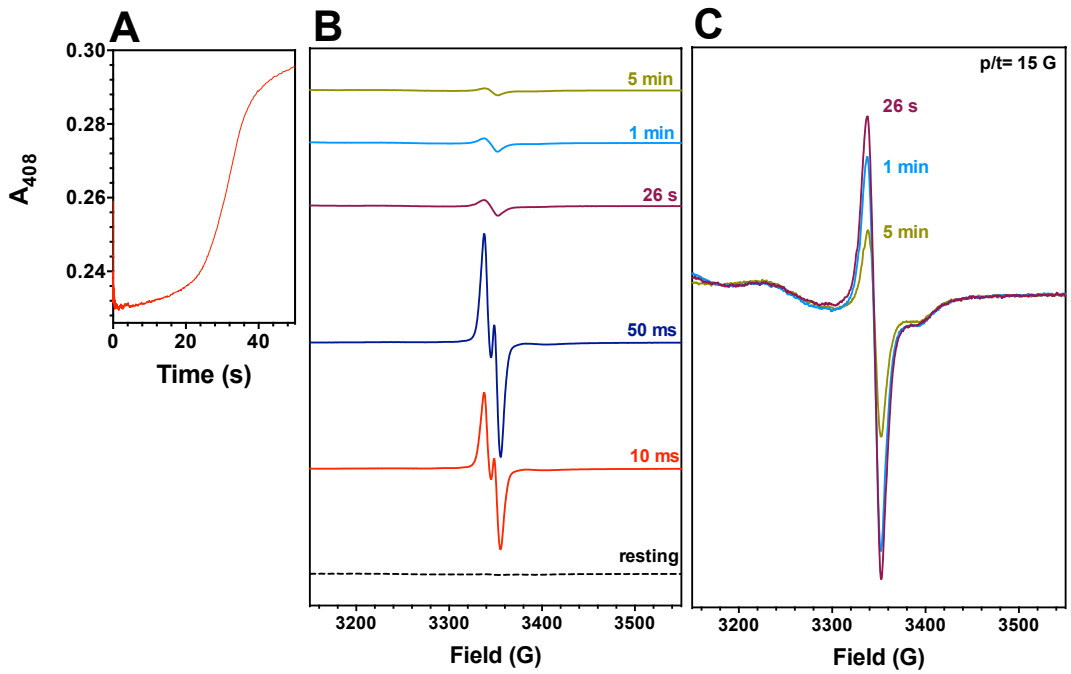

Figure 3.3.12. EPR spectra of freeze-quenched samples from reaction of W321/R418N KatG with H_2O_2 at pH 5. The stopped-flow trace monitoring return of ferric enzyme at 407.5 nm during W321F/R418N reaction with 66.7eq. H_2O_2 are shown in A. The g// component of the resting state as well as protein-based radicals (g ~ 2) of W321F/R418N are shown in B. The comparison of the singlet radical detected in samples quenched at 26 s, 1 min, and 5 min are shown in C. The molar proportions of enzyme to H_2O_2 used for stopped-flow experiments (1:66.7) were maintained for these experiments. Consequently, ferric enzyme (150 μM after mixing) was reacted with H_2O_2 (10 mM after mixing) for the time indicated prior to freeze-quenching. Reactions were carried out at 4 °C in 50 mM acetate, pH 5. The resting W321F/R418N KatG was prepared the same way except no H_2O_2 included and quenched manually. All spectra were recorded at 4.5 K, if not indicated otherwise. Spectrometer settings were as described under "Experimental procedures." Specifically, Instrument parameters were as follows: microwave frequency, 9.393 GHz; modulation amplitude, 2 G; modulation frequency, 100 kHz; microwave power, 1 milliwatt; time constant, 163.84 ms; sweep time 335.54 s; number of scans, 1; conversion, 327.68 ms; resolution, 1024 point; receiver gain, 1.0×10^4; and phase, 0 degrees.

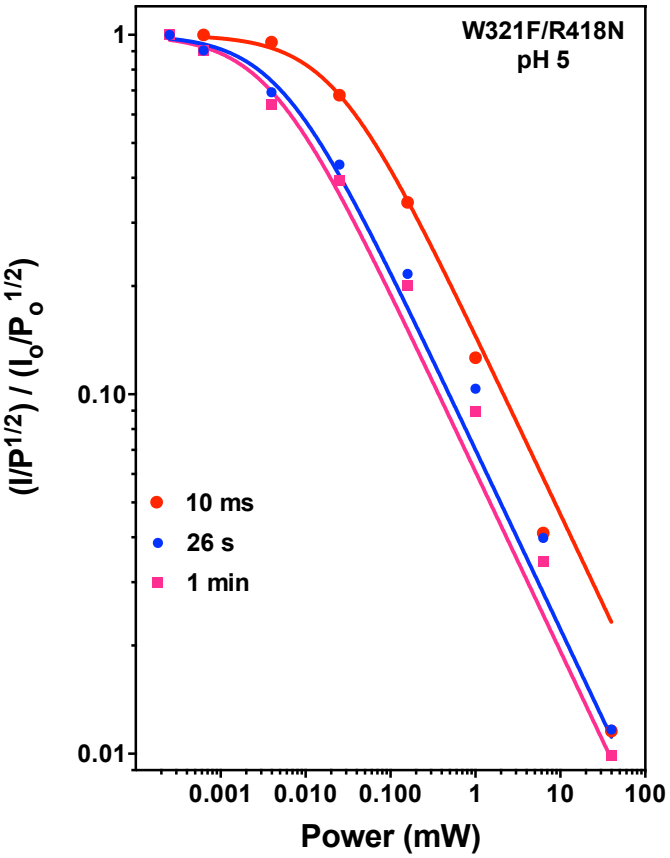

Figure 3.3.13. Power saturation profile of EPR spectra of freeze-quenched samples from reaction of W321/R418N KatG with H_2O_2 at pH 5. The normalized signal intensities for samples collected 10 ms, 26 s and 1 min after W321F/R418N KatG reaction with H_2O_2 at pH 5 as a function of microwave power are shown. For all these samples, the peak to trough intensity was used. Unless otherwise indicated, all spectra were recorded at 4.5 K with all other spectrometer settings as described in "Experimental procedures" Samples were prepared and evaluated as described for Fig. 3.3.12.

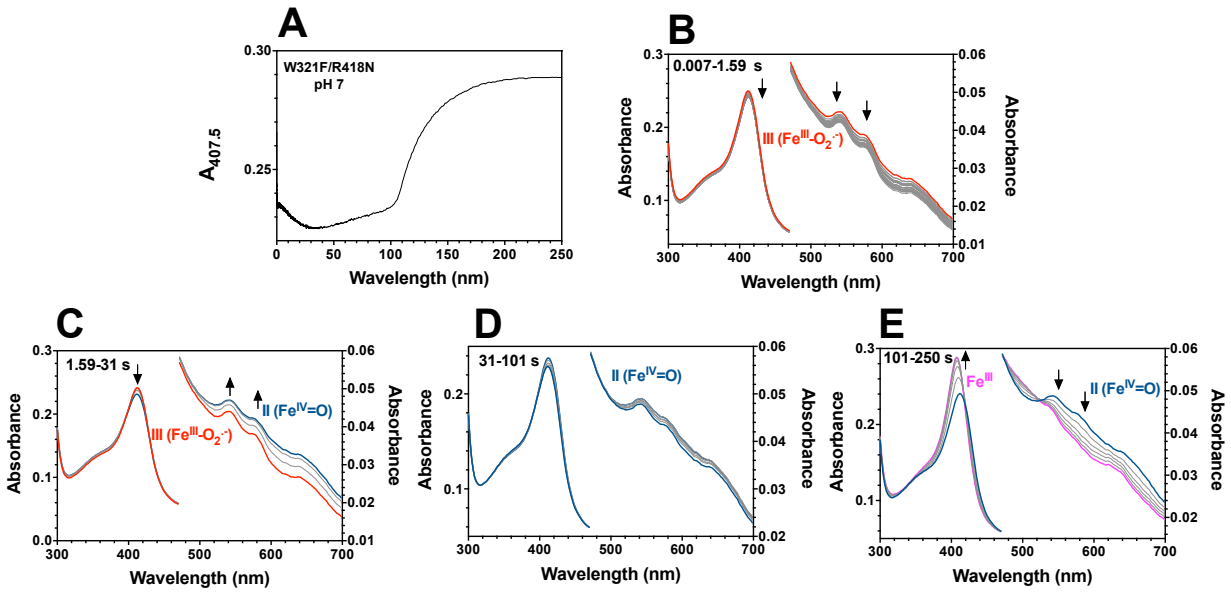

Figure 3.3.14. Spectra collected during reaction of W321F/R418N KatG with 2.0 mM H_2O_2 at pH 7. The change in absorbance at 408 nm over the entire course of the reaction (A) is shown. Spectra corresponded to 0.007-1.59 s (B), 1.59-31 s (C), and 31-101 s (D), 101-250 s following mixing of 3 μM enzyme and 2.0 mM H_2O_2. This reaction was carried out in 100 mM phosphate pH 7 at 4 °C.

R418N.

We observed the earliest spectra of W321F/R418N mixing with 2 mM H_2O_2 included a Soret at 416 nm and α, β bands maxima at 580 and 542 nm (Fig. 3.3.14B). This spectrum was consistent with the oxyferrous intermediate (i.e. Fe^{III}-$O_2^{\bullet-}$), catalase competent intermediate. We observed nearly identical spectra (i.e. Fe^{III}-$O_2^{\bullet-}$) at the earliest time points for R418N and *wt*KatG at both pH 5 and 7. This spectra stayed almost unchanged from 7 ms to 1.59 s, except very slight decrease in the Soret band. From 1.59 s to 31 s, we observed the broad increase in absorption above 520 nm, with α, β bands maxima at 584 and 546 nm (Fig. 3.3.14C), and diminished absorbance at 416 nm (the Soret peak). From 31 s to 101 s, α, β bands maxima stayed unchanged, but absorbance at 416 nm increased (Fig. 3.3.14D). After that, the slow return of the ferric enzyme was observed (Fig. 3.3.14E). We were not sure exactly how the intermediates changed during the whole reaction regime, but it seems the catalatic oxyferrous intermediate (i.e. Fe^{III}-$O_2^{\bullet-}$) gradually transitioned to a ferryl species after 1.59 s, indicative of the off-pathway electron transfer events. This is also supported by the slow return of the ferric enzyme.

Reaction of W321F/R418N with 667 eq. of H_2O_2 produced a nearly identical narrow doublet radical at 10 ms, as at pH 7 (Fig. 3.3.15B). This radical was also observed with the sample quench at 50 ms (Fig. 3.3.15B). Thus, similar to W321F/R418N KatG at H 5, the combination of our optical stopped-flow and RFQ-EPR data suggest that the dominant steady-state intermediate catalase activity at the earliest turnover at neutral pH is still consistent with Fe^{III}-$O_2^{\bullet-}$[MYW]$^{\bullet+}$. We observed the narrow singlet in the sample quenched at 12 s after mixing the double variant with H_2O_2. Similar to that at pH 5 was the persistence of the narrow singlet thereafter. Indeed, the narrow singlet was observed at a 5-min reaction time. Different from the reaction of R418N variant with H_2O_2 at pH 7 was that no exchange-coupled radical was detected,

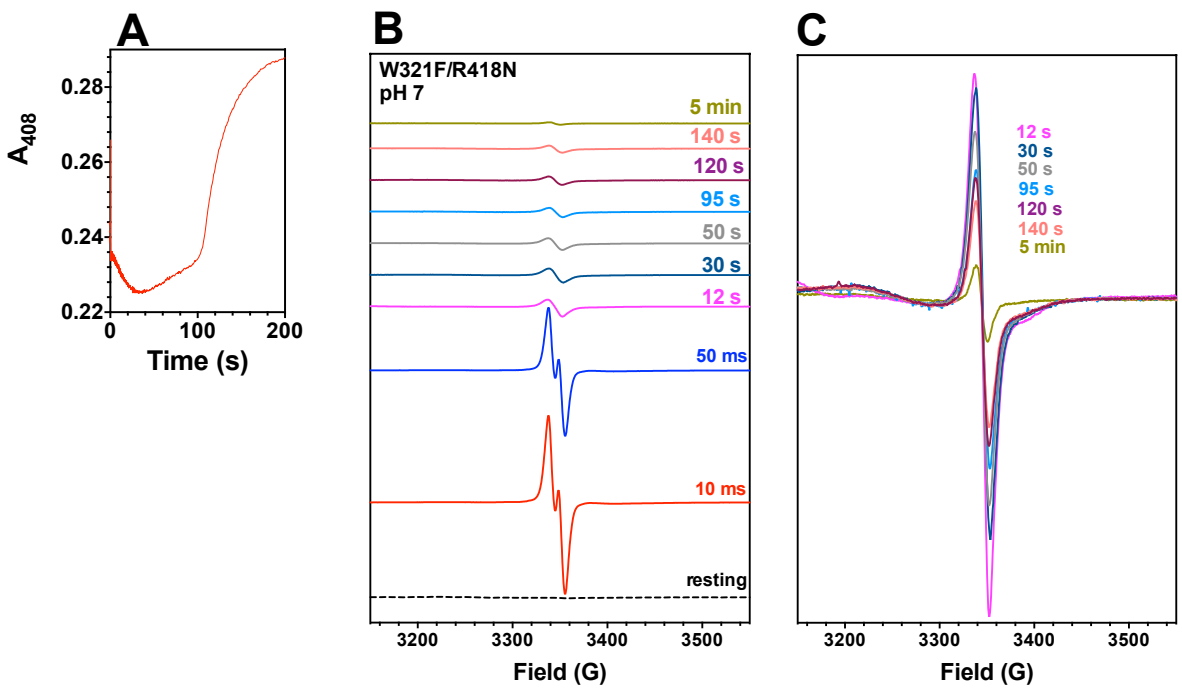

Figure 3.3.15. EPR spectra of freeze-quenched samples from reaction of W321/R418N KatG with H_2O_2 at pH 7. The stopped-flow trace monitoring return of ferric enzyme at 407.5 nm during W321F/R418N reaction with 667eq. H_2O_2 are shown in A. The g// component of the resting state as well as protein-based radicals (g ~ 2) of W321F/R418N are shown in B,C. The comparison of the singlet radical as well as g// component of the resting state are shown in C. The molar proportions of enzyme to H_2O_2 used for stopped-flow experiments (1:667) were maintained for these experiments. Consequently, ferric enzyme (150 μM after mixing) was reacted with H_2O_2 (100 mM after mixing) for the time indicated prior to freeze-quenching. Reactions were carried out at 4 °C in 50 mM acetate, pH 5. The resting W321F/R418N KatG was prepared the same way except no H_2O_2 included and quenched manually. All spectra were recorded at 4.5 K, if not indicated otherwise. Spectrometer settings were as described under "Experimental procedures." Specifically, Instrument parameters were as follows: microwave frequency, 9.393 GHz; modulation amplitude, 2 G; modulation frequency, 100 kHz; microwave power, 1 milliwatt; time constant, 163.84 ms; sweep time 335.54 s; number of scans, 1; conversion, 327.68 ms; resolution, 1024 point; receiver gain, 1.0×10^4; and phase, 0 degrees.

consistent with the hypothesis that the broadening feature is attributed to the $W321^{\bullet+}$. Consistent with absence of the exchange-coupled radical, the power saturation profile for the sample quenched at 12 s, 120 s and 5 min are quite similar and very susceptible to power saturation (Fig. 3.3.16). Notable, none of them are well-fitted suggestive of the multitude of radical species.

These data suggest that (1) the narrow doublet radical assigned to $MYW^{\bullet+}$ does not persist throughout the time course of turnover of H_2O_2; and (2) other route(s) bypassing W321 participates off-catalase protein oxidation.

3.3.8 The effect of PxEDs on protein-based radicals upon reaction of W321F/R418N with H_2O_2

To examine the effects of PxED on the intermediates formed upon reaction of W321F/R418N with H_2O_2, similar rapid freeze-quench EPR experiments at both pH 5 and 7 were performed in the presence of PxED (ABTS/ascorbate). We observed that the narrow doublet signal in samples quenched after 10-ms at either pH 5 or pH 7 (Fig. 3.3.17). Thus, PxED did not interfere with the formation of the catalatic-essential MYW cofactor radical at the earliest time regime. For the samples quenched at longer time points far after the reaction was completed, the samples with ABTS presence showed minimal accumulation of the protein-based radicals than those without ABTS (Fig. 3.3.18). This was applied to pH 5 and pH 7.

3.3.9 Conclusions

The absence of the Arg switch by orientation or by mutagenesis increases the susceptibility to H_2O_2-dependent inactivation of KatG, resulting from the increased frequency of off-pathway electron transfer. The proximal W321 is the primary residue to handle off-pathway electron transfer, in that (1) off-pathway electron transfer via W321 conduit forestalls the irreversible inactivation of KatG; and (2) off-pathway electron transfer bypassing W321 is mostly un-rescue-able by PxED oxidation.

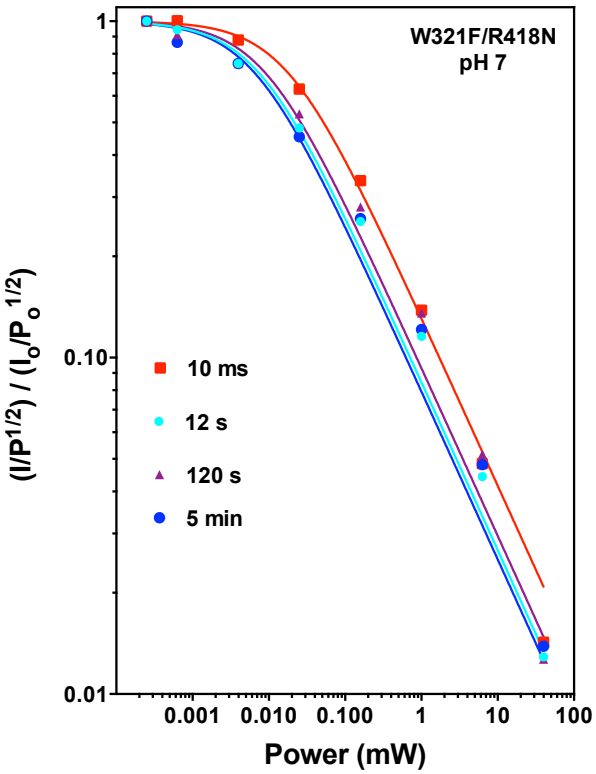

Figure 3.3.16. Power saturation profile of EPR spectra of freeze-quenched samples from reaction of W321/R418N KatG with H_2O_2 at pH 7. The normalized signal intensities for samples collected 10 ms, 12 s, 120 s and 5 min after W321F/R418N KatG reaction with H_2O_2 at pH 7 as a function of microwave power are shown. For all these samples, the peak to trough intensity was used. Unless otherwise indicated, all spectra were recorded at 4.5 K with all other spectrometer settings as described in "Experimental procedures" Samples were prepared and evaluated as described for Fig. 3.3.15.

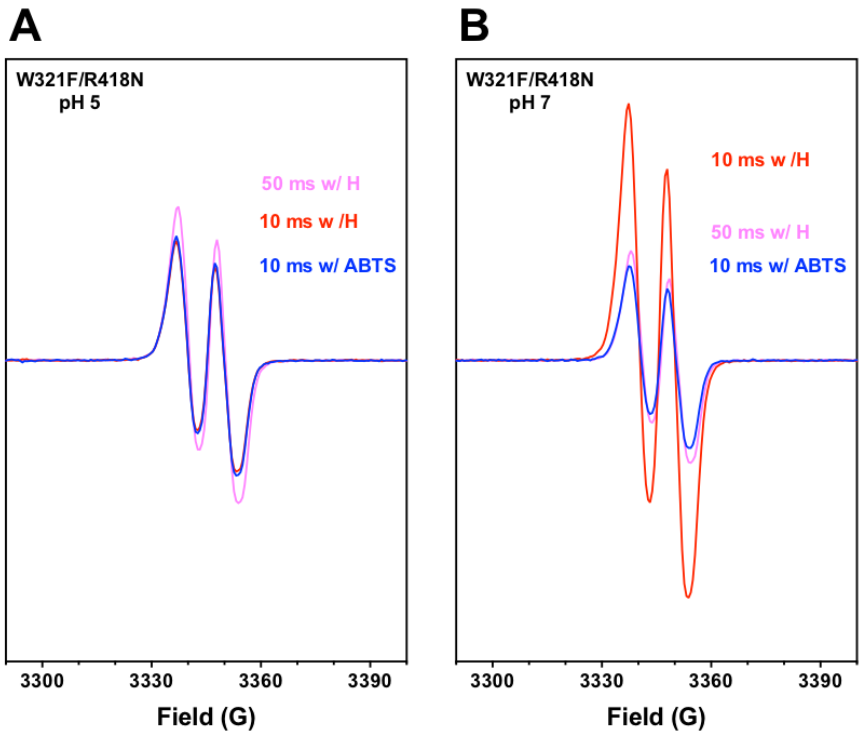

Figure 3.3.17. Comparison of EPR spectra for protein-based radicals 10 ms and 50 ms after mixing with H_2O_2, as well as 10 ms after mixing with H_2O_2 in the presence of ABTS at pH 5 (A) and at pH 7 (B) for W321F/R418N. Spectra were recorded at 77 K, minimizing power saturation of the radical observed at 4.5 K (see Fig. 3.2.12A and 3.2.13). All spectrometer settings were as described under "Experimental procedures."

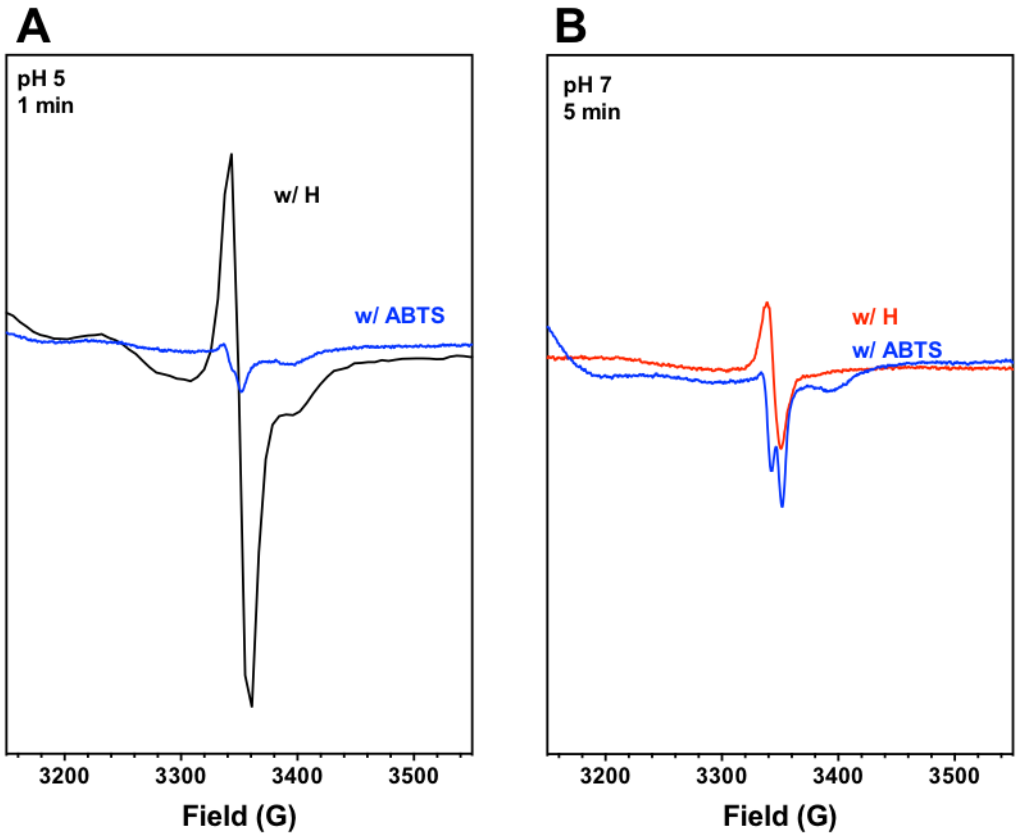

Figure. 3.3.18. Comparison of EPR spectra for protein-based radicals at later time points at pH 5 in the absence and presence of ABTS/ ascorbate (A), and at pH 7 in the absence and presence of ABTS/ascorbate (B) for W321F/R418N. Spectra were recorded at 4.5 K. All spectrometer settings were as described under "Experimental procedures."

3.4 Integrating the functional roles of R418 and W321 in KatG catalysis and inactivation

3.4.1 W321: friend or foe? Revisiting W321F

We previously reported that W321 is the hot spot for off-catalase protein oxidation in *wt*KatG and blocking W321 (i.e., W321F) leads to a higher initial rate of catalase activity (higher k_{cat}) at low pH where off-pathway electron transfer events are prominent, as well as less need for PxED intervention. These data are indicative of a deleterious role of Trp 321 oxidation during catalase turnover in KatG. Some time had passed when we pondered why this Trp 321 was preserved during evolutionary biology. However, our recent data suggest to evaluate if KatG or variant is robust catalase, not only the initial rate of catalase activity matters, but also its sustainability. Indeed, W321F reacting with 100,000-fold excess of H_2O_2 started with much higher initial rate than *wt*KatG at pH 5, however, it burned out itself more quickly with only 1/3 of the catalase cycle achieved prior to inactivation compared to *wt*KatG (Fig. 3.4.1A). These data suggest W321F is far more compromised in sustainability as a catalase than *wt*KatG in the situation where off-pathway electron transfer is a frequent event. Consistent with this, at pH 7 where off-pathway electron transfer was not an issue, W321F is as robust as *wt*KatG in terms of rate and sustainability. Therefore, the beneficial role of Trp 321 in catalase activity in the long run emerges.

3.4.2 Comparison of the vulnerability of 4 KatGs to H_2O_2-dependent inactivation.

We overlaid representatives of all the O_2 production traces of reacting KatGs (*wt*KatG, R418N, W321F, W321F/R418N) with 100,000 molar excess of H_2O_2 at pH 5 (Fig. 3.4.1A) and at pH 7 (Fig. 3.4.1B), to examine the effect of such mutation(s) on the resistance to H_2O_2-dependent inactivation. At pH 7, where off-catalase electron transfer was not a problem, W321F behaved nearly identical to *wt*KatG, in that both of them were able to deplete H_2O_2. R418N and

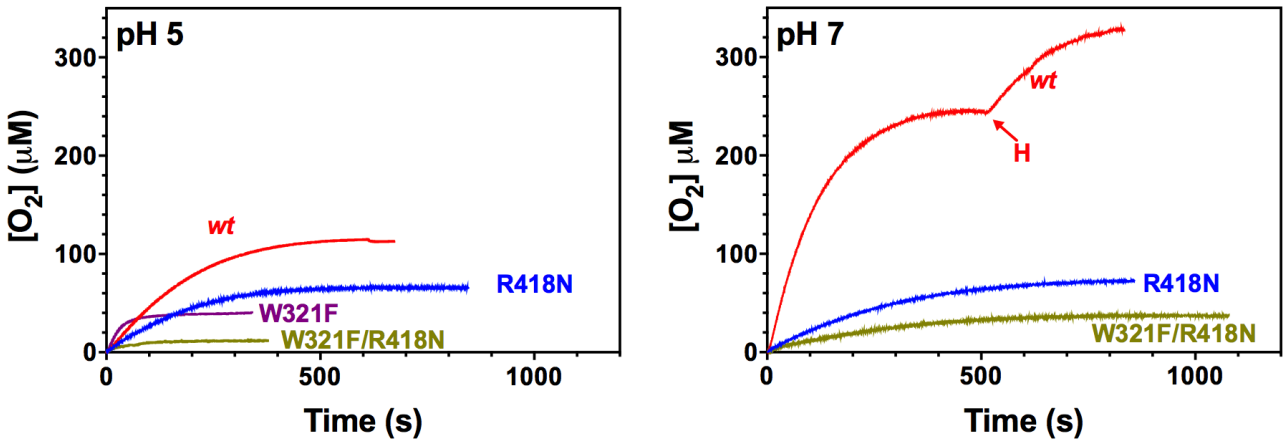

Figure 3.4.1. The effect of pH on catalatic O_2 production by *wt*, R418N, W321F, W321F/R418N KatG. All reactions contained 5 nM KatG, and were initiated by the addition of 0.5 mM H_2O_2. All reaction in Panel A, and the reactions of R418N and W321F/R418N in Panel B ceased due to enzyme inactivation, thus only the O_2 extent are shown. All reactions were carried out at 23 °C. Reactions at pH 5.0 (Panel A) were buffered with 50 mM acetate and reactions at pH 7.0 (Panel B) were buffered with 100 mM phosphate.

W321F/R418N were both inactivated during the reaction with the substantial amount of H_2O_2 left unreacted, suggesting elimination of the Arg switch favored inactivation, potentially due to higher frequency of off-catalase electron transfer. The double variant was more compromised than R418N, in that it achieved only half of the catalase cycle prior to inactivation compared to R418N, as judged by O_2 extent. These data suggest that the Trp-321 conduit is the strategy to cope with off-pathway electron transfer when occurs.

At pH 5 where off-pathway electron transfer was prominent, all four KatGs were inactivated, indicating that elimination of the Arg switch either by lower pH or mutagenesis leads to higher propensity for inactivation. At pH 5, *wt*KatG was the superior, as demonstrated by decent initial rate and the highest extent of O_2 production among all four KatG variants. Admittedly, it was compromised at this pH compared to pH 7. R418N was a worse catalase than *wt*KatG at pH 5 both in terms of sustainability. And this difference is likely due to the complete abolishment of Arg switch by mutagenesis in the variant. Interstingly, W321F was a much faster catalase than *wt*KatG. In fact, it is fastest catalase among all four variant in terms of the initial rate. However, W321F was far more compromised than *wt*KatG in sustainability, as demonstrated by the observation that it only accomplished 1/3 of the catalase cycles prior to inactivation, compared to *wt*KatG. Further, W321F was even inferior than R418N with respect to sustainability. These data suggest that while blocking the off-pathway electron transfer through Trp 321 (i.e., W321F) makes short-term gain in rates of catalase activity, but leads to long-term crisis in sustainability. On the other hand, *wt*KatG uses Trp 321 oxidation as a trade-off in order to be more sustainable in the long run. Also in support of the beneficial role of W321 is the hyper-vulnerability of W321F/R418N at pH 5. Indeed, W321F/R418N, in which the Arg switch was eliminated by mutagenesis to largely increase the frequency for off-pathway electron

transfer, and at the same time, Trp 321 was withdrawn as a solution for the off-pathway electron transfer, presented the worst case scenario.

We also compared the % of catalase activity remaining for KatG (i.e., *wt*KatG, R418N, W321F, W321F/R418N) post incubation with varying molar excess of H_2O_2 at pH 5 and pH 7 (Fig. 3.4.2), in order to examine the effect of such mutations(s) and pH on enzyme susceptibility to H_2O_2-dependent inactivation. At pH 7, where off-catalase electron transfer is not an issue, both *wt* and W321F KatG behaved nearly identical, and were relatively insensitive to H_2O_2-dependent inactivation. But at pH 5, where off-pathway electron transfer events are invited, both *wt* and W321F KatG were more susceptible to H_2O_2-dependent inactivation. However, strikingly, W321F KatG were far more compromised in sustaining catalase activity at pH 5. R418N KatG, where the arginine switch is eliminated by mutagenesis, was relatively more prone to H_2O_2-dependent inactivation at both pH 7 and pH 5. But the double variant W321F/R418N KatG, where the W321 is abolished, was far more vulnerable to H_2O_2-dependent inactivation both pH 5 and 7, compared to R418N KatG. In fact, W321F/R418N KatG at pH 7 and W321F KatG at pH 5 were highly similar in tolerance to H_2O_2. These data suggest that W321 was the major residue to handle off-catalase electron transfer events when they occur.

*wt*KatG was much less resistant to H_2O_2-dependent inactivation at pH 5 than at pH 7, indicating the conformation of the Arg switch ("*in*" and "*out*") preserved catalase activity. Indeed, *wt*KatG was similar to R418N with respect to vulnerability at pH 5, suggesting elimination of Arg switch by either manipulating pH or mutagenesis favored inactivation. Yet, *wt*KatG performed slightly better than R418N in coping with H_2O_2 assault, presumably because *wt*KatG still retained Arg switch, a small population of which could still adopt "*in*" conformation

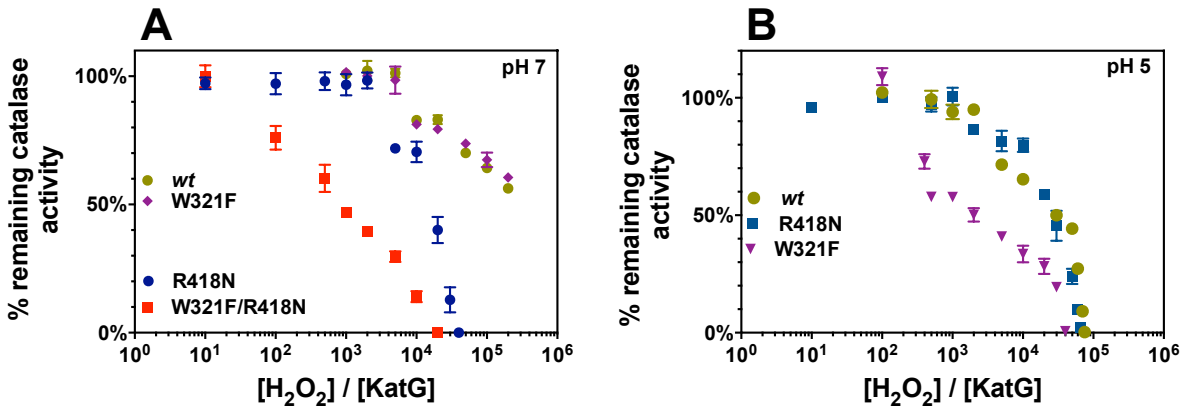

Figure 3.4.2. Effect of H_2O_2 preincubation and pH on the catalase activity of *wt* ,R418N, W321F, W321F/R418N KatG. KatG (200 nM) was preincubated with the indicated concentration of H_2O_2. Preincubations were carried out in either 100 mM phosphate, pH 7.0 or 50 mM acetate, pH 5.0. Following a 1 hour preincubation, an aliquot was withdrawn and catalase activity was measured with 10 mM H_2O_2 in 100 mM phosphate, pH 7.0 by O_2-senstive electrode. All reactions were carried out at 23 °C.

every once a while to mitigate inactivation process.

3.4.3 The effects of H_2O_2 concentration on k_{obs} for the H_2O_2-dependent inactivation.

We reacted KatGs with varying H_2O_2 concentrations at pH 5 and confirmed KatGs were inactivated in all cases of reaction afterwards by addition of enzyme or H_2O_2 after O_2 production ceased. We obtained the k_{obs} for the H_2O_2-dependent inactivation for all of the KatGs by fitting the O_2 production curve to the signal exponential equation. It is clear the k_{obs} for the H_2O_2-dependent inactivation of *wt*KatG and variants were independent of H_2O_2 concentration (Fig. 3.4.3A). This is consistent with the inactivation process starting after compound I formation. Moreover, we also observed a much higher value of k_{obs} for the H_2O_2-dependent inactivation by W321F/R418N and W321F than R418N and *wt*KatG. These results also indicate that Trp 321 is the residue to copy with the off-pathway electron transfer.

3.4.4 Conclusions

The presence and the conformation of the Arg switch preserves KatG catalase activity by limiting off-pathway electron transfer events. The proximal Trp 321 is the primary residue to handle this when it occurs.

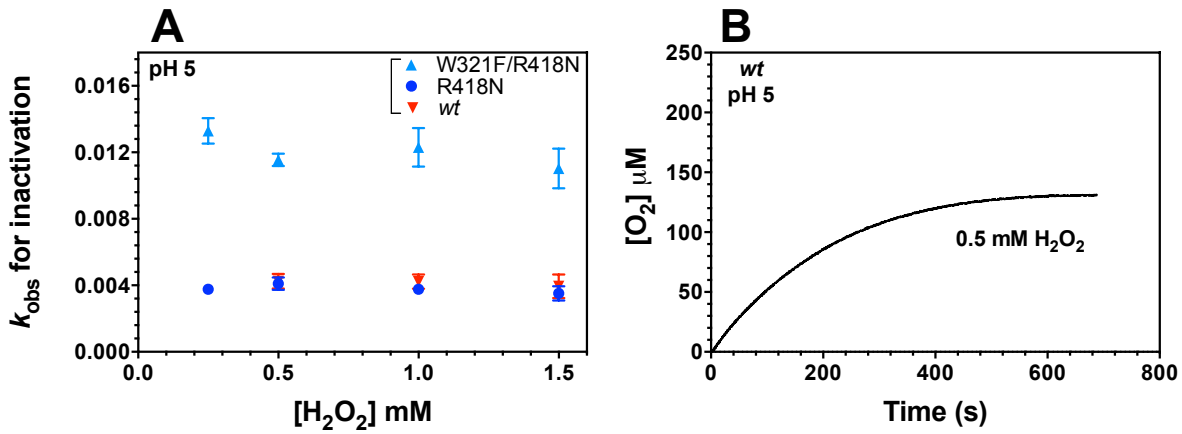

Figure 3.4.3. The effects of H_2O_2 concentration on k_{obs} for H_2O_2-dependent inactivation. The enzyme concentration was 10 nM, except for W321F/R418N, in which 30 nM was used to get better signal to noise ratio. All reactions were carried in 50 mM acetate, pH 5. All reactions were carried at 23 °C. One representative trace was shown in (B). Five replicates for each data point is were in (A).

3.5 Toward Identifying the Inactive Form of KatG

Our data show that (1) a transition from on-catalase radical to off-catalase radical during the reaction course of KatG with H_2O_2; and (2) a decreased intensity of later non-catalatic radicals over time; and (3) a decreased ability of PxEDs to rescue inactive species as time passes (data not shown). Accordingly, our working hypothesis is KatG uses the proximal Trp 321 route as primary antioxidants to absorb off-catalase oxidizing equivalents and as these frontline antioxidants are depleted, oxidative damage to structure(s) essential for KatG catalase activity ensue, which results in irreversible KatG inactivation. The early phase of inactivation is dominated by protein-based radicals and is reversible by inclusion of a PxED, whereas the later phase is dominated by amino acid oxygenation and other covalent modifications of the enzyme (i.e., heme oxidation) and cannot be reversed by inclusion of a PxED.

Our attempts to elucidate the covalent modifications of KatG, as well as the correlation of mutation(s) with the fate(s) of inactivation by mass spectrometry were not successful, due to the resistance of ionization of KatG in the ESI source. The on-going investigation is pursued by my co-workers.

3.5.1 Examination of UV-vis spectra of H_2O_2-preincubated KatG and % remaining catalase activity

In our preincubation experiments of KatG (*wt* and variants) with varying concentrations of H_2O_2 at pH 7 (Fig. 3.3.2) covered previously, we also withdraw the fractions to monitor the change of UV-vis spectra recorded for the post-reacted KatG in comparison to the unreacted enzyme (control) (Fig. 3.5.1). We aim to correlate the decrease of catalase activity with the change of enzyme spectra. Our data suggest the loss of KatG catalase activity was only observed above a threshold concentration of H_2O_2, for both *wt* and R418N at both pH. In sharp contrast, W321F/R418N showed loss of catalase activity starting by reacting with a handful of H_2O_2.

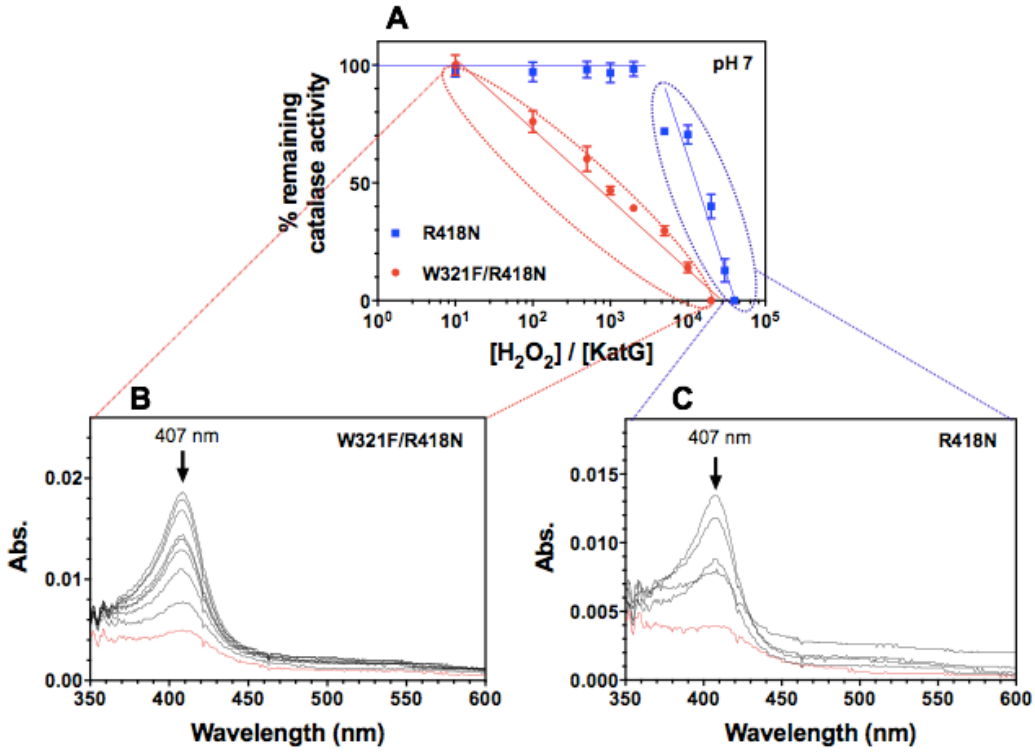

Figure. 3.5.1. UV-visible spectra of KatGs associated with residual catalase activity. Either R418N or W321F/R418N KatG (200 nM) was preincubated with the indicated concentration of H_2O_2 (A). Preincubations were carried out in 100 mM phosphate, pH 7.0. Following a 1 hour preincubation, an aliquot was withdrawn and catalase activity was measured with 10 mM H_2O_2 in 100 mM phosphate, pH 7.0 by O_2-senstive electrode. An aliquot was withdrawn, and UV-vis spectra were measured after centrifuge for 40 s. Spectra of W321F/R418N (B) and those of R418N (C) were shown. All reactions were carried out at 23 °C.

Interestingly, we observed that the bleaching of KatG's heme in corresponding samples with diminished catalase activity, irrespective of *wt* or variants. Indeed, no spectra changes of the post-reacted KatG were evident in samples that maintain a full level of catalase activity. Heme bleaching is indicative of either heme damage or less amounts of active enzyme in the solution or a combination of both. The possibility of less active enzyme in the solution can be resulted from enzyme precipitation due to the large-scale enzyme oxidative crosslinking and aggregation. We did not observe the precipitation after centrifuge of the fraction, however, that cannot rule out it as a possibility, considering the enzyme concentration in this experiment is very low (i.e., 200 nM). On the other hand, our attempts to seek heme degradation evidence by optical stopped-flow were not successful. We anticipate to differentiate these two possible outcomes by mass spectrometry in the future study.

Although no definitive answer(s) for the cause of heme bleaching that is associated with the loss of catalase activity, we think it represents protein extensive oxidation. Based on this assumption, our data suggest that devoid of Trp 321, both the substantial protein damage and the loss of catalase activity kick in for W321F/R418N almost immediately upon consuming a handful of H_2O_2 (Fig. 3.5.1A). Conversely, armed with Trp 321, *wt*KatG and R418N (Fig. 3.5.1B) both showed much better tolerance to H_2O_2. Indeed, while W321 is hot spot for oxidation upon reaction with 667 molar excess of H_2O_2 by *wt*KatG or R418N in the condition where off-pathway electron transfer events are prominent, both maintain a full level of catalase activity and no spectral change up to reacting with at least 1000 molar excess of H_2O_2. These data suggest that (1) Trp 321 is the frontline oxidative defense when the KatG encounters the self-inflicted oxidative stress in the active site due to uncommitted primary chemistry; and (2) withdrawal of this primary protective residue, KatG cannot ramp up its antioxidant capacity to handle the

uncommitted radical species in the dire situation, therefore oxidative damage to structures crucial for catalase function occurs within the first couple of catalase turnover, which fastens KatG inactivation.

Chapter Four: Discussion

The research of this dissertation has focused on two amino acids within the active site of KatG that have shown intriguing properties, but for whom a role in the function of the enzyme has remained unclear. The arginine switch (^{Sw}Arg) (Arg 418 in *Mt*KatG) adopts two conformations, the position of which is pH dependent. Above pH 6.5, its guanidinium side chain points predominantly toward the phenolate oxygen of the MYW tyrosine (i.e., "*in"* conformation), and below pH 6.5 it points away from the MYW cofactor and toward the protein surface (i.e., "*out*" conformation). We observed that susceptibility of KatG catalase to inactivation increases below pH 6.5. Our data suggest that these two pH-dependencies are connected. The proximal Trp (^{Px}Trp) is strictly conserved across all KatGs and even among other enzymes of its family (e.g., cytochrome *c* peroxidase [C*c*P]); its oxidation has been observed in a variety of reactions (e.g., KatG reaction with peracetic acid, CcP reaction with H_2O_2, etc.) However, in KatG ^{Px}Trp variants consistently retain catalase activity similar to the wild-type enzyme under standard assay conditions. Our previous investigations have suggested that ^{Px}Trp oxidation in KatG may be a step toward the inactivation of the enzyme.[129] Interestingly, results from computational studies have suggested the distribution of spin in the two-electron oxidized compound I state (i.e., Fe^{IV}=O[porphyrin]$^{\bullet+}$, Fe^{IV}=O[MYW]$^{\bullet+,}$ or Fe^{IV}=O[Trp]$^{\bullet+}$) is influenced by the position of the ^{Sw}Arg. Specifically, withdrawal of the ^{Sw}Arg and protonaton of the Tyr phenol oxygen of the MYW cofactor (both observed at low pH) favor the Fe^{IV}=O[Trp]$^{\bullet+}$ state over other two-electron oxidized forms of KatG.[135] Our own data have shown that a radical corresponding to the ^{Px}Trp replaces the MYW narrow-doublet radical as the catalase reaction rate slows and H_2O_2 consumption ceases. This is particularly apparent under acidic conditions (e.g.,

pH 5) where KatG also shows its greatest sensitivity to H_2O_2-dependent inactivation. Nevertheless, a coherent mechanism which connects all of these events has not been developed.

Although they may have other roles in function of KatG, the research described in this dissertation reveals that the ^{Sw}Arg and the ^{Px}Trp both function to extend KatG's capacity to degrade H_2O_2 by limiting/delaying peroxide-dependent inactivation. Furthermore, these residues appear to operate together to link preservation of KatG's catalase activity to its peroxidase activity. The data presented here suggest that the ^{Sw}Arg controls the frequency of off-catalase electron transfer events that occur during H_2O_2 decomposition by KatG, whereas the ^{Px}Trp is the point residue in a network of redox-active amino acids that effectively handles off-pathway electron transfer when occurs. By serving as a conduit to distribute sacrificial oxidation events away from the active site (e.g., to remote KatG protein components or an exogenous PxED), forestalling irreversible KatG inactivation.

A model summarizing the findings of this work is presented in Fig. 4.1.1. Following compound I (i.e., Fe^{IV}=O[porphyrin]$^{\bullet+}$) formation (**paths a**), the dominant pathway is the completion the KatG catalase cycle, specifically, intramolecular electron transfer to form compound I* (i.e., Fe^{IV}=O[MYW]$^{\bullet+}$) and subsequent catalatic oxidation of H_2O_2 by way of a Fe^{III}-$O_2^{\bullet-}$[MYW]$^{\bullet+}$ intermediate (abbreviated as **path b** in Fig. 4.1.1.). Consistent with this proposed mechanism, we capture the narrow doublet radical (i.e., MYW$^{\bullet+}$) and heme spectra reminiscent of a Fe^{III}-$O_2^{\bullet-}$ state at times corresponding to maximum catalase activity of KatG, regardless of *wt* or variants. Occasionally, off-catalase electron transfer events occur where the porphyrin radical is instead reduced by the proximal Trp (Trp 321) to form Fe^{IV}=O[Trp 321]$^{\bullet+}$ (reactions c). Accordingly, we observe by RFQ-EPR that Trp 321$^{\bullet+}$ accumulates and replaces MYW$^{\bullet+}$ as the dominant radical species by the time H_2O_2 consumption by the enzyme ceases.

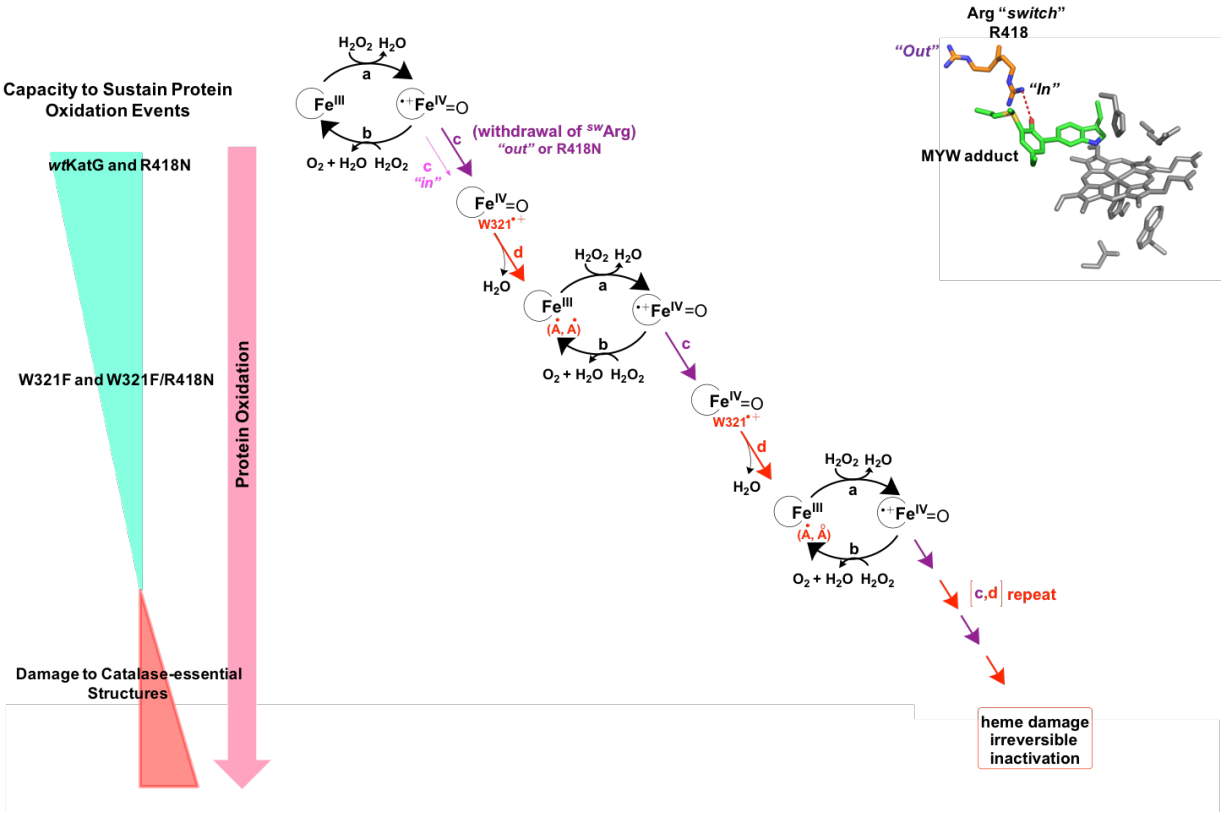

Figure 4.1.1. Proposed mechanism for inactivation of KatG catalase and the role of the Arg switch and Trp 321 in preserving KatG catalase activity.

From that point and well into the minute time scale, the Trp 321$^{\bullet+}$-dominated EPR spectrum diminishes in favor of signals that lack exchange broadening, suggesting radical transfer away from the active site towards the enzyme surface. In the reaction scheme (Fig. 4.1.1), this is represented by reactions d. In principle, radical transfer from the active site should regenerate the ferric KatG, enabling the enzyme to reengage in the catalatic mechanism. However, this will have come at the expense of the oxidation of enzyme structure remote from the active site.

Our results suggest that ^{Sw}Arg is a central player in controlling the frequency of reaction c (off-pathway electron transfer) *vs.* path b (catalase activity). Indeed, disruption of ^{Sw}Arg interaction with the MYW cofactor (either by pH or mutagenesis), generates an enzyme that in the absence of a PxED inactivates after fewer catalytic cycles and at lower concentrations of H_2O_2. In the presence of a PxED, such is evident by a robust peroxidase activity that coincides with a substantially expanded capacity to use its catalase mechanism to degrade H_2O_2. In the scheme (Fig. 4.1.1), this is reflected a higher propensity towards taking path c than when the ^{Sw}Arg is available and oriented toward the MYW cofactor. Based on H_2O_2 consumed relative to the accumulation of oxidized PxED, we estimate that *wt*KatG explores reaction c *vs.* path b around once per 140 catalase turnover at pH 5. Under similar conditions, the R418N variant does so about once per 12 catalase turnovers. The R418N variant favors reaction c much more at lower concentration of H_2O_2, such that around 25% of the substrate is used toward the oxidation of PxED in reaction where one molar equivalents of H_2O_2 is used. It appears that *wt*KatG also explores reaction c at pH 7, but to a far lesser extent. Accordingly, the enzyme is relatively insensitive to H_2O_2-dependent inactivation. Additional catalase turnover produces additional off-pathway electron transfer, represented by arrow c and d. But the restoration of the ferric enzyme in this context comes at the expense of protein oxidation. It is a cumulative process and, absent a

PxED, the enzyme has a finite capacity to sacrificially absorb these off-catalase electron transfer events. As such, the progression of protein oxidative damage eventually leads to damage to the catalase-essential components of the enzyme and irreversible inactivation of KatG.

On the other hand, we suggest that Trp 321, counterintuitively, is a primary conduit to handle the distribution of oxidizing equivalents to remote/surface protein substituents thereby limiting destructive reactions within the active site. Accordingly, the faster Trp 321 conduit depletes, the quicker the enzyme demise ensues. An inverse triangle is to represent the ability of KatG to sustain off-pathway protein oxidation. We show *wt*KatG and R418N with an oxidizable Trp have higher capacity to handle off-catalase protein oxidation than variants bearing W321F mutation (i.e., W321F, W321F/R418N). As KatG goes through off-catalase radical transfer in a vertical direction, it will eventually deplete the sacrificial amino acids, and then lead to damage to catalatic-essential components. Manifestly, Trp 321 is the major residue to handle off-catalase protein oxidation events. First, for *wt*KatG and R418N KatG, when they encounter off-pathway electron transfer, Trp 321 oxidation not only prolongs catalase activity of KatG, but also provides a hole-hopping mechanism for PxED-based prevention of KatG inactivation, if a PxED is present. Second, for W321F and W321F/R418N KatG, when face off-pathway electron transfer, off-catalase radicals handled by another route(s) appear to not only produce the more rapid demise of the enzyme as compared to variant where the proximal Trp was present, but also they are far less effective for PxED-based prevention of KatG inactivation.

We showed that at pH 7, where the off-catalase electron transfer is not an issue, the tolerance to H_2O_2-dependent inactivation followed *wt*KatG ≈ W321F >> R418N > W321F/R418N. At pH 5, where there is a much greater frequency of off-pathway electron transfer, the order followed *wt*KatG > R418N > W321F > W321F/R418N. All these data are

consistent with our model: (1) withdrawal of the arginine switch leads to more off-pathway protein oxidation, and more rapid depletion of the capacity provided by Trp 321, thus quicker to the demise of the enzyme; and (2) devoid of Trp 321 creates enzymes that have a lower capacity to handle off-pathway electron transfer events, when they occur.

We propose that inactive protein-based radical species dominated in the early phase will be replaced by the advanced covalent modifications of amino acid side chains (i.e., amino acid oxygenation, crosslinking) in the later phase. There are several lines of evidence to support this idea. First, the intensity of non-catalatic singlet radical signals diminishes over time upon reaction of KatG with H_2O_2 by RFQ-EPR. Second, while PxED can restore KatG catalase activity, the longer the enzyme reacts with H_2O_2 without a PxED, the less activity is recover-able. Third, CcP, KatG closest family member, showed extensive oxidation of protein after reacting with 10 molar excess of H_2O_2 in the absence of ferrocytochrome c.

A PxED, when present, could deliver electron from an exterior site via a conduit involving the Trp 321 to the active site. Since Trp 321 is not surface-exposed, we think that M377 as well as Y353 and/or W341 are also involved in the electron-hole transfer events. In this manner, PxED by its own oxidation rescues the inactive catalatic radical species at the early stage and protects KatG from advanced/irreversible inactivation primarily via Trp 321 conduit. This is supported by the observation that with a PxED included, only $MYW^{\bullet+}$ is detected at the earliest time point during KatG (*wt*KatG or R418N) reacting with H_2O_2, no other radical species accumulate when H_2O_2 depletion ceases or thereafter.

4.1 The ^{Sw}Arg: a central player minimizing propensity for off-catalase electron transfer

Our data suggest that inactivation of KatG during catalatic consumption of H_2O_2 occurs due to off-pathway intramolecular electron transfer and the ^{Sw}Arg is the central control minimizing off-pathway electron transfer events for self-preservation in KatG.

We have substantial evidence to suggest that elimination of the ^{Sw}Arg dramatically increases the through-protein electron transfer. First, R418N exhibits 60-fold, 30-fold and 150-fold increases in peroxidase activity (by k_{cat}/K_M with respect to [H_2O_2]) compared to *wt*KatG when ABTS, CPZ and TMPD were included as PxEDs, respectively. In a similar vein, R418N yields much higher yields of oxidized PxED (e.g., $ABTS^{\bullet+}$, $CPZ^{\bullet+}$/CPZSO, $TMPD^{\bullet+}$, etc) per H_2O_2 consumed during catalatic H_2O_2 consumption than does *wt*KatG, suggesting (1) much higher partition of peroxidase activity (off-pathway electron transfer) *vs.* catalase activity; and (2) while PxED oxidation corrects the catalase-inactive species, much more PxED intervention is required in the case of R418N.

Elimination of the ^{Sw}Arg by mutagenesis created an enzyme (i.e., R418N KatG) that has a higher propensity towards off-pathway electron transfer than that (i.e., *wt*KatG) by the manipulation of its orientation by pH. Though the dominant conformation of the ^{Sw}Arg at pH 5.0 is "*out*" (given an apparent pK_a of 6.5), the ability to occupy the "*in*" conformation for a limited time/to a limited extent appears to mitigate some of the enzyme's sensitivity to inactivation. These data are consistent with the proposed role of ^{Sw}Arg in this catalase mechanism, which tentatively facilitates the decomposition of compound III* (Fe^{III}-$O_2^{\bullet-}$[MYW]$^{\bullet+}$) through promoting the electron transfer from Fe^{III}-$O_2^{\bullet-}$ heme intermediate to the $MYW^{\bullet+}$ and release triplet O_2 by swing from the "*out*" conformation to "*in*" conformation.[113,123] Interestingly,

monofunctional peroxidases do not have this unique ^{Sw}Arg, and the ferric-superoxide species are inactive and the enzyme gets stuck in that form.

Based on the premise that off-pathway electron transfer will eventually lead to inactivation, the cases where the Arg switch is absence by either lower pH or by mutagenesis, should be more prone to inactivation. As expected, we show R418N is a more compromised catalase with respect to sustainability (i.e., the turnover number it sustains prior to irreversible inactivation) across the pH compared to *wt*KatG. At the representative pH 5 and 7, the order of susceptibility to H_2O_2-dependent inactivation follows R418N at pH 5 and pH 7 > *wt*KatG at pH 5 >> *wt*KatG at pH 7.

Although stopped-flow and RFQ-EPR experiments do not inform much about the frequency of off-catalase electron transfer *per se*, but they validate the occurrence of off-pathway through-protein hole hopping. Transition of the steady-state intermediates (the narrow doublet $MYW^{\bullet+}$ → exchange-coupled radical $W321^{\bullet+}$) during turnover of KatG (*wt*KatG at pH 5; R418N at pH 5 and 7) with H_2O_2 not only reflects facile off-catalase through-protein radical transfer occurring in KatG when the Arg switch is withdrawn, but also suggests W321 as the hotspot for oxidation.

Magliozzo and co-workers provided the 1st experimental evidence that disruption of the Arg switch enhances off-catalase protein oxidation with the *Mt*KatG R418L variant, suggested by the higher percentage of oligomerization after catalase turnover of R418L compared to *wt*KatG.[115] Surprisingly, no protein-based radical species other than the catalase-active narrow doublet (i.e., $MYW^{\bullet+}$) was detected in their reaction of R418L with H_2O_2 by RFQ-EPR, and the narrow doublet persisted throughout the catalase turnover of R418L. Since the EPR spectra they reported were recorded at 77 K, it is possible the $W321^{\bullet+}$ was not detected in their samples

because of unfavorable experimental conditions. Alternatively, either $W321^{\bullet+}$ was not formed in their samples at all, or too short-lived to accumulate to be detected, provided they seek for it at liquid helium temperature yet do not find it. Given the fact that they observed enhanced oligomerization in R418L reacting with H_2O_2 compared to *wt*KatG, lack of detection of any other protein-based radical(s) in their RFQ-EPR samples may indicate other radical species do not accumulate enough to be detected. Different substitutions may lead to different kinetics in terms of the formation and dissipation of other radical species in R418L and R418N. Stated another way, these two variants may behave differently, we noted R418N reacting with 50,000 molar excess of H_2O_2 at pH 5 and pH 7 yielded negligible oligomer after the reaction, indicating other oxidative modifications (i.e., oxygenation) may be preferred.

4.2 ^{Px}Trp: the primary site for off-catalase hole hopping

Our data suggest that W321 is the hot spot to initiate off-pathway electron transfer. We show the exchange-coupled radical consistent with what was previously assigned to the proximal Trp (W321 in *Mt*KatG and W330 in *Bp*KatG) replaces the narrow doublet radical during the catalatic turnover of R418N at both pH 5 and 7. We note the exchange-coupled radical is longer-lived, and also exhibits more prominent wing broadening in R418N reactions at pH 5 compared to pH 7. This may be because (1) pH difference could elicit H-bonding environment change, thus affecting the stability of W321 radical; and (2) W321 route has been used to a different extent at different pH conditions, thus the difference in lineshape simply reflects different percentage of the exchange-coupled species out of all radical species. But when PxED (ABTS, ascorbate) was present, no radical species expect the catalatic competent narrow doublet were detected. These data indirectly confirm (1) W321 is not directly involved in catalase mechanism; and (2) W321 is the conduit through which PxED rescues inactive species on the exterior of the protein.

The exchange-coupled radical species are not detected during the turnover of W321F/R418N with excess H_2O_2 at either pH 5 or 7, consistent with our thought that W321 is the radical site. Likewise, the exchange-coupled radical species are not detected during the turnover of W321F with excess H_2O_2 at pH 5 either, in contrast to *wt*KatG. This needs to practice with caution, because many other reasons can explain its lack of detection. For example, the time resolution of the sample is not good enough to capture it. Or W321 may be involved to facilitate the formation of exchange-coupled radical, rather than itself being the radical site. In addition, other Trp residue(s) closed to the heme can also be the candidate that holds the radical, in the magnetic coupling with the iron. However, in addition to RFQ-EPR data, our inactivation assays strongly argue for the participation of W321 as the radical site. This proximal Trp has been shown in several other contexts to be prone to oxidation. Reaction of KatGs with PAA generate compound I species, which include a radical at proximal Trp in *Mt*KatG and *Bp*KatG.[130,151] Calculations have shown that KatG compounds I (i.e. two-electron oxidized KatG) have substantial spin density associated with the proximal Trp, especially prominent when the arginine switch is oriented away from the MYW adduct.[135] Indeed, we previously captured the exchange-coupled radicals consistent with W321 radical accumulated during catalase turnover of wild-type *Mt*KatG at pH 5 exactly where the "*out*" conformation of the Arg switch dominates and where it is prone to inactivation. Interestingly, this species as well as the susceptibility to inactivation has been observed with R418N turnover of excess of H_2O_2 at both pH 5 and 7. Moreover, CcP, which resides in the same superfamily with KatG, forms compound ES (i.e., Fe^{IV}=O[Trp 191]$^{\bullet+}$) upon reaction with H_2O_2, in which Trp 191 is CcP's proximal Trp.[77]

4.3 Role of ^{Px}Trp: handle protein oxidation events

Recently, Gray and Winkler propose that a preponderance of oxidizable amino acids found in oxidoreductases protects the active-site components from oxidative inactivation by constituting pathways to release uncommitted oxidants.[33] Specifically, CcP has been recently shown to spare its cofactor heme from damage by extensive protein hole hopping revealed by LC-MS/MS. Based on the algorithms of Gray and Winkler, four pathways of redox chains in KatG have been proposed (Fig. 4.1.2). For this study, the hole hopping path that includes W321 is of high interest. Namely heme-Trp 321-Met 377-Tyr 353 and/ or Trp 341.

Our data suggest the proximal Trp 321 is the major internal antioxidant to handle self-inflicted oxidative stress resulted by off-pathway electron transfer during catalase turnover in two ways. First, the Trp 321 conduit (i.e., heme-Trp 321-Met 377-Tyr 353 and/ or Trp 341) serves as internal electron donors to resolve off-pathway radicals, in the absence of exogenous reducing substrates at the enzyme exterior. As such, the catalase activity of KatG prolongs. Second, the Trp-321 conduit bridges the active site and the reducing substrates on protein exterior provided PxEDs are available. Therefore, PxEDs can deliver electron to rescue inactive intermediates through this route as many times as necessary, provided this route is not blocked by oxidative modification. This makes this antioxidant mechanism even more effective since it is not a stoichiometric reactant.

We have substantial evidence to support the antioxidant role of Trp 321. First, we capture $W321^{\bullet+}$ upon reaction of KatG (i.e., *wt*KatG at pH 5; R418N at pH 5 and 7) with H_2O_2 in all three cases, however, the enzyme resists to the loss of catalase activity in these conditions, suggesting sacrificial oxidation of Trp 321 forestalls inactivation of KatG. Second, withdrawal of W321 while increasing the propensity towards off-pathway electron transfer (i.e., W321F at

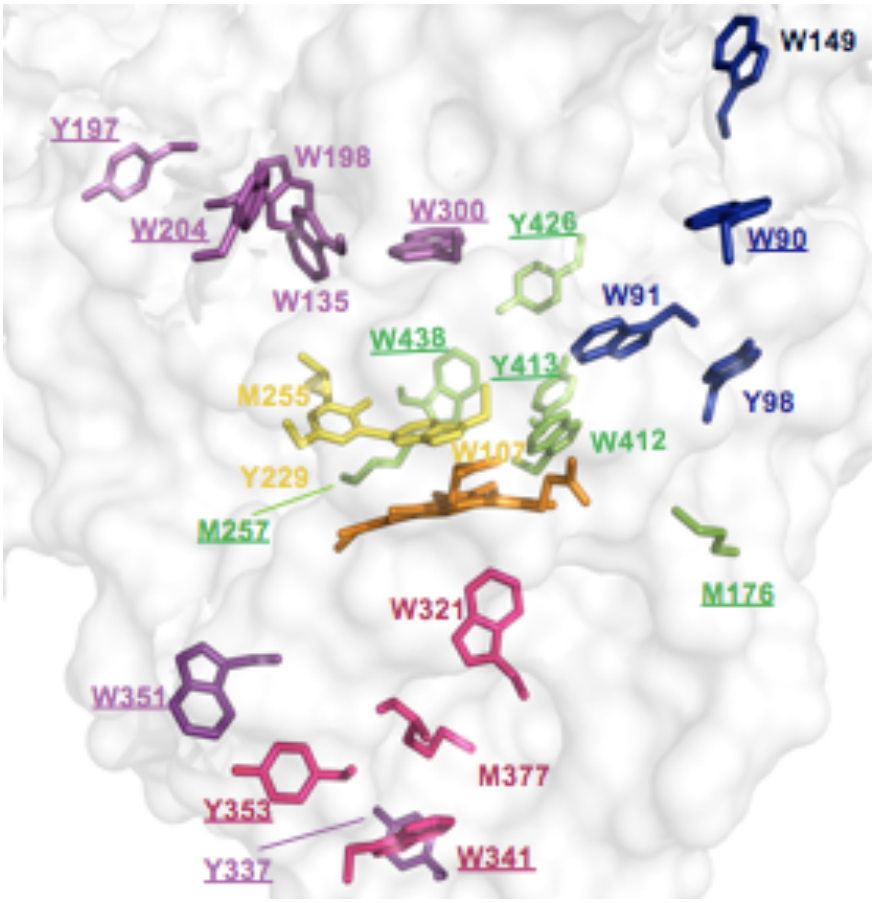

Figure 4.1.2 Oxidizable amino acids in KatG protein matrix. Four principal pathways are proposed. The *magenta* path connects to the heme via the proximal Trp (Trp 321). The *green* path connects to the heme via Trp 412. The *blue* path connects to the heme via Trp 91. The *purple* path is purported to connect to the heme via the MYW adduct Trp (Trp 107).

pH 5, and W321F/R418N irrespective of pH), we produced highly compromised KatG in terms of sustainability as a catalase. Specifically, *wt*KatG and W321F are nearly identical in terms of the kinetic parameters of the catalase activity (i.e., k_{cat}, K_{on}) and the tolerance to H_2O_2-dependent inactivation at pH 7, where off-pathway electron transfer is not an issue. However, at low pH (i.e., pH 5.0) where off-pathway electron transfer problem intensifies, W321F KatG is highly compromised in its ability to sustain catalase activity compared to *wt*KatG and even R418N, as judged by its much lower tolerance to H_2O_2-dependent inactivation. Indeed, it starts to loss catalase activity even after consumption with a handful molar excess of H_2O_2. Interestingly, the absence of the protective means (i.e., devoid of Trp 321 in W321F) hurts more than inviting the oxidative stress problems (i.e., withdraw ^{Sw}Arg in R418N), emphasizes the crucial role of the Trp-321 in coping with off-pathway protein oxidation. In the similar vein, W321F/R418N has much lower tolerance to H_2O_2-dependent inactivation compared to R418N. It is important pointing out that withdrawal of the arginine switch by mutagenesis not only greatly enhances the frequency of off-catalase electron transfer in KatG, but also leads to a **slower** catalase with respect to catalase rate, compared to *wt*KatG. The later point is consistent with the general proposal that ^{Sw}Arg facilitates the electron flow from the ferric-superoxide heme to MYW radical and releases O_2. Strikingly, R418N is slow but relatively sustainable as catalase *vs.* W321F/R418N is slow but hyper-susceptible to catalase inactivation. Clearly, devoid of antioxidant Trp 321 while encountering extensive off-pathway electron transfer (i.e., eradicate ^{Sw}Arg completely by mutagenesis) is detrimental. These data again suggest Trp-321 is the major strategy KatG uses to handle off-catalase protein oxidation when it occurs.

Likewise, the evidence to support the antioxidant role of W321 in the presence of PxEDs is followed. First, inclusion of a PxED washes out all the radicals except the catalase-essential

narrow doublet in the cases where susceptibility of inactivation is seen (i.e., *wt*KatG pH 5; R418N pH 5 and 7). These data suggest that through Trp 321, PxED can recycle enzyme back to catalase turnover and simultaneously optimize catalase activity. Second, PxED have less stimulatory effects on the catalase activity of W321F, compared to *wt*KatG. Likewise, it only have very marginal protective effects on catalase activity of W321F/R418N. These results suggest that devoid of Trp 321, PxED protective effect to KatG catalase activity is far less prominent than otherwise.

4.4 Novel aspects of catalase activity of KatG

Our data show that effective catalatic disproportionation of H_2O_2 by KatG not only requires the on-catalase mechanism but also the off-catalase mechanism (Trp 321 oxidation) when the primary chemistry fails. We showed the Trp 321 paradox in the KatG catalase function: the oxidation of Trp 321 initiates enzyme inactivation, however, devoid of this seeming culprit counterintuitively fastens the inactivation. As such, the off-catalase mechanism is essential to the sustainability of on-catalase mechanism provided the primary catalase fails. How to balance both activities so that off-catalase mechanism serves for the on-catalase mechanism for efficient disproportionation of H_2O_2, KatG uses a conformationally-dynamic ^{Sw}Arg. In this manner, the protective peroxidase activity will not outcompete/disrupt catalase activity, but rather, this protective mechanism only operates when needed. This paradox indicates evolution possibly makes compromise between success in its highly demanding job (i.e., catalase activity) and its self-preservation (by extension peroxidase activity, in which the Trp 321 route and/or external PxEDs could be the reducing substrates). Adding to the elegancy of method is that the build-in Trp-321 antioxidant route is sustainable in that it could recruit electrons from external PxEDs if there, instead of sacrificing themselves, although consuming themselves in the absence of

external PxEDs also provides KatG with decent protection to quench the fire in the stressed active site.

Considering many intracellular pathogens carry KatG to defend against host-derived H_2O_2 in mM concentration in the highly acidic (i.e, pH 5) and oxidizing environment of neutrophils and microphages, the inactivation phenomenon is very likely to be physiologically relevant. The mechanism by which KatG slows down/mitigates this process will contribute to the colonization and survival of the pathogens carrying it. Thus this deserves further studies, and it will contribute to our understanding of host-pathogen interaction, which will likely provide a treatment for a disease by enhancing host capability to fight the pathogen. In addition, our research also contributes to knowledge pool of how oxidoreductases protect themselves from damage by potentially destructive chemistry they are catalyzing, provided catalytic turnover fails. With the ability to form the highly oxidizing species during catalysis, these oxidoreductases can do amazing chemistry. However, even with fidelity slightly lower than 100%, the accumulated consequence is grave. How to minimize this detrimental effect due to uncommitted oxidizing bombs have been popularly investigated. KatG seems a good system to investigate. It capitalizes the comformationally-dynamic arginine switch to maximize the fidelity to its central catalase activity. Further, when the central catalase turnover fails, it directs the oxidizing equivalent to the Trp 321, the essential residue to handle off-pathway electron transfer, for self-preservation of KatG. This is tentatively achieved by modulation of oxidation potential of the protein internal electron donors (i.e., MYW *vs.* Trp 321) through its positive side chain and two conformations.

4.5 Unresolved issues

So far the comparisons and conclusions we discussed are based on the assumptions that mutation of R418 and/or W321 is not negatively affecting the integrity of the MYW adduct,

which may not be the case. Just mirrors that fact that KatG needs internal antioxidants to resolve the uncommitted oxidizing equivalents failed from catalase turnover during H_2O_2 dismutation, the formation of the covalent adduct cofactor from activated heme by H_2O_2 during KatG maturation is as demanding, if not more, compared to its catalase activity. Therefore, we think the process of forming intact MYW adduct also requires redox-active amino acids to absorb off-pathway electron transfer when occurs. When we mutate oxidizible Trp to non-oxidizable Phe, it is possible that two variants W321F and W321F/R418N are compromised already during their maturation stage. The extent to which they are compromised can vary and include many possibilities: (1) the integrity of MYW adduct is not 100%, with some of MYW irreversibly oxidized during maturation; (2) MYW is 100% intact, however, the redox-active amino acids that serve as antioxidants partly are damaged during the process of forming the adduct, which will pose disadvantage later on in the catalase function; and (3) heme is modified. We do not think these possibilities would be severe enough to negate our major conclusion in this study, for multiple reasons. First, we captured the MYW radical in all 4 variants we during its fastest catalase turnover with H_2O_2. Second, W321F is indistinguishable in every respect from *wt*KatG at neutral pH. Third, W321F/R418N has highly similar catalatic steady-state parameters as R418N at neutral pH. Fourth, even if a small portion of the enzyme is oxidatively damaged, we likely get rid of it by multiple steps of purification. Yet, all these do not rule out the possibility that W321 mutation are already compromised to a certain extent at the stage of MYW formation. This can be more likely in W321F/R418N. This leaves room for future work to examine the chemical form of four KatG variants by MS or crystallography.

4.6 Speculations

Our data suggest that KatG is full of compromises likely due to two factors. First, the harsh reality it confronts: both the hostile environment where it resides (i.e., the acidic phagolysosomes of neutrophils and macrophages) and the potentially highly oxidizing environment in the active site when the primary catalase fails. Second, it is a **peroxidase** but engineered by nature to be good at catalase activity approaching those of typical catalases. In a peroxidase active site, it employs a post-translationally generated MYW covalent adduct and a conformationally dynamic "arginine switch" ^{Sw}Arg. In KatG, MYW adduct needs to be the transient radical site for catalase mechanism. How to modulate the reduction potential of the MYW adduct to accommodate oxidation and reduction to give optimal catalase activity is challenging. In this regard, KatG seems to use a conserved conformationally dynamic ^{Sw}Arg to modulate the electronic structures of the active site by its swinging positive side chain between the two conformations. But this does not seem perfect, especially has been seen in a couple of KatG from bacterial sources that the pK_a (i.e., pH 6.5) gives 50/50 "*in*" and "*out*" conformations of arginine switch is a little off from the physiological relevant pH (i.e., pH 5.0). Interestingly, MagKatG2 from fungal exhibited a much acidic pK_a gives 50/50 "*in*" and "*out*" conformations of arginine switch. As such, its optimal catalase activity occurred at lower pH, which was proposed to better defend the organism against the host immune response. Why fungal MagKatG2 has a lower pK_a than its bacterial counterparts is not clear, but it is proposed to be affected by the protein environment (i.e., the interaction partner of arginine switch when it points away from the active site). It is speculated that evolution will manipulate the arginine switch pK_a of the "*in*" and "*out*" conformations to better serve the role in catalase activity. But evolutionary biology seems to realize this is tough. So nature seems to come with a strategy. It builds a

proximal Trp (Trp-321) on the opposite side of the MYW adduct, whose reduction potential is controled by the arginine switch. The coorperation of the arginine switch and Trp 321 makes sure the off-catalase (peroxidase activity) serves for its central catalatic disproportionation of H_2O_2. Whenever off-pathway electron transfer is needed, Trp-321 is the preferred conduit to cope with this. Although irreversible inactivation of KatG will come after protein oxidation depletes the antioxidant power within the protein and leads to catalase-crucial structure damage. But the sacrificial oxidation of Trp-321 forestalls the inactivation and prolongs the catalase activity.

Chapter Five: Summary and Future Studies

5.1 Summary

KatG is still full of mysteries after its initial discovery 30 years ago.

KatG masters catalatic disproportionation of H_2O_2 which rivals monofunctional catalases. Strikingly, it is the only member in peroxidase superfamily that is capable of doing this. Indeed, KatG relies on both on-catalase mechanism and off-catalase mechanism under the control of an invariant conformationally dynamic "arginine switch" ^{Sw}Arg to achieve this new function. The on-catalase mechanism has attracted intense attention across KatG field, but the off-catalase mechanism had just recently come into the radar. Our data reveal that off-catalase mechanism does not jeopardize catalatic detoxification of H_2O_2, counterintuitively, however, is an essential component to KatG H_2O_2-detoxification mechanism that ensures the sustainability of the on-catalase mechanism. We are the first to find out the ability to sustain the catalase activity is as important as the catalase activity itself in KatG system.

Our research makes a stride into a novel territory in KatG field and this has a couple of important ramifications. First, it facilitates the appreciation of the virulence of numerous bacterial and fungal pathogens that appear to use KatG as the frontline defense against host-derived H_2O_2. Second, this protective mechanism (off-catalase electron transfer) KatG employs aids our understanding of how oxidoreductases balance their demanding catalysis and self-preservation. A popular current theme proposed by Dr. Gray and Winkler is the oxidoreductases that form highly reactive intermediates should have protective mechanisms available provided the primary chemistry fails. They further suggested that the clusters of oxidizable amino acids serve as the conduits to off-load the uncommitted oxidizing equivalents to remote protein surface, where they can be reduced by cellular reductants if exist. In addition, they think that the

protective mechanism should not disrupt the primary enzyme function to be effective. Our data suggest all these above components have been incorporated to KatG structure during evolution. KatG has both the catalatic-essential MYW adduct cofactor, and antioxidant-essential Trp conduit in the repertoire. Whether to proceed with catalase activity or explore off-catalase electron transfer is deliberately controlled by a conformationally-dynamic ^{Sw}Arg so that the protective peroxidase activity will not outcompete/disrupt catalase activity, but rather, it only operates when needed. KatG is not alone, a couple of oxidoreductases have been reported to suffer inactivation due to either low fidelity to primary catalysis or absence of the substrates. Our data improve the understanding of the tradeoff that oxidoreductases use overall. Third, our research promotes the understanding of the control of electron transfer, a popular theme in enzymology.

5.2 Future Studies

Many knowledge gaps remain to be elucidated. First, what is the chemical form of the inactive KatG? Our preliminary data are indicative of a couple of possibilities: oxidative damage of the heme and/or the catalase-essential amino acid(s) and/or extensive enzyme crosslinking. These await the future investigations by LC-MS/MS. Second, what are the other conduits that involved in the off-pathway electron transfer, besides the proximal Trp? We show that PxEDs still have marginal protective effects on the catalase activity of W321F and W321F/R418N (to a much less extent in the double variant), suggesting other route(s) bypassing Trp 321 also participates in forestalling catalase inactivation of KatG. We anticipate LC-MS/MS will provide an answer. Third, does Trp 321 oxidation provides protection to the MYW adduct formation process? Based on our results and the proposal of Gray and Winkler, we think the formation of the covalent adduct cofactor from activated heme by H_2O_2 during KatG maturation is as

demanding as the catalase mechanism itself, if not more, and this process is very likely facilitated by using the same protective repertoire. We anticipate to reveal this possibility by comparing our reconstituted *wt*KatG and W321F KatG that lack the covalent adduct during the adduct formation.

Reference

(1) Pau, M. Y., Lipscomb, J. D., and Solomon, E. I. (2007) Substrate activation for O2 reactions by oxidized metal centers in biology. *Proceedings of the National Academy of Sciences 104*, 18355–18362.

(2) Imlay, J. A. (2003) Pathways of oxidative damage. *Annual Reviews in Microbiology 57*, 395–418.

(3) Cadenas, E. (1989) Biochemistry of oxygen toxicity. *Annual Review of biochemistry 58*, 79–110.

(4) Elstner, E. F. (1982) Oxygen activation and oxygen toxicity. *Annual Review of Plant Physiology 33*, 73–96.

(5) Wiseman, H., and Halliwell, B. (1996) Damage to DNA by reactive oxygen and nitrogen species: role in inflammatory disease and progression to cancer. *Biochemical Journal 313*, 17.

(6) Bandyopadhyay, U., Das, D., and Banerjee, R. K. (1999) Reactive oxygen species: oxidative damage and pathogenesis. *Current Science-Bangalore- 77*, 658–666.

(7) Sharma, P., Jha, A. B., Dubey, R. S., and Pessarakli, M. (2012) Reactive oxygen species, oxidative damage, and antioxidative defense mechanism in plants under stressful conditions. *Journal of Botany 2012*.

(8) Bartz, R. R., and Piantadosi, C. A. (2010) Clinical review: oxygen as a signaling molecule. *Critical Care 14*, 234.

(9) Balaban, R. S., Nemoto, S., and Finkel, T. (2005) Mitochondria, oxidants, and aging. *Cell 120*, 483–495.

(10) Aon, M. A., Cortassa, S., and O'Rourke, B. (2010) Redox-optimized ROS balance: a unifying hypothesis. *Biochimica et Biophysica Acta (BBA)-Bioenergetics 1797*, 865–877.

(11) Babior, B. M., Lambeth, J. D., and Nauseef, W. (2002) The neutrophil NADPH oxidase. *Archives of Biochemistry and Biophysics 397*, 342–344.

(12) Babior, B. M. (2004) NADPH oxidase. *Current Opinion in Immunology 16*, 42–47.

(13) Vergnaud, S., Paclet, M.-H., El Benna, J., Pocidalo, M.-A., and Morel, F. (2000) Complementation of NADPH oxidase in p67-phox-deficient CGD patients: p67-phox/p40-phox interaction. *European Journal of Biochemistry 267*, 1059–1067.

(14) Klebanoff, S. J. (2005) Myeloperoxidase: friend and foe. *Journal of Leukocyte Biology 77*, 598–625.

(15) Klebanoff, S. J., Kettle, A. J., Rosen, H., Winterbourn, C. C., and Nauseef, W. M. (2013) Myeloperoxidase: a front-line defender against phagocytosed microorganisms. *Journal of Leukocyte Biology 93*, 185–198.

(16) Fridovich, I. (1995) Superoxide radical and superoxide dismutases. *Annual Review of Biochemistry 64*, 97–112.

(17) Djaman, O., Outten, F. W., and Imlay, J. A. (2004) Repair of oxidized iron-sulfur clusters in Escherichia coli. *Journal of Biological Chemistry 279*, 44590–44599.

(18) Kono, Y., and Fridovich, I. (1982) Superoxide radical inhibits catalase. *Journal of Biological Chemistry 257*, 5751–5754.

(19) Blum, J., and Fridovich, I. (1985) Inactivation of glutathione peroxidase by superoxide radical. *Archives of Biochemistry and Biophysics 240*, 500–508.

(20) Forman, H. J., and Fridovich, I. (1973) Superoxide dismutase: a comparison of rate constants. *Archives of Biochemistry and Biophysics 158*, 396–400.

(21) Stadtman, E. R., and Berlett, B. S. (1998) Reactive oxygen-mediated protein oxidation in aging and disease. *Drug Metabolism Reviews 30*, 225–243.

(22) Stadtman, E. R. (1993) Oxidation of free amino acids and amino acid residues in proteins by radiolysis and by metal-catalyzed reactions. *Annual Review of Biochemistry 62*, 797–821.

(23) Levine, R. L., Moskovitz, J., and Stadtman, E. R. (2000) Oxidation of methionine in proteins: roles in antioxidant defense and cellular regulation. *IUBMB Life 50*, 301–307.

(24) Kiley, P. J., and Storz, G. (2004) Exploiting thiol modifications. *PLoS Biology 2*, e400.

(25) Stadtman, E. R., and Levine, R. L. (2000) Protein oxidation. *Annals of the New York Academy of Sciences 899*, 191–208.

(26) Choi, H.-J., Kim, S.-J., Mukhopadhyay, P., Cho, S., Woo, J.-R., Storz, G., and Ryu, S.-E. (2001) Structural basis of the redox switch in the OxyR transcription factor. *Cell 105*, 103–113.

(27) Giulivi, C., Traaseth, N. J., and Davies, K. J. A. (2003) Tyrosine oxidation products: analysis and biological relevance. *Amino acids 25*, 227–232.

(28) Uchida, K., and Kawakishi, S. (1993) 2-Oxo-histidine as a novel biological marker for oxidatively modified proteins. *FEBS letters 332*, 208–210.

(29) Holmgren, A. (1984) Enzymatic reduction-oxidation of protein disulfides by thioredoxin, in *Methods in Enzymology*, pp 295–300. Elsevier.

(30) Luo, S., and Levine, R. L. (2009) Methionine in proteins defends against oxidative stress. *The FASEB Journal 23*, 464–472.

(31) Brot, N., and Weissbach, H. (1983) Biochemistry and physiological role of methionine sulfoxide residues in proteins. *Archives of Biochemistry and Biophysics 223*, 271–281.

(32) Go, Y.-M., and Jones, D. P. (2013) The redox proteome. *Journal of Biological Chemistry 288*, 26512–26520.

(33) Gray, H. B., and Winkler, J. R. (2015) Hole hopping through tyrosine/tryptophan chains protects proteins from oxidative damage. *Proceedings of the National Academy of Sciences 112*, 10920–10925.

(34) Sundaresan, M., Yu, Z.-X., Ferrans, V. J., Irani, K., and Finkel, T. (1995) Requirement for generation of H2O2 for platelet-derived growth factor signal transduction. *Science 270*, 296–299.

(35) Rhee, S. G., Bae, Y. S., Lee, S.-R., and Kwon, J. (2000) Hydrogen peroxide: a key messenger that modulates protein phosphorylation through cysteine oxidation. *Science Signaling 2000*, pe1–pe1.

(36) Forman, H. J., Maiorino, M., and Ursini, F. (2010) Signaling functions of reactive oxygen species. *Biochemistry 49*, 835–842.

(37) Bakke, J., and Haj, F. G. (2015) Protein-tyrosine phosphatase 1B substrates and metabolic regulation, in *Seminars in Cell & Developmental Biology*, pp 58–65. Elsevier.

(38) Lee, J.-W., and Helmann, J. D. (2006) The PerR transcription factor senses H 2 O 2 by metal-catalysed histidine oxidation. *Nature 440*, 363.

(39) Kathiresan, M., Martins, D., and English, A. M. (2014) Respiration triggers heme transfer from cytochrome c peroxidase to catalase in yeast mitochondria. *Proceedings of the National Academy of Sciences 111*, 17468–17473.

(40) Berndt, C., Lillig, C. H., and Holmgren, A. (2007) Thiol-based mechanisms of the thioredoxin and glutaredoxin systems: implications for diseases in the cardiovascular system. *American Journal of Physiology-Heart and Circulatory Physiology 292*, H1227–H1236.

(41) Delaunay, A., Pflieger, D., Barrault, M.-B., Vinh, J., and Toledano, M. B. (2002) A thiol peroxidase is an H2O2 receptor and redox-transducer in gene activation. *Cell 111*, 471–481.

(42) Fuangthong, M., and Helmann, J. D. (2002) The OhrR repressor senses organic hydroperoxides by reversible formation of a cysteine-sulfenic acid derivative. *Proceedings of the National Academy of Sciences 99*, 6690–6695.

(43) Zheng, M., and Storz, G. (2000) Redox sensing by prokaryotic transcription factors. *Biochemical Pharmacology 59*, 1–6.

(44) Herbig, A. F., and Helmann, J. D. (2001) Roles of metal ions and hydrogen peroxide in modulating the interaction of the Bacillus subtilis PerR peroxide regulon repressor with operator DNA. *Molecular Microbiology 41*, 849–859.

(45) Volkov, A. N., Nicholls, P., and Worrall, J. A. (2011) The complex of cytochrome c and cytochrome c peroxidase: the end of the road? *Biochimica et Biophysica Acta (BBA)-Bioenergetics 1807*, 1482–1503.

(46) Jiang, H., and English, A. M. (2006) Phenotypic analysis of the ccp1Δ and ccp1Δ-ccp1W191F mutant strains of Saccharomyces cerevisiae indicates that cytochrome c peroxidase functions in oxidative-stress signaling. *Journal of Inorganic Biochemistry 100*, 1996–2008.

(47) Martins, D., Kathiresan, M., and English, A. M. (2013) Cytochrome c peroxidase is a mitochondrial heme-based H2O2 sensor that modulates antioxidant defense. *Free Radical Biology and Medicine 65*, 541–551.

(48) Charizanis, C., Juhnke, H., Krems, B., and Entian, K.-D. (1999) The mitochondrial cytochrome c peroxidase Ccp1 of Saccharomyces cerevisiae is involved in conveying an oxidative stress signal to the transcription factor Pos9 (Skn7). *Molecular and General Genetics MGG 262*, 437–447.

(49) Kathiresan, M., and English, A. M. (2017) LC-MS/MS suggests that hole hopping in cytochrome c peroxidase protects its heme from oxidative modification by excess H 2 O 2. *Chemical Science 8*, 1152–1162.

(50) Lim, J. M., Kim, G., and Levine, R. L. (2019) Methionine in Proteins: It's Not Just for Protein Initiation Anymore. *Neurochemical Research 44*, 247–257.

(51) Stadtman, E. R., Moskovitz, J., Berlett, B. S., and Levine, R. L. (2002) Cyclic oxidation and reduction of protein methionine residues is an important antioxidant mechanism, in *Oxygen/Nitrogen Radicals: Cell Injury and Disease*, pp 3–9. Springer.

(52) Benoit, S. L., and Maier, R. J. (2016) Helicobacter catalase devoid of catalytic activity protects the bacterium against oxidative stress. *Journal of Biological Chemistry 291*, 23366–23373.

(53) Requejo, R., Hurd, T. R., Costa, N. J., and Murphy, M. P. (2010) Cysteine residues exposed on protein surfaces are the dominant intramitochondrial thiol and may protect against oxidative damage. *The FEBS Journal 277*, 1465–1480.

(54) Hondorp, E. R., and Matthews, R. G. (2004) Oxidative stress inactivates cobalamin-independent methionine synthase (MetE) in Escherichia coli. *PLoS Biology 2*, e336.

(55) Winkler, J. R., and Gray, H. B. (2015) Electron flow through biological molecules: does hole hopping protect proteins from oxidative damage? *Quarterly Reviews of Biophysics 48*, 411–420.

(56) Winkler, J. R., and Gray, H. B. (2015) Could tyrosine and tryptophan serve multiple roles in biological redox processes? *Philosophical Transactions of the Royal Society A: Mathematical, Physical and Engineering Sciences 373*, 20140178.

(57) He, K., Bornheim, L. M., Falick, A. M., Maltby, D., Yin, H., and Correia, M. A. (1998) Identification of the heme-modified peptides from cumene hydroperoxide-inactivated cytochrome P450 3A4. *Biochemistry 37*, 17448–17457.

(58) Shevelkova, A. N., and Ryabov, A. D. (1996) Irreversible inactivation of Caldariomyces fumago chloroperoxidase by hydrogen peroxide. *IUBMB Life 39*, 665–670.

(59) Yukl, E. T., Williamson, H. R., Higgins, L., Davidson, V. L., and Wilmot, C. M. (2013) Oxidative damage in MauG: implications for the control of high-valent iron species and radical propagation pathways. *Biochemistry 52*, 9447–9455.

(60) Tarboush, N. A., Jensen, L. M., Yukl, E. T., Geng, J., Liu, A., Wilmot, C. M., and Davidson, V. L. (2011) Mutagenesis of tryptophan199 suggests that hopping is required for MauG-dependent tryptophan tryptophylquinone biosynthesis. *Proceedings of the National Academy of Sciences 108*, 16956–16961.

(61) Davidson, V. L., and Liu, A. (2012) Tryptophan tryptophylquinone biosynthesis: a radical approach to posttranslational modification. *Biochimica et Biophysica Acta (BBA)-Proteins and Proteomics 1824*, 1299–1305.

(62) Aubert, C., Vos, M. H., Mathis, P., Eker, A. P., and Brettel, K. (2000) Intraprotein radical transfer during photoactivation of DNA photolyase. *Nature 405*, 586.

(63) Byrdin, M., Eker, A. P., Vos, M. H., and Brettel, K. (2003) Dissection of the triple tryptophan electron transfer chain in Escherichia coli DNA photolyase: Trp382 is the primary donor in photoactivation. *Proceedings of the National Academy of Sciences 100*, 8676–8681.

(64) Holder, P. G., Pizano, A. A., Anderson, B. L., Stubbe, J., and Nocera, D. G. (2012) Deciphering radical transport in the large subunit of class I ribonucleotide reductase. *Journal of the American Chemical Society 134*, 1172–1180.

(65) Stubbe, J., and van der Donk, W. A. (1998) Protein radicals in enzyme catalysis. *Chemical Reviews 98*, 705–762.

(66) Zanetti-Polzi, L., Daidone, I., and Corni, S. (2019) Evidence of a Thermodynamic Ramp for Hole-Hopping to Protect a Redox Enzyme from Oxidative Damage. *The Journal of Physical Chemistry Letters*.

(67) Zamocky, M., Furtmüller, P. G., and Obinger, C. (2008) Evolution of catalases from bacteria to humans. *Antioxidants & Redox Signaling 10*, 1527–1548.

(68) Reid, T. J., Murthy, M. R., Sicignano, A., Tanaka, N., Musick, W. D., and Rossmann, M. G. (1981) Structure and heme environment of beef liver catalase at 2.5 A resolution. *Proceedings of the National Academy of Sciences 78*, 4767–4771.

(69) de Visser, S. P. (2006) What external perturbations influence the electronic properties of catalase compound I? *Inorganic Chemistry 45*, 9551–9557.

(70) Chelikani, P., Carpena, X., Fita, I., and Loewen, P. C. (2003) An electrical potential in the access channel of catalases enhances catalysis. *Journal of Biological Chemistry 278*, 31290–31296.

(71) Alfonso-Prieto, M., Biarnés, X., Vidossich, P., and Rovira, C. (2009) The molecular mechanism of the catalase reaction. *Journal of the American Chemical Society 131*, 11751–11761.

(72) Díaz, A., Loewen, P. C., Fita, I., and Carpena, X. (2012) Thirty years of heme catalases structural biology. *Archives of Biochemistry and Biophysics 525*, 102–110.

(73) Hillar, A., Nicholls, P., Switala, J., and Loewen, P. C. (1994) NADPH binding and control of catalase compound II formation: comparison of bovine, yeast, and Escherichia coli enzymes. *Biochemical Journal 300*, 531–539.

(74) Koua, D., Cerutti, L., Falquet, L., Sigrist, C. J., Theiler, G., Hulo, N., and Dunand, C. (2009) PeroxiBase: a database with new tools for peroxidase family classification. *Nucleic Acids Research 37*, D261–D266.

(75) Zámocký, M., and Obinger, C. (2010) Molecular phylogeny of heme peroxidases, in *Biocatalysis Based on Heme Peroxidases*, pp 7–35. Springer.

(76) Welinder, K. G. (1992) Superfamily of plant, fungal and bacterial peroxidases. *Current Opinion in Structural Biology 2*, 388–393.

(77) Sivaraja, M., Goodin, D. B., Smith, M., and Hoffman, B. M. (1989) Identification by ENDOR of Trp191 as the free-radical site in cytochrome c peroxidase compound ES. *Science 245*, 738–740.

(78) Hillar, A., Peters, B., Pauls, R., Loboda, A., Zhang, H., Mauk, A. G., and Loewen, P. C. (2000) Modulation of the Activities of Catalase- Peroxidase HPI of Escherichia coli by Site-Directed Mutagenesis. *Biochemistry 39*, 5868–5875.

(79) Regelsberger, G., Jakopitsch, C., Rüker, F., Krois, D., Peschek, G. A., and Obinger, C. (2000) Effect of distal cavity mutations on the formation of compound I in catalase-peroxidases. *Journal of Biological Chemistry 275*, 22854–22861.

(80) Jakopitsch, C., Auer, M., Regelsberger, G., Jantschko, W., Furtmüller, P. G., Rüker, F., and Obinger, C. (2003) The catalytic role of the distal site asparagine-histidine couple in catalase-peroxidases. *European Journal of Biochemistry 270*, 1006–1013.

(81) Klotz, M. G., and Loewen, P. C. (2003) The molecular evolution of catalatic hydroperoxidases: evidence for multiple lateral transfer of genes between prokaryota and from bacteria into eukaryota. *Molecular Biology and Evolution 20*, 1098–1112.

(82) Zámockỳ, M., Furtmüller, P. G., and Obinger, C. (2010) Evolution of structure and function of Class I peroxidases. *Archives of Biochemistry and Biophysics 500*, 45–57.

(83) Singh, R., Wiseman, B., Deemagarn, T., Jha, V., Switala, J., and Loewen, P. C. (2008) Comparative study of catalase-peroxidases (KatGs). *Archives of Biochemistry and Biophysics 471*, 207–214.

(84) Moore, R. L., Powell, L. J., and Goodwin, D. C. (2008) The kinetic properties producing the perfunctory pH profiles of catalase-peroxidases. *Biochimica et Biophysica Acta (BBA)-Proteins and Proteomics 1784*, 900–907.

(85) Zámockỳ, M., Gasselhuber, B., Furtmüller, P. G., and Obinger, C. (2012) Molecular evolution of hydrogen peroxide degrading enzymes. *Archives of Biochemistry and Biophysics 525*, 131–144.

(86) Zámockỳ, M., Gasselhuber, B., Furtmüller, P. G., and Obinger, C. (2014) Turning points in the evolution of peroxidase–catalase superfamily: molecular phylogeny of hybrid heme peroxidases. *Cellular and Molecular Life Sciences 71*, 4681–4696.

(87) ng Welinder, K. G. (1991) Bacterial catalase-peroxidases are gene duplicated members of the plant peroxidase superfamily. *Biochimica et Biophysica Acta (BBA)-Protein Structure and Molecular Enzymology 1080*, 215–220.

(88) Yamada, Y., Fujiwara, T., Sato, T., Igarashi, N., and Tanaka, N. (2002) The 2.0 \AA crystal structure of catalase-peroxidase from Haloarcula marismortui. *Nature Structural & Molecular Biology 9*, 691.

(89) Carpena, X., Switala, J., Loprasert, S., Mongkolsuk, S., Fita, I., and Loewen, P. C. (2002) Crystallization and preliminary X-ray analysis of the catalase–peroxidase KatG from Burkholderia pseudomallei. *Acta Crystallographica Section D: Biological Crystallography 58*, 2184–2186.

(90) Bertrand, T., Eady, N. A., Jones, J. N., Nagy, J. M., Jamart-Grégoire, B., Raven, E. L., and Brown, K. A. (2004) Crystal structure of Mycobacterium tuberculosis catalase-peroxidase. *Journal of Biological Chemistry 279*, 38991–38999.

(91) Dunford, H. B. (1999) Heme peroxidases. Wiley-vch.

(92) Santoni, E., Jakopitsch, C., Obinger, C., and Smulevich, G. (2004) Comparison between catalase-peroxidase and cytochrome c peroxidase. The role of the hydrogen-bond networks for protein stability and catalysis. *Biochemistry 43*, 5792–5802.

(93) Poulos, T. L., and Kraut, J. (1980) The stereochemistry of peroxidase catalysis. *Journal of Biological Chemistry 255*, 8199–8205.

(94) Vitello, L. B., Erman, J. E., Miller, M. A., Wang, J., and Kraut, J. (1993) Effect of arginine-48 replacement on the reaction between cytochrome c peroxidase and hydrogen peroxide. *Biochemistry 32*, 9807–9818.

(95) Baker, R. D., Cook, C. O., and Goodwin, D. C. (2004) Properties of catalase–peroxidase lacking its C-terminal domain. *Biochemical and Biophysical Research Communications 320*, 833–839.

(96) Carpena, X., Loprasert, S., Mongkolsuk, S., Switala, J., Loewen, P. C., and Fita, I. (2003) Catalase-peroxidase KatG of Burkholderia pseudomallei at 1.7 \AA resolution. *Journal of Molecular Biology 327*, 475–489.

(97) Zámockỳ, M., Garcia-Fernandez, Q., Gasselhuber, B., Jakopitsch, C., Furtmüller, P. G., Loewen, P. C., Fita, I., Obinger, C., and Carpena, X. (2012) High Conformational Stability of Secreted Eukaryotic Catalase-peroxidases ANSWERS FROM FIRST CRYSTAL STRUCTURE AND UNFOLDING STUDIES. *Journal of Biological Chemistry 287*, 32254–32262.

(98) Donald, L. J., Krokhin, O. V., Duckworth, H. W., Wiseman, B., Deemagarn, T., Singh, R., Switala, J., Carpena, X., Fita, I., and Loewen, P. C. (2003) Characterization of the catalase-peroxidase KatG from Burkholderia pseudomallei by mass spectrometry. *Journal of Biological Chemistry 278*, 35687–35692.

(99) Jakopitsch, C., Kolarich, D., Petutschnig, G., Furtmüller, P. G., and Obinger, C. (2003) Distal side tryptophan, tyrosine and methionine in catalase–peroxidases are covalently linked in solution. *Febs Letters 552*, 135–140.

(100) Ghiladi, R. A., Medzihradszky, K. F., and Ortiz de Montellano, P. R. (2005) Role of the Met- Tyr- Trp Cross-Link in Mycobacterium tuberculosis Catalase-Peroxidase (KatG) As Revealed by KatG (M255I). *Biochemistry 44*, 15093–15105.

(101) Ghiladi, R. A., Knudsen, G. M., Medzihradszky, K. F., and de Montellano, P. R. O. (2005) The met-Tyr-Trp cross-link in Mycobacterium tuberculosis catalase-peroxidase (KatG) autocatalytic formation and effect on enzyme catalysis and spectroscopic properties. *Journal of Biological Chemistry 280*, 22651–22663.

(102) Jakopitsch, C., Auer, M., Ivancich, A., Rüker, F., Furtmüller, P. G., and Obinger, C. (2003) Total conversion of bifunctional catalase-peroxidase (KatG) to monofunctional peroxidase by exchange of a conserved distal side tyrosine. *Journal of Biological Chemistry 278*, 20185–20191.

(103) Yu, S., Girotto, S., Zhao, X., and Magliozzo, R. S. (2003) Rapid formation of compound II and a tyrosyl radical in the Y229F mutant of Mycobacterium tuberculosis catalase-peroxidase disrupts catalase but not peroxidase function. *Journal of Biological Chemistry 278*, 44121–44127.

(104) Regelsberger, G., Jakopitsch, C., Furtmüller, P. G., Rueker, F., Switala, J., Loewen, P. C., and Obinger, C. (2001) The role of distal tryptophan in the bifunctional activity of catalase-peroxidases. Portland Press Limited.

(105) Buse, G., Soulimane, T., Dewor, M., Meyer, H. E., and Blüggel, M. (1999) Evidence for a copper-coordinated histidine–tyrosine cross-link in the active site of cytochrome oxidase. *Protein Science 8*, 985–990.

(106) Ostermeier, C., Harrenga, A., Ermler, U., and Michel, H. (1997) Structure at 2.7 \AA resolution of the Paracoccus denitrificans two-subunit cytochrome c oxidase complexed with an antibody FV fragment. *Proceedings of the National Academy of Sciences 94*, 10547–10553.

(107) Ito, N., Phillips, S. E., Yadav, K. D., and Knowles, P. F. (1994) Crystal structure of a free radical enzyme, galactose oxidase. *Journal of Molecular Biology 238*, 704–814.

(108) Díaz, A., Horjales, E., Rudiño-Piñera, E., Arreola, R., and Hansberg, W. (2004) Unusual Cys-Tyr covalent bond in a large catalase. *Journal of Molecular Biology 342*, 971–985.

(109) Proshlyakov, D. A., Pressler, M. A., DeMaso, C., Leykam, J. F., DeWitt, D. L., and Babcock, G. T. (2000) Oxygen activation and reduction in respiration: involvement of redox-active tyrosine 244. *Science 290*, 1588–1591.

(110) Whittaker, J. W. (2005) The radical chemistry of galactose oxidase. *Archives of Biochemistry and Biophysics 433*, 227–239.

(111) Maté, M. J., Sevinc, M. S., Hu, B., Bujons, J., Bravo, J., Switala, J., Ens, W., Loewen, P. C., and Fita, I. (1999) Mutants that alter the covalent structure of catalase hydroperoxidase II from Escherichia coli. *Journal of Biological Chemistry 274*, 27717–27725.

(112) Carpena, X., Wiseman, B., Deemagarn, T., Herguedas, B., Ivancich, A., Singh, R., Loewen, P. C., and Fita, I. (2006) Roles for Arg426 and Trp111 in the modulation of NADH oxidase activity of the catalase-peroxidase KatG from Burkholderia pseudomallei inferred from pH-induced structural changes. *Biochemistry 45*, 5171–5179.

(113) Gasselhuber, B., Graf, M. M., Jakopitsch, C., Zamocky, M., Nicolussi, A., Furtmüller, P. G., Oostenbrink, C., Carpena, X., and Obinger, C. (2016) Interaction with the redox cofactor MYW and functional role of a mobile arginine in eukaryotic catalase-peroxidase. *Biochemistry 55*, 3528–3541.

(114) Carpena, X., Wiseman, B., Deemagarn, T., Singh, R., Switala, J., Ivancich, A., Fita, I., and Loewen, P. C. (2005) A molecular switch and electronic circuit modulate catalase activity in catalase-peroxidases. *EMBO Reports 6*, 1156–1162.

(115) Zhao, X., Khajo, A., Jarrett, S., Suarez, J., Levitsky, Y., Burger, R. M., Jarzecki, A. A., and Magliozzo, R. S. (2012) Specific function of the Met-Tyr-Trp adduct radical and residues Arg418 and Asp137 in the atypical catalase reaction of catalase-peroxidase KatG. *Journal of Biological Chemistry* jbc–M112.

(116) Jakopitsch, C., Auer, M., Regelsberger, G., Jantschko, W., Furtmüller, P. G., Rüker, F., and Obinger, C. (2003) Distal site aspartate is essential in the catalase activity of catalase-peroxidases. *Biochemistry 42*, 5292–5300.

(117) Deemagarn, T., Wiseman, B., Carpena, X., Ivancich, A., Fita, I., and Loewen, P. C. (2007) Two alternative substrate paths for compound I formation and reduction in catalase–peroxidase KatG from Burkholderia pseudomallei. *PROTEINS: Structure, Function, and Bioinformatics 66*, 219–228.

(118) Suarez, J., Ranguelova, K., Jarzecki, A. A., Manzerova, J., Krymov, V., Zhao, X., Yu, S., Metlitsky, L., Gerfen, G. J., and Magliozzo, R. S. (2009) An oxyferrous heme/protein-based radical intermediate is catalytically competent in the catalase reaction of Mycobacterium tuberculosis catalase-peroxidase (KatG). *Journal of Biological Chemistry 284*, 7017–7029.

(119) Zhao, X., Suarez, J., Khajo, A., Yu, S., Metlitsky, L., and Magliozzo, R. S. (2010) A radical on the Met-Tyr-Trp modification required for catalase activity in catalase-peroxidase is established by isotopic labeling and site-directed mutagenesis. *Journal of the American Chemical Society 132*, 8268–8269.

(120) Zhao, X., Yu, S., Ranguelova, K., Suarez, J., Metlitsky, L., Schelvis, J. P., and Magliozzo, R. S. (2009) Role of the oxyferrous heme intermediate and distal side adduct radical in the catalase activity of Mycobacterium tuberculosis KatG revealed by the W107F mutant. *Journal of Biological Chemistry 284*, 7030–7037.

(121) Jakopitsch, C., Vlasits, J., Wiseman, B., Loewen, P. C., and Obinger, C. (2007) Redox intermediates in the catalase cycle of catalase-peroxidases from Synechocystis PCC 6803, Burkholderia pseudomallei, and Mycobacterium tuberculosis. *Biochemistry 46*, 1183–1193.

(122) Loewen, P. C., Carpena, X., Vidossich, P., Fita, I., and Rovira, C. (2014) An ionizable active-site tryptophan imparts catalase activity to a peroxidase core. *Journal of the American Chemical Society 136*, 7249–7252.

(123) Kruft, B. I., Magliozzo, R. S., and Jarzęcki, A. A. (2015) Density Functional Theory Insights into the Role of the Methionine–Tyrosine–Tryptophan Adduct Radical in the KatG Catalase Reaction: O2 Release from the Oxyheme Intermediate. *The Journal of Physical Chemistry A 119*, 6850–6866.

(124) Vlasits, J., Jakopitsch, C., Bernroitner, M., Zamocky, M., Furtmüller, P. G., and Obinger, C. (2010) Mechanisms of catalase activity of heme peroxidases. *Archives of Biochemistry and Biophysics 500*, 74–81.

(125) Njuma, O. J., Ndontsa, E. N., and Goodwin, D. C. (2014) Catalase in peroxidase clothing: Interdependent cooperation of two cofactors in the catalytic versatility of KatG. *Archives of Biochemistry and Biophysics 544*, 27–39.

(126) Ivancich, A., Jakopitsch, C., Auer, M., Un, S., and Obinger, C. (2003) Protein-based radicals in the catalase-peroxidase of synechocystis PCC6803: a multifrequency EPR investigation of wild-type and variants on the environment of the heme active site. *Journal of the American Chemical Society 125*, 14093–14102.

(127) Jakopitsch, C., Ivancich, A., Schmuckenschlager, F., Wanasinghe, A., Pöltl, G., Furtmüller, P. G., Rüker, F., and Obinger, C. (2004) Influence of the Unusual Covalent Adduct on the Kinetics and Formation of Radical Intermediates in Synechocystis Catalase Peroxidase A STOPPED-FLOW AND EPR CHARACTERIZATION OF THE MET275, TYR249, AND ARG439 VARIANTS. *Journal of Biological Chemistry 279*, 46082–46095.

(128) Ivancich, A., Donald, L. J., Villanueva, J., Wiseman, B., Fita, I., and Loewen, P. C. (2013) Spectroscopic and kinetic investigation of the reactions of peroxyacetic acid with Burkholderia pseudomallei catalase-peroxidase, KatG. *Biochemistry 52*, 7271–7282.

(129) Njuma, O. J., Davis, I., Ndontsa, E. N., Krewall, J. R., Liu, A., and Goodwin, D. C. (2017) Mutual synergy between catalase and peroxidase activities of the bifunctional enzyme KatG is facilitated by electron hole-hopping within the enzyme. *Journal of Biological Chemistry 292*, 18408–18421.

(130) Singh, R., Switala, J., Loewen, P. C., and Ivancich, A. (2007) Two [Fe (IV) O Trp•] Intermediates in M. tuberculosis Catalase-Peroxidase Discriminated by Multifrequency (9- 285 GHz) EPR Spectroscopy: Reactivity toward Isoniazid. *Journal of the American Chemical Society 129*, 15954–15963.

(131) Yu, S., Chouchane, S., and Magliozzo, R. S. (2002) Characterization of the W321F mutant of Mycobacterium tuberculosis catalase–peroxidase KatG. *Protein Science 11*, 58–64.

(132) Vidossich, P., Alfonso-Prieto, M., Carpena, X., Loewen, P. C., Fita, I., and Rovira, C. (2007) Versatility of the electronic structure of compound I in catalase-peroxidases. *Journal of the American Chemical Society 129*, 13436–13446.

(133) Claiborne, A., and Fridovich, I. (1979) Purification of the o-dianisidine peroxidase from Escherichia coli B. Physicochemical characterization and analysis of its dual catalatic and peroxidatic activities. *Journal of Biological Chemistry 254*, 4245–4252.

(134) Ndontsa, E. N., Moore, R. L., and Goodwin, D. C. (2012) Stimulation of KatG catalase activity by peroxidatic electron donors. *Archives of Biochemistry and Biophysics 525*, 215–222.

(135) Vidossich, P., Alfonso-Prieto, M., Carpena, X., Loewen, P. C., Fita, I., and Rovira, C. (2007) Versatility of the electronic structure of compound I in catalase-peroxidases. *Journal of the American Chemical Society 129*, 13436–13446.

(136) Baker, R. D., Cook, C. O., and Goodwin, D. C. (2006) Catalase- Peroxidase Active Site Restructuring by a Distant and "Inactive" Domain. *Biochemistry 45*, 7113–7121.

(137) Jakopitsch, C., Wanasinghe, A., Jantschko, W., Furtmüller, P. G., and Obinger, C. (2005) Kinetics of Interconversion of Ferrous Enzymes, Compound II and Compound III, of Wild-type Synechocystis Catalase-peroxidase and Y249F PROPOSAL FOR THE CATALATIC MECHANISM. *Journal of Biological Chemistry 280*, 9037–9042.

(138) Chouchane, S., Lippai, I., and Magliozzo, R. S. (2000) Catalase-peroxidase (Mycobacterium tuberculosis KatG) catalysis and isoniazid activation. *Biochemistry 39*, 9975–9983.

(139) Chouchane, S., Girotto, S., Kapetanaki, S., Schelvis, J. P., Yu, S., and Magliozzo, R. S. (2003) Analysis of heme structural heterogeneity in Mycobacterium tuberculosis catalase-peroxidase (KatG). *Journal of Biological Chemistry 278*, 8154–8162.

(140) Colin, J., Jakopitsch, C., Obinger, C., and Ivancich, A. (2010) The reaction of synechocystis catalase–peroxidase (KatG) with isoniazid investigated by multifrequency (9–285 GHz) EPR spectroscopy. *Applied Magnetic Resonance 37*, 267.

(141) Suarez, J., Ranguelova, K., Schelvis, J. P., and Magliozzo, R. S. (2009) Antibiotic resistance in Mycobacterium tuberculosis peroxidase intermediate bypass causes poor isoniazid activation by the S315G mutant of M. Tuberculosis catalase-peroxidase (KatG). *Journal of Biological Chemistry 284*, 16146–16155.

(142) Svistunenko, D. A., Worrall, J. A., Chugh, S. B., Haigh, S. C., Ghiladi, R. A., and Nicholls, P. (2012) Ferric haem forms of Mycobacterium tuberculosis catalase-peroxidase probed by EPR spectroscopy: Their stability and interplay with pH. *Biochimie 94*, 1274–1280.

(143) Kudalkar, S. N., Njuma, O. J., Li, Y., Muldowney, M., Fuanta, N. R., and Goodwin, D. C. (2015) A role for catalase-peroxidase large loop 2 revealed by deletion mutagenesis: control of active site water and ferric enzyme reactivity. *Biochemistry 54*, 1648–1662.

(144) Lukat-Rodgers, G. S., Wengenack, N. L., Rusnak, F., and Rodgers, K. R. (2000) Spectroscopic comparison of the heme active sites in WT KatG and its S315T mutant. *Biochemistry 39*, 9984–9993.

(145) Wengenack, N. L., Todorovic, S., Yu, L., and Rusnak, F. (1998) Evidence for differential binding of isoniazid by Mycobacterium tuberculosis KatG and the isoniazid-resistant mutant KatG (S315T). *Biochemistry 37*, 15825–15834.

(146) Ivancich, A., Mazza, G., and Desbois, A. (2001) Comparative electron paramagnetic resonance study of radical intermediates in turnip peroxidase isozymes. *Biochemistry 40*, 6860–6866.

(147) Khindaria, A., and Aust, S. D. (1996) EPR detection and characterization of lignin peroxidase porphyrin π-cation radical. *Biochemistry 35*, 13107–13111.

(148) Ivancich, A., Jouve, H. M., Sartor, B., and Gaillard, J. (1997) EPR investigation of compound I in Proteus mirabilis and bovine liver catalases: formation of porphyrin and tyrosyl radical intermediates. *Biochemistry 36*, 9356–9364.

(149) Ivancich, A., Dorlet, P., Goodin, D. B., and Un, S. (2001) Multifrequency high-field EPR study of the tryptophanyl and tyrosyl radical intermediates in wild-type and the W191G mutant of cytochrome c peroxidase. *Journal of the American Chemical Society 123*, 5050–5058.

(150) Jakopitsch, C., Obinger, C., Un, S., and Ivancich, A. (2006) Identification of Trp106 as the tryptophanyl radical intermediate in Synechocystis PCC6803 catalase-peroxidase by multifrequency electron paramagnetic resonance spectroscopy. *Journal of Inorganic Biochemistry 100*, 1091–1099.

(151) Colin, J., Wiseman, B., Switala, J., Loewen, P. C., and Ivancich, A. (2009) Distinct role of specific tryptophans in facilitating electron transfer or as [Fe (IV)= O Trp•] intermediates in the peroxidase reaction of Bulkholderia pseudomallei catalase-peroxidase: A multifrequency EPR spectroscopy investigation. *Journal of the American Chemical Society 131*, 8557–8563.

(152) 'Round-the-horn site-directed mutagenesis - OpenWetWare.

(153) Varnado, C. L., and Goodwin, D. C. (2004) System for the expression of recombinant hemoproteins in Escherichia coli. *Protein Expression and Purification 35*, 76–83.

(154) Smith, K. M. (1975) Porphyrins and metalloporphyrins. Elsevier Amsterdam.

(155) Scott, S. L., Chen, W. J., Bakac, A., and Espenson, J. H. (1993) Spectroscopic parameters, electrode potentials, acid ionization constants, and electron exchange rates of the 2, 2'-azinobis (3-ethylbenzothiazoline-6-sulfonate) radicals and ions. *The Journal of Physical Chemistry 97*, 6710–6714.

(156) Michaelis, L., Schubert, M., and Granick, S. (1939) The free radicals of the type of Wurster's salts. *Journal of the American Chemical Society 61*, 1981–1992.

(157) Goodwin, D. C., Aust, S. D., and Grover, T. A. (1995) Evidence for veratryl alcohol as a redox mediator in lignin peroxidase-catalyzed oxidation. *Biochemistry 34*, 5060–5065.

(158) Nelson, D. P., and Kiesow, L. A. (1972) Enthalpy of decomposition of hydrogen peroxide by catalase at 25 C (with molar extinction coefficients of H2O2 solutions in the UV). *Analytical Biochemistry 49*, 474–478.

(159) Goodwin, D. C., Yamazaki, I., Aust, S. D., and Grover, T. A. (1995) Determination of rate constants for rapid peroxidase reactions. *Analytical Biochemistry 231*, 333–338.

(160) Goodwin, D. C., and Hertwig, K. M. (2003) Peroxidase-catalyzed oxidation of capsaicinoids: steady-state and transient-state kinetic studies. *Archives of Biochemistry and Biophysics 417*, 18–26.

(161) Heering, H. A., Indiani, C., Regelsberger, G., Jakopitsch, C., Obinger, C., and Smulevich, G. (2002) New insights into the heme cavity structure of catalase-peroxidase: A spectroscopic approach to the recombinant Synechocystis enzyme and selected distal cavity mutants. *Biochemistry 41*, 9237–9247.

(162) Wiseman, B., Colin, J., Smith, A. T., Ivancich, A., and Loewen, P. C. (2009) Mechanistic insight into the initiation step of the reaction of Burkholderia pseudomallei catalase-peroxidase with peroxyacetic acid. *JBIC Journal of Biological Inorganic Chemistry 14*, 801–811.